

Technical Report Documentation Page

1. REPORT No.

FHWA/CA/TL-2000/08

2. GOVERNMENT ACCESSION No.**3. RECIPIENT'S CATALOG No.****4. TITLE AND SUBTITLE**

A Modal Parameter Based Technique to Inspect Welded Reinforcement Splices during Construction

5. REPORT DATE

June 2000

6. PERFORMING ORGANIZATION**7. AUTHOR(S)**

N. Stubbs, R.W. Bolton, S. Park, S. Choi, E. Miller, A.H. Price, and C. Sikorsky

8. PERFORMING ORGANIZATION REPORT No.**9. PERFORMING ORGANIZATION NAME AND ADDRESS**

Texas Engineering Experimental Station
College Station, Texas 77843

10. WORK UNIT No.**11. CONTRACT OR GRANT No.**

Contract #5940073

12. SPONSORING AGENCY NAME AND ADDRESS

California Department of Transportation,
Engineering Service Center
1801 30th Street. Sacramento, CA 95816

13. TYPE OF REPORT & PERIOD COVERED

January 1998- June 1999

14. SPONSORING AGENCY CODE

F 98 SD 01

15. SUPPLEMENTARY NOTES**16. ABSTRACT**

The objective of this study was to investigate the technical feasibility of using a modal-parameter based method to evaluate, quantitatively, welded reinforcement splices during the construction process. At the outset of the project, an experiment was performed to demonstrate that the modal-based method could detect a 1/32 inch flaw in a #6 and a #9 rods, in accordance with ANSI/AWS Specifications. The notion of damage was defined and relationships between damage and the strength of a material were reviewed and applied to the welded splice. The fractional loss in stiffness in the weld region was taken as the measure of damage. An experiment to nondestructively measure the fractional stiffness changes, using changes in modal parameters and systems identification, in the weld region of twenty seven welded reinforcing rods was performed. Destructive tests to measure the yield strength, yield load, tensile strength, and ultimate load of the same specimens were also performed. The predicted strengths of the weld systems, obtained using the strength-damage models and the nondestructively measured fractional stiffness change, and the measured strengths obtained from the destructive tests were compared. Finally, how the proposed methodology may be extended to field conditions was investigated. Results indicate that the method is a feasible alternative to inspect welded reinforcement splices during the construction process.

17. KEYWORDS

Welded connections; nondestructive damage evaluation, modal parameters, continuum damage mechanics, quality control, X-Radiography

18. No. OF PAGES:

229

19. DRI WEBSITE LINK

http://www.dot.ca.gov/hq/research/researchreports/1997-2001/inspect_weld.pdf

20. FILE NAME

inspect_weld.pdf

**A Modal Parameter Based Technique to Inspect Welded
Reinforcement Splices during Construction**

FINAL REPORT

Prepared by

N. Stubbs¹, R.W. Bolton², S. Park³, S. Choi⁴, E. Miller⁵, A.H. Price⁶
Texas Engineering Experiment Station
College Station, Texas 77843

and

C. Sikorsky⁷
State of California
Department of Transportation
Sacramento, CA 95816

Submitted to:

State of California
Department of Transportation
Sacramento, CA 95816

TEES CONTRACT 32525-55090CE

June 2000

-
1. A.P. and Florence Wiley Professor
 2. Assistant Professor
 3. Research Associate
 4. Research Associate
 5. Structural Engineer
 6. Assistant Professor
 7. Senior Bridge Engineer

1. Report No. FHWA/CA/TL-2000/08		2. Government Accession No.		3. Recipient's Catalog No.	
4. Title and Subtitle A Modal Parameter Based Technique to Inspect Welded Reinforcement Splices during Construction				5. Report Date June 2000	
				6. Performing Organization Code	
				8. Performing Organization Report No.	
7. Author's N. Stubbs, R.W. Bolton, S. Park, S. Choi, E. Miller, A.H. Price, and C. Sikorsky				10. Work Unit No. (TRAIS)	
9. Performing Organization Name and Address Texas Engineering Experimental Station College Station, Texas 77843				11. Contract or Grant No. Contract #5940073	
				13. Type of Report and Period Covered January 1998 – June 1999	
12. Sponsoring Agency Name and Address California Department of Transportation, Engineering Service Center 1801 30th Street, Sacramento, CA 95816				14. Sponsoring Agency Code F 98 SD 01	
				15. Supplementary Notes	
16. Abstract The objective of this study was to investigate the technical feasibility of using a modal-parameter based method to evaluate, quantitatively, welded reinforcement splices during the construction process. At the outset of the project, an experiment was performed to demonstrate that the modal-based method could detect a 1/32 inch flaw in a #6 and a #9 rods, in accordance with ANSI/AWS Specifications. The notion of damage was defined and relationships between damage and the strength of a material were reviewed and applied to the welded splice. The fractional loss in stiffness in the weld region was taken as the measure of damage. An experiment to nondestructively measure the fractional stiffness changes, using changes in modal parameters and systems identification, in the weld region of twenty seven welded reinforcing rods was performed. Destructive tests to measure the yield strength, yield load, tensile strength, and ultimate load of the same specimens were also performed. The predicted strengths of the weld systems, obtained using the strength-damage models and the nondestructively measured fractional stiffness change, and the measured strengths obtained from the destructive tests were compared. Finally, how the proposed methodology may be extended to field conditions was investigated. Results indicate that the method is a feasible alternative to inspect welded reinforcement splices during the construction process.					
17. Key Words Welded connections, nondestructive damage evaluation, modal parameters, continuum damage mechanics, quality control, X-Radiography			18. Distribution Statement No restrictions. This document is available to the public through the National Technical Information Service, Springfield, Virginia 22161		
19. Security Classif. (of this report) Unclassified		20. Security Classif. (of this page) Unclassified		21. No. of Pages	22. Price

DISCLAIMER: The opinions, findings, and conclusions expressed in this publication are those of the authors and not necessarily those of the STATE OF CALIFORNIA

TABLE OF CONTENTS

	Page
TABLE OF CONTENTS	iii
LIST OF TABLES	vii
LIST OF FIGURES.....	xii
CHAPTER	
1 INTRODUCTION	1
1.1. BACKGROUND	1
1.2. POTENTIAL SOLUTION	2
1.3. RESEARCH OBJECTIVE AND METHODOLOGY	3
1.4. ORGANIZATION OF THE REPORT.....	4
2 QUANTITATIVE EVALUATION OF WELD CAPACITY	5
2.1. INTRODUCTION	5
2.2. ESTIMATION OF WELD CAPACITY	6
2.3. ESTIMATION OF WELD CAPACITY USING CONTINUUM DAMAGE MECHANICS	8
2.4. SUMMARY.....	11
3 MEASUREMENT OF FRACTIONAL STIFFNESS CHANGES IN WELDMENTS	13
3.1. INTRODUCTION	13
3.2. OVERVIEW OF METHODOLOGY.....	13
3.3. DESCRIPTION OF WELDED REINFORCING ROD SPECIMENS	14
3.4. EXPERIMENTAL DETERMINATION OF MODAL PARAMETERS OF RODS	15
3.4.1. Experimental Arrangement.....	15
3.4.2. Test Procedure	15
3.4.3. Extraction of Modal Parameters.....	16
3.5. GENERATION OF BASELINE MODELS OF RODS	17
3.6. DETERMINATION OF FRACTIONAL STIFFNESS CHANGES IN THE WELD.....	18
3.7. SUMMARY.....	19

TABLE OF CONTENTS (continued)

CHAPTER	Page	
4	YIELD STRENGTHS AND TENSILE STRENGTHS OF FIELD PREPARED REINFORCING ROD.....	32
	4.1. INTRODUCTION	32
	4.2. TEST FACILITIES AND TEST PROCEDURES	32
	4.3. TENSILE TEST RESULTS	33
	4.4. DISCUSSION OF TENSILE TEST RESULTS.....	33
	4.5. SUMMARY.....	34
5	COMPARISON BETWEEN MEASURED MEASURED WELD CAPACITY AND PREDICTED WELD CAPACITY	45
	5.1. INTRODUCTION	45
	5.2. COMPUTING THE PREDICTED WELD CAPACITY	45
	5.3. FAILURE MODEL OF THE WELD-ROD SYSTEM	46
	5.4. RESULTS OF THE COMPARISON BETWEEN THE PREDICTED AND MEASURED WELD CAPACITIES	46
	5.5. DISCUSSION OF RESULTS	48
	5.5.1. Interpretation of the Results	48
	5.5.2. Accuracy of the Results.....	49
	5.5.3. Areas for Potential Improvement in the Prediction.....	49
	5.5.4. Field Implementation of the Methodology.....	50
	5.6. SUMMARY.....	52
6	SUMMARY AND CONCLUSIONS	63
	6.1. SUMMARY.....	63
	6.2. CONCLUSIONS	64
	REFERENCES.....	66
APPENDICES		
A.	A METHODOLOGY TO IDENTIFY STRUCTURAL PROPERTIES OF THE BASE LINE AND THE EXISTING STRUCTURES	A-1
	A.1. SYSTEM IDENTIFICATION SCHEME FOR THE BASELINE STRUCTURE	A-1
	A.2. DAMAGE LOCALIZATION THEORY (DAMAGE INDEX METHOD).....	A-3
	A.3. DAMAGE SEVERITY ESTIMATION	A-9

TABLE OF CONTENTS (continued)

CHAPTER	Page
A.4. IDENTIFICATION OF STIFFNESS OF EXISTING STRUCTURE	A-10
B. VALIDATION OF THE METHODOLOGY VIA LABORATORY EXPERIMENTS FOR A 1/32" SURFACE DEFECT IN A #6 AND #9 BAR	B-1
B.1. INTRODUCTION	B-1
B.2. MATERIALS AND EQUIPMENT	B-1
B.2.1. Description of Materials	B-1
B.2.2. Description of Equipment	B-2
B.3. SUMMARY OF MODAL TESTING.....	B-3
B.3.1. Description of Equipment Setup.....	B-3
B.3.2. Specimen Preparation	B-3
B.3.3. Quantification of the Number of Impact Locations Using Shannon's Sampling Theorem	B-4
B.3.4. Description of Experimental Procedure.....	B-5
B.3.5. Description of Experiments	B-7
B.3.5.1. Description of Preliminary Experiments	B-7
B.3.5.2. Description of Final Experiments	B-8
B.4. DESCRIPTION OF RESULTS	B-12
B.4.1. Overview.....	B-12
B.4.2. Mode Shape Repeatability	B-12
B.4.3. Verification of Free-free Boundary Assumption	B-13
B.4.4. Support Interaction	B-13
B.4.5. Verification of Concept.....	B-14
B.5. SUMMARY AND CONCLUSIONS	B-14
C. MODAL ANALYSIS AND SYSTEM IDENTIFICATION RESULTS FOR REINFORCING ROD SPECIMENS	C-1
C.1. MODAL ANALYSIS RESULTS FOR FIELD WELDMENTS.	C-1
C.2. MODAL ASSURANCE CRITERIA.....	C-32
C.3. SYSTEM IDENTIFICATION RESULTS.....	C-43
D. TXDOT TENSILE TEST RESULTS FOR WELDED REINFORCING ROD SPECIMENS.....	D-I

TABLE OF CONTENTS (continued)

CHAPTER	Page
E. INDEPENDENT NON-DESTRUCTIVE EVALUATION OF WELDED REINFORCING ROD SPECIMENS	E-1
E.1. INTRODUCTION.....	E-1
E.2. DYE PENETRANT INSPECTION PROCEDURES.....	E-1
E.3. RESULTS OF VISUAL/ DYE PENETRANT INSPECTION....	E-2
E.4. INTERPRETATION OF RADIOGRAPHIC RECORDS	E-4
E.5. DISCUSSION OF RESULTS.....	E-7
E.6. SUMMARY AND CONCLUSIONS.....	E-7

LIST OF TABLES

TABLE		Page
3.1	Welded Specimen Designation Codes and Lot Sources	21
3.2	Modal Test Parameters for Reinforcing Rod Specimen Testing	21
3.3	Measured Resonant Frequencies	22
3.4	Initial Values of Material Properties for FE Models.....	23
3.5	Stiffness Sensitivity Matrix F for Specimen #11 BP1	23
3.6	System Identification for Specimen #11 BP1	23
3.7	Identified Average Stiffness Parameter (EI) for Baseline Models.....	24
3.8	Fractional Changes of the Bending Stiffness for Welded Specimens.....	25
4.1	Code of Bent Reinforcing Rod Specimens.....	36
4.2	Yield Strength of Reinforcing Rod Specimens	37
4.3	Tensile Strength of Reinforcing Rod Specimens	38
4.4	Breaking Strength of Reinforcing Rod Specimens	39
4.5	Young's Modulus of Reinforcing Rod Specimens.....	40
4.6	Total Grip Displacement for Reinforcing Rod Specimens	41
4.7	Percent Elongation of Reinforcing Rod Specimens	42
5.1	Comparison of Predicted and Measured Yield Strength Using Stiffness Changes Based on First Bending Mode	53
5.2	Comparison of Predicted and Measured Yield Load Using Stiffness Changes Based on First Bending Mode	54
5.3	Comparison of Predicted and Measured Tensile Strength Using Stiffness Changes Based on First Bending Mode	55
5.4	Comparison of Predicted and Measured Ultimate Load Using Stiffness Changes Based on First Bending Mode	56
5.5	Comparison of Proposed Approach and Qualitative Approach with Laboratory Test	57
B.1	Experimentation Sequence (UW = Unwelded; W = Welded).....	B-16
B.2	Modal Assurance Criteria for Specimen 6_3 and 6_1.....	B-18
B.3	Modal Assurance Criteria for Specimen 6_3 and 6_2.....	B-18

LIST OF TABLES (continued)

TABLE		Page
B.4	Modal Assurance Criteria for Specimen 6_3 and 6_4.....	B-18
B.5	Modal Assurance Criteria for Specimen 6_1 and 6_2.....	B-18
B.6	Modal Assurance Criteria for Specimen 6_1 and 6_4.....	B-19
B.7	Modal Assurance Criteria for Specimen 6_2 and 6_4.....	B-19
B.8	Modal Assurance Criteria for #6 FE Model and Specimen 6_3	B-19
B.9	Modal Assurance Criteria for Specimen 9_1 and 9_2.....	B-19
B.10	Modal Assurance Criteria for Specimen 9_1 and 9_3.....	B-20
B.11	Modal Assurance Criteria for Specimen 9_2 and 9_3.....	B-20
B.12	Modal Assurance Criteria for #9 FE Model and Specimen 9_2	B-20
C.1	Modal Assurance Criteria (FE Model vs. Measured) for #14 Unwelded Reinforcing Rod Specimen	C-33
C.2	Modal Assurance Criteria (FE Model vs. Measured) for #14 BP1 Reinforcing Rod Specimen	C-33
C.3	Modal Assurance Criteria (FE Model vs. Measured) for #14 BP2 Reinforcing Rod Specimen	C-33
C.4	Modal Assurance Criteria (FE Model vs. Measured) for #14 BP3 Reinforcing Rod Specimen	C-34
C.5	Modal Assurance Criteria (FE Model vs. Measured) for #14 PH3 Reinforcing Rod Specimen	C-34
C.6	Modal Assurance Criteria (FE Model vs. Measured) for #14 S1 Reinforcing Rod Specimen	C-34
C.7	Modal Assurance Criteria (FE Model vs. Measured) for #14 S2 Reinforcing Rod Specimen	C-35
C.8	Modal Assurance Criteria (FE Model vs. Measured) for #14 S3 Reinforcing Rod Specimen	C-35
C.9	Modal Assurance Criteria (FE Model vs. Measured) for #14 W1 Reinforcing Rod Specimen.....	C-35
C.10	Modal Assurance Criteria (FE Model vs. Measured) for #14 W2 Reinforcing Rod Specimen.....	C-36

LIST OF TABLES (continued)

TABLE		Page
C.11	Modal Assurance Criteria (FE Model vs. Measured) for #11 Unwelded Reinforcing Rod Specimen.....	C-36
C.12	Modal Assurance Criteria (FE Model vs. Measured) for #11 BP1 Reinforcing Rod Specimen	C-36
C.13	Modal Assurance Criteria (FE Model vs. Measured) for #11 BP2 Reinforcing Rod Specimen	C-37
C.14	Modal Assurance Criteria (FE Model vs. Measured) for #11 BP3 Reinforcing Rod Specimen	C-37
C.15	Modal Assurance Criteria (FE Model vs. Measured) for #11 PH2 Reinforcing Rod Specimen	C-37
C.16	Modal Assurance Criteria (FE Model vs. Measured) for #11 S1 Reinforcing Rod Specimen	C-38
C.17	Modal Assurance Criteria (FE Model vs. Measured) for #11 S2 Reinforcing Rod Specimen	C-38
C.18	Modal Assurance Criteria (FE Model vs. Measured) for #11 S3 Reinforcing Rod Specimen	C-38
C.19	Modal Assurance Criteria (FE Model vs. Measured) for #11 W1 Reinforcing Rod Specimen.....	C-39
C.20	Modal Assurance Criteria (FE Model vs. Measured) for #11 W2 Reinforcing Rod Specimen.....	C-39
C.21	Modal Assurance Criteria (FE Model vs. Measured) for #8 Unwelded Reinforcing Rod Specimen.....	C-39
C.22	Modal Assurance Criteria (FE Model vs. Measured) for #8 BP1 Reinforcing Rod Specimen	C-40
C.23	Modal Assurance Criteria (FE Model vs. Measured) for #8 BP2 Reinforcing Rod Specimen	C-40
C.24	Modal Assurance Criteria (FE Model vs. Measured) for #8 BP3 Reinforcing Rod Specimen	C-40
C.25	Modal Assurance Criteria (FE Model vs. Measured) for #8 PH1 Reinforcing Rod Specimen	C-41

LIST OF TABLES (continued)

TABLE		Page
C.26	Modal Assurance Criteria (FE Model vs. Measured) for #8 S1 Reinforcing Rod Specimen	C-41
C.27	Modal Assurance Criteria (FE Model vs. Measured) for #8 S2 Reinforcing Rod Specimen	C-41
C.28	Modal Assurance Criteria (FE Model vs. Measured) for #8 S3 Reinforcing Rod Specimen	C-42
C.29	Modal Assurance Criteria (FE Model vs. Measured) for #8 W1 Reinforcing Rod Specimen.....	C-42
C.30	Modal Assurance Criteria (FE Model vs. Measured) for #8 W2 Reinforcing Rod Specimen.....	C-42
C.31	System Identification for #14 Unwelded Reinforcing Rod Specimen	C-44
C.32	System Identification for #14 BP1 Reinforcing Rod Specimen.....	C-44
C.33	System Identification for #14 BP2 Reinforcing Rod Specimen.....	C-44
C.34	System Identification for #14 BP3 Reinforcing Rod Specimen.....	C-45
C.35	System Identification for #14 PH3 Reinforcing Rod Specimen	C-45
C.36	System Identification for #14 S1 Reinforcing Rod Specimen	C-45
C.37	System Identification for #14 S2 Reinforcing Rod Specimen	C-46
C.38	System Identification for #14 S3 Reinforcing Rod Specimen	C-46
C.39	System Identification for #14 W1 Reinforcing Rod Specimen.....	C-46
C.40	System Identification for #14 W2 Reinforcing Rod Specimen.....	C-47
C.41	System Identification for #11 Unwelded Reinforcing Rod Specimen	C-47
C.42	System Identification for #11 BP1 Reinforcing Rod Specimen.....	C-47
C.43	System Identification for #11 BP2 Reinforcing Rod Specimen.....	C-48
C.44	System Identification for #11 BP3 Reinforcing Rod Specimen.....	C-48
C.45	System Identification for #11 PH2 Reinforcing Rod Specimen	C-48
C.46	System Identification for #11 S1 Reinforcing Rod Specimen	C-49
C.47	System Identification for #11 S2 Reinforcing Rod Specimen	C-49

LIST OF TABLES (continued)

TABLE		Page
C.48	System Identification for #11 S3 Reinforcing Rod Specimen	C-49
C.49	System Identification for #11 W1 Reinforcing Rod Specimen.....	C-50
C.50	System Identification for #11 W2 Reinforcing Rod Specimen.....	C-50
C.51	System Identification for #8 Unwelded Reinforcing Rod Specimen	C-50
C.52	System Identification for #8 BP1 Reinforcing Rod Specimen.....	C-51
C.53	System Identification for #8 BP2 Reinforcing Rod Specimen.....	C-51
C.54	System Identification for #8 BP3 Reinforcing Rod Specimen.....	C-51
C.55	System Identification for #8 PH1 Reinforcing Rod Specimen	C-52
C.56	System Identification for #8 S1 Reinforcing Rod Specimen	C-52
C.57	System Identification for #8 S2 Reinforcing Rod Specimen	C-52
C.58	System Identification for #8 S3 Reinforcing Rod Specimen	C-53
C.59	System Identification for #8 W1 Reinforcing Rod Specimen.....	C-53
C.60	System Identification for #8 W2 Reinforcing Rod Specimen.....	C-53
C.61	Summary of Identified Baseline Stiffness Parameters (E).....	C-54
E.1	Welded Specimens Sorted by Relative Weld Quality.....	E-9
E.2	Relative Weld Quality of Specimens Sorted by Specimen Size and Code.....	E-10

LIST OF FIGURES

FIGURE		Page
2.1	A Rod Containing Weld Subjected to an Axial Force	12
3.1	Schematic for Estimating Stiffness Change in Weldments.....	26
3.2	A Typical Welded Rod Specimen.....	27
3.3	Experiment Model Setup with Free-free Boundary	27
3.4	Impact Head and Slider Assembly for the Experiment.....	28
3.5	Instrumentation for Experimental Modal Testing	28
3.6	A Typical Configuration of Rod Specimen (#11 BP1).....	29
3.7	Mode Shapes of #11 BP1 Specimen	30
3.8	Schematic of FE Model for #11 2 BP1 Specimen.....	31
4.1	Tensile Test of #11 Welded Reinforcement Rod Specimen	43
4.2	End and Side View of Failed #11 Control Specimen.....	43
4.3	End and Side View of Failed #11 BP2 Specimen.....	44
4.4	End and Side View of Failed #8 S1 Specimen.....	44
5.1	Correlation of Predicted and Measured Yield Strength Using Stiffness Changes Based on First Bending Mode	58
5.2	Correlation of Predicted and Measured Yield Load Using Stiffness Changes Based on First Bending Mode	59
5.3	Correlation of Predicted and Measured Tensile Strength Using Stiffness Changes Based on First Bending Mode	60
5.4	Correlation of Predicted and Measured Ultimate Load Using Stiffness Changes Based on First Bending Mode	61
5.5	Prototype of Clamping Device	62
5.6	Schematic of Field Test Specimen.....	62
A.1	Flawed Structure and Estimate of Flawless Structure.....	A-11
B.1	Supports and Pendulum.....	B-21
B.2	Pendulum and Materials Used.....	B-21
B.3	Equipment and Setup	B-22

LIST OF FIGURES (continued)

FIGURE		Page
B.4	Weak and Strong Axis.....	B-22
B.5	Milling out Impact and Accelerometer Locations.....	B-23
B.6	Inflicting Damage with Hacksaw	B-23
B.7	Milling out U-groove for Weld Joint	B-24
B.8	Welding of Joint Using GMAW (ER70S-6).....	B-24
B.9	Effect of Random Vibration in the Data on Mode 1 Curvatures.....	B-25
B.10	Accelerometer Attachment.....	B-25
B.11	Conducting Modal Test.....	B-26
B.12	Catching Hammer after Impact	B-26
B.13	Dampening out Vibrations between Impacts	B-27
B.14	Effect on Mode 1 Curvatures due to Variation in the Data Caused by the Experimental Procedure	B-27
B.15	Damage Localization for Specimen S_1 with 1/8 inch Deep Saw Cut...	B-28
B.16	Damage Localization for Specimen S_2 with 1/16 inch Deep Saw Cut.	B-28
B.17	Damage Localization for Specimen 6_3 with 1/32 inch Deep Saw Cut .	B-28
B.18	Mode 1 Symmetry Comparison between Experiment 4, 7, and 7a.....	B-29
B.19	Damage Localization for Specimen 6_1 for SC1 (Locations 2.5 and 7.5) with 0.02 inch Deep Saw Cut.....	B-29
B.20	Damage Localization for Specimen 6_1 for SC2 (Locations 3.5 and 6.5) with 0.02 inch Deep Saw Cut.....	B-30
B.21	Mode 1 Curvatures for Specimen 6_1 from Experiments 9b and 9c for SC1 and SC2 with 0.02 inch Deep Saw Cut	B-31
B.22	Damage Localization for Specimen 9_2 with 0.02 inch Deep Saw Cut .	B-31
B.23	Damage Localization for Specimen 9_2 with 1/32 inch Deep Saw Cut .	B-32
B.24	Damage Localization for Specimen 9_3 with 1/32 inch Deep Saw Cut .	B-32
B.25	Damage Localization for Welded Specimen 9_3 with 1/32 inch Deep Saw Cut	B-33

LIST OF FIGURES (continued)

FIGURE		Page
B.26	Damage Localization for Welded Specimen 6_3 with 0.04 inch Deep Saw Cut	B-34
B.27	Damage Localization for Welded Specimen 6_1 with 0.02 inch Deep Saw Cut	B-35
C.1	Modal Analysis Reporting Sheet for #14 Unwelded Reinforcing Rod Specimen	C-2
C.2	Modal Analysis Reporting Sheet for #14 BP1 Reinforcing Rod Specimen	C-3
C.3	Modal Analysis Reporting Sheet for #14 BP2 Reinforcing Rod Specimen	C-4
C.4	Modal Analysis Reporting Sheet for #14 BP3 Reinforcing Rod Specimen	C-5
C.5	Modal Analysis Reporting Sheet for #14 PH3 Reinforcing Rod Specimen	C-6
C.6	Modal Analysis Reporting Sheet for #14 S1 Reinforcing Rod Specimen	C-7
C.7	Modal Analysis Reporting Sheet for #14 S2 Reinforcing Rod Specimen	C-8
C.8	Modal Analysis Reporting Sheet for #14 S3 Reinforcing Rod Specimen	C-9
C.9	Modal Analysis Reporting Sheet for #14 W1 Reinforcing Rod Specimen	C-10
C.10	Modal Analysis Reporting Sheet for #14 W2 Reinforcing Rod Specimen	C-11
C.11	Modal Analysis Reporting Sheet for #11 Unwelded Reinforcing Rod Specimen	C-12
C.12	Modal Analysis Reporting Sheet for #11 BP1 Reinforcing Rod Specimen	C-13
C.13	Modal Analysis Reporting Sheet for #11 BP2 Reinforcing Rod Specimen	C-14

LIST OF FIGURES (continued)

FIGURE		Page
C.14	Modal Analysis Reporting Sheet for #11 BP3 Reinforcing Rod Specimen	C-15
C.15	Modal Analysis Reporting Sheet for #11 PH2 Reinforcing Rod Specimen	C-16
C.16	Modal Analysis Reporting Sheet for #11 S1 Reinforcing Rod Specimen	C-17
C.17	Modal Analysis Reporting Sheet for #11 S2 Reinforcing Rod Specimen	C-18
C.18	Modal Analysis Reporting Sheet for #11 S3 Reinforcing Rod Specimen	C-19
C.19	Modal Analysis Reporting Sheet for #11 W1 Reinforcing Rod Specimen	C-20
C.20	Modal Analysis Reporting Sheet for #11 W2 Reinforcing Rod Specimen	C-21
C.21	Modal Analysis Reporting Sheet for #8 Unwelded Reinforcing Rod Specimen	C-22
C.22	Modal Analysis Reporting Sheet for #8 BP1 Reinforcing Rod Specimen	C-23
C.23	Modal Analysis Reporting Sheet for #8 BP2 Reinforcing Rod Specimen	C-24
C.24	Modal Analysis Reporting Sheet for #8 BP3 Reinforcing Rod Specimen	C-25
C.25	Modal Analysis Reporting Sheet for #8 PH1 Reinforcing Rod Specimen	C-26
C.26	Modal Analysis Reporting Sheet for #8 S1 Reinforcing Rod Specimen	C-27
C.27	Modal Analysis Reporting Sheet for #8 S2 Reinforcing Rod Specimen	C-28
C.28	Modal Analysis Reporting Sheet for #8 S3 Reinforcing Rod Specimen	C-29

LIST OF FIGURES (continued)

FIGURE	Page
C.29 Modal Analysis Reporting Sheet for #8 W1 Reinforcing Rod Specimen	C-30
C.30 Modal Analysis Reporting Sheet for #8 W2 Reinforcing Rod Specimen	C-31
D.1 TxDOT Tensile Test Report for #14 Unwelded Reinforcing Rod Specimen	D-2
D.2 TxDOT Tensile Test Report for #14 BP1 Reinforcing Rod Specimen	D-3
D.3 TxDOT Tensile Test Report for #14 BP2 Reinforcing Rod Specimen	D-4
D.4 TxDOT Tensile Test Report for #14 BP3 Reinforcing Rod Specimen	D-5
D.5 TxDOT Tensile Test Report for #14 PH3 Reinforcing Rod Specimen	D-6
D.6 TxDOT Tensile Test Report for #14 S1 Reinforcing Rod Specimen	D-7
D.7 TxDOT Tensile Test Report for #14 S2 Reinforcing Rod Specimen	D-8
D.8 TxDOT Tensile Test Report for #14 S3 Reinforcing Rod Specimen	D-9
D.9 TxDOT Tensile Test Report for #14 W1 Reinforcing Rod Specimen	D-10
D.10 TxDOT Tensile Test Report for #14 W2 Reinforcing Rod Specimen	D-11
D.11 TxDOT Tensile Test Report for #11 Unwelded Reinforcing Rod Specimen	D-12
D.12 TxDOT Tensile Test Report for #11 BP1 Reinforcing Rod Specimen	D-13
D.13 TxDOT Tensile Test Report for #11 BP2 Reinforcing Rod Specimen	D-14

LIST OF FIGURES (continued)

FIGURE	Page
D.14 TxDOT Tensile Test Report for #11 BP3 Reinforcing Rod Specimen	D-15
D.15 TxDOT Tensile Test Report for #11 PH2 Reinforcing Rod Specimen	D-16
D.16 TxDOT Tensile Test Report for #11 S1 Reinforcing Rod Specimen	D-17
D.17 TxDOT Tensile Test Report for #11 S2 Reinforcing Rod Specimen	D-18
D.18 TxDOT Tensile Test Report for #11 S3 Reinforcing Rod Specimen	D-19
D.19 TxDOT Tensile Test Report for #11 W1 Reinforcing Rod Specimen	D-20
D.20 TxDOT Tensile Test Report for #11 W2 Reinforcing Rod Specimen	D-21
D.21 TxDOT Tensile Test Report for #8 Unwelded Reinforcing Rod Specimen	D-22
D.22 TxDOT Tensile Test Report for #8 BP1 Reinforcing Rod Specimen	D-23
D.23 TxDOT Tensile Test Report for #8 BP2 Reinforcing Rod Specimen	D-24
D.24 TxDOT Tensile Test Report for #8 BP3 Reinforcing Rod Specimen	D-25
D.25 TxDOT Tensile Test Report for #8 PH1 Reinforcing Rod Specimen	D-26
D.26 TxDOT Tensile Test Report for #8 S1 Reinforcing Rod Specimen	D-27
D.27 TxDOT Tensile Test Report for #8 S2 Reinforcing Rod Specimen	D-28
D.28 TxDOT Tensile Test Report for #8 S3 Reinforcing Rod Specimen	D-29

LIST OF FIGURES (continued)

FIGURE		Page
D.29	TxDOT Tensile Test Report for #8 W1 Reinforcing Rod Specimen	D-30
D.30	TxDOT Tensile Test Report for #8 W2 Reinforcing Rod Specimen	D-31
E.1	A Typical Sample Bar with Irregular Surfaces (Welds apparently were slightly ground)	E-11
E.2	The Same Bar after the Developer Was Applied (Note that surface irregularities precluded proper cleaning of the weld area.)	E-11

1. INTRODUCTION

1.1 BACKGROUND

Quality assurance of the various types of splices is accomplished using nondestructive testing (NDT) techniques, preapproved installation procedures, and visual inspection. For example, visual inspection of lap splices is sufficient, since the strength of the connection is a function of the length of the lap. Mechanical couplers are preapproved based on laboratory testing prior to their installation in the field. While inspection of welded splices could be accomplished via a visual inspection during the actual welding of the splice, radiographs of the welded joint are usually required as described in the contract documents.

The Structural Welding Code (ANSI/AWS D1.4, 1992) defines acceptance of a welded splice as a function of the maximum dimension of any single porosity or fusion type discontinuity. Procedures used to determine acceptance of a welded reinforcement splice are based on a statistical analysis of imperfections in welded splices collected from welds tested in the laboratory. Detection of a given defect is dependent on such factors as location, orientation and shape of the defect, material, inspector, and inspection environment (Chang et al., 1993). Failure to account for these factors during the radiographing process could result in inconclusive radiographs.

Potential weaknesses exist in current testing and acceptance procedures for welded reinforcement splices. For local NDT methods such as radiography to be used successfully, the location of damage or the defect must be known a priori. It should also be noted here that radiography requires the use of a hazardous substance which results in logistical problems during inspection. Also, the time interval between taking the initial radiograph and the report of the final interpretation could be significant. Finally, quality control and acceptance procedures mainly identify a defect; the quantification of the impact of the defect on the weld system is not performed.

Given the magnitude of the seismic retrofit program in California, including the retrofit and replacement of the toll structures, a more rational and quantitative field inspection method for welded splices in steel reinforcement bars is needed. A more reliable and responsive nondestructive field test method must be developed to verify that a welded reinforcement splice will perform as designed. Related needs are the problem of nondestructively evaluating the integrity of composite components used in bridges and welds cast in concrete.

1.2 POTENTIAL SOLUTION

Universal interest exists in the capability to monitor a structure and detect defects at the earliest possible stage. Current damage detection methods use either visual inspection or local methods such as acoustic or ultrasonic methods, magnetic field methods, radiographs, eddy-current methods, and thermal field methods. These techniques require that the vicinity of the damage be known, a priori, and that the portion of the structure being inspected is readily accessible. Generally, these experimental methods can detect potential damage on or near the surface of the structure. In addition, the damage has to be subjectively interpreted to assess the impact of the damage. What is needed is an objective method of quantifying the state of damage at a given location in a member and a set of analytical expressions that relate the state of damage to the strength of the member.

Another approach to NDT comprises the so-called "Global" Methods. The term "Global" refers to the fact that the integrity of a structure is interrogated using properties that belong to the entire structure (e.g., resonant frequencies and mode shapes). Methods that examine changes in the vibrational characteristics of the structure to detect defects and estimate the severity of the defects have recently received much attention (Doebbling et al., 1996; Rytter, 1992). Caltrans funded a modest research program to explore developing nondestructive damage evaluation (NDE) schemes that use the vibrational properties of a structure to locate and quantify damage in the structure. The first project (Contract #59A048) demonstrated a state-of-the-art process to detect and assess damage

in bridges (Stubbs et al., 1997). Another project (Contract #59A132), used this same NDE technique to assess the condition of Span #10 of the Benicia-Martinez Crossing (Stubbs et al., 1995). A third project (Contract #59A0022) periodically evaluated the structural integrity of a bridge found to have been constructed with potentially reactive aggregate, using the same NDE scheme (Stubbs et al., 1999).

The NDE methods using modal parameters supported by Caltrans have been deemed successful by other independent sources. A recent study at Los Alamos National Labs, for example, reviewed the efficacy of operationalizing various damage detection schemes found in the literature (Farrar and Jauregui, 1996). In that work, Farrar and Jauregui (1996) applied the results from an experimental modal analysis of a steel plate girder bridge to five different damage identification algorithms. One of those algorithms, the Damage Index Method is the NDE scheme supported by Caltrans. There are several noteworthy results from the Los Alamos study pertinent to this work. First, the Damage Index Method was the only damage identification scheme which did not give false negative readings (i.e., damage exist but damage is not predicted). Second, the Damage Index Method was the only method that had specific statistical criteria for determining if damage had occurred at a particular location. Third, the Damage Index Method was the only method that correctly detected and located all levels of inflicted damage. The Los Alamos study is important in that an independent credible source confirmed the efficacy of the NDE scheme proposed for this study.

1.3 RESEARCH OBJECTIVE AND METHODOLOGY

The objective of this project is to investigate the technical feasibility of using the Damage Index Method to evaluate, quantitatively, welded reinforcement splices during the construction process. The overall approach utilized to meet this objective was driven by the following logic: (1) experimentally demonstrate that the Damage Index Method could detect minimum-sized flaws as specified by ANSI/AWS (1992), (2) identify or develop models that relate strength of a member to the damage in that member, (3) design

an experiment to test the model, (4) perform the experiment and (5) extend the results to the field.

1.4 ORGANIZATION OF THE REPORT

The remainder of this report is organized as follows. In Chapter 2, the notion of damage is defined and relationships between damage and the strength of a material are developed. In Chapter 3, an experiment to nondestructively measure the relative stiffness change in the weld region, using twenty seven welded reinforcing rods, is described. In Chapter 4, an experiment to measure the yield strength, yield load, tensile strength, and ultimate load of the same specimens described in Chapter 3, is described. In Chapter 5, the results of the comparison of the strength of the weld systems using the strength damage models developed in Chapter 2 and the strengths measured in the experiment described in Chapter 4 are described. How the proposed methodology may be extended to field conditions is also discussed in Chapter 5. Finally, in Chapter 6, a summary of the project along with a list of significant findings is presented.

Five appendices support this work. Appendix A summarizes the Damage Index Method and the system identification approach used in Chapter 3. Appendix B describes an independent experiment, the objective of which was to demonstrate in accordance with ANSI/AWS specifications, that the Damage Index Method could, indeed, detect a flaw 1/32 inches deep in a #6 and a #9 rods (ANSI/AWS D1.4, 1992). In Appendix C, data supporting the modal analysis, system identification of the rods, and the stiffness change calculations utilized in Chapter 3 are summarized. The raw data in the form of uniaxial load-extension plots, for the 30 reinforcing rod specimens described in Chapter 4, are catalogued in Appendix D. Finally, an evaluation of the welds using Dye Penetrant and an interpretation of the radiographs of the welds provided by Caltrans is presented in Appendix E.

2. QUANTITATIVE EVALUATION OF WELD CAPACITY

2.1 INTRODUCTION

Nondestructive evaluation methods such as Dye Penetrant and X-Ray inspection yield only a qualitative description of surface and internal flaws in a weld system. Even if the geometry of a flaw were known, Fracture Mechanics or other strength predicting methods must be utilized to estimate the strength or useful life of a structural element. In addition, if the geometry of the defect is complex, such as in the case of a defective weld, the application of Fracture Mechanics, which applies mostly to isolated flaws with simple geometric configurations, is limited.

In the discipline of Continuum Damage Mechanics, damage and damage growth is related to the initial state of damage in a material and the loading environment to which the material is subjected. However, in that field, the consensus is that damage is treated as an unobservable internal thermodynamic variable. Physically, damage has been related to the fraction of voids in a plane intersecting a material and the reduction in the elastic modulus of the material. More specifically, Kachanov (1986) considered the damage variable as a surface density of intersections of cracks and cavities.

In recent years, the authors have developed and refined a nondestructive methodology that can locate, as well as quantify, damage in a structural element or a larger structure. In the present usage, the measure of damage is the fractional loss in stiffness at some location in a structure. To date, however, the technique has been only used to estimate stiffness changes or effective reduction in moduli of structures or structural elements. Certainly, the value of the methodology could be significantly enhanced, if it were possible to utilize the measured damage, or stiffness increase, of a weldment to predict load capacity of a welded reinforcing rod.

In this chapter a relationship between the damage in a material and the strength of the material is developed. Two approaches are used. First, independent of Continuum Damage Mechanics, a relationship between the yield strength and tensile strength of a

welded reinforcing rod is developed. Second, the validity of the results is checked using the results from Continuum Damage Mechanics.

2.2 ESTIMATION OF WELD CAPACITY

A rod containing a weld and subjected to an axial force P is shown in Figure 2.1. Let the weld system consist of the filler material and the interface between the filler material and the base metal. Restricting this analysis to failure in the filler material, let the yield strength and cross-sectional area of the weld system without any defects be σ_y and A_U , respectively. Then, the load, P_{Uy} , to cause yield in the weld system without defects is given by:

$$P_{Uy} = \sigma_y A_U \quad (2.1)$$

Assume that defects in the form of cracks, voids, porosity, incomplete fusion, etc., are introduced into the weld system such that the cross-sectional area is reduced to $A_D < A_U$. Then the load, P_{Dy} , to cause yield in the weld system with defects becomes:

$$P_{Dy} = \sigma_y A_D \quad (2.2)$$

Dividing Equation (2.2) by Equation (2.1) yields:

$$\begin{aligned} \frac{P_{Dy}}{P_{Uy}} &= \frac{A_D}{A_U} \\ &= \frac{Er^2 A_D}{Er^2 A_U} = \frac{EI_D}{EI_U} \end{aligned} \quad (2.3)$$

where E , r , and I are, respectively, Young's modulus, the radius of gyration of the cross-section, and the second moment of area of the cross section. Here it is assumed that the damaged region is small compared to the cross-sectional area and the radius of gyration is

not affected. According to Equation (2.3), the ratio of loads to cause yield equals the ratio of the bending stiffnesses of the defect-free and defected weld systems.

Note that the ratio EI_D/EI_U is the damage index, DI , utilized by Stubbs et al. (1992) in the so-called Damage Index Method (See also Appendix A). That is,

$$\frac{EI_D}{EI_U} = DI = (1 + \alpha) \quad (2.4)$$

where α is the fractional change in stiffness of a section, the measure of damage in the Damage Index Method. Theoretically, α ranges from -1 to $+\infty$. If $\alpha < 0$, the interpretation is damage; if $\alpha > 0$, stiffening has occurred. Combining Equation (2.3) and (2.4),

$$P_{Dy} = P_{Uy} (1 + \alpha) \quad (2.5)$$

Dividing both sides of Equation (2.5) by A_U yields:

$$\sigma_{Dy} = \sigma_y (1 + \alpha) \quad (2.6)$$

From the theory outlined in Appendix A, α can be measured nondestructively by utilizing the modal parameters of the structure containing the weld. Since the intent here is to inspect the weld by measuring α after welding, the analysis ignores damage growth subsequent to loading. This situation is analogous to a rod with a circular hole that is loaded to yield. In such a case, a strength of materials analysis indicates no change in the geometry of the hole at full yield. Furthermore, the yield strength, σ_y , can be associated with the nominal properties of the weld. Thus, Equations (2.5) and (2.6) predict the load and strength at yield for a defective weld, given the damage and the nominal properties of a defect-free weld system.

If the yield strength is replaced in Equations (2.1) to (2.6) with the tensile strength, σ_T , of the defect-free weld system, the predictions for the maximum load, P_{DT} , and the tensile strength, σ_{DT} , of the defective specimen are as follows:

$$P_{DT} = P_{UT}(1 + \alpha) \quad (2.7)$$

$$\sigma_{DT} = \sigma_T(1 + \alpha) \quad (2.8)$$

In Equations (2.7) and (2.8), the damage, α , is measured and P_{UT} and σ_T are the nominal values associated with the tensile strength and the load corresponding to the tensile strength.

2.3 ESTIMATION OF WELD CAPACITY USING CONTINUUM DAMAGE MECHANICS

In Continuum Damage Mechanics, damage refers collectively to all entities, considered to be of a microscopic scale, which are capable of changing their characteristic dimensions under thermomechanical loadings (Talreja, 1994). Continuum Damage Mechanics offers an alternative logic to developing estimates of the capacity of damaged systems. For convenience, the concepts of damage variable, effective stress, and the Principle of Strain-Equivalence will be reviewed. From these results, estimates of the values of yield and tensile strengths of virgin (undamaged) and damaged specimens will be developed.

Consider the same rod depicted in Figure 2.1. Consider also a plane through the weld region perpendicular to the axial load. Let the total area of the cross-section be A and the area of the voids be given by A_v . Rabotnov (1969) interpreted damage, w , as the area fraction of voids given by

$$w = \frac{A_v}{A} \quad (2.9)$$

Note that:

- a) $w = 0$ corresponds to the undamaged state,
- b) $w = 1$ corresponds to separation of the material, and
- c) $0 \leq w < 1$ characterizes the damage state.

At some arbitrary damage state, w , the effective cross-sectional area resisting the load is \tilde{A} , where

$$\tilde{A} = A - A_d = A(1 - w) \quad (2.10)$$

By definition, the “effective stress,” $\tilde{\sigma}$, is

$$\tilde{\sigma} = P / \tilde{A} = P / A(1 - w) = \sigma / (1 - w) \quad (2.11)$$

Note that $\sigma = P/A$ is referred to as the “usual stress”.

Note also that :

- a) $\tilde{\sigma} \geq \sigma$:
- b) $\tilde{\sigma} = \sigma$ for a virgin material, and
- c) $\tilde{\sigma} \rightarrow \infty$ at separation.

According to Lemaitre and Chaboche (1990), the Principal of Strain Equivalence for a damaged material may be stated as follows: “Any deformation behavior of a damaged material is represented by the constitutive laws of the virgin material in which the usual stress is replaced by the effective stress”. In the uniaxial case presented in Figure 2.1, the usual stress is $\sigma = P/A$ and the effective stress is $\tilde{\sigma} = \sigma / (1 - w)$. Thus, if ϵ_c is the strain experienced by the damaged body subjected to stress σ , ϵ_c is also the strain in the equivalent virgin material subjected to stress $\tilde{\sigma}$. That is,

$$\epsilon_c = \frac{\tilde{\sigma}}{E} = \frac{\sigma}{(1 - w)E} \quad (2.12)$$

where E is the Young's modulus of the virgin material. Rearranging Equation (2.12),

$$\tilde{\sigma} = \sigma / (1 - w) = E \varepsilon_c \quad (2.13)$$

or, for the damaged body subjected to stress σ ,

$$\sigma = E(1 - w) \varepsilon_c = \tilde{E} \varepsilon_c \quad (2.14)$$

Thus, the quantity $E(1 - w) = \tilde{E}$ can be interpreted as the Young's modulus of the material with damage w . Eliminating σ and ε_c from Equation (2.13) and Equation (2.14) yields

$$\frac{\tilde{E}}{E} = 1 - w \quad (2.15)$$

Thus the Principle of Strain Equivalence leads to a relationship between damage and the change in the Young's modulus of the material.

The relationship between damage and various strength measures can be developed by manipulating Equation (2.14). A material with yield strength σ_y would yield when the effective stress is $\tilde{\sigma} = \sigma_y$. That is, setting $\tilde{\sigma} = \sigma_y$, the usual stress at yield, σ_{yw} , becomes

$$\sigma_{yw} = \sigma_y (1 - w) \quad (2.16)$$

Similarly, if σ_T is the tensile strength, the material with damage w will have a tensile strength, σ_{Tw} , given by

$$\sigma_{Tw} = \sigma_T (1 - w) \quad (2.17)$$

In summary, note the similarity between Equation (2.6) and Equation (2.16) and Equation (2.8) and Equation (2.17). The two sets of equations are identical, if $w = -\alpha$. Note also that the ratio \tilde{E}/E is analogous to the damage index, DI, introduced in Equation (2.4).

2.4 SUMMARY

In this chapter, a relationship between the damage in a material and the strength of the material was developed. Two approaches were used. First, independent of Continuum Damage Mechanics, a relationship between the yield strength and tensile strength of a welded reinforcing rod was developed. Second, the validity of the results was checked using the results from Continuum Damage Mechanics. There is a strong agreement between the damage physically measured in the Damage Index Method and the internal variable used to characterize damage in Continuum Damage Mechanics.

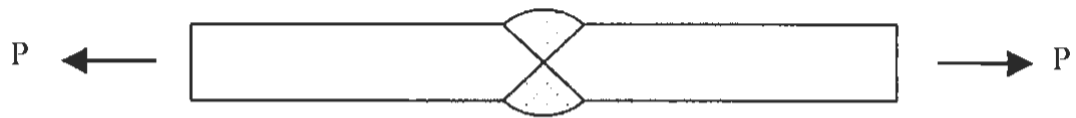


Figure 2.1 A Rod Containing Weld Subjected to an Axial Force

3. MEASUREMENT OF FRACTIONAL STIFFNESS CHANGES IN WELDMENTS

3.1 INTRODUCTION

Caltrans fabricated twenty-seven welded reinforcing rod specimens and collected radiographic images of each specimen weld prior to shipment to Texas A&M. This chapter presents the results of nondestructive testing and weld stiffness analyses performed on twenty-seven welded reinforcing rod specimens. The remainder of the chapter is organized into five sections. First, an overview of the evaluation methodology is presented. Second, the reinforcing rod specimens are described. Third, modal tests results for the specimens are discussed. Fourth, the development of the baseline models for the specimens is presented. Finally, the stiffness changes in the welded specimens are generated. A second independent nondestructive evaluation (NDE) of weld quality was also performed at Texas A&M and is presented in Appendix E.

3.2 OVERVIEW OF METHODOLOGY

An overview of the damage evaluation methodology used here to identify the fractional stiffness changes in the welded rod specimens is shown in Figure 3.1. Modal tests are performed on the test specimens and from an analysis of the measured response, modal parameters are extracted. The modal parameters of interest here are resonant frequencies and corresponding mode shapes. In order to perform the identification of the test specimen, modal parameters of the test specimen as well as the modal parameters of the baseline model are needed. The baseline modal parameters may be estimated using measured frequencies for the test specimen as well as the FE model of the test specimen (See Appendix A for details). Once a corresponding set of measured modal parameters for the test specimen and baseline modal parameters are available, the damage evaluation methodology (See Appendix A for details) can be used to estimate the fractional change in the weldment.

3.3 DESCRIPTION OF WELDED REINFORCING ROD SPECIMENS

A total of thirty 48 inch (nominal) Grade 60 reinforcing rod specimens fabricated by Caltrans were delivered to Texas A&M for evaluation. The thirty specimen set consisted of three, ten-specimen subsets fabricated from #8, #11, and #14 size rods. Each ten-specimen subset included one unwelded rod that served as a control. Table 3.1 summarizes the coding system used to identify each rod in the ten-specimen subsets. Similar designations were used for all rod sizes. Observations of differences in reinforcement ridge patterns and vendor code numbers on the #11 rods indicate that these rods came from two different rod stocks. The #8 and the #14 rods all appear to have come from common #8 and #14 rod stocks. These variations are indicated in Table 3.1 by the lot identifier.

Visual inspection of the welded specimens indicated that each rod was originally saw-cut to a 48-inch length and then bevel cut again at the center of the rod to form the groove geometry for a butt weld. The final lengths of the specimens after welding were approximately 0.5 to 1.0 inch longer than their original lengths. No attempt was made to shorten the specimens to the original 48-inch length. Measured dimensions for each specimen are shown in Appendix C. A typical welded test specimen is shown in Figure 3.2. The backing plate attached to each specimen during the welding process is also noted in Figure 3.2. All specimens were tested and evaluated with backing plates attached. The reinforcing rods were welded with the SMAW process using 1/8" diameter E8018-C3 electrodes. The joint geometry was a single V with a 45 degree included angle and 1/4" root. Stringer beads were applied with cleaning after each bead using chipping and brushing only, no grinding was performed on the specimens. Short arc lengths were maintained and generator CC welding machines set at 125 amps were used.

3.4 EXPERIMENTAL DETERMINATION OF MODAL PARAMETERS OF RODS

3.4.1 Experimental Arrangement

The experimental setup used in the modal testing of the reinforcing rod specimens is shown in Figure 3.3. A fixed response - roving input test method was used to collect the response data. The test specimen shown in Figure 3.3 was suspended with two flexible cables to simulate a free-free boundary configuration in the horizontal plane. A response accelerometer was attached to the back of the specimen slightly off center and in the horizontal plane. The impact head/slider assembly noted in Figure 3.3 was aligned along the horizontal center-line of the specimen and used to impact the specimen at specific locations along its length. The custom-fabriacted impact head/slider assembly was designed to maintain a horizontal impact vector perpedicuar to the specimen as the assembly was moved to each impact location. An enlargement of the impact head assembly is shown in Figure 3.4. Impact positions were marked on the slider assembly to insure positional repeatability during the testing.

Instrumentation used to conduct the modal tests consisted of a PCB 298A10 piezoelectric load cell mounted in a spring-loaded impact head/slider assembly, a PCB 352A10 piezoelectric response accelerometer attached to the specimen, a 4-channel DSP Technology 20-42 Digital Signal Processor (DSP), and a portable computer (PC). Data acquisition software was provided by the DSP vendor, Siglab Version V3.10 (11-Sep-98). The DSP unit and portable computer used in these tests are shown in Figure 3.5. Instrumentation and test settings used for the modal tests are summarized in Table 3.2.

3.4.2 Test Procedure

All of the specimens under test had 13 uniformly distributed impact locations and 1 accelerometer response location. These locations are shown for each specimen in Appendix C. A typical impact/ response location configuration is shown in Figure 3.6. The Frequency Response Functions (FRFs) measured at each impact location were derived from an average of 10 response measurements.

The experimental modal testing procedure consisted of the following steps:

1. Mark the impact locations;
2. Attach the response accelerometer to the specimen with an adhesive (Quick Grab Clear Silicon Adhesive, Quick Grab, Inc. Scottsdale, AZ);
3. Position the specimen in the supports in a horizontal position with the accelerometer in the horizontal plane of the specimen;
4. Align and adjust the relative position of specimen and the impact/slider assembly so that the impact head is perpendicular to the specimen and travels along the horizontal centerline of the specimen;
5. Arm the acquisition system to record the data;
6. Trigger a response measurement by retracting and releasing the impact head plunger assembly;
7. After completion of the measurement, gently grasp the specimen to damp out the remaining vibrations and stop the specimen from swinging;
8. Repeat Steps 6 to 7 ten times;
9. Manually record the maximum value for the five monitored response peaks of the average FRF and store the data on disk; and
10. Repeat Steps 1 to 9 for each impact location.

3.4.3 Extraction of Modal Parameters

Time data from the response accelerometer and impact head were converted in the DSP hardware to the frequency domain and the associated frequency response functions (FRFs) were generated. It was possible to extract modal parameters (i.e. frequencies and mode shapes) directly from the FRF data because of the low damping, widely-spaced frequencies, and simple geometry of the experimental test configuration. The modal parameters were obtained from the plot of frequency response function using the peak picking method (Ewins, 1984). The mode shapes for each specimen were drawn by measuring the magnitude of frequency response functions corresponding to impact location 1 through impact location 13 at specific frequencies (e.g. resonant frequencies of

the first five modes). The measured resonant frequencies for each specimen are presented in Table 3.3.

The five measured resonant frequencies of the #8 specimens ranged approximately from 70 Hz to 950Hz. It was observed that the specimen without weldment had higher frequency values than most of welded specimens as means and coefficient of variations of frequencies indicate in Table 3.3. Ignoring the variations in material and measurement errors that might be attributed to the increase in length due to weldment and/or poor weldment, the same phenomena were observed in #11 and #14 specimens for which the first five resonant frequencies span approximately from 100 Hz to 1300Hz and from 120 Hz to 1600 Hz, respectively. Overall, resonant frequencies were very consistent and uniform across all modes and rod sizes, as indicated by the small coefficients of variation for each size and frequency group which ranged from 1.2% to 2.5%. More variability in resonant frequencies was observed in #8 specimens than in the larger rod sizes. The modal test results are provided in Appendix C. A typical set of measured mode shapes (#14 BP1 specimen) are plotted in Figure 3.7. In the figure, the modes represent the first through the fifth bending mode in the horizontal direction.

3.5 GENERATION OF BASELINE MODELS OF RODS

The baseline model for each specimen was constructed using the resonant frequencies extracted from the modal testing. Note that the baseline structure is assumed to be damage-free with resonant frequencies near those of the welded specimens. To develop such a baseline model, a finite element (FE) model of the welded reinforcing bar specimen was developed (ABAQUS 1994). A schematic of the FE model for #14 BP1 specimen is shown in Figure 3.8. The specimen was modeled using 768 beam elements. Also, linear spring elements were used to model the cable to suspend the specimen in free-free boundary condition. The spring elements have negligible stiffness and mass properties. The other specimens were modeled based on the measured length, location of the weldments, location of the sensors, and location of the support cables. All beam members of the FE models were assigned to one group and initial material properties (E)

were summarized in Table 3.4. The correlation between the baseline modes and experiment modes was established using modal assurance criteria (MAC). The resulting MAC values for each specimen are presented in Appendix C.

The procedure of baseline parameter identification for the #11 BPI specimen is illustrated here as a typical example. With the initial estimates of material properties and with the appropriate group stiffness reduced by a known amount, the stiffness sensitivity matrix, F , which relates changes in element stiffness to changes in resonant frequencies (See Appendix A for details), was developed. The elements of the sensitivity matrix F for the specimen are listed in Table 3.5. The six-step algorithm (See Appendix A for details) was utilized until the system converged. The convergence of the system identification scheme is demonstrated in Table 3.6. After two iterations, the percent differences in the corresponding five frequencies of the specimen and the FE model have been reduced from, respectively, 5.58%, 6.98%, 5.71%, 6.80% and 5.67% to 0.32%, 0.11%, 0.09%, 0.06% and 0.01%. Therefore, the updated model with frequencies of 99.68 Hz for the first mode, 274.68 Hz for the second mode, 533.00 Hz for the third mode, 878.88 Hz for the fourth mode and 1295.5 Hz for the fifth mode is designated as the baseline model. The corresponding material parameter for each specimen is provided in Table 3.7. The baseline parameter identification results for the other specimens are summarized in Appendix C.

3.6 DETERMINATION OF FRACTIONAL STIFFNESS CHANGES IN THE WELD

The fractional stiffness changes in the weld were assessed using the following six steps.

1. Assume that the appropriate baseline model identified in the previous section represents the reference unwelded specimen;
2. Define a single location, k , the same size as the weld, in which the stiffness can change;

3. Generate the k^{th} column of the sensitivity matrix, F_{ik} , for the weld location using the first five bending modes;
4. Assume that the measured modal parameters are associated with the modified system;
5. Compute the fractional eigenvalue changes, z_i ($i = 1, 2, \dots, 5$), using modal parameters defined in Step 1 and Step 4; and
6. Compute the fractional changes in the stiffness at the weld location, using the sensitivity matrix F_{ik} and eigensensitivity z_i .

Note that all entries of F_{ik} are positive, while the z_i 's may be negative, zero, or positive. A positive value of z_i is associated with stiffening while a negative z_i is associated with stiffness loss. It is quite common when using field data for the z_i 's in a single experiment to assume both positive and negative values for various modes. It should also be noted that the relative magnitudes of the sensitivities associated with the individual modes may differ considerably. In the present arrangement, the dominant mode is the first bending mode. The sensitivities of the even modes are orders of magnitude less than the odd modes. This observation led to the choice of one consistent method of estimating damage: use only the dominant first bending mode to estimate damage.

The identified fractional changes in the effective stiffness of the weldment are summarized in Table 3.8. In Table 3.8, negative values indicate that the stiffness of a welded splice is less than the effective stiffness of the corresponding unwelded specimen. Note that the fractional change in effective stiffness is based on the baseline stiffness value of each specimen presented in Table 3.7.

3.7 SUMMARY

The results of modal tests and fractional stiffness changes on twenty seven welded rod specimens were presented. First, the welded specimens were described. Second, the instrumentation, modal test procedures, and modal results were presented. Third, the

generation of specimen baseline models was discussed. Finally, the results of the fractional changes in stiffness of welded specimens were presented.

Table 3.1 Welded Specimen Designation Codes and Lot Sources

Size	#8		#11		#14	
Designation	Code	Lot	Code	Lot	Code	Lot
	BP1	1	BP1	2	BP1	4
	BP2	1	BP2	3	BP2	4
	BP3	1	BP3	2	BP3	4
	PH1	1	PH2	3	PH3	4
	S1	1	S1	2	S1	4
	S2	1	S2	3	S2	4
	S3	1	S3	3	S3	4
	W1	1	W1	2	W1	4
	W2	1	W2	2	W2	4
	Control	1	Control	2	Control	4

Table 3.2 Modal Test Parameters for Reinforcing Rod Specimen Testing

Parameter	Setting	Notes/Units
Accelerometer channels	--	PCB 352A10
Impact head	--	PCB 208A10
Analyzer	--	DSP Technology 20-42
Sample frequency	5000	Hz
Sample length	8192	Samples per channel
Spectral Resolution	1.5625	Hz
Number of repetitions	10	Linear average
Channel gain	Varied	Set to maximize resolution
Trigger method	+ 18% hammer FS	Pre-trigger save all channels
Accelerometer window	Exponential	99% down at end
Hammer window	Rectangular	10% Window width

Table 3.3 Measured Resonant Frequencies

Size	Specimen	Frequencies (Hz)				
		Mode 1	Mode 2	Mode 3	Mode 4	Mode 5
#14	No Weld	124.38	339.38	660.63	1081.3	1595.6
	BP1	124.38	340.00	659.38	1082.5	1594.4
	BP2	118.75	327.50	633.13	1041.3	1528.8
	BP3	121.88	335.63	649.38	1068.8	1569.4
	PH3	121.88	334.38	647.50	1065.0	1565.6
	S1	120.63	330.63	641.88	1052.5	1551.3
	S2	121.88	334.38	649.38	1064.4	1568.8
	S3	122.50	335.63	651.25	1066.9	1573.1
	W1	121.25	332.50	645.00	1058.8	1558.8
	W2	122.50	338.75	654.38	1078.1	1580.6
	Mean*	122.00	334.38	647.92	1064.3	1565.6
COV**	0.0136	0.0115	0.0116	0.0117	0.0118	
#11	No Weld	103.13	283.13	551.88	906.25	1341.9
	BP1	100.00	274.38	532.50	879.38	1295.6
	BP2	100.00	276.25	533.75	883.13	1299.4
	BP3	100.63	276.88	536.88	886.25	1305.0
	PH2	100.63	276.25	535.63	883.75	1302.5
	S1	100.00	276.88	536.25	885.63	1304.4
	S2	100.63	276.88	537.50	886.88	1308.1
	S3	100.63	276.25	536.88	883.75	1306.3
	W1	100.63	277.50	536.25	888.13	1311.9
	W2	103.75	285.63	555.00	912.50	1349.4
	Mean	100.77	277.43	537.85	887.71	1309.2
COV	0.0115	0.0115	0.0123	0.0109	0.0121	
#8	No Weld	74.375	205.63	401.88	662.50	985.00
	BP1	73.125	200.63	389.38	645.00	953.13
	BP2	73.125	200.00	388.75	643.13	952.50
	BP3	78.125	210.00	405.00	674.38	991.25
	PH1	73.750	206.88	398.75	665.00	976.25
	S1	72.500	200.63	390.00	646.88	955.63
	S2	72.500	199.38	388.13	642.50	951.25
	S3	73.125	200.63	390.63	645.63	956.25
	W1	71.875	198.75	384.38	639.38	941.88
	W2	72.500	200.63	388.13	646.25	950.63
	Mean	73.403	201.95	391.46	649.79	958.75
COV	0.0252	0.0189	0.0162	0.0181	0.0159	

* Mean of resonant frequencies for welded specimens

** Coefficient of variation of resonant frequencies for welded specimens

Table 3.4 Initial Values of Material Properties for FE Models

Properties	Value
E (lb/in ²)	30 x 10 ⁶
ρ (lb.s ² /in ⁴)	0.000733

Table 3.5 Stiffness Sensitivity Matrix F for Specimen #11 BP1

Mode	Bar
1	1.0
2	1.0
3	1.0
4	1.0
5	1.0

Table 3.6 System Identification for Specimen #11 BP1

Mode	Frequency of Initial FE model	Updated Frequencies (Hz)			Frequency of Target Structure	Error (%)	
		Iter. 1	Iter. 2	Iter. 3		Initial	Final
1	105.58	99.65	99.68		100.00	5.58	0.32
2	293.53	274.67	274.68		274.38	6.98	0.11
3	562.93	532.81	533.00		532.50	5.71	0.09
4	939.16	878.85	878.88		879.38	6.80	0.06
5	1369.1	1295.0	1295.5		1295.6	5.67	0.01

**Table 3.7 Identified Average Stiffness Parameter (EI)
for Baseline Models**

Welded Specimen		Average Stiffness (EI)
Size	Specimen	(lb-in ²)
#14	BP1	10.698E6
	BP2	10.686E6
	BP3	10.695E6
	PH3	10.750E6
	S1	10.585E6
	S2	10.878E6
	S3	10.951E6
	W1	10.643E6
	W2	10.803E6
#11	BP1	5.097E6
	BP2	5.048 E6
	BP3	5.078 E6
	PH2	5.028 E6
	S1	5.099 E6
	S2	5.029 E6
	S3	5.078 E6
	W1	5.102 E6
	W2	5.096E6
#8	BP1	1.311 E6
	BP2	1.317 E6
	BP3	1.446 E6
	PH1	1.428 E6
	S1	1.313 E6
	S2	1.311 E6
	S3	1.312 E6
	W1	1.307 E6
	W2	1.313E6

Table 3.8 Fractional Changes of the Bending Stiffness for Welded Specimens

Welded Specimen		Fractional Change of Bending Stiffness, α
Size	Specimen	
#14	BP1	0.067
	BP2	-0.052
	BP3	-0.052
	PH3	0.015
	S1	0.013
	S2	-0.004
	S3	0.034
	W1	0.011
	W2	-0.115
#11	BP1	0.082
	BP2	0.012
	BP3	0.055
	PH2	0.092
	S1	-0.061
	S2	0.023
	S3	0.056
	W1	0.008
	W2	0.004
#8	BP1	0.264
	BP2	0.271
	BP3	0.730
	PH1	-0.217
	S1	-0.063
	S2	0.074
	S3	0.146
	W1	0.063
	W2	0.044

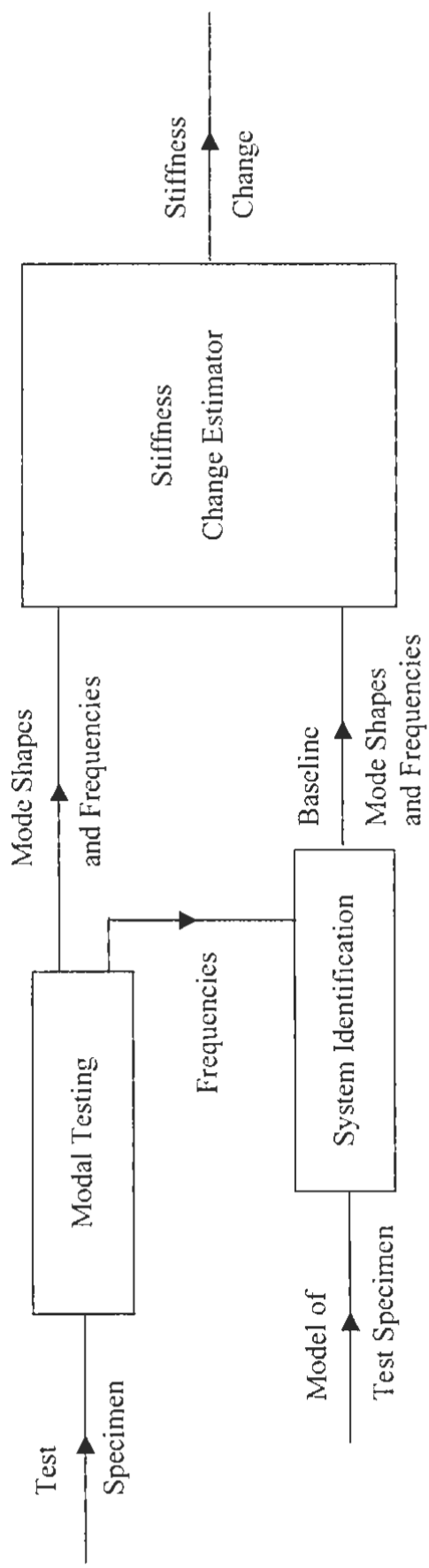


Figure 3.1 Schematic for Estimating Stiffness Change in Weldments

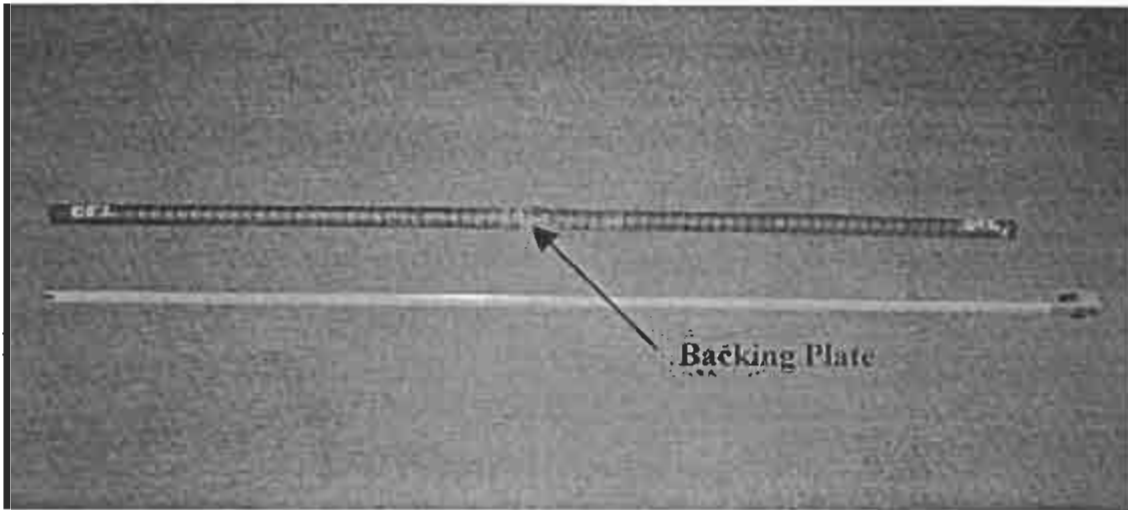


Figure 3.2 A Typical Welded Rod Specimen

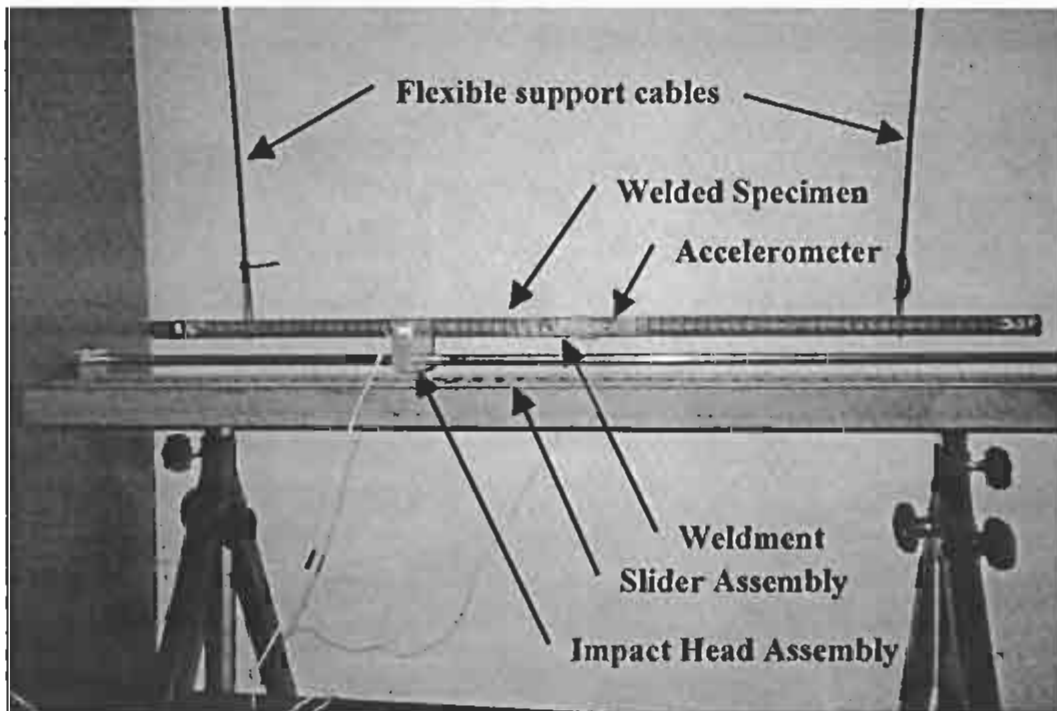


Figure 3.3 Experiment Model Setup with Free-free Boundary.

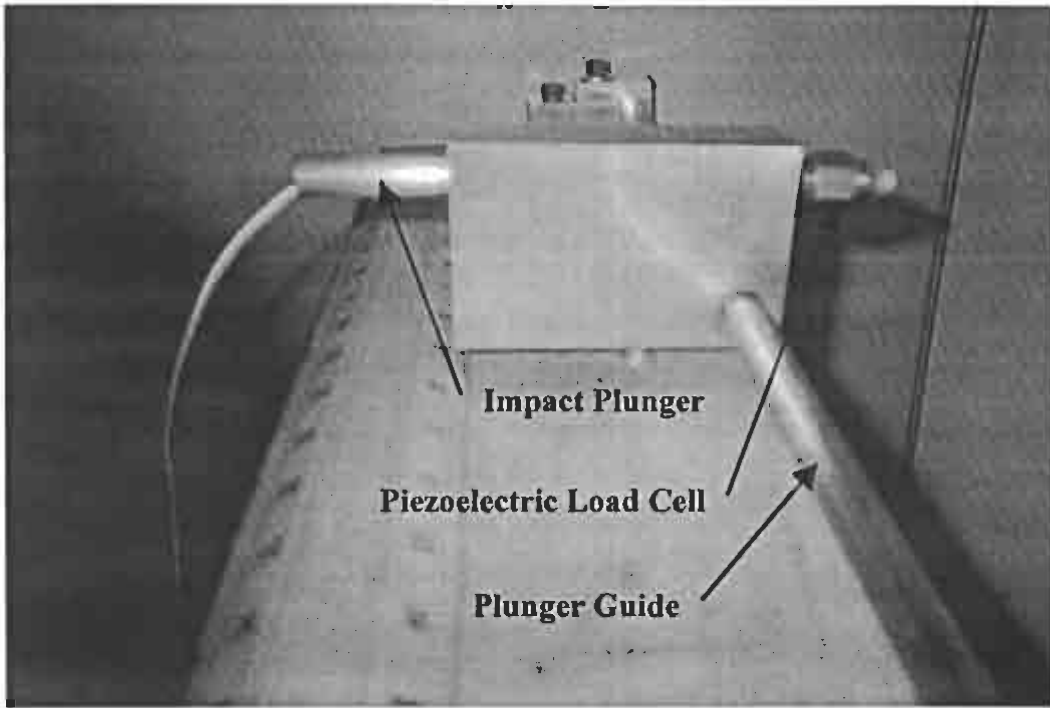
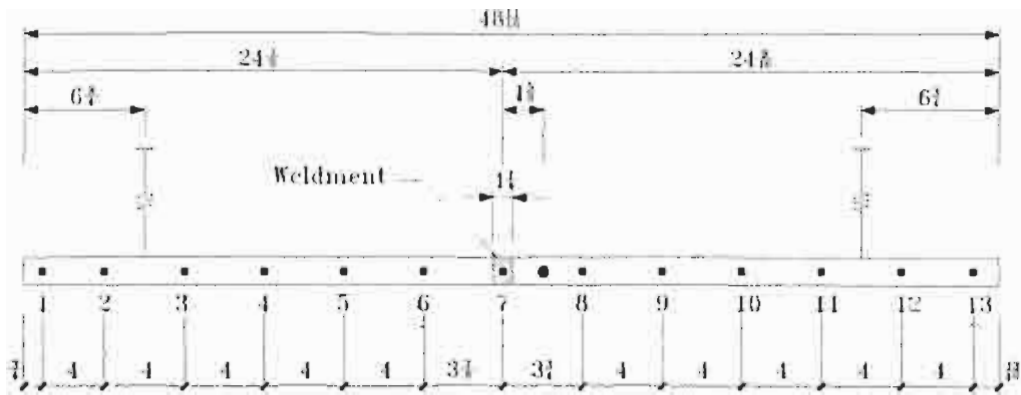


Figure 3.4 Impact Head and Slider Assembly for the Experiment

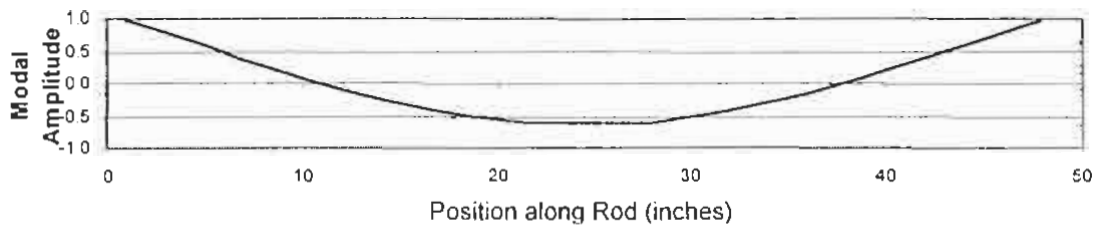


Figure 3.5 Instrumentation for Experimental Modal Testing.

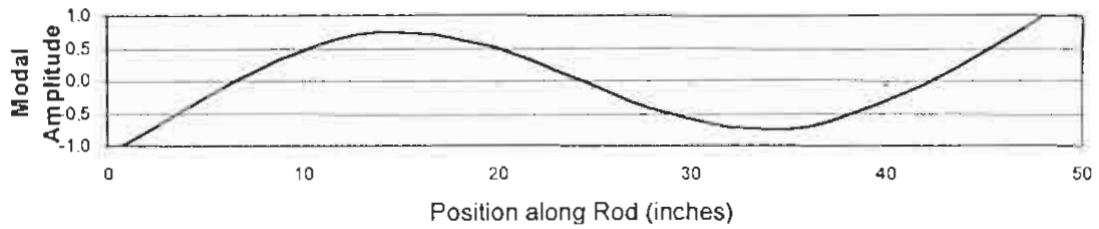


- : accel location
 - : impact locations
- Unit = inch

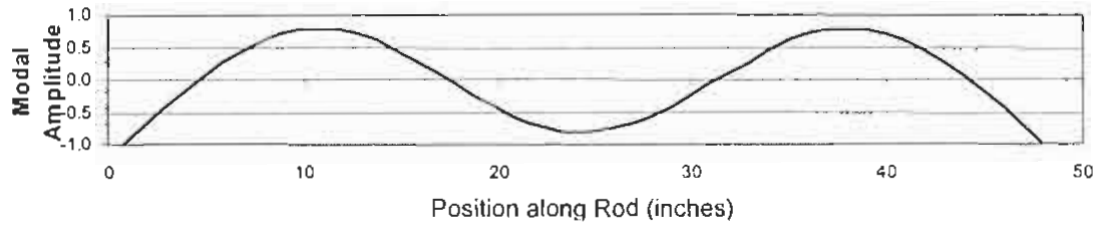
Figure 3.6 A Typical Configuration of Rod Specimen (#11 BP1)



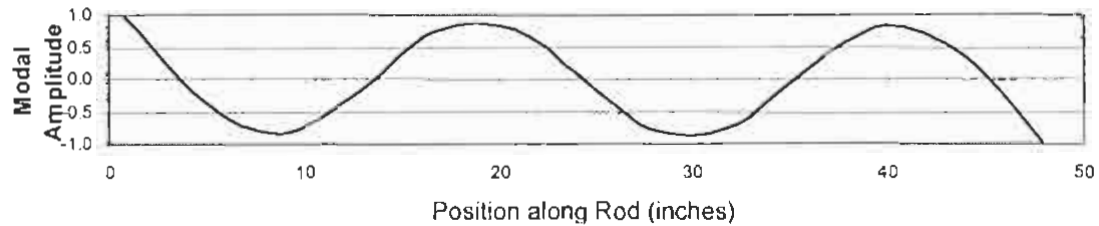
(a) Mode 1



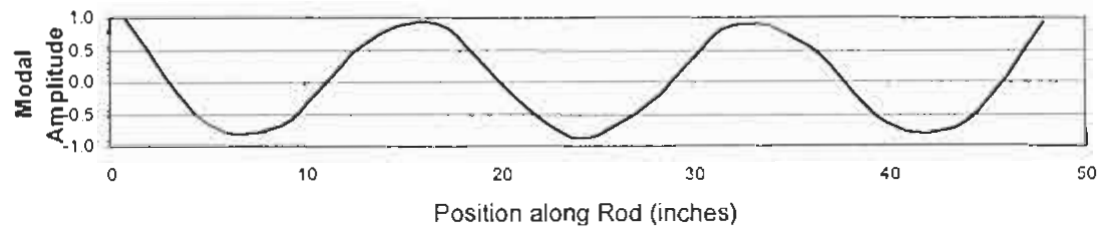
(b) Mode 2



(c) Mode 3

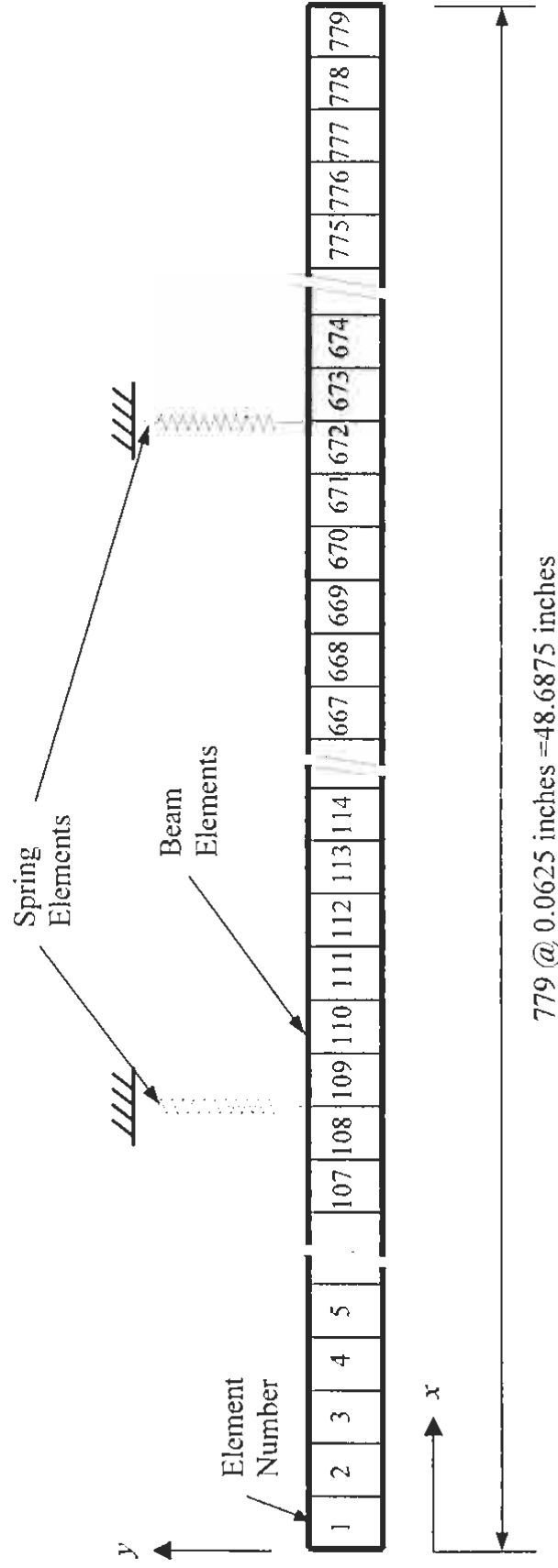


(d) Mode 4



(e) Mode 5

Figure 3.7 Mode Shapes of #11 BP1 Specimen



* Spring elements in x direction are not shown in this figure

Figure 3.8 Schematic of FE Model for #11 BP1 Specimen

4. YIELD STRENGTHS AND TENSILE STRENGTHS OF FIELD PREPARED REINFORCING ROD

4.1 INTRODUCTION

This chapter presents the results of destructive tensile tests performed on the thirty welded reinforcement rod specimens that were discussed in the last chapter. Yield strength and tensile strength results from these specimens will be used in combination with the predicted yield and tensile strengths to evaluate the accuracy of the models proposed in Chapter 2. A description of the specimens is provided in the proceeding chapter. Table 3.1 lists the identification code assigned to each specimen which are referred to in several tables in this chapter.

The object of these tests was to determine selected mechanical properties of each welded specimen. The mechanical properties of interest included the yield strength, tensile strength, breaking strength, Young's modulus, and percent elongation. The remainder of the chapter is organized into the following sections; a description of test facilities and procedures, the results of tensile tests, a discussion of the results relative to several control specimens, and a summary of this project task.

4.2 TEST FACILITIES AND TEST PROCEDURES

The final tests on the thirty welded reinforcement rod specimens were conducted at the Texas Department of Transportation (TxDOT) Materials and Test Laboratory in Austin, Texas. This laboratory is responsible for maintaining the quality of construction materials used in Texas state contracted highway construction. These responsibilities include the measurement of mechanical properties of steel reinforcing rods and the evaluation of various connection technologies.

Tensile tests of the thirty specimens were conducted over the two-day period, spanning 6 April 2000 to 7 April 2000. Destructive tensile tests were conducted in accordance with ASTM Procedures and Standards A370 and A615. The reported data included yield strength, tensile strength, breaking strength, load-displacement plots, and percent

elongation. Percent elongation was calculated using the position of the upper and lower grips at the beginning of the test and at fracture. Young's modulus was also reported for the #8 and the #11 specimens using data from an 8-inch gage length extensometer. The attachment clips of the extensometer could not be adjusted to fit the #14 rods. Thus, measurements of Young's modulus were omitted for the #14 specimen tests.

A 400 Kip Baldwin-Satec testing machine was used for all tests. The distance between the upper and lower grips was 16 inches, with the weld centered between grips. Figure 4.1 shows a typical test of a #11 rod specimen with the extensometer attached. After the application of a touch load to tension the load string, a linear displacement rate of 0.50 in./min. was applied until the specimen yielded. At yield, the extensometer was removed and a higher linear displacement rate of 2.0 in./min. was used until the specimen failed.

4.3 TENSILE TEST RESULTS

Table 4.2 through Table 4.7 list measured mechanical properties for each of the welded specimen. These properties include; yield strength, tensile strength, breaking strength, Young's modulus, total elongation, and percent elongation, respectively. Included in the tables are the average value and standard deviation, by rod size, for each measured mechanical property. The original test data sheets prepared by TxDOT for the tensile tests are located in Appendix D.

4.4 DISCUSSION OF TENSILE TEST RESULTS

All welded specimens failed in or very near the welded connection. Unwelded control specimens failed near one of the grips. Several specimens exhibited significant bending at the welded joint. These specimens are identified in Table 4.1. Specimen failures generally occurred in the weld perpendicular to the longitudinal axis of the specimen. Figure 4.2 presents the end and side view of the #11 control specimen failure surface. Necking of the specimen is apparent in the side view of the specimen near the failure surface. Figure 4.3 presents a similar end and side view of the #11 BP-2 specimen. The

specimen exhibited a perpendicular failure through the weld (i.e., the typical failure mode noted above). Several specimens, particularly the #8 rod specimens, had angular failures along the beveled fusion line between the weld and base material. Figure 4.4 presents two views of this failure mode for the #8 S-1 specimen. Visible necking was not apparent in welded specimens. A review of the data in Table 4.2 through Table 4.7 indicates that the effect of bending in the specimens listed in Table 4.1 did not have a significant impact on measured mechanical properties. A single exception to this observation may be the fact that the #11 BP3 specimen has a relatively low Young's Modulus of 23,200 ksi.

In general, welded specimens exhibited somewhat lower strength properties than the unwelded control specimen of the same size. Yield strengths of the welded specimens were 6% lower on average than those of the control specimens. Specimen yield strength varied across rod sizes. The #14 specimens exhibited a higher overall yield strength (approximately 5 ksi higher), relative to the #8 and the #11 specimens.

Tensile strengths in the welded specimens were 21% lower, on average, than the corresponding control specimens. No significant trends were noted in regard to rod size, as was found in the yield strength data. The computed Young's modulus for the #8 and the #11 specimens did not show significant variation with respect to their respective control specimens. Percent elongation showed a 60% reduction, on average, for the welded specimens compared to the control specimens.

4.5 SUMMARY

Tensile tests were conducted on thirty 48-inch welded reinforcing rod specimens at the TxDOT Materials and Tests Laboratory in Austin, TX. The thirty-specimen set was divided into three 10-specimen subsets consisting of #8, #11, and #14 reinforcing rod sizes. An unwelded control specimen was included in each subset. Reported mechanical properties included yield strength, tensile strength, breaking strength, Young's modulus, total elongation, and percent elongation. Overall, the welded specimens exhibited

somewhat lower overall strength properties, minimal change in elastic modulus, and decreased ductility relative to the control specimens of the same size.

Table 4.1 Code of Bent Reinforcing Rod Specimens

<i>Size</i>		
<i>#8</i>	<i>#11</i>	<i>#14</i>
BP2	BP3	BP1
BP3	PH2	
PH1		

Table 4.2 Yield Strength of Reinforcing Rod Specimens

Code	Size		
	#8 (psi)	#11 (psi)	#14 (psi)
BP1	63,933	60,258	73,698
BP2	64,276	61,517	73,434
BP3	64,086	*59,600	69,118
PH1	64,527	N/A	N/A
PH2	N/A	70,190	N/A
PH3	N/A	N/A	69,491
S1	64,113	59,855	73,720
S2	64,732	70,583	69,463
S3	64,291	71,252	69,587
W1	62,751	57,433	*73,300
W2	62,673	59,752	69,160
Mean	63,931	63,382	71,219
STD	731	5,575	2,209
Unwelded	65,800	71,400	73,400

* Computed from load-displacement curve

Table 4.3 Tensile Strength of Reinforcing Rod Specimens

Code	Size		
	#8 (psi)	#11 (psi)	#14 (psi)
BP1	87,808	85,732	80,812
BP2	90,595	78,532	81,587
BP3	82,809	85,159	83,196
PH1	94,802	N/A	N/A
PH2	N/A	96,705	N/A
PH3	N/A	N/A	90,481
S1	86,241	84,410	90,353
S2	89,094	85,781	87,931
S3	94,687	84,855	88,442
W1	82,967	67,923	79,444
W2	79,191	81,422	78,240
Mean	87,577	83,391	84,498
STD	5,366	7,595	4,820
Unwelded	106,300	109,900	106,100

Table 4.4 Breaking Strength of Reinforcing Rod Specimens

Code	Size		
	#8 (psi)	#11 (psi)	#14 (psi)
BP1	87,500	*	80,800
BP2	88,100	*	81,600
BP3	80,200	*	83,200
PH1	92,000	N/A	N/A
PH2	N/A	*	N/A
PH3	N/A	N/A	89,300
S1	79,000	*	90,100
S2	85,700	85,800	87,600
S3	94,700	85,000	86,200
W1	78,900	*	77,500
W2	47,300	63,400	73,800
Mean	81,500	78,000	83,300
STD	14,000	**	5,500
Unwelded	96,900	*	71,800

* Not recorded

** Not computed

Table 4.5 Young's Modulus of Reinforcing Rod Specimens

Code	Size		
	#8 (ksi)	#11 (ksi)	#14 (ksi)
BP1	28,300	26,900	*
BP2	28,600	26,300	*
BP3	26,400	23,200	*
PH1	*	N/A	N/A
PH2	N/A	27,800	N/A
PH3	N/A	N/A	*
S1	26,800	25,800	*
S2	28,200	27,500	*
S3	27,500	27,700	*
W1	26,500	26,000	*
W2	27,100	27,100	*
Mean	27,400	26,500	
STD	900	1,400	
Unwelded	27,500	27,400	*

* Not recorded

Table 4.6 Total Grip Displacement for Reinforcing Rod Specimens

Code	Size		
	#8 (inches)	#11 (inches)	#14 (inches)
BP1	1.41	2.50	1.69
BP2	1.51	1.38	1.83
BP3	1.14	2.50	2.56
PH1	1.47	N/A	N/A
PH2	N/A	2.25	N/A
PH3	N/A	N/A	3.30
S1	1.28	2.25	2.25
S2	1.45	1.63	2.91
S3	1.69	1.94	2.13
W1	1.30	1.00	1.93
W2	1.12	1.88	2.31
Mean	1.37	1.92	2.32
STD	0.18	0.51	0.52
Unwelded	3.78	5.50	4.76

Table 4.7 Percent Elongation of Reinforcing Rod Specimens

Code	Size		
	#8 (%)	#11 (%)	#14 (%)
BP1	8.8	15.6	10.5
BP2	9.4	8.6	11.4
BP3	7.1	15.6	16.0
PH1	9.2	N/A	N/A
PH2	N/A	14.1	N/A
PH3	N/A	N/A	20.6
S1	8.0	14.1	14.1
S2	9.1	10.2	18.2
S3	10.5	12.1	13.3
W1	8.1	6.3	12.1
W2	7.0	11.8	14.4
Mean	8.6	12.0	14.5
STD	1.1	3.2	3.3
Unwelded	23.6	34.4	29.8

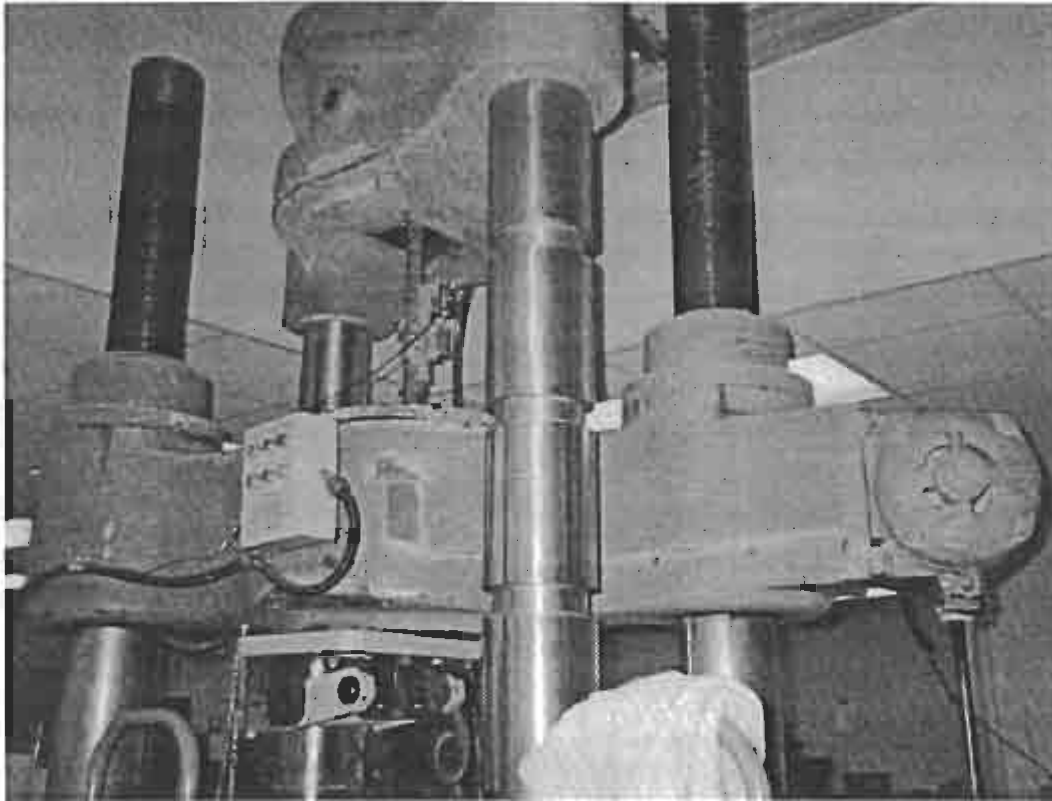


Figure 4.1 Tensile Test of #11 Welded Reinforcement Rod Specimen.

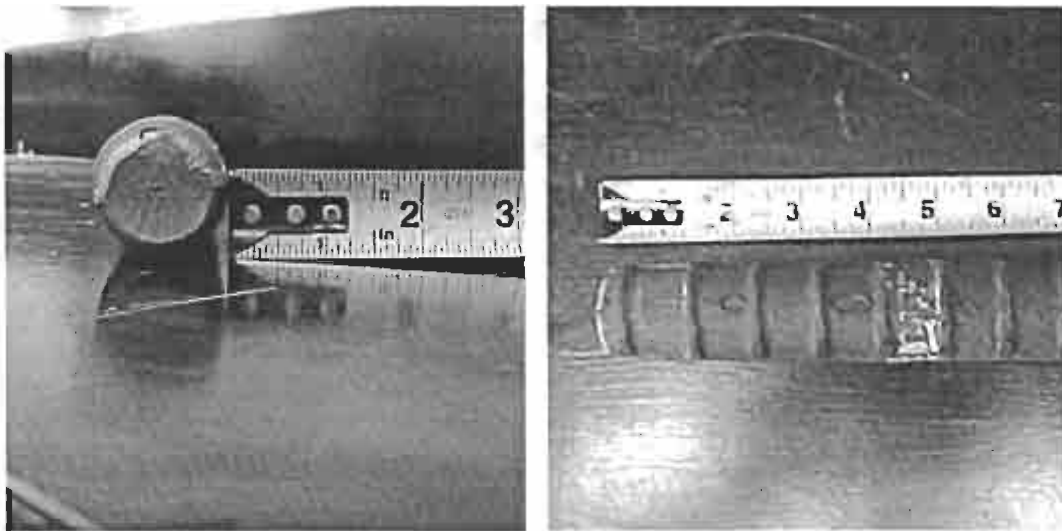


Figure 4.2 End and Side View of Failed #11 Control Specimen.

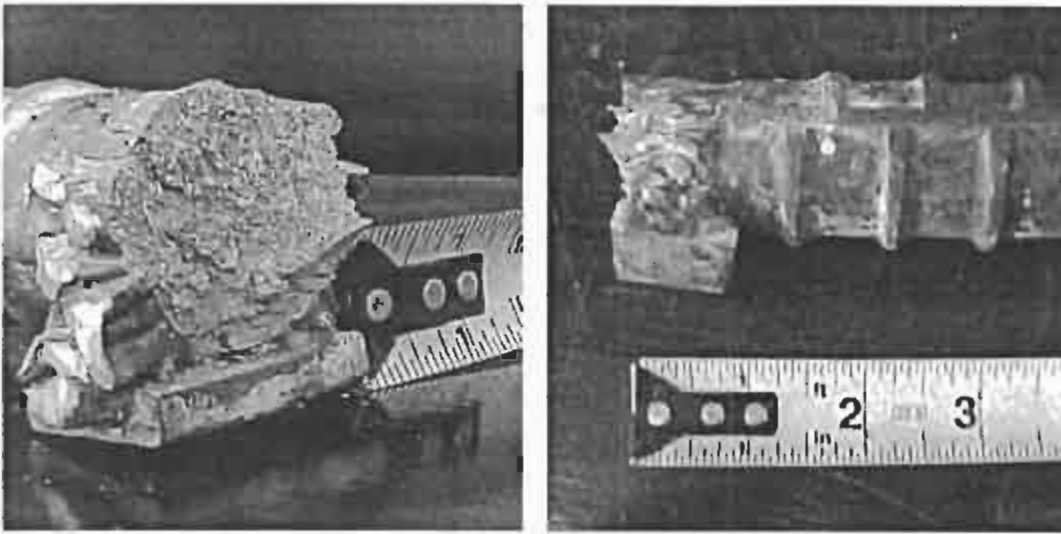


Figure 4.3 End and Side View of Failed #11 BP2 Specimen.

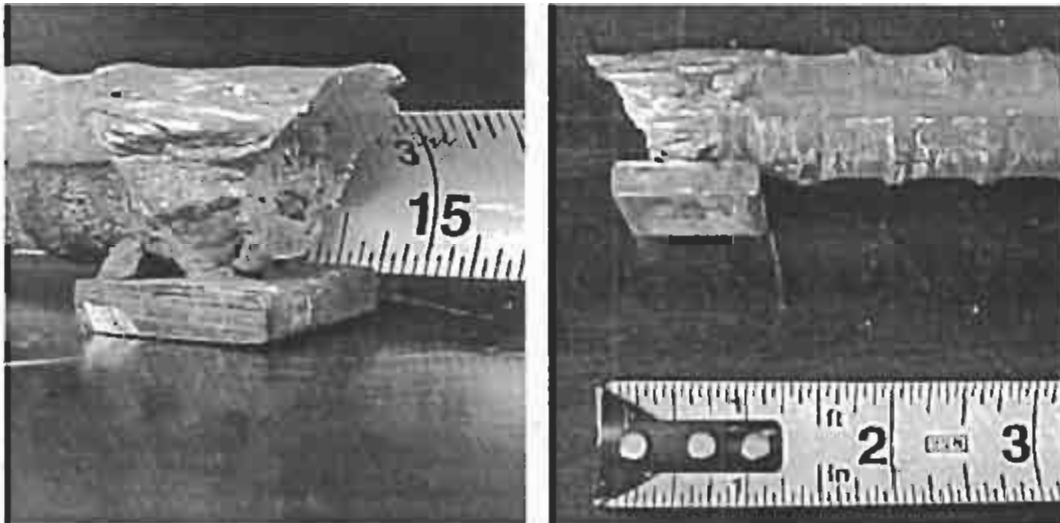


Figure 4.4 End and Side View of Failed #8 S1 Specimen.

5. COMPARISON BETWEEN MEASURED WELD CAPACITY AND PREDICTED WELD CAPACITY

5.1 INTRODUCTION

In Chapter 2, expressions for the capacity of a weld were developed using limit state concepts and Continuum Damage Mechanics. Depending upon the interpretation of damage, both approaches yielded the same result. In Chapter 3, fractional stiffness changes of the welded region relative to the unwelded rod were nondestructively measured for the twenty-seven specimens. In Chapter 4, the same set of specimens in addition to three controlled specimens (one for each rod size) were tested to failure and various mechanical properties, which included yield strength and tensile strength, were measured for welded and unwelded specimens. A welded system consists of the weld, the rod, and the interfaces between the weld and the rod. The objective of this chapter is to compare the predicted magnitudes of the capacity of a weld-rod system with the measured values for the system. System capacity is determined in terms of the yield strengths of the weld and the rod, the loads that correspond to yield, and the tensile strengths of the weld and the rod. In the remaining portions of this chapter, the equations and the parameters used to estimate weld capacities are identified, a simple failure model of the rod-weld-interface system summarized, the results of the comparison summarized, and the results discussed.

5.2 COMPUTING THE PREDICTED WELD CAPACITY

The equations to predict the yield strength, σ_{Dy} , and the load corresponding to the yield strength, P_{Dy} , are given by Equations (2.6) and (2.5). For convenience, here we will refer to the load at yield as the yield load. The values of the stiffness changes, α , are provided in Table 3.8. Note that the stiffness changes are based on the estimate using only the first bending mode. The value of σ_y used in this exercise is $\sigma_y = 67$ Ksi, since E8018-C3 electrodes were used in the welding process (See ANSI/AWS D1.4, 1992). The value of P_{Uy} in Equation (2.5) is obtained using the equation $P_{Uy} = \sigma_y A_n$, where A_n is the nominal area of the reinforcing rod. The nominal areas taken here for the #8, #11, and #14 rods are, respectively 0.79 in.^2 , 1.56 in.^2 , and 2.25 in.^2 . The predicted weld capacity for the

tensile strength and the load in the rod at the tensile strength are provided by Equations (2.8) and (2.7), respectively. The value of σ_T for the E8018-C3 electrode is taken as 80 Ksi. (Sec ANSI/AWS D1.4, 1992). The load P_{UT} (i.e., the ultimate load) in Equation (2.7) is calculated using the equation $P_{UT} = \sigma_T A_n$.

5.3 FAILURE MODEL OF THE WELD-ROD SYSTEM

The system being evaluated in this study consists of the rod comprising the base metal, the weld itself, and the interface between the weld and the base metal. When subjected to an axial load, the system will fail when any one of the elements (i.e., the rod, weld, or interface) comprising the system fails. Since the system described here is a weakest link (Series) system, the predicted strength of the system is the strength of the weakest element. Note that the yield strength and tensile strength for unwelded #8, #11, and #14 control rods are provided in Table 4.2 and Table 4.3. In summary, the predicted yield strength and tensile strength of the rod-weld system are given by:

$$\sigma_{y(\text{system})} = \text{Min} \{ \sigma_{y(\text{rod})}, \sigma_{y(\text{weld})}, \sigma_{(\text{interface})} \} \quad (5.1)$$

$$\sigma_{T(\text{system})} = \text{Min} \{ \sigma_{T(\text{rod})}, \sigma_{T(\text{weld})}, \sigma_{T(\text{interface})} \} \quad (5.2)$$

Because we have no information on the strength properties of the weld-base metal interface, it will be assumed that the yield strength and the tensile strength of the interface are equal to the yield strength and tensile strength of the filler material.

5.4 RESULTS OF THE COMPARISON BETWEEN THE PREDICTED AND MEASURED WELD CAPACITIES

The predicted and measured weld capacities using the values for the fractional stiffnesses computed on the basis of the first bending mode only are listed in Table 5.1 to Table 5.4. Table 5.1 summarizes the comparison between the measured yield strengths described in the last chapter and the predicted yield strength using Equation (2.6). Note that in order to predict the yield strengths in the table, only the nominal yield strength of the E8018-C3

electrode and the estimated fractional stiffness change based on the first bending mode were utilized. To provide an indication of the accuracy of the prediction of the yield strength, the deviation between the measured yield strength and the predicted yield strength is provided in the last two columns of the table. Note also that the mean and standard deviation of the percentage error between the predicted and the measured values is provided for each rod size as well as for the entire test sample. Cases in which the failure of the weld did not control the failure of the system are indicated in the table. The results in Table 5.1 are presented graphically in Figure 5.1. Note that a line of unit slope has been included in the figure, to aid in the interpretation of the accuracy of the results. Table 5.2 summarizes the comparison of the measured and predicted yield load (see Equation (2.5)). Whereas the “measured” load was obtained directly from the test, the predicted load uses the nominal area of the reinforcing rod along with the predicted yield strength. Statistics, similar to those presented in Table 5.1, on the accuracy of prediction are also provided in Table 5.2. A graphical description of the numerical results presented in Table 5.2 is presented in Figure 5.2. Table 5.3 and Table 5.4 present comparisons of the predicted tensile strength and the predicted ultimate load using Equation (2.8) and Equation (2.9), respectively. The corresponding information is presented graphically in Figure 5.3 and Figure 5.4. Note again that the predictions presented in Table 5.1 to Table 5.4 are based on the estimate of stiffness change using the first bending mode.

The results of the laboratory tests, predictions of the proposed method and the assessment based on the dye penetrant and x-ray evidence were also compared in another fashion. First, the welding expert was asked to select the welds that were considered acceptable. The following welds were designated as acceptable. Specimens BP1, BP2, and PH3 for the #14 size rods; Specimens BP1, BP3, and S1 for the #11 size rods; and Specimens BP, BP2, and BP3 for the #8 size rods. The remaining 18 specimens were rejected (see Table E.1). Second, the laboratory results presented in the second column of Table 5.1 were used to evaluate the quality of the weld systems. If the measured yield strength was equal to or greater than 60 Ksi, the weld was accepted; if the measured yield strength was less than 60 Ksi, the weld was rejected. One specimen, Specimen W1 of the #11 size rods, was rejected. All other 26 specimens were accepted. Third, the yield strengths predicted using the method proposed here was used as a basis for determining

the acceptability of the welds. If the predicted yield strength was greater than or equal to 60 Ksi, the weld was accepted. If the yield strength was less than 60 Ksi, the weld was rejected. Again one specimen, Specimen PH1 of the #8 rods, was rejected. These results are listed in Table 5.5. If the measure of quality of the welds defined on the basis of laboratory tests is taken as the true measure of the quality, the proposed approach and the traditional NDE approaches can be compared more quantitatively. Out of a total of 27 specimens, the proposed approach accepted one weld that should have been rejected (#11 W1) and rejected one weld that should have been accepted (#8 Ph1). For the same 27 specimens, the traditional NDE approach rejected 17 specimens that should have been accepted.

5.5 DISCUSSION OF RESULTS

Given the results presented in the last section, in this portion of the chapter, the following four issues will be discussed: (1) how to interpret the results, (2) the accuracy of the results, (3) areas for potential improvement in the accuracy of the predictions and (4) field implementation of the methodology.

5.5.1 Interpretation of the Results

In the common methods of NDE, the location and geometry of a flaw, or a system of flaws, is detected by some means and the impact of the flaw on the performance of the structural element evaluated. The evaluation may be qualitative, as in the case of the Dye Penetrant Method, or quantitative, as in the case of the Ultrasonic-Fracture Mechanics combination. As noted earlier, the use of fracture mechanics is limited if the flaw distribution and geometry are complex. The approach proposed here attempts to provide the nondestructive evaluation of a system with complex distributive damage such as that found in welds. The inputs to the method are the tensile strength and yield strength of the filler material and the base metal, the nominal area of the member, and a nondestructive measure of the fractional stiffness change in the weld relative to the undamaged rod. The output of the method is a prediction of the resisting capacity of the weld system. Whether the system is adequate or inadequate depends upon the load demand in a specific application. In Table 5.5 an evaluation based on the system with resisting yield

strength equal to or greater than 60 Ksi was presented. If a weld system is evaluated using the method presented here, the information passed on to the designer is an estimate of the resistance of the system in terms of its yield strength and tensile strength.

5.5.2 Accuracy of the Results

The measures of accuracy utilized in this report are the magnitude of deviation and the percent deviation of the predicted capacity from the measured capacity. As noted above, here capacity is measured in terms of yield strength, yield load, tensile strength, and ultimate load of the system. If one considers the predictions based on stiffness changes using only the first bending mode, as shown in Table 5.1, the mean deviation percent error of the predictions for all specimens is 0.77%. The smallest mean deviation percent error (0.11%) coincides with the #8 rods, while the largest mean deviation percent error (8.97%) resides with the #14 rods. Since the yield load is related to the yield stress through the nominal area of the rod, the error distribution for the predicted yield load, in terms of percent error of the deviation, is identical to the error distribution of the yield strength. Figure 5.1 and Figure 5.2 indicate that the predicted and measured yield strength and yield load tend to cluster around the line of unit slope. Again, on considering the predictions based on stiffness changes using only the first bending mode, as shown in Table 5.3 and 5.4, the mean deviation percent error of the predictions of the tensile strength and the ultimate load for all specimens is -1.84%. The smallest mean deviation percent error (-0.57%) coincides with the #11 rods; while the largest mean deviation error (-6.04%) resides with the #11 rods. Figure 5.3 and Figure 5.4 indicate that the predicted and measured yield strength and yield load tend to cluster around the line of unit slope.

5.5.3 Areas for Potential Improvement in the Predictions

Even though the methodology proposed here to predict the capacity of a weld-rod system is quite good, there are still many areas for potential improvement in the accuracy of the predictions. Three obvious areas include the following: (1) improving the strength-damage models, (2) accounting for uncertainties in the parameters used to predict the

strength, and (3) reducing errors associated with experimental measurements and stiffness change determination.

The strength-damage model for weld systems can be improved or refined in several ways. First, the model may be extended to include the strength properties of the interface and/or changes in the properties of the base metal in the heat affected zone. Second, the impact of the incremental damage incurred during loading on the strength may be considered. Finally, the irregular geometry in the weld zone and the impact of the mass due to the weld and the backing can be included in the analysis.

The equations used in this study assumed that all of the parameters used in this study, such as yield strengths, tensile strengths, and nominal areas, are deterministic. In reality these variables are random variables. Thus, the model can be significantly improved by treating the parameters as random variables. To accomplish this task, statistical descriptions of the parameters of interest must be developed.

For scientific reasons, the dynamic testing portion of this study involved a weld reinforcing rod system that had precisely defined boundary conditions; namely, free-free boundary conditions. Such ideal conditions are unlikely to be encountered in the field. Measurement of modal parameters must be accomplished for systems with more complicated boundary conditions and system identification procedures must be extended to account for the variable boundary conditions. The system identification technique used in this work is capable of identifying such variable boundary conditions. The capability to deal with more complicated boundary conditions is key to extending the technique to the field. The technique forms the basis of a prototype apparatus, to be described below, for the evaluation of weld capacity in the field.

5.5.4 Field Implementation of the Methodology

The method demonstrated in this study can be implemented in two phases. The objective of the first phase would be to nondestructively measure the stiffness changes of the welded region in the field. To accomplish this objective several subobjectives would

have to be accomplished. First, a clamping device that could isolate the weld from the rest of the structure has to be designed, fabricated, and field-tested. Such a device is needed so that only a small part of the structure is dynamically excited. Second, in the field testing phase, the capability of exciting the region around the weld and extracting local modal parameters must be demonstrated. In a laboratory setting, modal parameters can be extract quite rapidly using the method referred to as “peak picking.” The modal parameter reported in Appendix C were determined using peak picking. Third, a system identification, which is robust to variable boundary conditions, must be made of the weld-clamp system, using the field-derived modal parameters. Finally, either using mode shapes or frequency changes, the stiffness changes at the weld location must be determined.

The objective of the second phase would be to predict the weld capacity using Equations (2.5), (2.6), (2.7), (2.8), (5.1) and (5.2). This task would entail knowing the appropriate strength properties of the rod and the electrodes utilized as well as the rod sizes.

A prototype of such a clamping device to isolate the weld from the surrounding structure is shown in Figure 5.6. The device is essentially an extension of the free-free beam described in Chapter 3. Here clamps are ideally rigidly attached to a very stiff beam with bending rigidity very large compared to the bending rigidity of the reinforcing rod. A span of the rod containing the weld is clamped creating something close to a fixed-fixed beam. Modal testing is performed on the section in the usual way and the subsequent analysis based on the local vibrational modes. The model to be identified using systems identification is shown in Figure 5.7. In the figure note that the clamp is modeled as a combination of torsional and axial springs. The stiffness of the springs inturn depend upon the rotational rigidity of the clamp, which may differ from end to end, and the magnitude of the clamping force. Variations in boundary conditions may be reduced by tightening the clamps with a torque wrench. The additional equipment needed to perform the test is shown in Figure 3.5. Space and weight requirement are minimal, except for the clamping device that may weigh 60 to 80 pounds.

5.5 SUMMARY

The objective of this chapter was to compare the predicted magnitudes of the capacity of a weld-rod system with the measured values of the system. The capacity of the system was expressed in terms of the yield strength, yield load, tensile strength, and ultimate load of the weld-rod system. The equations and parameters used to predict the capacity of the weld were summarized, failure models for the weld-rod system were proposed, and the results of the comparison between the predicted and measured results for twenty-seven specimens were described. Finally, the results were discussed with respect to (1) how they should be interpreted, (2) the accuracy of the predictions, (3) areas for potential improvements in the accuracy of the predictions, and (4) the implementation of the methodology in the field.

Table 5.1 Comparison of Predicted and Measured Yield Strength Using Stiffness Changes Based on First Bending Mode

Rod Designation	Yield Strength (psi)		Error (%)	Deviation	
	Measured	*Predicted			
#14	BP1	73698	71489	-3.00	-2209
	BP2	73434	63516	-13.51	-9918
	BP3	69118	63516	-8.10	-5602
	PH3	69491	68005	-2.14	-1486
	S1	73720	67871	-7.93	-5849
	S2	69463	66732	-3.93	-2731
	S3	69587	69278	-0.44	-309
	W1	73300	67737	-7.59	-5563
	W2	69160	59295	-14.26	-9865
	Mean (Standard Deviation)			-6.77 (4.86)	-4837 (3470)
#11	BP1	60258	**71400	18.49	11142
	BP2	61517	67804	10.22	6287
	BP3	59600	70685	18.60	11085
	PH2	70190	**71400	1.72	1210
	S1	59855	62913	5.11	3058
	S2	70583	68541	-2.89	-2042
	S3	71252	70752	-0.70	-500
	W1	57433	67536	17.59	10103
	W2	59752	67268	12.58	7516
	Mean (Standard Deviation)			8.97 (8.47)	5318 (5073)
#8	BP1	63933	**65800	2.92	1867
	BP2	64276	**65800	2.37	1524
	BP3	64086	**65800	2.67	1714
	PH1	64527	52461	-18.70	-12066
	S1	64113	62779	-2.08	-1334
	S2	64732	**65800	1.65	1068
	S3	64291	**65800	2.35	1509
	W1	62751	**65800	4.86	3049
	W2	62673	**65800	4.99	3127
	Mean (Standard Deviation)			0.11 (7.35)	51 (4725)
Mean			0.77	177	
Standard Deviation			9.44	6029	

* Assuming properties of Electrode E8018-C3

** Rod Controlled

Table 5.2 Comparison of Predicted and Measured Yield Load Using Stiffness Changes Based on First Bending Mode

Rod Designation	Yield Load (lb)		Error (%)	Deviation	
	Measured	Predicted*			
#14	BP1	165820	160850	-3.00	-4970
	BP2	165230	142911	-13.51	-22319
	BP3	155510	142911	-8.10	-12599
	PH3	156350	153011	-2.14	-3339
	S1	165870	152710	-7.93	-13160
	S2	156290	150147	-3.93	-6143
	S3	156570	155876	-0.44	-694
	W1	164925	152408	-7.59	-12517
	W2	155610	133414	-14.26	-22196
	Mean (Standard Deviation)			-6.77 (4.86)	-10882 (7808)
#11	BP1	94002	**111384	18.49	17382
	BP2	95966	105774	10.22	9808
	BP3	92976	110269	18.60	17293
	PH2	109500	**111384	1.72	1884
	S1	93374	98144	5.11	4770
	S2	110110	106924	-2.89	-3186
	S3	111150	110373	-0.70	-777
	W1	89595	105356	17.59	15761
	W2	93212	104938	12.58	11726
	Mean (Standard Deviation)			8.97 (8.47)	8296 (7913)
#8	BP1	50507	**51982	2.92	1475
	BP2	50778	**51982	2.37	1204
	BP3	50628	**51982	2.67	1354
	PH1	50976	41444	-18.70	-9532
	S1	50650	49595	-2.08	-1055
	S2	51139	**51982	1.65	843
	S3	50790	**51982	2.35	1192
	W1	49573	**51982	4.86	2409
	W2	49511	**51982	4.99	2471
	Mean (Standard Deviation)			0.11 (7.35)	40 (3733)
Mean			0.77	-849	
Standard Deviation			9.44	10314	

* Assuming properties of Electrode E8018-C3

** Rod Controlled

Table 5.3 Comparison of Predicted and Measured Tensile Strength Using Stiffness Changes Based on First Bending Mode

Rod Designation	Tensile Strength (psi)		Error (%)	Deviation
	Measured	Predicted*		
#14				
BP1	80812	85360	5.63	4548
BP2	81587	75840	-7.04	-5747
BP3	83196	75840	-8.84	-7356
PH3	90481	81200	-10.26	-9281
S1	90353	81040	-10.31	-9313
S2	87931	79680	-9.38	-8251
S3	88442	82720	-6.47	-5722
W1	79444	80880	1.81	1436
W2	78240	70800	-9.51	-7440
Mean (Standard Deviation)			-6.04 (5.77)	-5236 (4901)
#11				
BP1	85732	86560	0.97	828
BP2	78532	80960	3.09	2428
BP3	85159	84400	-0.89	-759
PH2	96705	87360	-9.66	-9345
S1	84410	75120	-11.01	-9290
S2	85781	81840	-4.59	-3941
S3	84855	84480	-0.44	-375
W1	67923	80640	18.72	12717
W2	81422	80320	-1.35	-1102
Mean (Standard Deviation)			-0.57 (8.63)	-982 (6621)
#8				
BP1	87808	101120	15.16	13312
BP2	90595	101680	12.24	11085
BP3	82809	**106300	28.37	23491
PH1	94802	62640	-33.93	-32162
S1	86241	74960	-13.08	-11281
S2	89094	85920	-3.56	-3174
S3	94687	91680	-3.18	-3007
W1	82967	85040	2.50	2073
W2	79191	83520	5.47	4329
Mean (Standard Deviation)			1.11 (17.87)	518 (16021)
Mean			-1.84	-1900
Standard Deviation			11.88	10297

* Assuming properties of Electrode E8018-C3

** Rod Controlled

Table 5.4 Comparison of Predicted and Measured Ultimate Load Using Stiffness Changes Based on First Bending Mode

Rod Designation	Ultimate Load (lb)		Error (%)	Deviation
	Measured	Predicted*		
#14				
BP1	181830	192060	5.63	10230
BP2	183570	170640	-7.04	-12930
BP3	187190	170640	-8.84	-16550
PH3	203580	182700	-10.26	-20880
S1	203290	182340	-10.31	-20950
S2	197840	179280	-9.38	-18560
S3	198990	186120	-6.47	-12870
W1	178750	181980	1.81	3230
W2	176040	159300	-9.51	-16740
Mean (Standard Deviation)			-6.04 (5.77)	-11780 (11025)
#11				
BP1	133740	135034	0.97	1294
BP2	122510	126298	3.09	3788
BP3	132850	131664	-0.89	-1186
PH2	150860	136282	-9.66	-14578
S1	131680	117187	-11.01	-14493
S2	133820	127670	-4.60	-6150
S3	132370	131789	-0.44	-581
W1	105960	125798	18.72	19838
W2	127020	125299	-1.35	-1721
Mean (Standard Deviation)			-0.57 (8.64)	-1532 (10329)
#8				
BP1	69368	79885	15.16	10517
BP2	71570	80327	12.24	8757
BP3	65419	**83977	28.37	18558
PH1	74894	49486	-35.93	-25408
S1	68130	59218	-13.08	-8912
S2	70384	67877	-3.56	-2507
S3	74803	72427	-3.18	-2376
W1	65544	67182	2.50	1638
W2	62561	65981	5.47	3420
Mean (Standard Deviation)			1.11 (17.87)	410 (12656)
Mean			-1.84	-4301
Standard Deviation			11.88	12215

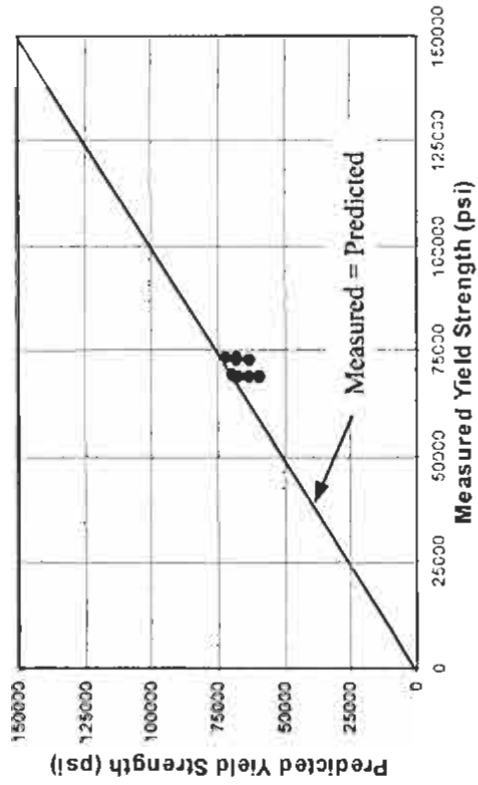
* Assuming properties of Electrode E8018-C3

** Rod Controlled

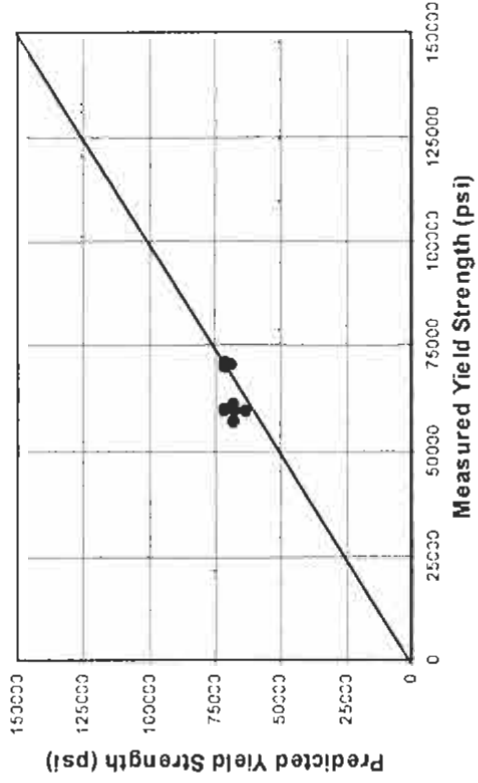
Table 5.5 Comparison of Proposed Approach and Qualitative Approach with Laboratory Tests

ROD DESIGNATION	BASIS OF JUDGEMENT			DYE PENETRANT RADIOGRAPHY***	
	LABORATORY TESTS	PROPOSED APPROACH			
#14	BP1	Accept	Accept	Accept	
	BP2	Accept	Accept	Accept	
	BP3	Accept	Accept	Reject	
	PH3	Accept	Accept	Accept	
	S1	Accept	Accept	Reject	
	S2	Accept	Accept	Reject	
	S3	Accept	Accept	Reject	
	W1	Accept	Accept	Reject	
	W2	Accept	Borderline	Reject	
	#11	BP1	Accept	Accept	Accept
		BP2	Accept	Accept	Reject
		BP3	Borderline	Accept	Accept
		PH2	Accept	Accept	Reject
		S1	Borderline	Accept	Accept
S2		Accept	Accept	Reject	
S3		Accept	Accept	Reject	
W1		Reject	Accept	Reject	
W2		Borderline	Accept	Reject	
#8		BP1	Accept	Accept	Accept
		BP2	Accept	Accept	Accept
		BP3	Accept	Accept	Accept
		PH1	Accept	Reject	Reject
		S1	Accept	Accept	Reject
	S2	Accept	Accept	Reject	
	S3	Accept	Accept	Reject	
	W1	Accept	Accept	Reject	
	W2	Accept	Accept	Reject	

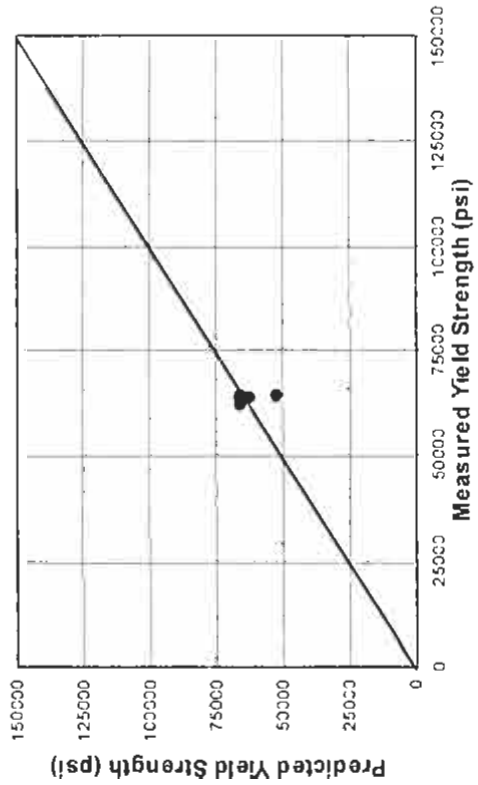
*Accept if measured yield stress \geq 60 ksi
 **Accept if predicted yield stress \geq 60 ksi
 ***Expert Opinion



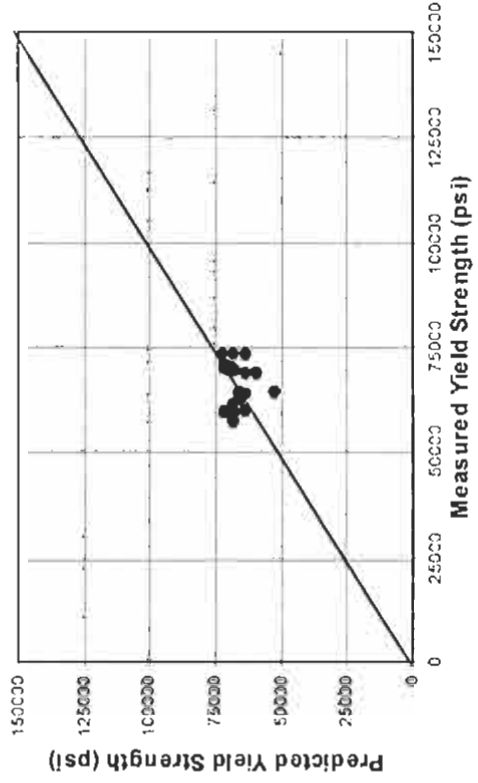
(a) #14



(b) #11



(c) # 8



(d) All Data

Figure 5.1 Correlation between Predicted and Measured Yield Strength Using Stiffness Changes Based on First Bending Mode

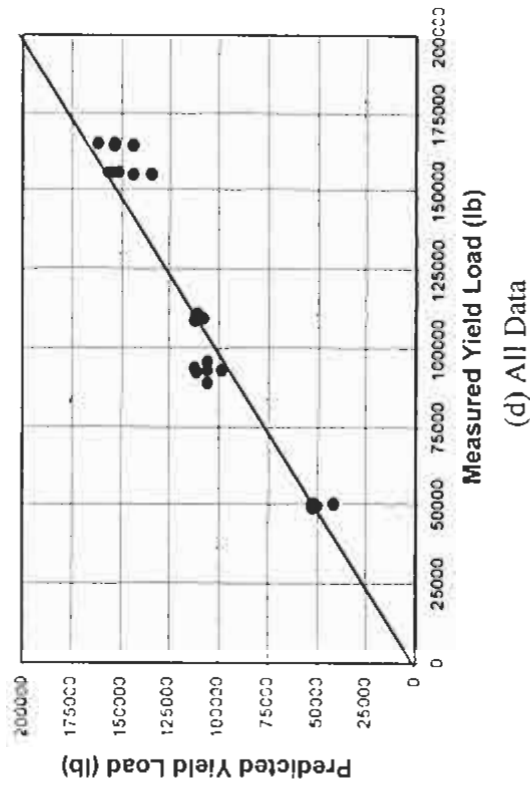
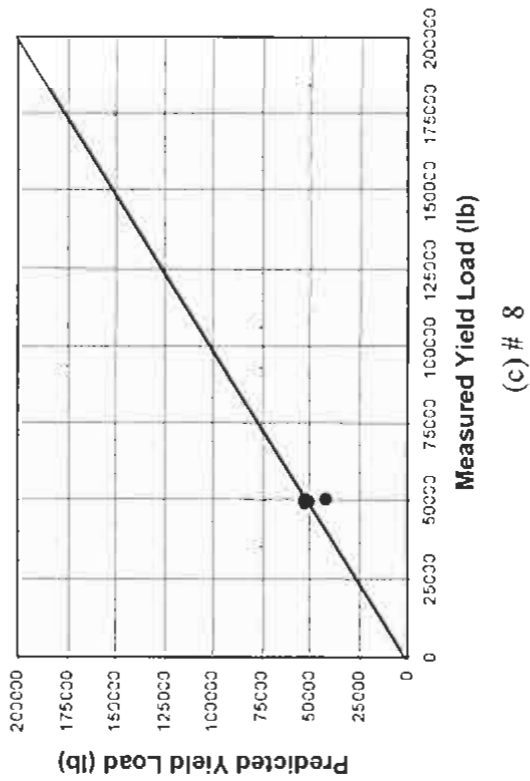
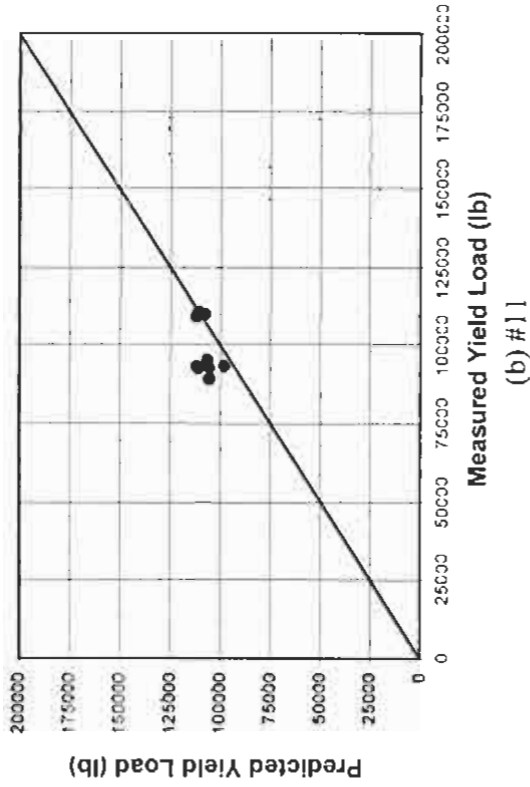
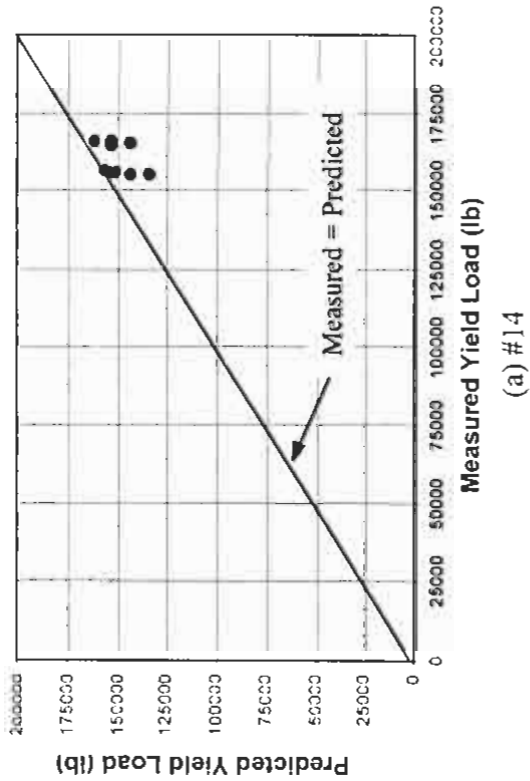
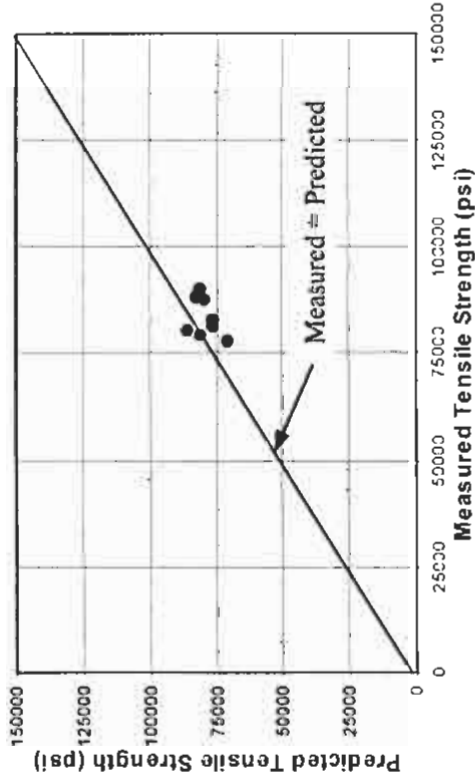
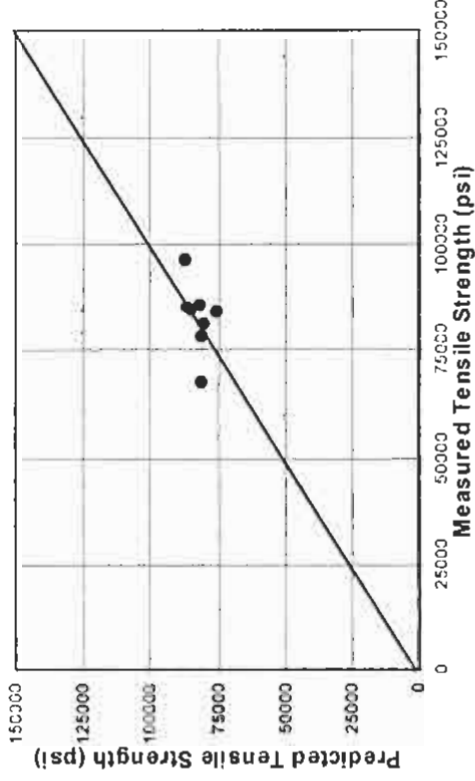


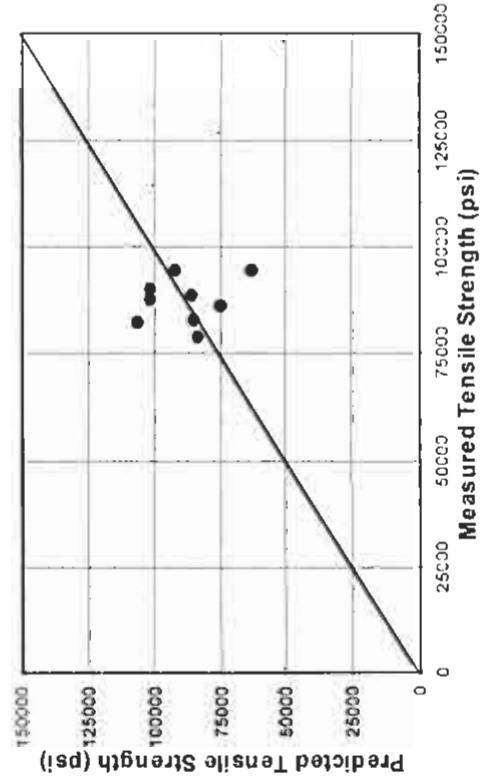
Figure 5.2 Correlation between Predicted and Measured Yield Load Using Stiffness Changes Based on First Bending Mode



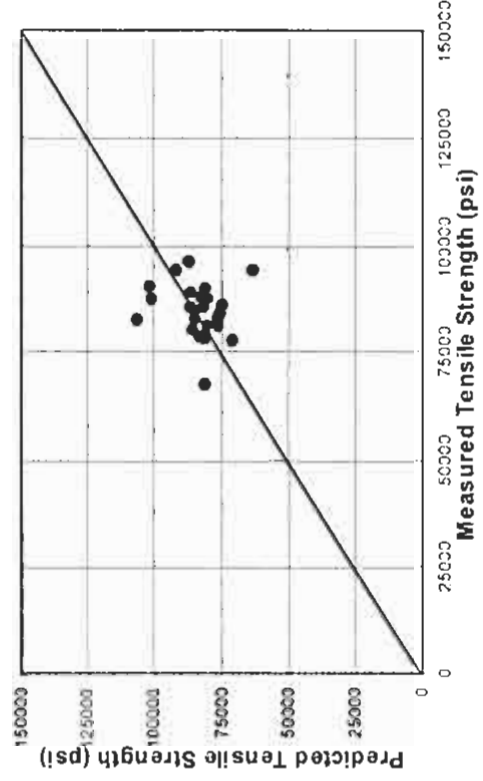
(a) #14



(b) #11

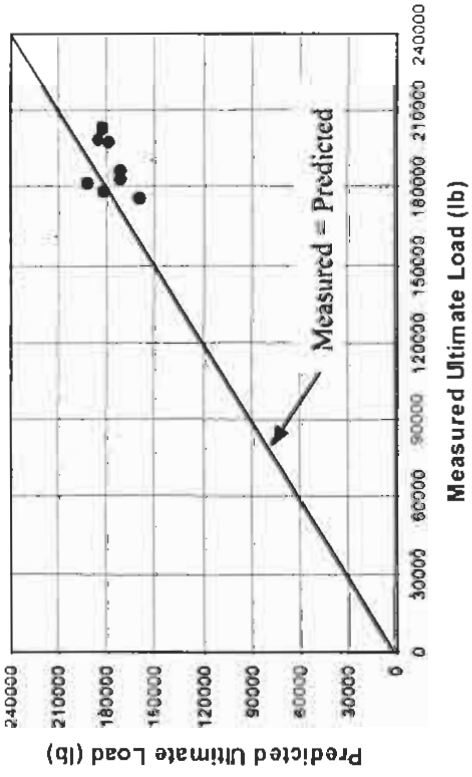


(c) # 8

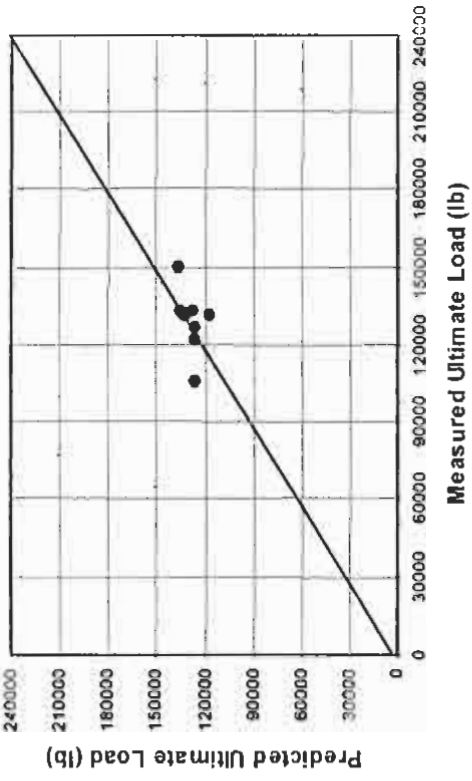


(d) All Data

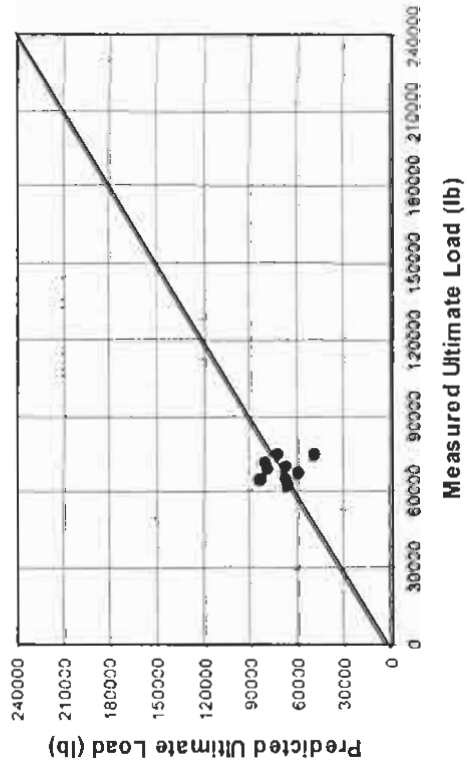
Figure 5.3 Correlation between Predicted and Measured Tensile Strength Using Stiffness Changes Based on First Bending Mode



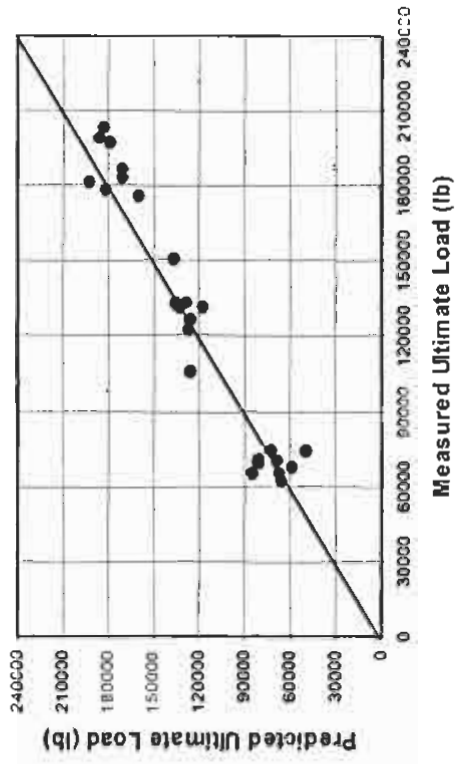
(a) #14



(b) #11



(c) # 8



(d) All Data

Figure 5.4 Correlation between Predicted and Measured Ultimate Load Using Stiffness Changes Based on First Bending Mode

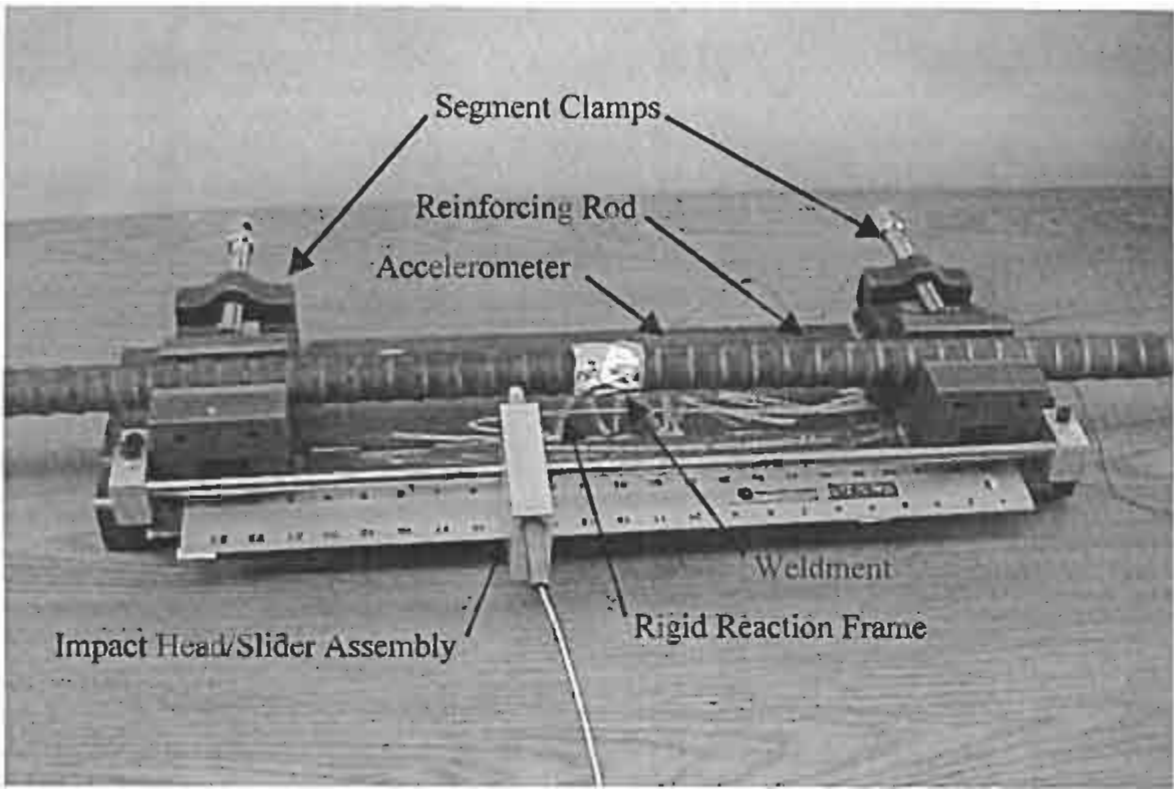


Figure 5.6 Prototype of Clamping Device

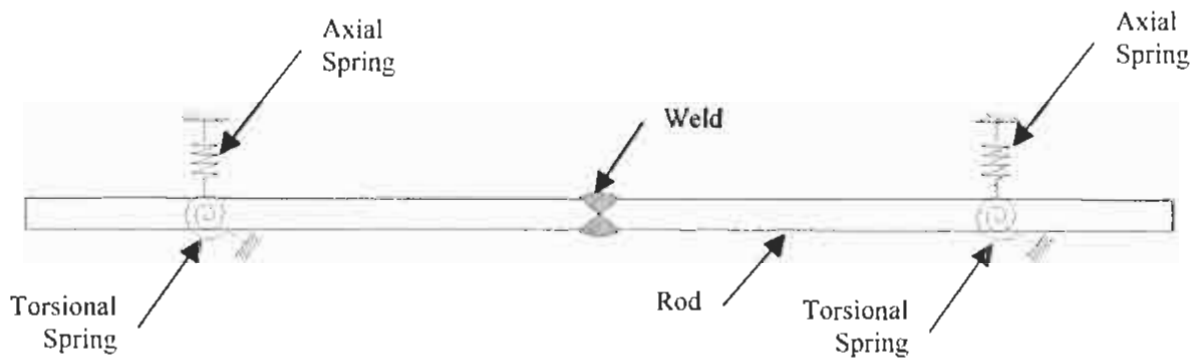


Figure 5.7 Schematic of Field Test Specimen

6. SUMMARY AND CONCLUSIONS

6.1 SUMMARY

The objective of this study was to investigate the technical feasibility of using a proven NDE scheme (the Damage Index Method) developed for large structures to evaluate, quantitatively, welded reinforcement splices during construction. At the outset of the project, an experiment was performed to demonstrate that the modal-based method could detect a 1/32 inch flaw in a #6 and a #9 rods in accordance with ANSI/AWS Specifications. Details of the experiment are provided in Appendix B.

In Chapter 2, a relationship between the damage in a material and the strength of the material was developed. Two approaches were used. First, independent of Continuum Damage Mechanics, a relationship between the yield strength and tensile strength of a welded reinforcing rod was developed. Second, the validity of the results was checked using the results from Continuum Damage Mechanics. A strong agreement between the damage measure of in the Damage Index Method (the fractional change in stiffness) and the internal variable used to characterize damage in Continuum Damage Mechanics exists.

In Chapter 3, the results of the modal testing and the subsequent stiffness evaluation for twenty seven welded rod specimens were presented. First, the welded specimens were described. Second, the instrumentation, modal test procedures, and modal results were presented. Third, the generation of specimen baseline models was discussed. Finally, the results of the fractional change in stiffness of the welds were presented.

In Chapter 4, tensile tests were conducted on thirty 48-inch welded reinforcing rod specimens at the TxDOT Materials and Tests Laboratory in Austin, TX. The thirty-specimen set was divided into three, 10-specimen subsets consisting of #8, #11, and #14 reinforcing rod sizes. An unwelded control specimen was included in each subset. Reported mechanical properties included yield strength, tensile strength, breaking strength, Young's modulus, total elongation, and percent elongation.

Finally, in Chapter 5, the predicted magnitudes of the capacity of a weld-rod system with the measured values of the system were compared. The capacity of the system was expressed in terms of the yield strength, yield load, tensile strength, and ultimate load of the weld-rod system. The equations and parameters used to predict the capacity of the weld were summarized, failure models for the weld-rod system were proposed, and the results of the comparison between the predicted and measured results for twenty-seven specimens were described. Also the evaluation of the weld using the proposed method, x-ray examination and dye penetrant were compared to the quality of the weld based on laboratory testing of the welds. Finally, the results were discussed with respect to (1) how they should be interpreted, (2) the accuracy of the predictions, (3) areas for potential improvements in the accuracy of the predictions, and (4) the implementation of the methodology in the field.

6.2 CONCLUSIONS

On the basis of the results presented in the main text and the supporting information catalogued in the appendices, the following findings ensue from this study:

1. The Damage Index Method is capable of detecting a 1/32 inch deep flaw in a #6 and a #9 rod, satisfying AWS Specifications (See Appendix B);
2. The performance, measured by the tensile strength and the yield strength, of a welded joint can be related to the fractional change in stiffness at the joint location due to the weld (See Chapter 2);
3. Fractional stiffness changes at the location of a weld can be routinely measured using modal-based methods (See Chapter 3);
4. Good agreement exist between predicted strengths of weld-rod systems and the corresponding strengths measured in the laboratory (See Chapters 4 and 5);
5. A model device that may allow the method to be used directly in the field has been constructed;
6. All theory, software, hardware and special sensors now exist to support the field application;

7. Finding 2, Finding 3, and Finding 4 imply that the method is quantitative;
8. Finding 1 and Finding 4 imply that the method is feasible; and
9. Finding 5 (given that such a device can be built) and Finding 6 (given that supporting instrumentation and theory to evaluate the weld exists) imply that the proposed methodology is feasible (i.e., practicable) under field conditions.

REFERENCES

- ABAQUS (1994). *Version 5.4 User Manual*. Hibbitt, Karlsson & Sorensen, Inc., Providence, Rhode Island.
- ANSI/AWS D1.4-92 (1992). *Structural Welding Code – Reinforcing Steel*. 4th Edition. American Welding Society. Miami, FL.
- Chang, C., Chen, I., Shee, H., and Chen, H. (1993). “X-ray Inspection Reliability for Welded Joints.” *Proceedings of the Sixth International Conference on Structural Safety and Reliability*, Vol. 2, pp. 991-996, August.
- Craig, R.R. (1981). *Structural Dynamics - An Introduction to Computer Methods*. John Wiley & Sons, New York, New York.
- Doebling, S., Farrar, C., Prime, M., and Shevitz, D. (1996). *Damage Identification and Health Monitoring of Structural and Mechanical Systems from Changes in Their Vibrational Characteristics: A Literature Review*. Los Alamos National Laboratory, Report # LA-13070-MS, Los Alamos, New Mexico, May.
- Ewins, D. J. (1984). *Modal Testing: Theory and Practice*. Research Studies Press, London, England.
- Farrar C., and Jauregui, D. (1996). *Damage Detection Algorithms Applied to Experimental and Numerical Modal Data from the I-40 Bridge*. Los Alamos National Laboratory Report # LA-13074-MS, Los Alamos, New Mexico, January.
- Garcia, G.V. (1996). *Evaluation of Relative Performance of Classification Algorithms for Nondestructive Damage Detection*. Ph.D. Dissertation, Texas A&M University, College Station, Texas.
- Gibson, J.D., and Melsa, J.L. (1975). *Introduction to Nonparametric Detection with Applications*. Academic Press, New York, New York.
- Kachanov, L., M. (1986). *Introduction to Continuum damage mechanics*. Kluwer Academic Publishers, Dordrecht, The Netherlands.
- Lemaitre, J., and Chaboche, J. -L. (1990). *Mechanics of Solid Materials*. Cambridge University Press, New York, New York..
- Nadler, M., and Smith, E.P. (1993). *Pattern Recognition Engineering*. John Wiley, New York, New York.
- Rabotnov, Y., N. (1969). *Creep Problems in Structural Members*. North-Holland, Amsterdam, The Netherlands.

- Rytter, A. (1993). *Vibrational Based Inspection of Civil Engineering Structures*. Ph.D. Thesis, University of Aalborg, Aalborg, Denmark.
- Stubbs, N., and Osegueda, R. (1990). "Global Non-Destructive Damage Evaluation in Solids." *International Journal of Analytical and Experimental Modal Analysis*, Vol. 5, No. 2, pp. 67-79.
- Stubbs, N., and Kim, J.T. (1996). "Damage Localization in Structures without Baseline Modal Parameters.", *AIAA Journal*, Vol. 34, No. 8, pp. 1644-1649.
- Stubbs, N., Kim, J.T., and Topole, K. (1992). "An Efficient and Robust Algorithm for Damage Localization in Offshore Platforms." *ASCE 10th Structures Congress '92*, San Antonio, Texas, pp. 543-546.
- Stubbs, N., Park, S., and Sikorsky, C. (1995). *Nondestructive Damage Evaluation of Span #10, Bridge #28-153*. Final Report # NDD-04-96-04, Caltrans, December.
- Stubbs, N., Park, S., and Sikorsky, C. (1997). *A Global Methodology to Nondestructively Evaluate Bridge Structural Safety*. Final Report # NDD 04-97-04, Caltrans, January.
- Stubbs, N., Park, S., Bolton, R.W., Choi, S., and Sikorsky, C. (1999). *Non-destructive Estimate of the Rate of Change of Structural Degradation of the Lavic Road Overcrossing*. Final Report # FHWA/CA/ESC/TEES 1-9/99, Caltrans, October.
- Talreja, R., (1994). "Damage Characterization by Internal Variables, Chapter 2." *Damage Mechanics of Composite Materials*, Composite Materials Series, Vol. 9. Elsevier Science B. V., Amsterdam, The Netherlands.

APPENDIX A

A METHODOLOGY TO IDENTIFY STRUCTURAL PROPERTIES OF THE BASELINE AND THE EXISTING STRUCTURES

A.1 SYSTEM IDENTIFICATION SCHEME FOR THE BASELINE STRUCTURE

The rationale behind the development of the baseline model can be explained with the aid of Figure A.1. Suppose a flawed (i.e., damaged) structure (Refer to Figure A.1(a)) is given with field-measured mode shapes Φ_j^* and eigenfrequencies ω_j^* . Assume that the magnitude of the flaw is small in comparison to a flawless (i.e., baseline) structure. Suppose that an estimate of the flawless structure can be identified, shown in Figure A.1(b), using only the frequency information from the flawed structure. Then the identified baseline model (Refer to Figure A.1(b)) will have the same eigenfrequencies ω_j^* (in the least square sense) of the flawed model (Refer to Figure A.1(a)) but the mode shapes of the two structures will be different in the neighborhood of the flaw. This difference in the mode shapes of the identified baseline structure and the measured mode shapes of the existing structure may then be exploited to localize the flaw.

Here, a system identification methodology to identify baseline modal responses of a structure is outlined (Stubbs and Kim, 1996). Consider a linear skeletal structure with NE members and N nodes. Suppose \mathbf{k}_j^* is the unknown stiffness of the j^{th} member of the structure for which M eigenvalues are known. Also, suppose \mathbf{k}_j is a known stiffness of the j^{th} member of a FE model for which the corresponding set of M eigenvalues are known. Then, relative to the FE model, the fractional stiffness change of the j^{th} member of the structure, α_j , and the stiffnesses are related according to the following equation:

$$\mathbf{k}_j^* = \mathbf{k}_j (1 + \alpha_j) \quad (\text{A.1})$$

The fractional stiffness change of NE members may be obtained using the following equation (Stubbs and Osegueda, 1990):

$$\mathbf{Z} = \mathbf{F}\alpha \quad (\text{A.2})$$

where α is a $NE \times 1$ matrix containing the fractional changes in stiffness between the FE model and the structure, \mathbf{Z} is a $M \times 1$ matrix containing the fractional changes in eigenvalues between the two systems, and \mathbf{F} is a $M \times NE$ stiffness sensitivity matrix relating the fractional changes in stiffnesses to the fractional changes in eigenvalues.

The $M \times NE$, \mathbf{F} matrix can be determined as follows: first, M eigenvalues are numerically generated from the initial FE model; second, the stiffness of the first member of the FE model is modified by a known amount; third, the corresponding set of M eigenvalues are numerically generated for the modified FE model; fourth, the fractional changes between the M initial eigenvalues and M eigenvalues of the modified structure are computed; fifth, each component of the first column of the \mathbf{F} matrix (i.e., the $M \times 1$, \mathbf{F} matrix) is computed by dividing the fractional changes in each eigenvalue by the magnitude of the modification at member one; and finally, the $M \times NE$, \mathbf{F} matrix is generated by repeating the entire procedures for all NE members.

Using the above rationale as a basis, the following 6-step algorithm is proposed to identify a given structure:

1. Select a target structure (e.g., a post-damage state of the structure) for which sufficient eigenfrequencies that can be used to identify the baseline structure are available. (Note that the mode shapes of the damaged structure in defining the target structure are ignored.)
2. Select an initial FE model of the structure, utilizing all possible knowledge about the design and construction of the structure.
3. As outlined above, compute the sensitivity matrix of the FE model.
4. As outlined above, compute the fractional changes in eigenvalues between the FE model and the target structure.
5. Fine-tune the FE model by first solving Equation (A.2) to estimate stiffness changes

(i.e., to compute the $NE \times 1, \alpha$ matrix) and next solving Equation (A.1) to update the stiffness parameters of the FE model.

6. Repeat steps 1~5 until $Z \cong 0$ or $\alpha \cong 0$ (i.e., as they approach zero) when the parameters of the FE model are identified.

The converged FE model is the baseline model. It has the frequencies of the damaged (i.e., target) structure but none of its members are damaged. Furthermore, the mode shapes of the baseline model differ from those of the damaged structure. Once the baseline model is identified, its modal parameters can be numerically generated (e.g., using commercial software ABAQUS (1994)).

A.2 DAMAGE LOCALIZATION THEORY (DAMAGE INDEX METHOD)

In the field of Nondestructive Damage Detection (NDD) using modal parameters, one of the more difficult problems is that of making a statement regarding the integrity of a relatively small portion of a structure when very few modal parameters are available. In such cases, inverse methods using systems of equations usually result in unsolvable systems with few equations but many unknowns. The discipline of pattern recognition provides a way to deal with such heavily underdetermined systems (Nadler and Smith, 1993).

In pattern recognition, physical world data are transduced into the so-called pattern space. Using techniques of dimensionality reduction, the pattern space is reduced to a smaller dimension known as the feature space. Data in the feature space are introduced to a decision algorithm and the elements of the feature space are classified into a finite number of clusters. In the problem at hand, the dynamic response of the structure in the time domain represents the physical world data and the modal parameters represent the pattern space. The feature space is represented by indicators that are a function of measurable pre-damage and post-damage modal parameters. These indicators can be selected in such a manner that they reflect internal structure in the data. The decision

algorithm is a means by which the data space is partitioned into D_n clusters (decision spaces). In this study, $n = 2$ and the decision spaces correspond to the cases: (a) a structure is not damaged at a given location, and (b) a structure is damaged at a given location. For each instance the indicator of damage will fall into one of the two categories.

The damage index method utilizes the change in mode shapes of the pre-damage and post-damage structure to detect and locate damage in a structure (Stubbs et al., 1992). Consider a linear, undamaged, skeletal structure with NE elements and N nodes. After writing the equations of motion for the structure and solving the eigenvalue problem, the i^{th} modal stiffness, K_i , of the arbitrary structure is given by (Craig, 1981)

$$K_i = \Phi_i^T C \Phi_i \quad (\text{A.3})$$

where Φ_i is the i^{th} modal vector and C is the system stiffness matrix. From matrix structural analysis, the contribution of the j^{th} member to the i^{th} modal stiffness, K_{ij} , is given by

$$K_{ij} = \Phi_i^T C_j \Phi_i \quad (\text{A.4})$$

where C_j is the contribution of the j^{th} member to the system stiffness matrix. The fraction of modal energy for the i^{th} mode that is concentrated in the j^{th} member (i.e., the element sensitivity of the j^{th} member to the i^{th} mode) is given by

$$F_{ij} = K_{ij}/K_i \quad (\text{A.5})$$

Let the corresponding modal parameters in Equations (A.3) to (A.5) associated with a subsequently damaged structure be characterized by asterisks. Then for the damaged structure,

$$F_{ij}^* = K_{ij}^* / K_i^* \quad (\text{A.6})$$

where K_{ij}^* and K_i^* are given by, respectively

$$K_{ij}^* = \Phi_i^{*T} C_j^* \Phi_i^* \quad (\text{A.7})$$

and

$$K_i^* = \Phi_i^{*T} C^* \Phi_i^* \quad (\text{A.8})$$

Again, from matrix structural analysis, the stiffness matrices C_j and C_j^* in Equations (A.4) and (A.7) may be written as follows:

$$C_j = k_j C_{j0} \quad (\text{A.9})$$

and

$$C_j^* = k_j^* C_{j0} \quad (\text{A.10})$$

where the scalars k_j and k_j^* , respectively, are parameters representing the material stiffness properties of the undamaged and damaged j^{th} member of the structure, and the matrix C_{j0} involves only geometric quantities (and possibly terms containing Poisson's ratio). The quantities F_{ij} and F_{ij}^* are related by the equation:

$$F_{ij}^* = F_{ij} + dF_{ij} \quad (\text{A.11})$$

where dF_{ij} is related to the change in the fraction of modal energy of the j^{th} member in the i^{th} mode. The quantity dF_{ij} can be obtained from the expression:

$$dF_{ij} = \frac{K_{ij}}{K_i} \left[\frac{dK_{ij}}{K_{ij}} - \frac{dK_i}{K_i} \right] \quad (\text{A.12})$$

Assuming that the structure is damaged at a single location j and the resulting change in F_{ij}

is only a function of k_j , a first order approximation of dK_{ij} can be obtained from the expression:

$$dK_{ij} \cong \frac{\partial K_{ij}}{\partial k_j} dk_j + \frac{\partial K_{ij}}{\partial u_{ij}} \frac{\partial u_{ij}}{\partial k_j} dk_j \quad (\text{A.13})$$

where

$$u_{ij} = \Phi_i^T C_{j0} \Phi_i \quad (\text{A.14})$$

Using Equations (A.4) and (A.9), it can be shown that

$$\frac{\partial K_{ij}}{\partial k_j} = u_{ij} \quad (\text{A.15})$$

and

$$\frac{\partial K_{ij}}{\partial u_{ij}} = k_j \quad (\text{A.16})$$

Next, introducing the modal force vector associated with the j^{th} member and the i^{th} mode, A_{ij} , given by

$$A_{ij} = C_j \Phi_i \quad (\text{A.17})$$

it can be shown that by using Equations (A.9), (A.14), and (A.17),

$$u_{ij} = \frac{1}{k_j^2} A_{ij}^T C_{j0}^1 A_{ij} \quad (\text{A.18})$$

Therefore, if it is assumed that the modal force A_{ij} remains constant while k_j changes (note that the assumption is true in the case of a statically determinant system), then

$$\frac{\partial u_{ij}}{\partial k_j} = -\frac{2u_{ij}}{k_j} \quad (\text{A.19})$$

Since it has been assumed that the structure is damaged in only one location, it follows readily that $dK_{ij} = dK_i$. Also, since $K_i \gg K_{ij}$, from Equation (A.12)

$$dF_{ij} \cong \frac{dK_{ij}}{K_i} = -\frac{u_{ij}}{K_i} dk_j = -F_{ij} \alpha_j \quad (\text{A.20})$$

where $a_j = dk_j/k_j$, the fractional change in the stiffness of Element j . Substituting the result of Equation (A.20) into Equation (A.11), and substituting for F_{ij}^* using Equations (A.6) to (A.11), it can be shown that

$$\frac{k_j^*}{K_i^*} = k_j \frac{u_{ij}}{K_i} (1 - \alpha_j) \quad (\text{A.21})$$

Substituting for $a_j = (k_j^* - k_j)/k_j$ in Equation (A.21), and rearranging, one obtains:

$$\frac{k_j}{k_j^*} = \left(\frac{u_{ij}^*}{K_i^*} + \frac{u_{ij}}{K_i} \right) / 2 \frac{u_{ij}}{K_i} \quad (\text{A.22})$$

Setting $f_{ij}^* = u_{ij}^*/K_i^*$ and $f_{ij} = u_{ij}/K_i$, Equation (A.22) reduces to

$$DI_{ij} = \frac{k_j}{k_j^*} = \frac{f_{ij}^*/f_{ij} + 1}{2} \quad (\text{A.23})$$

where DI_{ij} is the indicator of damage in the j^{th} member using the i^{th} mode. If $DI_{ij} > 1$, damage may exist. From Equation (A.23), the fundamental indicator of damage is the quotient f_{ij}^*/f_{ij} . Note that the one in the numerator is, essentially, a shifting factor while the two in the denominator is a scaling factor. Equation (A.23) becomes singular when $f_{ij} \rightarrow 0$: a condition

which will occur when, simultaneously, the element size approaches zero and the element is located at a node of a mode. Here the division-by-zero difficulty can be overcome by simply shifting the axis of reference for the sensitivities. For example, if the origin is shifted from $f_{ij} = 0$ to $f_{ij} = -1$, then

$$f'_{ij} \rightarrow 1 + f_{ij} \quad (\text{A.24})$$

and

$$f'_{ij} \rightarrow 1 + f_{ij}^* \quad (\text{A.25})$$

So the new indicator function, DI_{ij} , which will also form the basis of feature space (in the pattern recognition sense), becomes

$$DI_{ij} = \frac{f_{ij}^* + 1}{f_{ij} + 1} \approx \left[\frac{\Phi_i^{*T} C_{j_0} \Phi_i^* + \Phi_i^{*T} C \Phi_i^*}{\Phi_i^T C_{j_0} \Phi_i + \Phi_i^T C \Phi_i} \right] \frac{\Phi_i^T C \Phi_i}{\Phi_i^{*T} C \Phi_i^*} \quad (\text{A.26})$$

There are two important characteristics of the indicator DI_{ij} given by Equation (A.26): first, the expression attempts to express the changes in stiffness at a specific location in terms of measurable pre-damage and post-damage mode shapes (Φ_i and Φ_i^*); and second, the term C_{j_0} on the right hand side of Equation (A.26) can be determined from a knowledge of the geometry of the structure. Thus for each damage location j , there are as many DI_{ij} 's available as there are mode shapes. As noted above, in the context of pattern recognition, the latter values of DI_{ij} define the feature space. The following expression will be the convenient form of damage index DI_j for a single location if several modes (NM) are used

$$DI_j = \frac{\sum_{i=1}^{NM} (\Phi_i^{*T} C_{j_0} \Phi_i^* + \Phi_i^{*T} C \Phi_i^*) \Phi_i^T C \Phi_i}{\sum_{i=1}^{NM} (\Phi_i^T C_{j_0} \Phi_i + \Phi_i^T C \Phi_i) \Phi_i^{*T} C \Phi_i^*} \quad (\text{A.27})$$

The final step in damage localization is classification. Classification analysis addresses itself to the problem of assigning an object to one of a number of possible groups on the basis of observations made on the objects. In this study, the objects are the members of the structure. There are two groups: undamaged elements and damaged elements. Finally, the observations made on the objects are the DI_j 's. Many techniques are available to accomplish the end. Examples of these methods include classification on the basis of: (1) Bayes' rule (from which the well known Linear Discriminant Analysis and Quadratic Discriminant Analysis are derived), (2) nearest distance, and (3) hypothesis testing (Gibson and Melsa 1975). While other approaches are available (Garcia 1996), the authors currently have utilized primarily techniques from hypothesis testing. The criteria for damage localization is established based on statistical reasoning. The values, $DI_1, DI_2, DI_3, \dots, DI_{NE}$ for each element, are considered as realization of a random variable. The normalized damage indicator is given by

$$z_j = \frac{DI_j - \mu_{DI}}{\sigma_{DI}} \quad (A.28)$$

where μ_{DI} and σ_{DI} represent mean and standard deviation of the damage index, DI_j , respectively. Let H_0 be the hypothesis that the structure is not damaged at member j , and let H_1 be the hypothesis that the structure is damaged at member j . The following decision rules may be used to assign damage to member j : (1) choose H_1 if $z_j \geq \lambda$ and (2) choose H_0 if $z_j < \lambda$ where λ is a threshold which assigns a level of significance.

A.3 DAMAGE SEVERITY ESTIMATION

Note that in Equation (A.23) the indicator of damage is the ratio of the undamaged stiffness to the damaged stiffness. Such a number exists for each potentially damaged member. For example, in the case of a truss there is a DI_j associated with every member j . Here the damage is expressed as the fractional change in stiffness of an element:

$$\alpha_j = \frac{k_j^* - k_j}{k_j} = \frac{1}{DI_j} - 1 \quad (\text{A.29})$$

Thus if there is no damage, $\alpha_j = 0$; if there is damage, $\alpha_j < 0$. Note that if $\alpha_j = -1$, all stiffness capacity is completely lost.

A.4 IDENTIFICATION OF STIFFNESS OF EXISTING STRUCTURE

Having stiffness parameters for the baseline structure, location of damage, and the severity of damage, the stiffness properties of the existing structure can be obtained from the equation:

$$k_j^{(\text{existing})} = k_j^{(\text{baseline})} [1 + \alpha_j] \quad (\text{A.30})$$

Note that if there is no damage at location j , the stiffness properties of the baseline and the existing structures are the same.

(a) Flawed Structure: Φ_j^*, ω_j^*



(b) Estimate of Flawless Structure: Φ_j, ω_j



Figure A.1 Flawed Structure and Estimate of Flawless Structure

APPENDIX B

VALIDATION OF THE METHODOLOGY VIA LABORATORY EXPERIMENTS FOR A 1/32" SURFACE DEFECT IN A #6 AND #9 BAR

B.1. INTRODUCTION

Laboratory experiments on unwelded and welded reinforcing rod specimens were performed to verify the damage detectability of the Damage Index Method. Surface cracks, the smallest depth of 1/50 inch to the greatest depth of 2/50 inch, are artificially made in #6 and #9 reinforcing rod specimens for the experiments. To meet the objective the following four tasks are performed. First, materials and equipment used in the experiment are described. Next, the details of the experiment are described. Third, the modal testing performed to extract the modal parameters, i.e., frequencies and mode shapes, are summarized. Finally, the modal parameters and the damage estimation results employing the Damage Index Method are summarized.

B.2. MATERIALS AND EQUIPMENT

In this section, the experimental configurations utilized to determine the modal characteristics of the specimen are described. These configurations include the types and dimensions of the specimens used in the experiment and modal testing equipment.

B.2.1. Description of Materials

Typical #6 and #9 reinforcing rods were selected in this experiment. All specimens were 24 inches long. A specimen length within 1/4 inches of the nominal value was considered acceptable. It should be noted that lengths of 44 and 48 inches were discussed earlier. Due to the physical size of the latter specimens, shorter specimens were preferred. The shorter specimens had higher natural frequencies, which in turn were easier to excite with the impact hammer used here. Note that #6 specimens has a nominal diameter of 3/4 inches and #9 specimen has a nominal diameter of 1.125 inches. All specimens were designated ASTM A60 and were purchased locally.

For the purpose of this study, a free-free beam was selected as the test configuration, because of the confidence in the knowledge of the boundary conditions. In order to simulate a free-free boundary condition, two lengths of 18 gauge wire approximately 24 inches in length were used. The support wires were tied to a pair of shelf brackets at one end and a noose at the other end (Refer to Figure B.1). A piece of sponge was placed between the specimen and the support wires at the lower end, to isolate the specimen from the supports and to create a free-free condition (Refer to Figure B.1). On the surface of the sponge in contact with the specimen, two strips of rubber bands were glued together in order to increase friction. This action was taken in an attempt to prevent the specimen from rotating about longitudinal axis as a result of the hammer impacts.

A pendulum device to impact the free-free specimen was constructed (Refer to Figure B.1). The purpose for selecting the pendulum device was to reduce variations in the magnitude and location of the hammer impacts. A permanent marker was utilized to indicate the designated points of impact for each specimen. A ruler was used to measure the magnitude of the inflicted damage. A hacksaw was used to introduce the intended damage to the specimen. Also, a 3/8 inches diameter ball end mill bit was used for weld joint preparation. All the materials used in the experiment are indicated in Figure B.2.

B.2.2. Description of Equipment

Figure B.3 depicts the equipment utilized in this study. The equipment consisted of a 4-channel Digital Signal Processor (DSP), an impact hammer, a piezoelectric accelerometer and a personal computer (PC) equipped with Siglab software version V3.10 (11-Sep-98 or later version). The DSP and Siglab software, designated model 20-42, were manufactured by the Signal Analysis Group. The impact hammer was a Piczotronics (PCB) model 086C01. Several impact tips were supplied with the hammer. The white nylon (084B04) and metal tip (084B03) were the ones finally used because they produced a flatter auto-spectrum in the frequency ranges corresponding to the first four resonant frequencies for both the #6 and #9 specimen sizes. The accelerometer utilized in the experiment was a PCB model 303A03.

B.3. SUMMARY OF MODAL TESTING

B.3.1. Description of Equipment Setup

The following summary highlights some of the Siglab settings used. Siglab's overload reject was set to "on". This setting meant that if there was an overload in one or both inputs, no data would be taken. Siglab's Record Length was set to collect the maximum number of samples, 8192. The record length is an intrinsic Siglab function that sets the number of samples taken and the sample time. Anti-aliasing filters were set to "on". The use of the filters eliminated any frequency content above the upper cut-off frequency of the bandwidth specified by the experimenter. The bandwidth was set to 5 KHz the resulting frequency error was ± 1.5625 Hz. The use of a 5 KHz bandwidth was sufficient to span the first 6 bending modes. The frequency error is a tolerance set by Siglab based on the bandwidth selected by the experimenter.

The #6 specimens required hammer and accelerometer sensitivity settings of 5V and 2.5V, respectively. The #9 specimens required hammer and accelerometer sensitivity settings of 10V and 5V, respectively. The sensitivity settings were sufficient to reduce the time required to conduct a modal test by eliminating repeated input overloads.

B.3.2. Specimen Preparation

The preparation of each specimen was accomplished in four steps. First, each specimen was cut to the appropriate length of 24 inches and surface grit was removed with a wire brush. Second, nine impact locations were milled on the weak axis three inches apart between centers of milled out sections (Refer to Figures B.4 and B.5). Third, the specimens were rotated 180° and one accelerometer location milled out 9 inches from the end corresponding to Location 1. Finally, the impact locations were labeled 1 through 9 with a permanent marker. Also, each specimen was assigned a number. For example, 6_2 designated a #6 rod specimen and specimen two.

To simulate a surface crack, an ordinary hacksaw was used to cut a groove in the surface of the specimen (Refer to Figure B.6). A hacksaw was used for two reasons: 1) it yielded

better control over the amount of material removed (as opposed to an electric band saw or power hacksaw); and 2) the hacksaw was faster than an arbor mill. The width of the inflicted crack was on the order of 0.0345 inches as measured with a pair of feeler gages. Note that an ordinary hacksaw approximately 0.02 inches in width was used to cut a groove in the surface of the reinforcing rod specimen and the depth of the groove was measured using a ruler.

Full penetration butt welds were tested. A double U-groove was preferred to a V-groove for at least three reasons. First, in order to prepare a V-groove, each specimen had to be cut into two pieces. This situation resulted in an alignment problem when an attempt was made to weld the two pieces together. Second, welding of a full penetration V-groove generated excessive heat that in turn resulted in specimen warping. Finally, a double U-groove was easier to mill than was a double V-groove.

Preparation of the complete weld joint required four steps. First, a 3/8 inch ball end mill was used to cut out a U-groove through half the diameter of a specimen at location 6 (refer to Figure B.7). Second, the groove was welded and cooled (refer to Figure B.8). Third, a second U-groove was cut on the opposite side of the first U-groove to a depth greater than half the diameter of the specimen to ensure full penetration. Finally, the second groove was welded and cooled. The welding was accomplished using Gas Metal Arc Welding (GMAW) and electrode specification ER70S-6.

B.3.3. Quantification of the Number of Impact Locations Using Shannon's Sampling Theorem

The number of impact locations for the modal testing was determined based on the Shannon's Sampling Theorem. The theorem states that in order to completely reconstruct a continuous time signal from a sample set requires that the sampling frequency should be greater than twice the highest frequency of interest contained in the original signal. Shannon's Theorem may be stated as follows:

$$f_s \geq 2 f_{max} \quad [\text{time domain}] \quad (\text{B.1})$$

where f_s is the sampling frequency and f_{max} represents the maximum frequency to be reconstructed. Analytical results for a simply supported rod show that the bending modes in the spatial domain are sinusoidal.

$$Y = C \sin\left(\frac{m\pi x}{L}\right) \quad (\text{B.2})$$

Where Y is the bending mode shape amplitude, C is an arbitrary constant, m is the mode number of the highest bending mode to be reconstructed and L represents the rod length. Hence, if the original signal is continuous and periodic, then the spatial domain equivalent of Equation (B.1) can be stated as follows:

$$N \geq 2K + 1 \quad [\text{Spatial domain}] \quad (\text{B.3})$$

where N is the number of sample points and K represents the highest harmonic to be reconstructed. For example, if we wanted to reconstruct the fourth harmonic of a signal ($K = 4$), then $N \geq 9$. In order to use the Damage Index Method, curvatures have to be computed numerically. Independent experimentation demonstrated that for values of $N > 9$, the resulting curvatures were undesirable. Here, undesirable refers to the non-smooth, asymmetrical appearance of Mode 1 curvatures obtained in experiments using 13 data points (Refer to Figure B.9). Figure B.9 demonstrates that the experiments using 9 data points resulted in curvatures that were more smooth and symmetrical. Therefore, the number of impact locations was set to 9 instead of 13. This adjustment allowed the first four bending modes to be used in the damage detection algorithm based on Equation (B.3).

B.3.4. Description of Experiment Procedure

The experimental procedures described below are applicable to both #6 and #9 rod specimens. Typically in modal testing, multiple sensors are used and the structure is

impacted at one location. Transfer frequency response functions (FRF) for all locations are then produced simultaneously. Since the FRF matrix is symmetric, an alternative modal testing method is to use one sensor and multiple impacts at each impact location (i.e., the fixed accelerometer - roving hammer method). The latter method is valid if the system is linear and if the hammer impacts are repeatable (Ewins, 1986). The procedure consists of the following nine steps:

1. Attach the accelerometer to the specimen (refer to Figure B.10);
2. Place the specimen into the supports (refer to Figure B.10)
3. Adjust the impact hammer in the vertical position so that it is perpendicular to the specimen and even with the center of the impact location (This procedure is an eyeball adjustment that reduces errors in the data due to the misalignment between the accelerometer and hammer which causes the accelerometer to sense non-bending modes);
4. Set the swing angle of the hammer by adjusting the pendulum's angle adjustment feature (refer to Figures B.1 and B.3);
5. Firmly hold the base of the pendulum with one hand, simultaneously raise the hammer with the other until the hammer is in contact with the angle adjustment stop, release the hammer and impact the specimen, then catch the hammer immediately after impact to prevent a double hit (refer to Figures B.11 and B.12);
6. Once the green light on the DSP starts flashing gently, grasp the specimen to dampen out the remaining vibrations and stop the specimen from swinging (Refer to Figure B.13);
7. Repeat Steps 1 to 6 three times;
8. (After the third impact at an impact location, Siglab displays an averaged FRF of the specimen on the PC monitor.) Record by hand the maximum value for the first four peaks of the FRF and store the data on disk. Siglab also provided the sign of the displacement (positive or negative); and
9. Repeat Steps 1 to 8 for each impact location.

By following the procedure outlined above, the magnitude of the system response at location i (accelerometer location: Location 4) due to an excitation at location j ($j = 1$ to 9) can be measured. At the conclusion of the modal test, a complete set of mode shapes for the first four modes was collected.

B.3.5. Description of Experiments

The experiment was conducted in two steps: preliminary and final experiments (Refer to Table B.1). The preliminary experiment (Experiment Number 1 through 1c) was performed on a homogeneous steel rod (Specimen S_1), to gain insight into how varying certain parameters would affect damage detection using the current NDD algorithm. The preliminary specimen was not welded. The final experiment (Experiment Number 2 through 23) was conducted on the non-welded and welded reinforcing rod specimens. The #6 and #9 specimens were used in the final experiment.

B.3.5.1. Description of Preliminary Experiments

In order to determine the smallest detectable defect, the depth of the groove was initially set at 0.02 inches. However, the current NDD algorithm showed that at this depth damage detection was not repeatable. Consequently, the damage was incrementally increased until the NDD algorithm could detect the damage repeatedly.

During the preliminary testing stage, the same type of boundary conditions (i.e., free-free boundary condition) were used for all specimens (Refer to Figures B.1 and B.3). The parameters of interest were the specimen length, hammer impact repeatability, number of impact locations and the accelerometer and damage locations. First, preliminary results indicated that if 13 data points were used, both 24 inches and 48 inches specimens had asymmetrical and non-smooth curvatures for Mode 1, which led to the use of 24 inches specimens (Refer to Figure B.14). Second, a pendulum was constructed in an attempt to improve hammer impact repeatability. Impact repeatability is essential if good data were to be collected using a non-contact excitation method such as an instrumented impact hammer. Third, the number of impact points was decreased from 13 to 9. This decision was made in an attempt to improve the quality of the curvature of Mode 1 (Refer to

Figure B.14). A cubic spline numerical routine was used to compute curvatures at intermediate impact points. In actual field testing, the number of measurable mode shapes may be limited; thus the reason for the emphasis being placed on Mode 1. Last, preliminary results from Experiments 1-1c (Refer to Table B.1) conducted on Specimen S_1, showed that if the accelerometer and damage locations were not at the specimen's midpoint, damage was detectable using the current NDD algorithm (Damage was at $x=16$: Element 60) (Refer to Figure B.15). This finding is attributable to the fact that the midpoint corresponds to a node point for modes two and four. Therefore, in moving the accelerometer and damage locations off center, the first four modes could be used for damage detection.

B.3.5.2. Description of Final Experiment

The objective of this section is to provide a general description of the experiments conducted and an experimental proof of concept for the approach. Here, the proof of concept refers to repeatedly detecting specific sized defects in unwelded #6 and #9 rod specimens using the current NDD algorithm. Proof of concept will also be extended to include full penetration butt welds. In this study damage was a cut inflicted with an ordinary hacksaw. Note that saw cut depths of interests ranged from 0.02 inches to 0.04 inches.

Unless otherwise stated, all specimens had the same support locations (Locations 2.5 and 7.5) and 9 data / impact points (3 inches pitch). The accelerometer was attached at Location 4 and damage was inflicted at Location 6. In this study, Location 1 corresponds to $x = 0$ inches, Location 2 corresponds to $x = 3$ inches, and so on. Based on the data gathered, the threshold value to be used for hypothesis testing was $z_0 = 0.45$, which corresponds the smallest encountered value for which damage was correctly predicted. The threshold value corresponds to a 67.36 % level of significance of correctly predicting the damage. When viewing a damage indicator, z , graph for a specimen, the damage location corresponds to element number 30 (Location 6: $x=15$ inches). The element length used in the NDD algorithm was 0.5 inches. The element corresponding to damage (DE) can be computed with the following expression:

$$DE = x / \text{Element Length} = \frac{(\text{Damage Location Number} - 1) * \text{pitch}}{\text{Element Length}} \quad (\text{B.4})$$

The homogeneous steel rod, Specimen S_2, had support locations at 2.5 and 5.5 and 7 impact points (4 inch pitch). For the steel rod, Location 1 corresponds to $x = 0$ inches, Location 2 corresponds to $x = 4$ inches, and so on. The accelerometer was attached at Location 3 and damage was inflicted at Location 5. The element number corresponding to damage is 32 for Specimen S_2. The element length used in the NDD algorithm was 0.5 inches. A listing of the experiments conducted along with the experimental objectives and results are presented in Table B.1.

Experiments 2 – 3b were conducted on unwelded Specimen S_2 (3/4 inch diameter) using the set-up previously defined. Specimen S_2 was inflicted with two damage sizes, 1/16 inches and 1/14 inches. Experimental results showed that the current NDD algorithm could be used to detect damage at Element 32 as small as 1/16 inches (Refer to Figure B.16) using all modes. This finding in conjunction with the findings from Experiments 1 – 1c provided proof of repeatability. The next step would be to extend the concept to actual rod specimens and damage less than or equal to 1/32 inches.

In Experiments 4 – 6, several iterations of modal testing were conducted on Specimens 6_3 and 6_3a. Baseline and damaged mode shapes collected demonstrated that a 1/32 inch defect was detectable combining all modes using the current NDD algorithm (Refer to Figure B.17, Element 30). At the conclusion of Experiments 4 through 6, proof of concept and repeatability of procedure were established. The next question to be answered was whether or not changing support locations might have an effect on damage detection.

In Experiments 7 and 7a, Specimen 6_3 was tested in an attempt to determine the effect of changing the support locations. Specimen 6_3 was re-tested with two different sets of support locations: 1) Support 1 had supports at Locations 3.5 and 6.5; and 2) Support 2

had supports at Locations 1.5 and 8.5. The level of damage was the same as in Experiments 4 through 6. Combining all modes both, support location scenarios predicted damage at the proper location. The curvatures for Mode 1 were not as symmetric here as compared to the ones generated in Experiments 4 – 6 (Refer to Figure B.18). Mode 1 curvatures in Figure B.18 correspond to those of damaged Specimen 6_3.

In Experiments 9 through 9d, Specimen 6_1 was tested in an attempt to address the asymmetry effect associated with changing support locations. Two different sets of support locations (SC1 and SC2) were used: 1) SC1 had support locations 2.5 and 7.5; and 2) SC2 had support locations at 3.5 and 6.5. For each support case, baseline and damaged mode shapes were collected. The level of damage was 0.02 inches. SC1 correctly predicted damage with modes 1,2 and 4 and combining all modes (Refer to Figure B.19). SC2 correctly predicted damage with only Mode 4 (Refer to Figure B.20). Results indicate that it would be better to use SC1 for future experiments. Note here that the results of Experiments 9 – 9d did not yield Mode 1 curvatures that were anymore symmetric than for Experiments 7 and 7a (Refer to Figure B.21). Experiment 9d was a re-test of Specimen 6_1, which successfully verified repeatability.

In Experiments 10 and 11, tests were conducted on Specimens 6_2 and 6_4. Only baseline mode shape data were collected. At the conclusion of Experiment 11, Specimens 6_1, 6_2 and 6_4 could be welded and tested.

Unwelded #9 rod Specimen 9_2 was tested in Experiments 12 – 12f. Due to the natural frequencies of Specimen 9_2 being higher than the corresponding modes for the #6 specimens, a metal impact tip was used instead of a nylon tip. The metal tip provided a better auto-spectrum for the impact hammer; also, a harder tip was recommended in the PCB owner's manual for higher frequencies. The test results showed that a defect of 0.02 inches and 1/32 inches were detectable using the current NDD algorithm (Refer to Figures B.22 and B.23).

In Experiments 13 – 13a, tests were conducted on Specimens 6_3 and 9_1. Specimen 6_3 was welded at Location 6 with a 50° V-groove using GMAW and electrode specification ER70S-6. The width of the weld was approximately 0.5 inches. The weld joint was prescribed by current Caltrans specifications.

In preparing the welded joint, two problems surfaced: 1) there was difficulty in the alignment of the weld joint surfaces; and 2) warpage resulted in Specimen 6_3 due to heat transfer. The mode shapes of the baseline and welded specimens were generated in independent tests. Specimen 9_1 was not welded, and both the baseline and damaged (1/32 inches defect) mode shapes were generated via independent tests. Test results showed that a 1/32 inches defect was undetectable in Specimen 9_1 using the current NDD algorithm.

In Experiments 14 and 14a, Specimen 9_3 was tested. Both the baseline and damaged mode shapes were generated via independent tests. The inflicted damage level was a 1/32 inch deep saw cut. Test results indicate that a 1/32 inch defect could be detected using the current NDD algorithm (Refer to Figure B.24). Experiment 14b was conducted on welded Specimen 6_3. The level of damage was 0.02 inches at Location 6. This level of damage was undetectable using the current NDD algorithm.

In Experiment 15, the level of damage in Specimen 6_3 was increased to 1/32 inches. At this level of damage, the current algorithm was able to detect the damage location with only Mode 4.

Experiment 16 was a re-test of Specimen 6_3 with the level of damage increased to 0.04 inches. Results of the current tests were similar to the ones reported in Experiment 15. The current results show that Modes 1 and 4 detected the damage (Refer to Figure B.26).

Experiments 18, 21 and 23 were performed on Specimen 6_1. Specimen 6_1 was welded at Location 6 using a double U-groove weld joint. A welded baseline was taken, then a 0.02 inch deep saw cut was inflicted at Location 6. Subsequently the damaged mode

shapes were taken. To better localize the damage using the current algorithm, the element size was reduced to 3/20 inches. The damaged element corresponds to Element 100 (refer to Figure B.27). Results indicate that a 0.02 inch defect is detectable and repeatable. The results also verified the proof of concept for #6 welded rod splices.

B.4. DISCUSSION OF RESULTS

B.4.1. Overview

The validation results for the proposed methodology and experimental procedure are discussed here. First, mode shape repeatability is discussed using the proposed experimental procedure. Second, verification of the assumed free-free boundary based on computed Modal Assurance Criteria (MAC) values is discussed. Third, the effects of support interaction are presented. Finally, verification of concept based on the proposed methodology and experimental procedure are presented.

B.4.2. Mode Shape Repeatability

The effect that the number of data points had on the curvature of Mode 1 is seen in Figure B.14. Seven data points yielded curvatures that were smoother and more symmetric as compared to mode shapes generated using 9 and 13 data points. It is hypothesized that the primary cause of the reduction in smoothness and symmetry for the 9 and 13 data point experiments may be caused by a variation in the data due to a lack of precision of the experimental procedure. Here precision refers to the ability to accurately center the impact hammer's tip with the impact locations. The current experimental procedure requires the experimenter to reposition the impact hammer at each impact location. If, for example at Location 4 the hammer was positioned slightly to the left or right and the specimen impacted, the resulting data would not be truly accurate for Location 4. The hypothesis being made here is that variations, due to experimental procedure, in the data taken resulted in asymmetrical curvatures for 13 data point experiments (Refer to Figure B.16). It is also hypothesized that specimen inhomogeneities and support interactions caused secondary variations in the data. Here inhomogeneities are rib pattern variations, manufacturer lettering and cross-sectional area differences.

The MAC values for the experimental mode shapes for the rod specimens were computed using Equation (C.1) (See Appendix C for details) and are displayed in Tables B.2 – B.7 and B.9 – B.11. The MAC values for both the #6 and #9 rod specimen are consistently greater than 0.99. This finding indicates a very strong correlation between experimental mode shapes and finite element mode shapes. This finding also indicates that as long as the support locations are kept reasonably close to Locations 2.5 and 7.5 mode shapes will not be effected too much. The repeatability of the experimental procedure is demonstrated by the high MAC values, since support conditions had apparently little effect on mode shapes. It is known that MAC values do not take into account systematic errors such as improper scaling of mode shapes or poor modal analysis of the measured data. However, if significant systematic errors had been present the MAC values would have been lower indicating poor correlation but this eventuality was not the case observed here.

B.4.3. Verification of Free-Free Boundary Assumption

In Tables B.8 and B.12, the MAC values for specimens 6_3 and 9_2 indicate a very strong correlation with the FE results. In the FE model the specimen was modeled as a free-free beam. Computed MAC values, which are greater than 0.99, indicate that the hypothesized free-free experimental boundary condition were closely related to the FE model generated free-free boundary conditions.

B.4.4. Support Interaction

Upon inspection of Figures B.19 and B.20, it appears that the location of the supports has an effect on the damage detection and localization. In the case where the supports are further away from the accelerometer and damage locations (Support condition SC1), the value of the damage indicator is 2. Based a standard normal distribution, $z = 2$ corresponds to a 97.72 % level of significance, indicating that the damage location was clearly detected. Whereas in the case where the supports are closer to the accelerometer and damage locations (Support condition SC2), the damage indicator value is negative which is an indication that the damage was clearly undetectable. The discrepancy

between support locations is probably due to boundary movement during the test and signal dampening by the supports.

B.4.5. Verification of Concept

The results of Experiment 1 (Refer to Figure B.15) verified the proof of concept by detecting a 1/8 inch defect using the current NDD algorithm. Subsequent experiments (refer to Figures B.16 through B.27) showed repeatability of results. The current NDD algorithm was able to detect defects as small as 0.02 inches and 1/32 inches in both #6 and #9 specimens. If we consider a defect size to rod diameter ratio (r), our current value for $r = (0.02 \text{ inches}) / (0.75 \text{ inches}) = 0.026$. Where the defect size is 0.02 inches and the nominal diameter of a #6 specimen is 0.75 inches. For the #9 rod, the $r = 0.02 / 1.125 = 0.0178$. Figure B.27 shows that the current NDD concept was applicable to welded specimen ($r = 0.026$). Note that the current algorithm successfully predicted damage at the proper location repeatedly.

B.5. SUMMARY AND CONCLUSIONS

The objective of this experiment was to verify the current field tested NDD algorithm developed at Texas A&M University via laboratory experiment. To meet the objective the following four tasks were performed. First, materials and equipment used in the experiment are described. Second, the experimental configurations were described. Next, the details of the modal tests were described. Finally, the Damage Index Method was employed to localize and estimate the inflicted known damage.

On the basis of the observations on the results from the experiment, the following conclusions are drawn:

1. By decreasing the number of impact points from 13 to 9 improved the curvature of Mode 1. (It is hypothesized that the reduction of impact points reduces the affects of variation in the data due to the experimental procedure used);
2. Initially it was hypothesized that the optimal location for the accelerometer and the damage was the midpoint of the specimen. However, if this configuration had been

used, Modes 2 and 4 would have been of no use, because the midpoint corresponds to a node point for all even modes. By locating the accelerometer and the damage locations at Locations 4 and 6 respectively, allowed the first four bending modes to be used for damage detection and localization. By increasing the number of useable modes (information) to be used for damage detection and localization, the possibility of detecting damage was increased. This finding was witnessed in Experiment 23 which shows Modes 1,2 and 4 correctly predicted the inflicted damage. It is worth mentioning that in Experiment 23, Modes 2 and 4 were very sensitive to the inflicted damage;

3. At this time, the extent of support interaction is not fully understood. However, experimental results indicated that the closer the support locations are to the accelerometer and damage locations, the lower the chances of predicting the inflicted damage;
4. Note that there were support location differences between the baseline and damage configurations. The support location differences were a result of having to remove the specimen and then to re-place the specimen into the supports. Provided that reasonable care is used, experimental results show that small support location differences alone are not sufficient to prevent damage detection.

In conclusion, it has been shown that the current NDD method is sensitive enough to detect damage in both #6 and #9 reinforcing rod specimen. For the #6 specimen, a 0.02 inch defect in both the unwelded and welded beams was detectable. For a unwelded #9 specimen a 1/32 inch defect was detectable.

Table B.1 Experimentation Sequence (UW = Unwelded; W = Welded)

Exp. No.	Specimen	Configuration	Damage Magnitude	Objectives of Test	Results of Tests
1 – 1c	S_1	UW	1/8”(3.2mm), 1/4”(6.4mm) 3/8”(9.6mm)	Collect baseline and damaged mode shapes. Verify proof of concept.	Successful for all 3 damages
2 – 2a	S_2	UW	1/16” (1.6mm) 1/14” (1.8mm)	Collect baseline and damaged mode shapes. Verify proof of concept.	Successful for both damages
3 – 3b	S_2	UW	1/14” (1.8 mm)	Retest of S_2 with same size damage. Confirm repeatability.	Successful
4 – 4a	6_3	UW	1/32” (0.8 mm)	Collect baseline and damaged mode shapes. Verify proof of concept.	Successful
5 – 5a	6_3a	UW	1/32” (0.8 mm)	Collect baseline and damaged mode shapes. Verify proof of concept.	Successful
6	6_3 6_3a	UW	1/32” (0.8 mm)	Confirm repeatability.	Successful for both.
7 – 7a	6_3	UW	1/32” (0.8 mm)	To determine if changing boundary locations has an affect on mode shapes and damage detection.	Boundary location has an affect.
9 – 9c	6_1	UW	0.02” (0.5 mm)	Collect baseline and damage mode shapes with different boundary locations for the same specimen. Verify proof of concept.	Successfully detected damage Successful with boundary
9d	6_1	UW	0.02” (0.5 mm)	Confirm repeatability.	Successful
10	6_2	UW	None	Collect baseline mode shapes.	Successful
11	6_4	UW	None	Collect baseline mode shapes.	Successful
12 – 12f	9_2	UW	1/32” (0.8 mm) 0.02” (0.5 mm)	Collect baseline and damaged mode shapes. Verify proof of concept.	Successful

Table B.1 (continued)

Exp. No.	Specimen	Configuration	Damage Magnitude	Objectives of Test	Results of Tests
13 – 13a	6_3	W	None	Collect baseline mode shapes of welded specimen.	Successful
	9_1	UW	1/32” (0.8 mm)	Collect baseline and damaged mode shapes. Verify proof of concept.	Not successful
14 – 14a	6_3	W	0.02” (0.5 mm)	Collect damaged welded mode shapes. Verify proof of concept.	Not successful
	9_3	UW	None	Collect baseline and damaged mode shapes. Verify proof of concept.	Successful
15	6_3	W	1/32” (0.8 mm)	Verify proof of concept	Not successful
16	6_3	W	0.04” (1 mm)	Verify proof of concept	Not successful
18, 21 & 23	6_1	W	0.02” (0.5 mm)	Collect welded baseline. Verify proof of concept. Verify repeatability.	Successful Successful Successful

Table B.2 Modal Assurance Criteria for Specimen 6_3 and 6_1

Mode	1 (6_1)	2 (6_1)	3 (6_1)	4 (6_1)
1 (6_3)	0.9992	0.0001	0.1349	0.0012
2 (6_3)	0.0006	0.9985	0.0003	0.1585
3 (6_3)	0.1512	0.0011	0.9983	0.0013
4 (6_3)	0.0022	0.1678	0.0032	0.9978

Table B.3 Modal Assurance Criteria for Specimen 6_3 and 6_2

Mode	1 (6_2)	2 (6_2)	3 (6_2)	4 (6_2)
1 (6_3)	0.9993	0.0001	0.1596	0.0002
2 (6_3)	0.0001	0.9983	0.0033	0.1797
3 (6_3)	0.1519	0.0004	0.9935	0.0002
4 (6_3)	0.0016	0.1603	0.0006	0.9934

Table B.4 Modal Assurance Criteria for Specimen 6_3 and 6_4

Mode	1 (6_4)	2 (6_4)	3 (6_4)	4 (6_4)
1 (6_3)	0.9997	0.0002	0.1470	0.0024
2 (6_3)	0.0001	0.9989	0.0000	0.1637
3 (6_3)	0.1494	0.0010	0.9992	0.0024
4 (6_3)	0.0013	0.1672	0.0039	0.9983

Table B.5 Modal Assurance Criteria for Specimen 6_1 and 6_2

Mode	1 (6_2)	2 (6_2)	3 (6_2)	4 (6_2)
1 (6_1)	0.9998	0.0001	0.1618	0.0000
2 (6_1)	0.0003	0.9994	0.0007	0.1811
3 (6_1)	0.1384	0.0000	0.9953	0.0000
4 (6_1)	0.0016	0.1538	0.0002	0.9948

Table B.6 Modal Assurance Criteria for Specimen 6_1 and 6_4

Mode	1 (6_4)	2 (6_4)	3 (6_4)	4 (6_4)
1 (6_1)	0.9998	0.0012	0.1498	0.0039
2 (6_1)	0.0003	0.9998	0.0007	0.1664
3 (6_1)	0.1359	0.0002	0.9994	0.0033
4 (6_1)	0.0013	0.1602	0.0026	0.9995

Table B.7 Modal Assurance Criteria for Specimen 6_2 and 6_4

Mode	1 (6_4)	2 (6_4)	3 (6_4)	4 (6_4)
1 (6_2)	0.9998	0.0005	0.1505	0.0031
2 (6_2)	0.0000	0.9990	0.0002	0.1587
3 (6_2)	0.1605	0.0008	0.9947	0.0008
4 (6_2)	0.0001	0.1803	0.0000	0.9932

Table B.8 Modal Assurance Criteria for #6 FE Model and Specimen 6_3

Mode	1 (6_3)	2 (6_3)	3 (6_3)	4 (6_3)
1 (FE)	0.9983	0.0000	0.1552	0.0007
2 (FE)	0.0001	0.9972	0.0018	0.1823
3 (FE)	0.1494	0.0017	0.9965	0.0021
4 (FE)	0.0001	0.1585	0.0000	0.9953

Table B.9 Modal Assurance Criteria for Specimens 9_1 and 9_2

Mode	1 (9_2)	2 (9_2)	3 (9_2)	4 (9_2)
1 (9_1)	0.9997	0.0001	0.1376	0.0000
2 (9_1)	0.0000	0.9995	0.0001	0.1542
3 (9_1)	0.1368	0.0001	0.9997	0.0006
4 (9_1)	0.0000	0.1511	0.0001	0.9995

Table B.10 Modal Assurance Criteria for Specimens 9_1 and 9_3

Mode	1 (9_3)	2 (9_3)	3 (9_3)	4 (9_3)
1 (9_1)	0.9993	0.0001	0.1455	0.0002
2 (9_1)	0.0001	0.9986	0.0000	0.1599
3 (9_1)	0.1325	0.0000	0.9977	0.0000
4 (9_1)	0.0000	0.1425	0.0002	0.9975

Table B.11 Modal Assurance Criteria for Specimens 9_2 and 9_3

Mode	1 (9_3)	2 (9_3)	3 (9_3)	4 (9_3)
1 (9_2)	0.9997	0.0003	0.1512	0.0001
2 (9_2)	0.0001	0.9994	0.0000	0.1623
3 (9_2)	0.1390	0.0000	0.9986	0.0000
4 (9_2)	0.0000	0.1482	0.0000	0.9984

Table B.12 Modal Assurance Criteria for #9 FE Model and Specimen 9_2

Mode	1 (9_2)	2 (9_2)	3 (9_2)	4 (9_2)
1 (FE)	0.9997	0.0003	0.1484	0.0001
2 (FE)	0.0000	0.9994	0.0003	0.1638
3 (FE)	0.1490	0.0000	0.9991	0.0007
4 (FE)	0.0000	0.1622	0.0001	0.9986

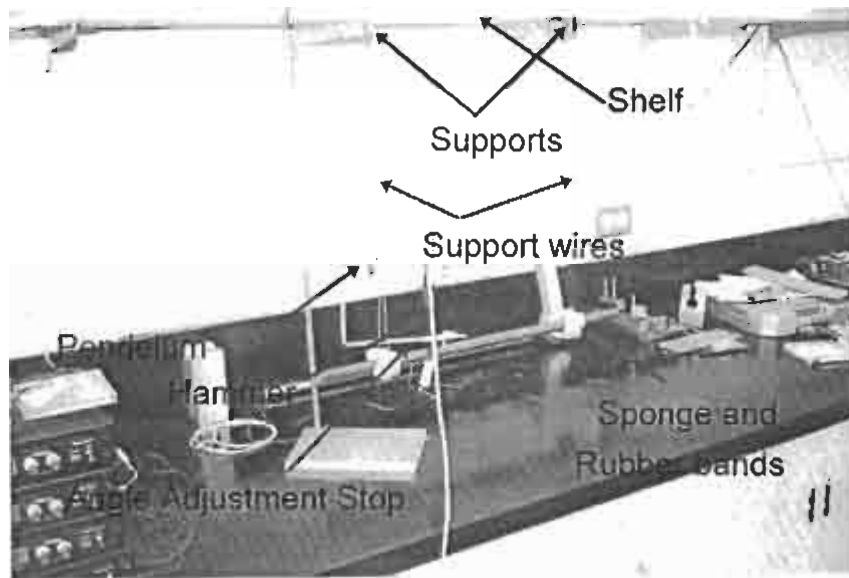


Figure B.1 Supports and Pendulum

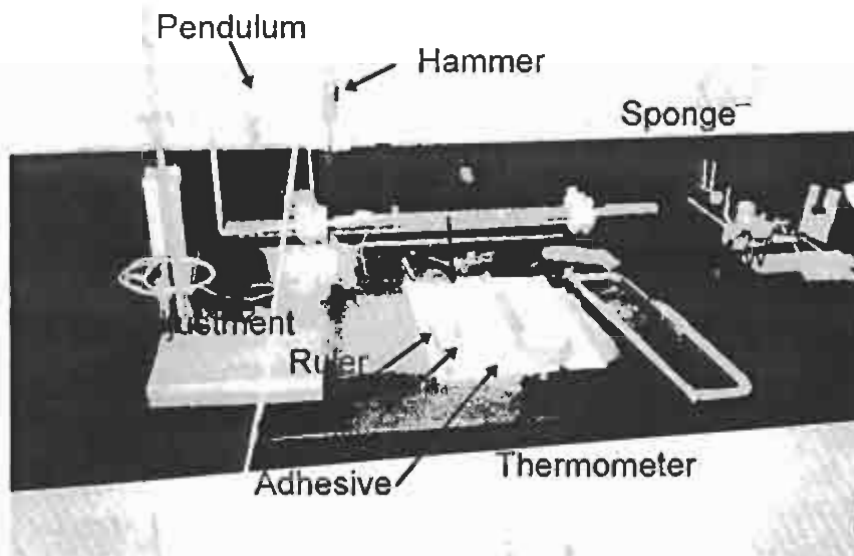


Figure B.2 Pendulum and Materials Used

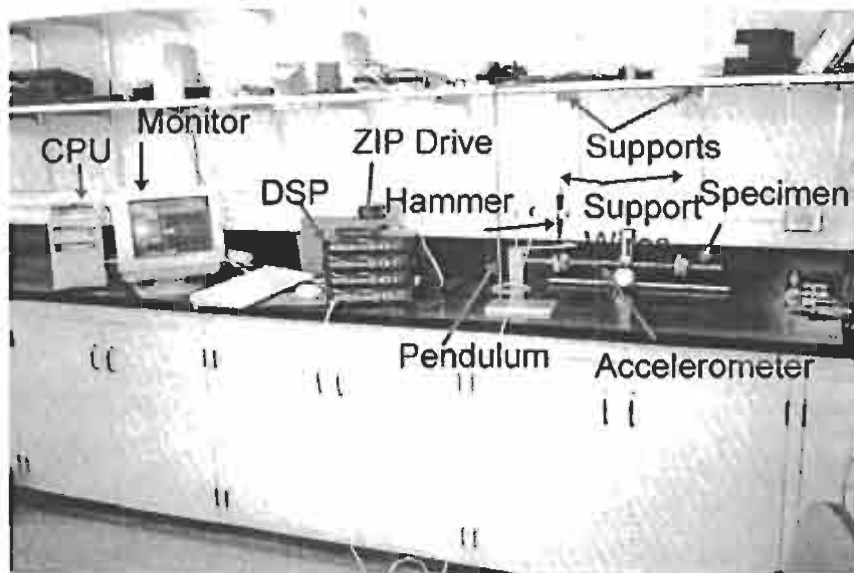


Figure B.3 Equipment and Setup

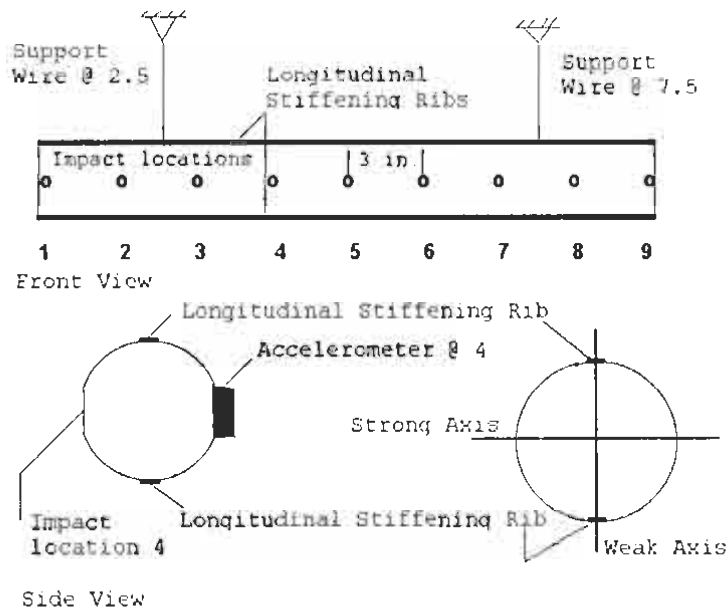


Figure B.4 Weak and Strong Axis

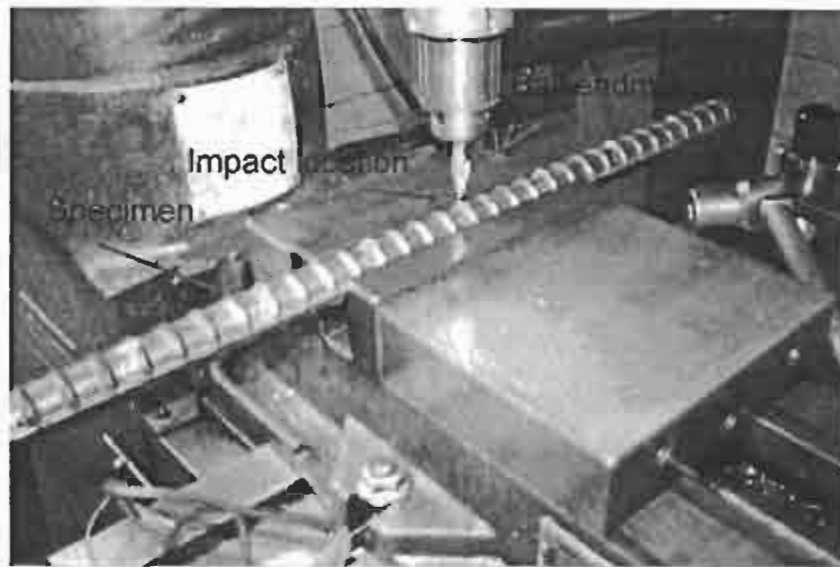


Figure B.5 Milling out Impact and Accelerometer Locations

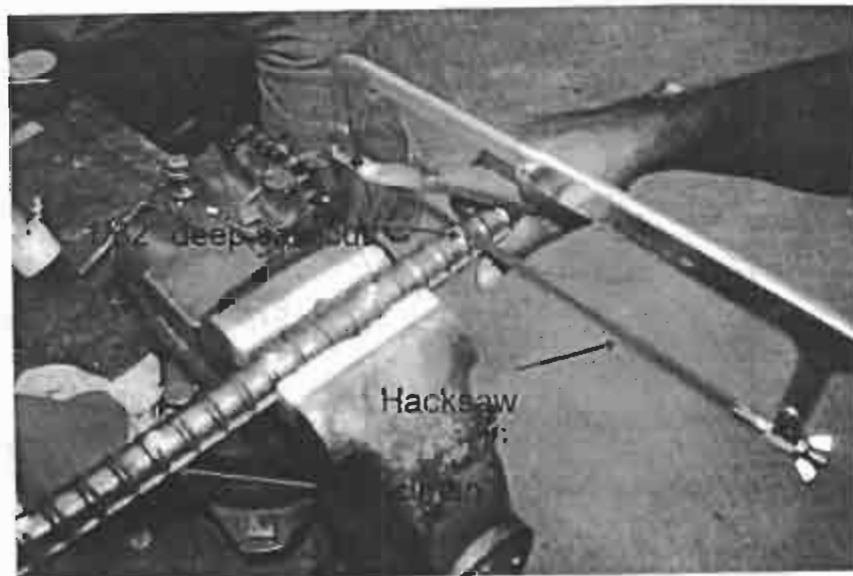


Figure B.6 Inflicting Damage with Hacksaw

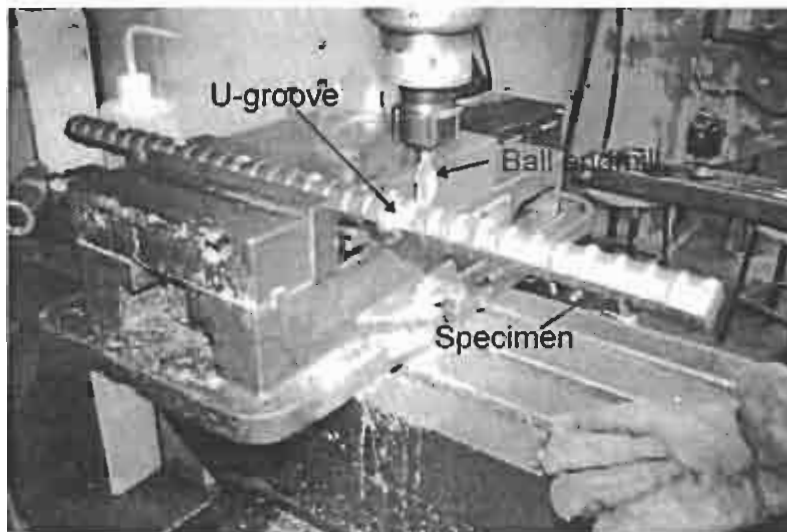


Figure B.7 Milling out U-groove for Weld Joint



Figure B.8 Welding of Joint Using GMAW (ER70S-6)

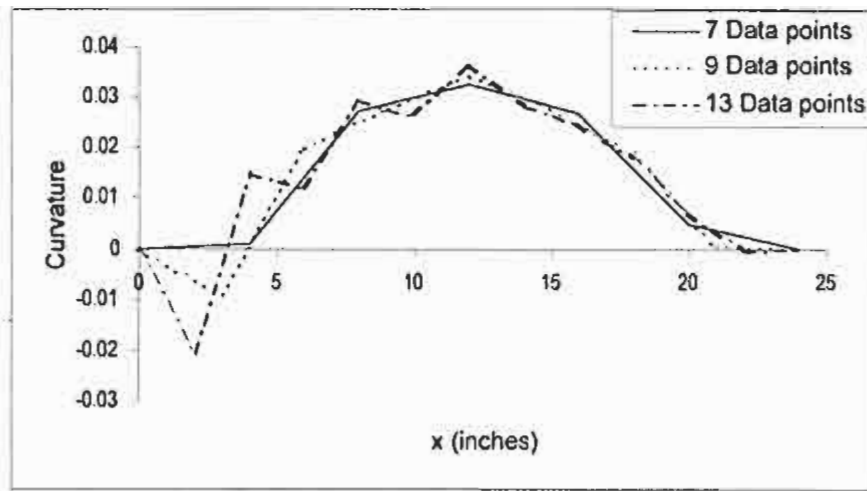


Figure B.9 Effect of Random Vibration in the Data on Mode 1 Curvatures

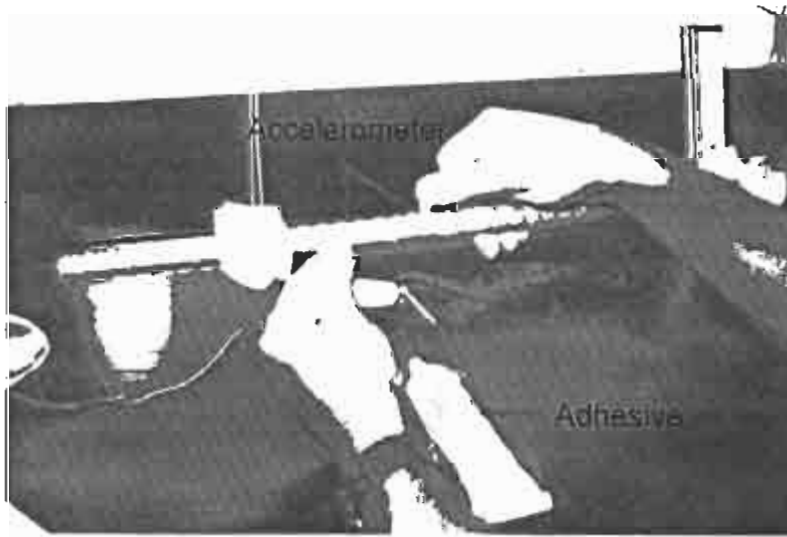


Figure B.10 Accelerometer Attachment



Figure B.11 Conducting Modal Test



Figure B.12 Catching Hammer after Impact



Figure B.13 Dampening out Vibrations between Impacts

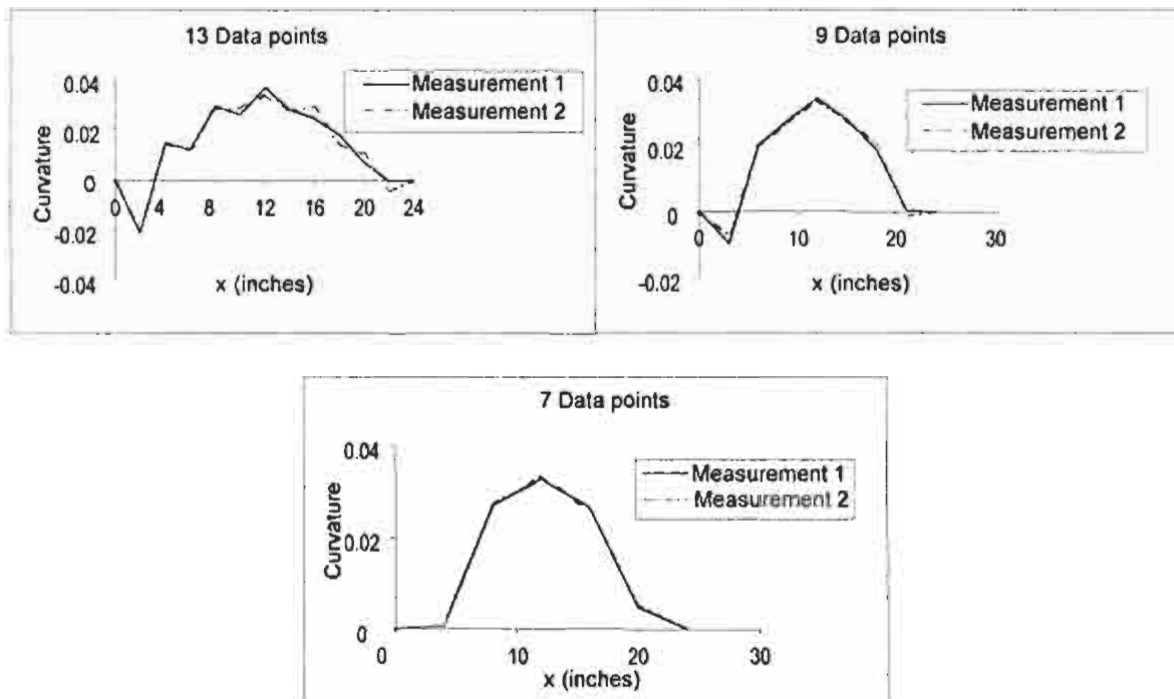


Figure B.14 Effect on Mode 1 Curvatures due to Variation in the Data Caused by the Experimental Procedure

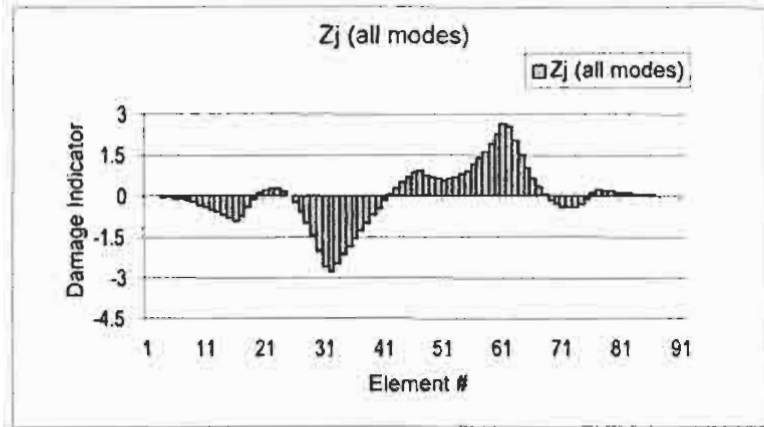


Figure B.15 Damage Localization for Specimen S_1 with 1/8 inch Deep Saw Cut

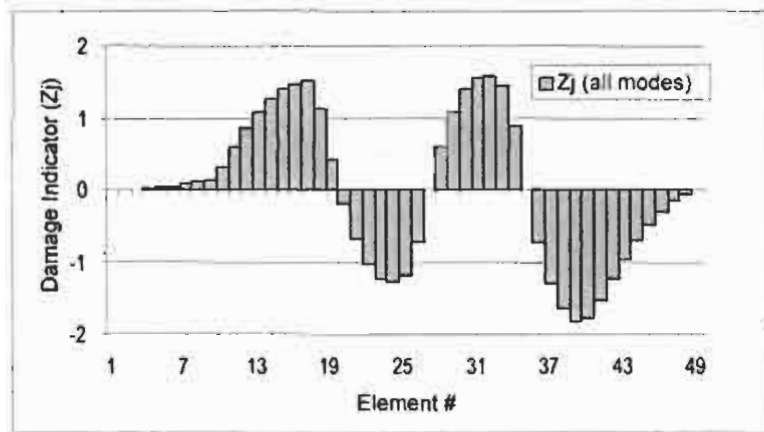


Figure B.16 Damage Localization for Specimen S_2 with 1/16 inch Deep Saw Cut

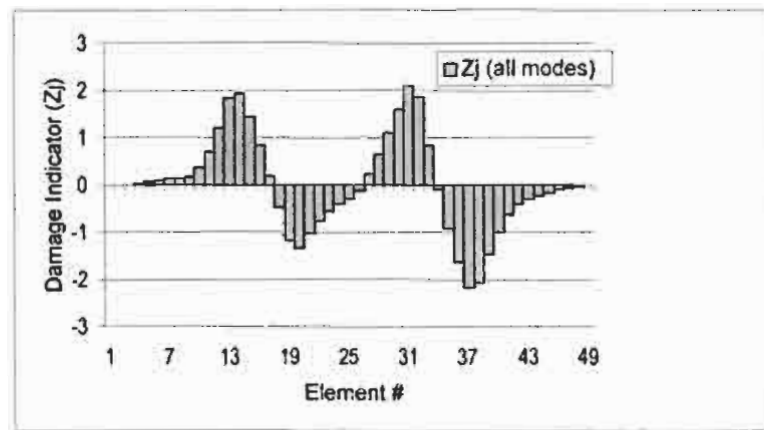


Figure B.17 Damage Localization for Specimen 6_3 with 1/32 inch Deep Saw Cut

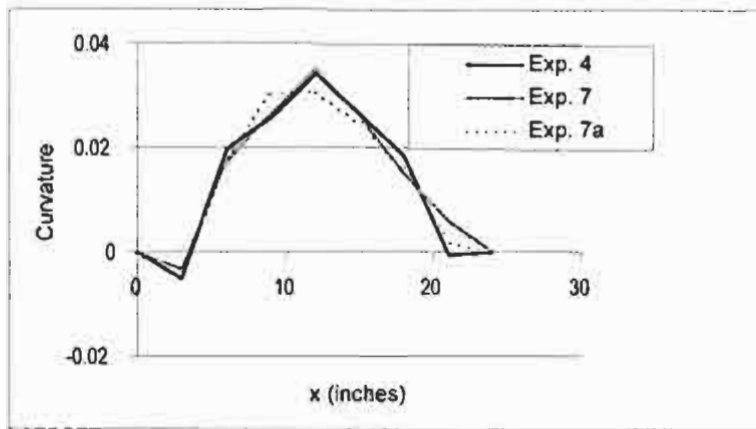


Figure B.18 Mode 1 Symmetry Comparison between Experiment 4, 7, and 7a

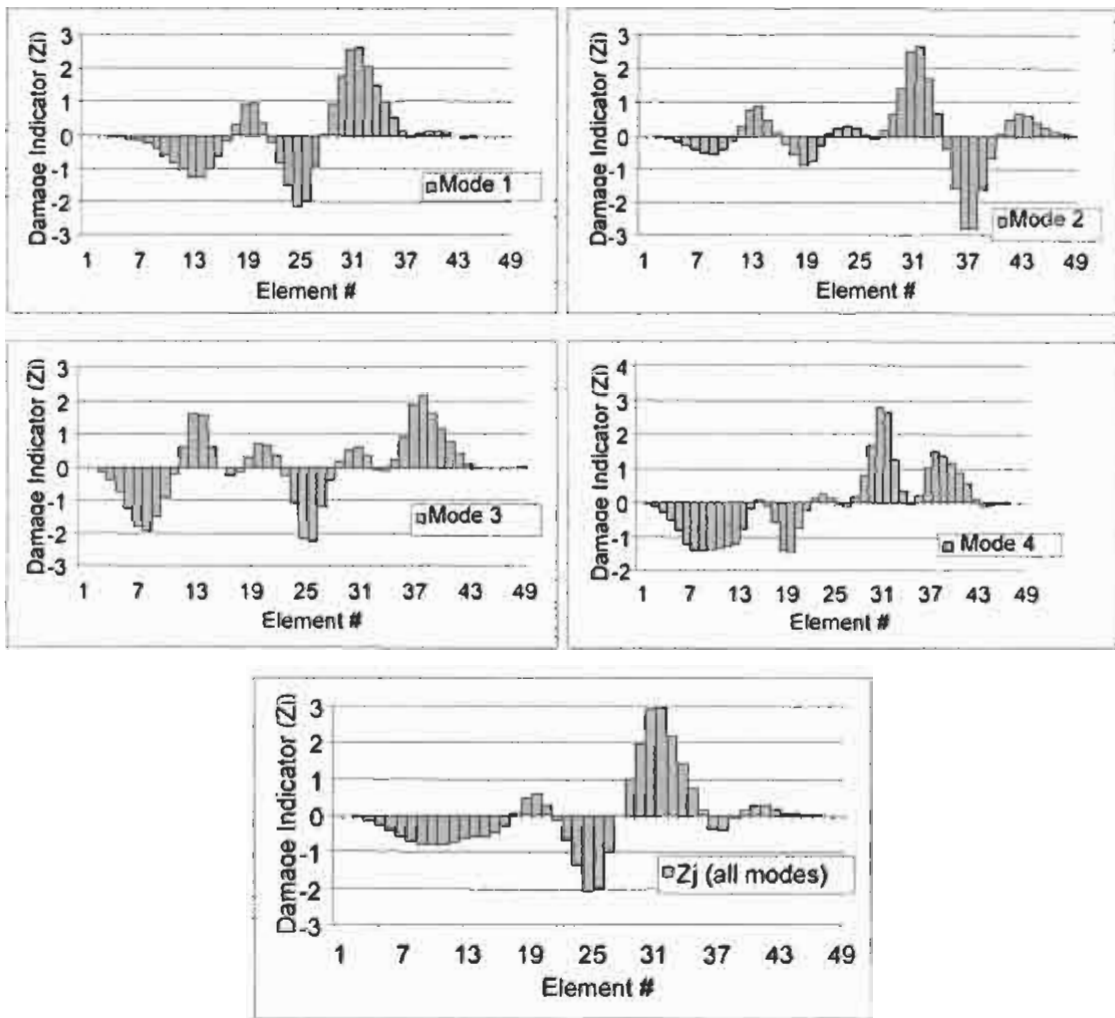


Figure B.19 Damage Localization for Specimen 6_1 for SC1 (Locations 2.5 and 7.5) with Deep 0.02 inch Saw Cut

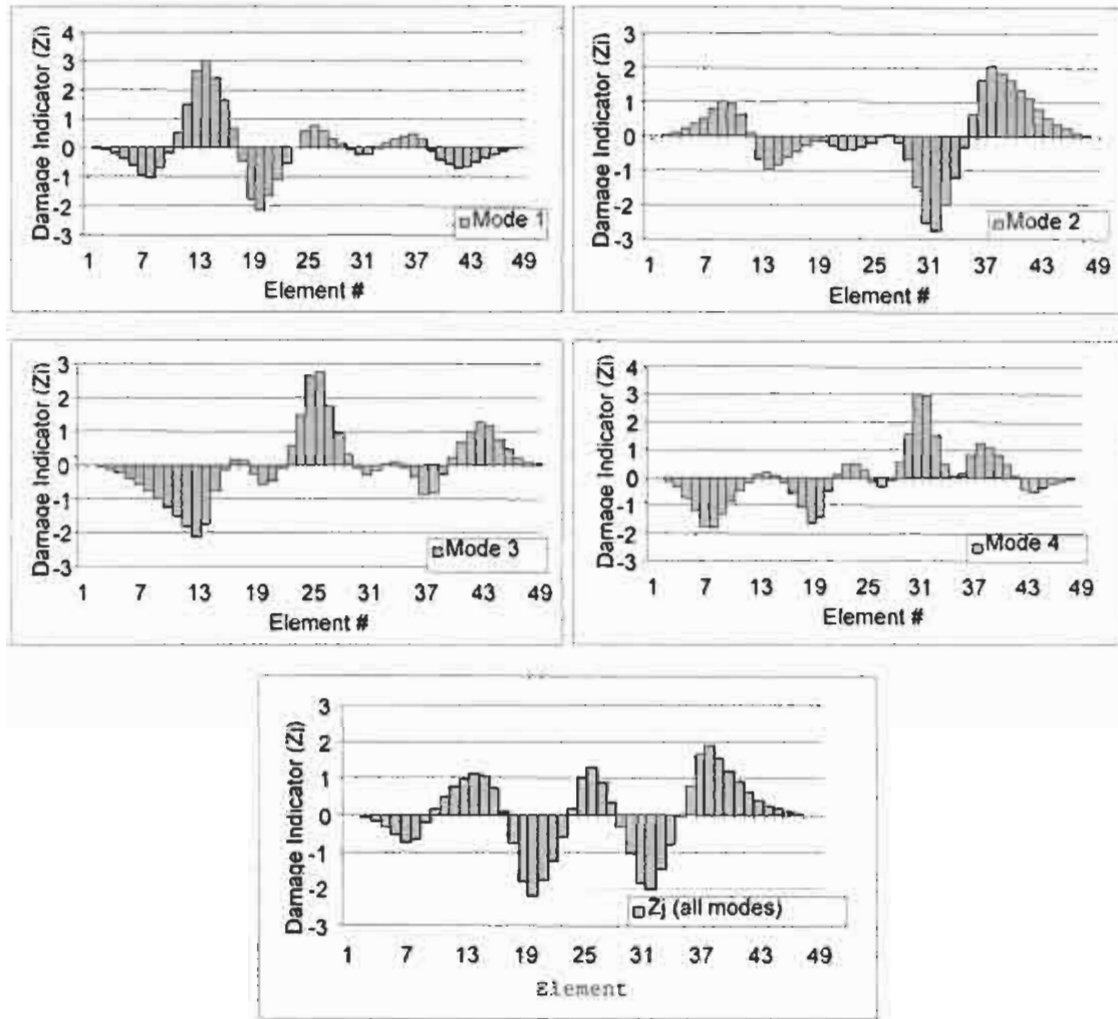


Figure B.20 Damage Localization for Specimen 6_1 for SC2 (Locations 3.5 and 6.5) with 0.02 inch Deep Saw Cut

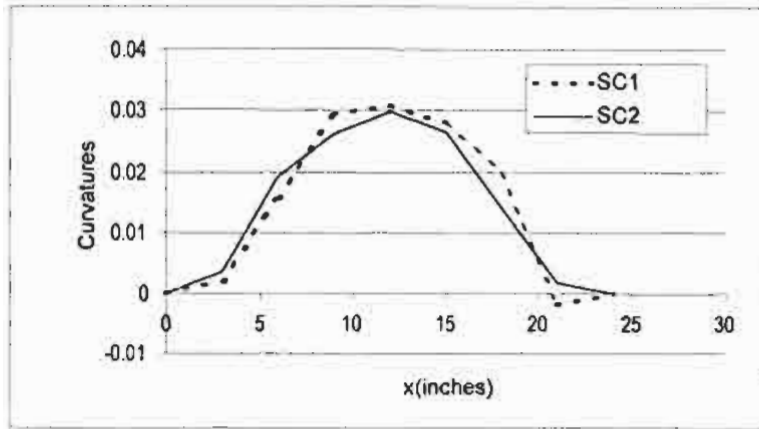


Figure B.21 Mode 1 Curvatures for Specimen 6_1 from Experiments 9b and 9c for SC1 and SC2 with 0.02 inch Deep Saw Cut

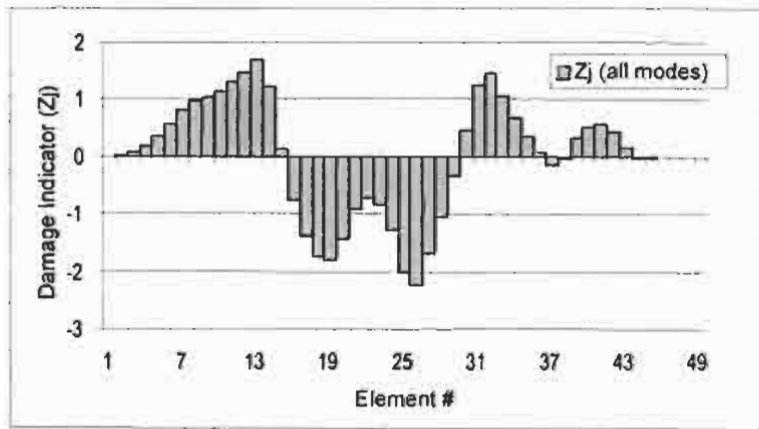


Figure B.22 Damage Localization for Specimen 9_2 with 0.02 inch Deep Saw Cut

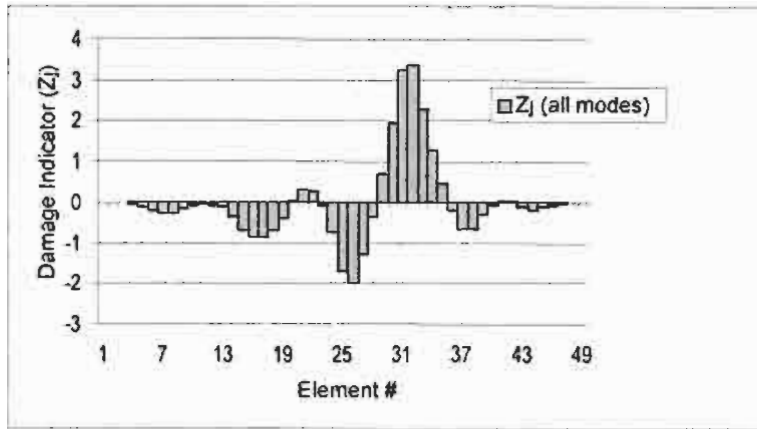


Figure B.23 Damage Localization for Specimen 9_2 with 1/32 inch Deep Saw Cut

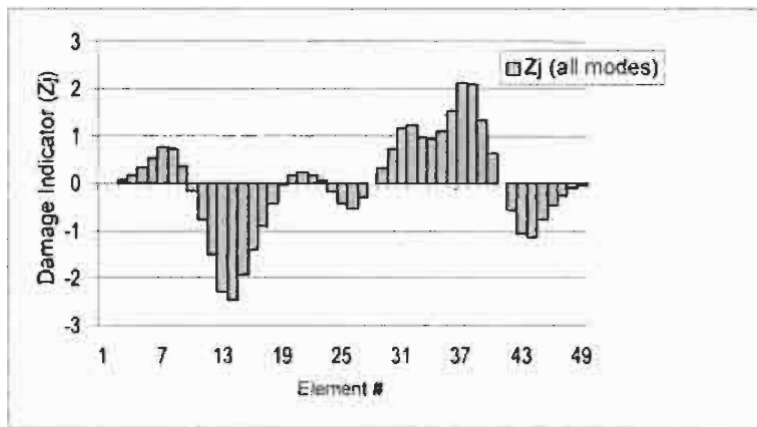


Figure B.24 Damage Localization for Specimen 9_3 with 1/32 inch Deep Saw Cut

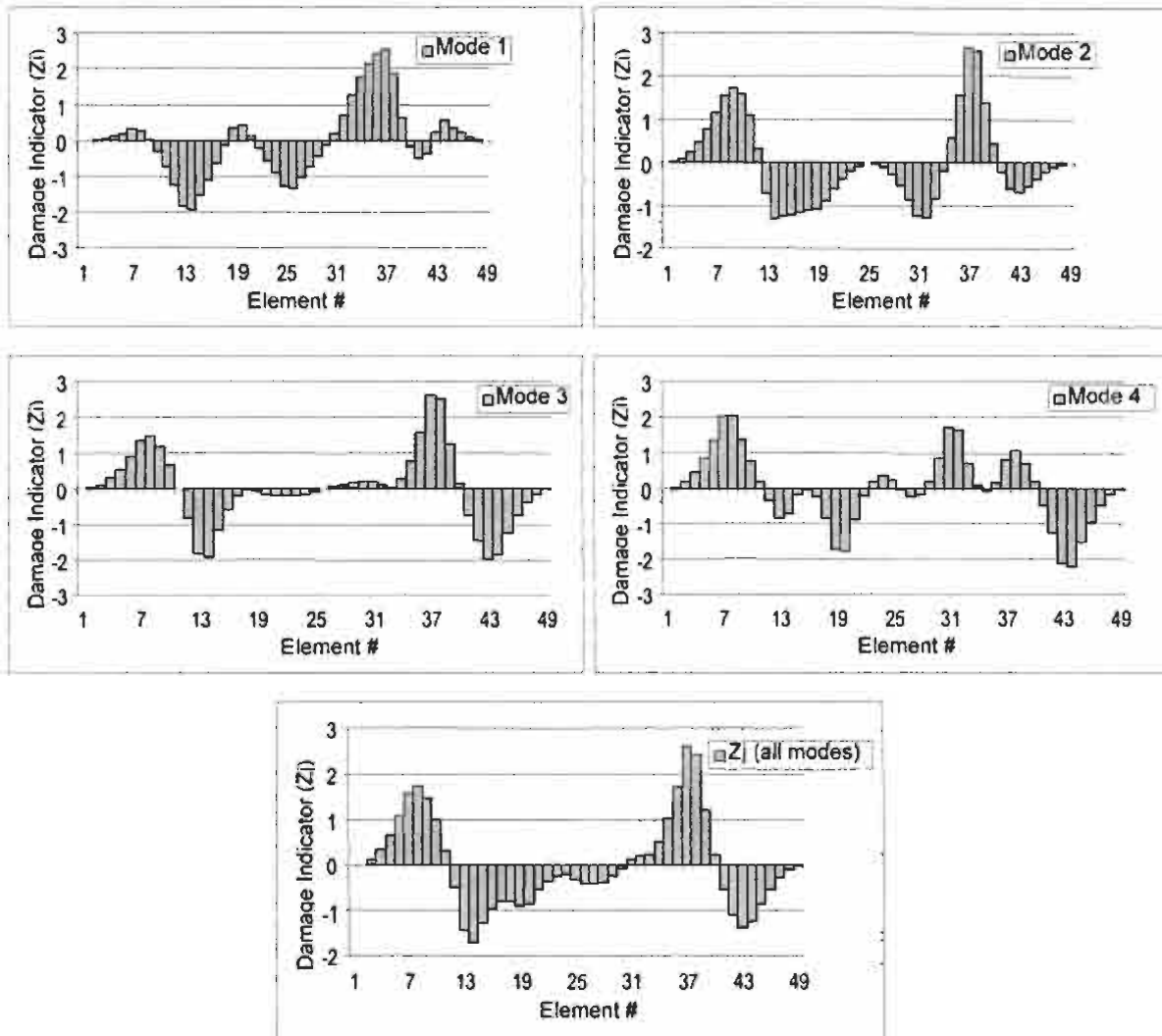


Figure B.25 Damage Localization for Welded Specimen 9_3 with 1/32 inch Deep Saw Cut

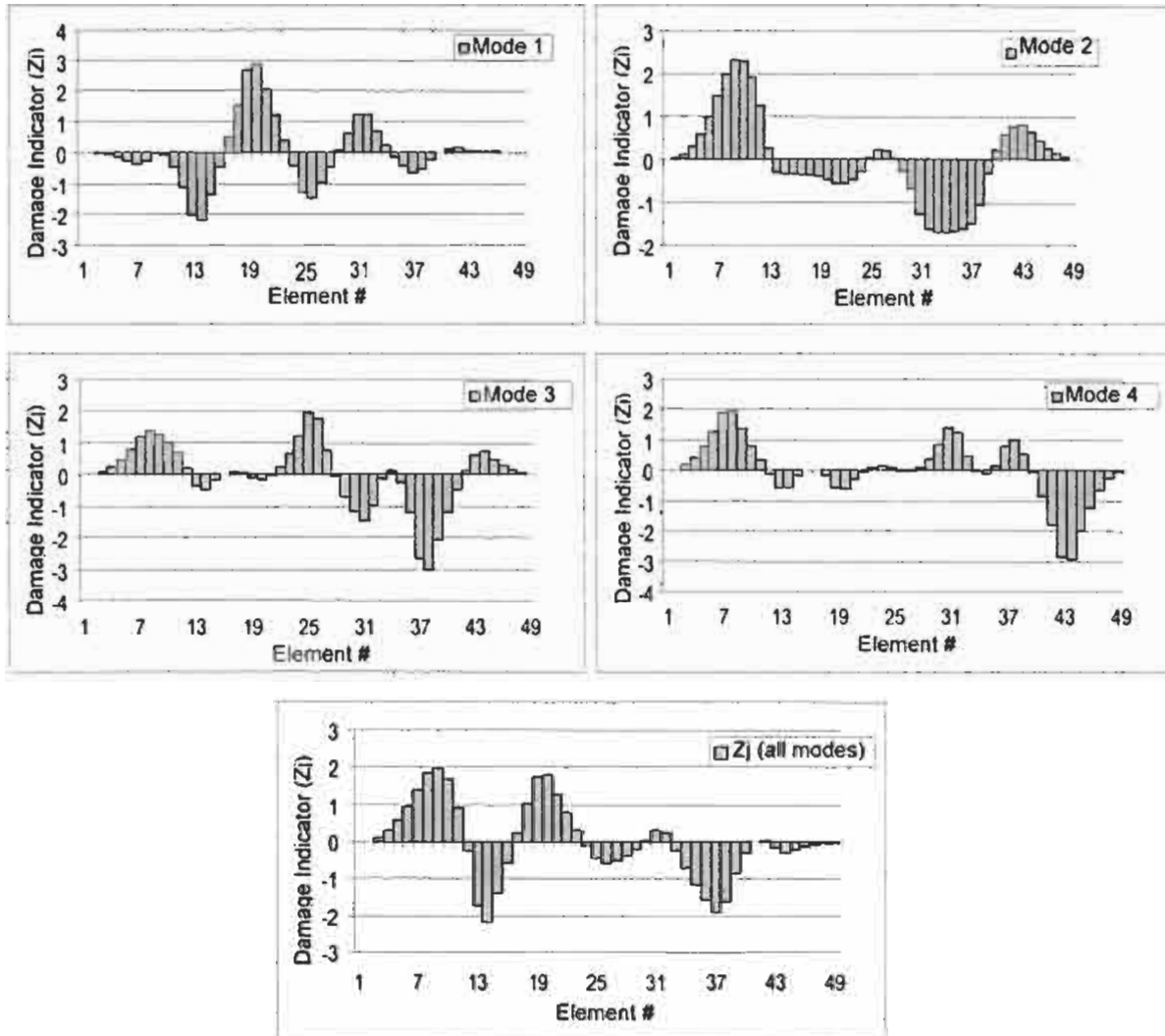


Figure B.26 Damage Localization for Welded Specimen 6_3 with 0.04 inch Deep Saw Cut

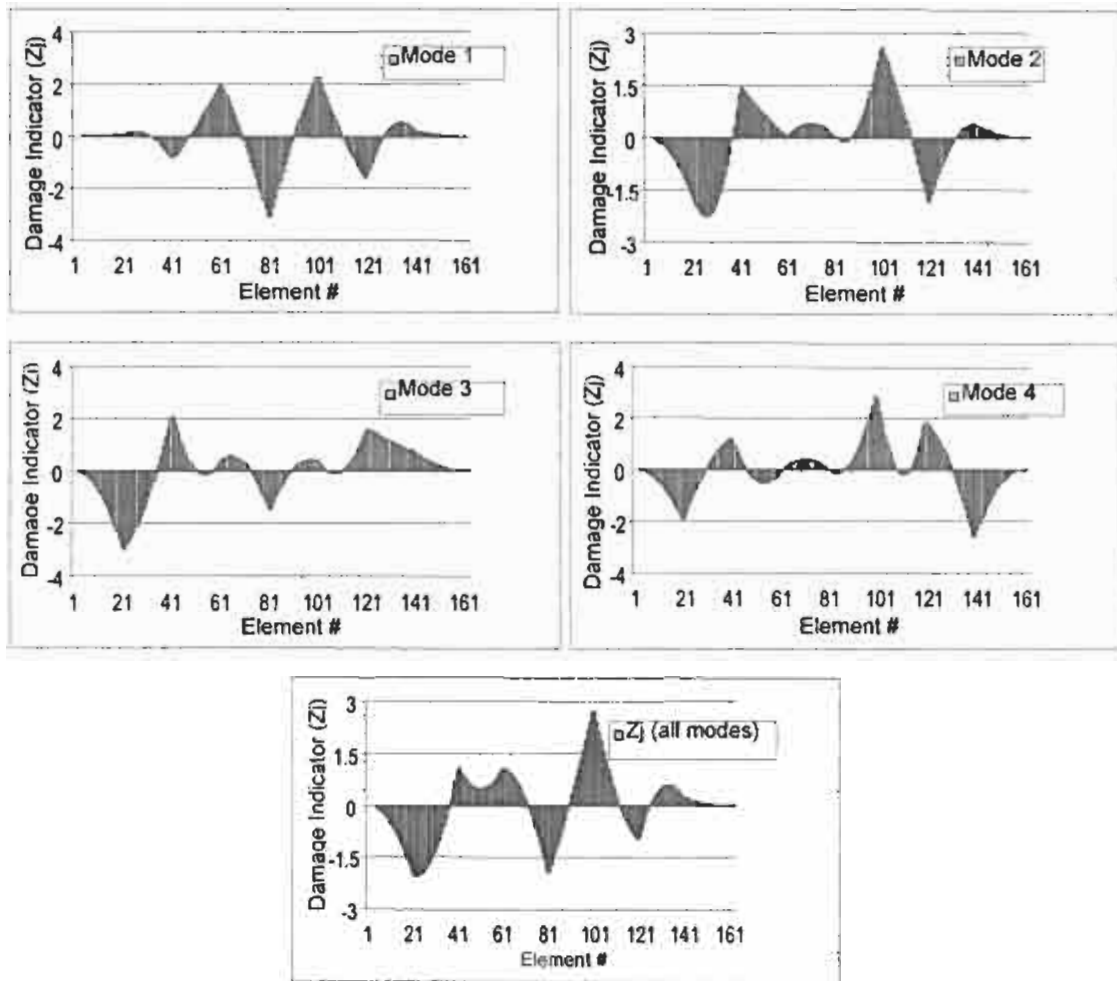


Figure B.27 Damage Localization for Welded Specimen 6_1 with 0.02 inch Deep Saw Cut

APPENDIX C

MODAL ANALYSIS AND SYSTEM IDENTIFICATION RESULTS FOR REINFORCING ROD SPECIMENS

C.1. MODAL ANALYSIS RESULTS FOR FIELD WELDMENTS

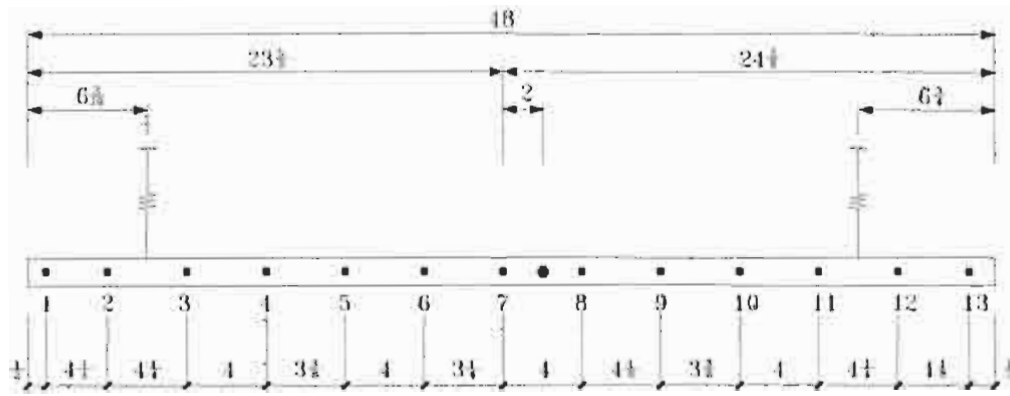
The results of modal analysis performed on the thirty reinforcing rod specimens discussed in Chapters 3 through 5 are presented here. Figures C.1 through C.10 present the results for the #14 specimens. Dimensions shown at the top of the figure include the specimen length and the locations of the response sensors and impact points. The table at the bottom of the figure presents extracted resonant frequencies and modal amplitudes of first five bending modes. The results for #11 and #8 specimens are presented in Figures C.11 through C.20 and Figures C.21 through C.30, respectively.

Date: 3/22/2000

Specimen: #14 Unwelded

of Average: 10

Sensitivity: Ch1 (Hammer: 10V) Ch2 (Accelerometer: 0.16V)



- : accel location
- : impact locations

Unit = inch

Location	Mode 1 124.375 Hz	Mode 2 339.375 Hz	Mode 3 660.625 Hz	Mode 4 1081.25 Hz	Mode 5 1595.625 Hz
1	1.276329	-1.145695	-7.522711	2.625223	9.989457
2	0.719392	-0.294250	0.320810	-0.840936	-5.671723
3	0.194711	0.406394	5.084199	-1.945810	-5.179162
4	-0.229361	0.773209	4.605553	-0.196035	5.849179
5	-0.513026	0.787481	0.963348	1.682112	7.858977
6	-0.733816	0.474287	-4.000925	1.904190	-2.172142
7	-0.806941	0.058728	-5.972417	0.251319	-8.569771
8	-0.737406	-0.468224	-4.058122	-1.897834	-2.327856
9	-0.508710	-0.787823	1.054724	-1.672288	7.956505
10	-0.220214	-0.766168	4.621854	0.238485	5.625322
11	0.203921	-0.394456	5.006230	1.983516	-5.270992
12	0.719013	0.311202	0.143028	0.779231	-5.363556
13	1.236178	1.124022	-7.294550	-2.626894	9.702783

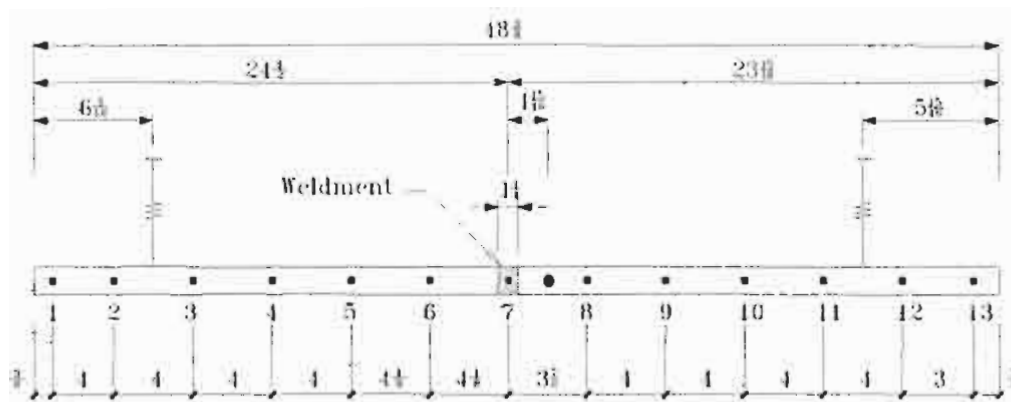
Figure C.1 Modal Analysis Reporting Sheet for #14 Unwelded Reinforcing Rod Specimen

Date: 2/11/2000

Specimen: #14 BP1

of Average: 10

Sensitivity: Ch1 (Hammer: 10V) Ch2 (Accelerometer: 0.16V)



- : accel location
- : impact locations

Unit = inch

Location	Mode 1 124.375 Hz	Mode 2 340.00 Hz	Mode 3 659.375 Hz	Mode 4 1082.50 Hz	Mode 5 1594.375 Hz
1	1.404909	-1.282583	-4.783577	2.931191	4.927509
2	0.929618	-0.486502	-0.325953	-0.800917	-3.399085
3	0.389350	0.344592	3.538561	-2.841161	-5.121664
4	-0.160435	0.946174	4.161955	-1.017281	2.569802
5	-0.584583	1.045914	1.151759	2.265089	6.174643
6	-0.855003	0.668857	-2.948812	2.888652	-0.764019
7	-0.943852	-0.040678	-4.705144	-0.220718	-5.880666
8	-0.827059	-0.718310	-2.611217	-3.037034	0.121370
9	-0.574500	-1.049508	1.272662	-2.249495	6.373253
10	-0.130890	-0.943017	4.405890	1.254697	2.183606
11	0.393484	-0.339983	3.670367	2.942045	-5.291241
12	0.944467	0.530165	-0.495022	0.742080	-3.379922
13	1.472204	1.442209	-5.836123	-3.486152	6.103178

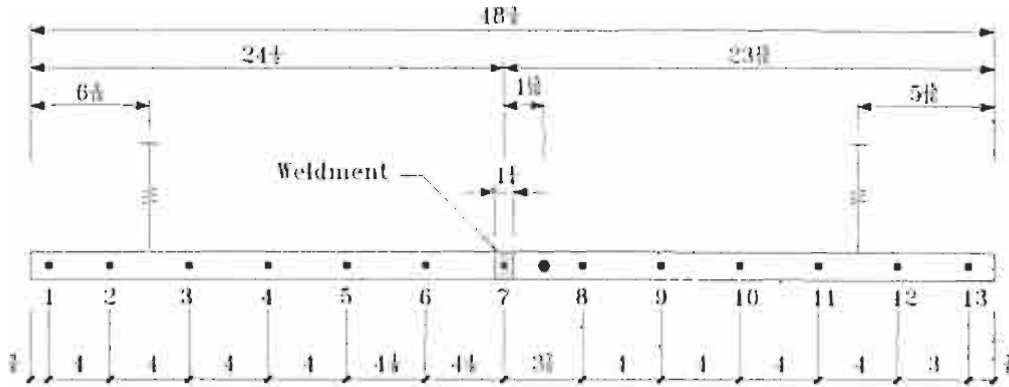
**Figure C.2 Modal Analysis Reporting Sheet for #14 BP1
Reinforcing Rod Specimen**

Date: 2/14/2000

Specimen: #14 BP2

of Average: 10

Sensitivity: Ch1 (Hammer: 10V) Ch2 (Accelerometer: 0.16V)



- : accel location
- : impact locations

Unit = inch

Location	Mode 1 118.75 Hz	Mode 2 327.50 Hz	Mode 3 633.125 Hz	Mode 4 1041.25 Hz	Mode 5 1528.75 Hz
1	1.185648	-1.003541	-5.613608	3.415163	6.707610
2	0.815483	-0.438287	-0.948728	-0.434863	-2.943713
3	0.396632	0.159413	3.254346	-2.998906	-6.601202
4	-0.049163	0.636882	4.647780	-1.794422	1.046932
5	-0.409880	0.777134	2.105518	1.790009	7.433197
6	-0.672038	0.549790	-2.383654	3.277059	1.004603
7	-0.775476	0.064047	-4.841553	0.452969	-6.822301
8	-0.699062	-0.497460	-2.978033	-3.032635	-0.688017
9	-0.479599	-0.768670	1.182918	-2.391609	7.053168
10	-0.205032	-0.739836	3.979064	0.409231	4.624547
11	0.231595	-0.356193	4.116735	2.969395	-4.894674
12	0.713830	0.281216	0.240489	1.305334	-4.843040
13	1.193242	1.018440	-5.672058	-3.494898	7.028580

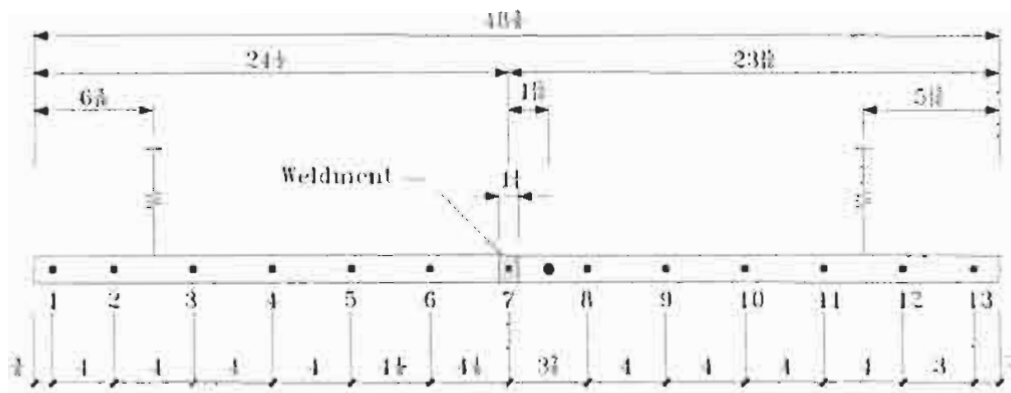
Figure C.3 Modal Analysis Reporting Sheet for #14 BP2 Reinforcing Rod Specimen

Date: 2/14/2000

Specimen: #14 BP3

of Average: 10

Sensitivity: Ch1 (Hammer: 10V) Ch2 (Accelerometer: 0.16V)



- : accel location
- : impact locations

Unit = inch

Location	Mode 1 118.75 Hz	Mode 2 327.50 Hz	Mode 3 633.125 Hz	Mode 4 1041.25 Hz	Mode 5 1528.75 Hz
1	1.274309	-2.021691	-5.337311	4.323769	4.128648
2	0.748864	-0.510144	0.546670	-2.058585	-3.307057
3	0.323412	0.599040	3.857264	-4.108704	-3.693482
4	-0.155644	1.470516	4.362866	-1.452708	2.014722
5	-0.559339	1.584594	0.867044	3.491465	4.361446
6	-0.807500	0.911403	-3.511331	3.810481	-1.355518
7	-0.862795	-0.075399	-4.942903	-0.334971	-4.530640
8	-0.779950	-1.050095	-2.997278	-4.184684	-0.357607
9	-0.513233	-1.625242	1.511559	-3.033541	4.811690
10	-0.084170	-1.384560	4.693422	2.188171	1.163817
11	0.409376	-0.428714	3.590119	4.121020	-4.331180
12	0.809768	0.625243	0.139058	1.689735	-3.161086
13	1.244653	1.871658	-4.863157	-3.635895	3.381602

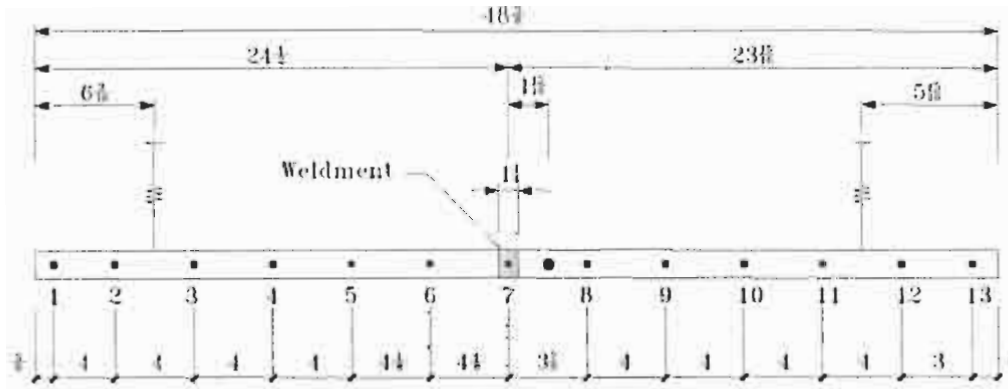
**Figure C.4 Modal Analysis Reporting Sheet for #14 BP3
Reinforcing Rod Specimen**

Date: 2/14/2000

Specimen: #14 PH3

of Average: 10

Sensitivity: Ch1 (Hammer: 10V) Ch2 (Accelerometer: 0.16V)



- : accel location
- : impact locations

Unit = inch

Location	Mode 1 121.875 Hz	Mode 2 334.375 Hz	Mode 3 647.000 Hz	Mode 4 1065.00 Hz	Mode 5 1565.625 Hz
1	1.514647	-2.158968	-5.388621	5.901907	4.646202
2	0.800734	-0.297988	1.386563	-3.981096	-4.748459
3	0.191373	1.037105	4.612207	-5.469604	-2.635669
4	-0.232531	1.642122	4.278944	-1.466827	3.097421
5	-0.720132	1.664884	0.217675	5.668621	4.770097
6	-0.971804	0.905777	-3.780717	5.192900	-2.240653
7	-1.010579	-0.231505	-4.644254	-1.514499	-5.049224
8	-0.863041	-1.342388	-1.943406	-5.990089	1.643481
9	-0.494310	-1.763122	2.644444	-2.521583	5.513736
10	-0.068508	-1.427140	4.688407	3.405508	0.731203
11	0.510405	-0.357132	3.251757	5.349266	-5.034881
12	1.037936	0.909044	-0.719231	1.127673	-2.548647
13	1.552162	2.239238	-5.660893	-6.470678	5.350400

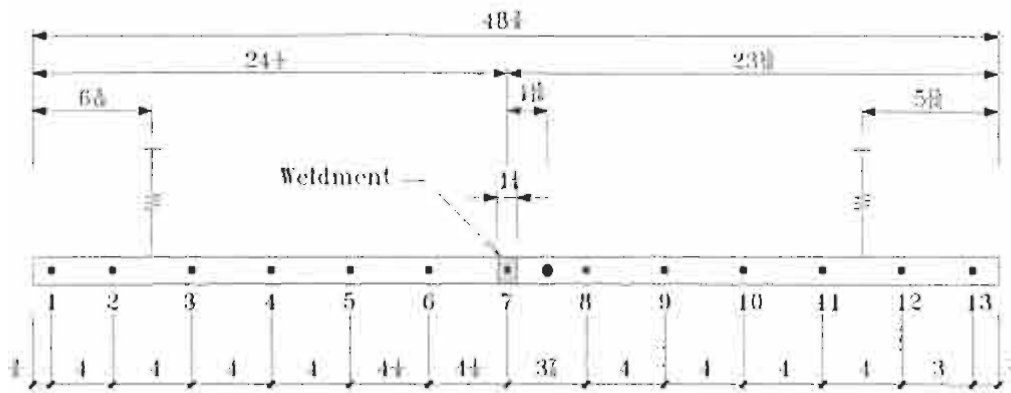
Figure C.5 Modal Analysis Reporting Sheet for #14 PH3 Reinforcing Rod Specimen

Date: 2/15/2000

Specimen: #14 S1

of Average: 10

Sensitivity: Ch1 (Hammer: 10V) Ch2 (Accelerometer: 0.16V)



- : accel location
- : impact locations

Unit = inch

Location	Mode 1 118.75 Hz	Mode 2 327.50 Hz	Mode 3 633.125 Hz	Mode 4 1041.25 Hz	Mode 5 1528.75 Hz
1	1.176926	-1.630588	-4.307001	4.066268	3.683925
2	0.653647	-0.310681	0.795598	-2.442919	-3.395014
3	0.258142	0.557444	3.370062	-4.119456	-3.122748
4	-0.185521	1.207444	3.347150	-0.811856	2.634397
5	-0.521489	1.232227	0.406483	3.782482	3.901730
6	-0.718298	0.711503	-2.810562	3.757185	-1.384498
7	-0.773375	-0.121148	-3.819561	-0.744497	-3.994191
8	-0.684143	-0.848672	-2.129720	-4.116724	0.070441
9	-0.415389	-1.269331	1.630299	-2.314063	4.215388
10	-0.075136	-1.059278	3.542783	2.100654	0.913459
11	0.390728	-0.259687	2.502427	3.814889	-3.705138
12	0.785881	0.631100	-0.429662	0.947805	-2.033865
13	1.148283	1.548830	-3.902781	-3.858491	3.208955

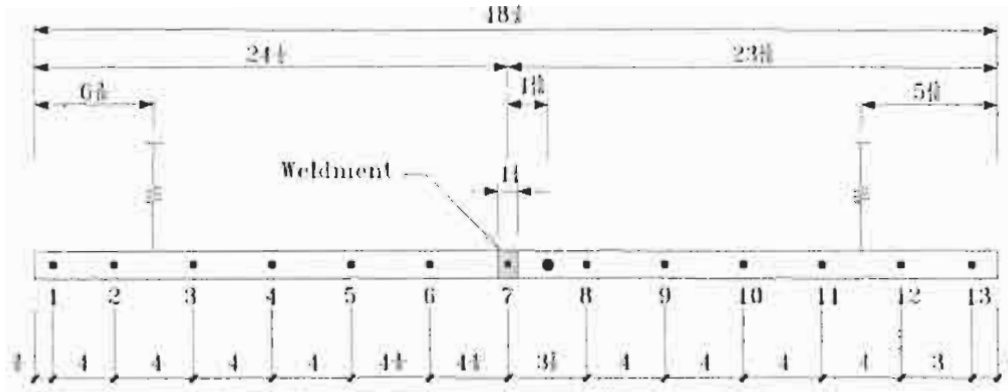
**Figure C.6 Modal Analysis Reporting Sheet for #14 S1
Reinforcing Rod Specimen**

Date: 2/16/2000

Specimen: #14 S2

of Average: 10

Sensitivity: Ch1 (Hammer: 10V) Ch2 (Accelerometer: 0.16V)



- : accel location
- : impact locations

Unit = inch

Location	Mode 1 118.75 Hz	Mode 2 327.50 Hz	Mode 3 633.125 Hz	Mode 4 1041.25 Hz	Mode 5 1528.75 Hz
1	1.461763	-1.095001	-6.089436	2.897752	8.917595
2	0.880165	-0.298082	0.427110	-1.286041	-6.319191
3	0.432832	0.251212	4.144212	-2.791844	-8.181819
4	-0.064847	0.716247	5.310952	-1.673344	1.375179
5	-0.524442	0.877529	2.451770	1.595983	9.519840
6	-0.852113	0.648255	-2.489347	2.987455	1.962129
7	-0.996686	0.134371	-5.466800	0.803214	-8.761017
8	-0.953018	-0.405148	-4.514275	-2.264385	-4.952101
9	-0.704257	-0.823852	0.155462	-2.701124	8.051594
10	-0.290731	-0.837715	4.441241	0.218061	6.865249
11	0.279139	-0.415344	4.847935	2.798042	-6.303506
12	0.923516	0.327812	0.218970	1.194587	-6.416607
13	1.542556	1.162459	-6.631076	-3.343786	10.785730

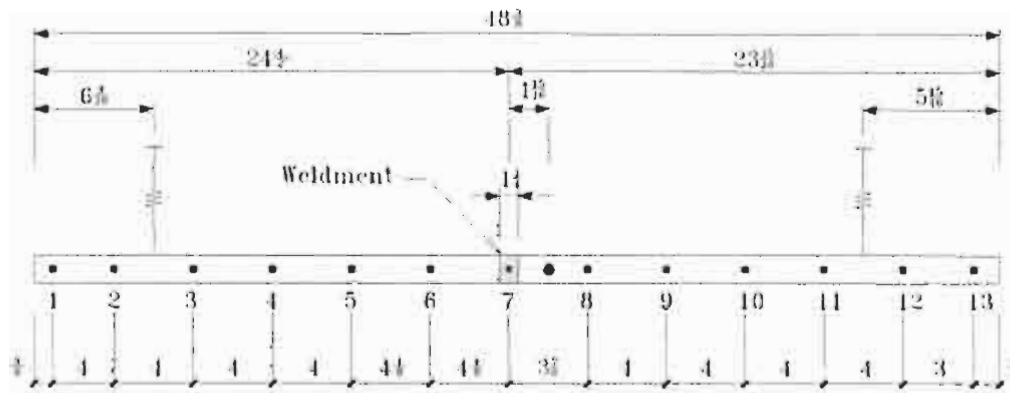
**Figure C.7 Modal Analysis Reporting Sheet for #14 S2
Reinforcing Rod Specimen**

Date: 2/15/2000

Specimen: #14 S3

of Average: 10

Sensitivity: Ch1 (Hammer: 10V) Ch2 (Accelerometer: 0.16V)



- : accel location
- : impact locations

Unit = inch

Location	Mode 1 122.50 Hz	Mode 2 335.625 Hz	Mode 3 651.25 Hz	Mode 4 1066.875 Hz	Mode 5 1573.125 Hz
1	1.267950	-0.858566	-5.049547	2.503551	6.332195
2	0.842709	-0.306157	-0.145108	-0.870515	-4.701522
3	0.311583	0.275413	3.942708	-2.591585	-6.116153
4	0.095444	0.593356	4.474490	-1.291559	2.154899
5	-0.514285	0.690004	1.454120	1.907996	7.954417
6	-0.780154	0.443331	-2.940635	2.670783	-0.849622
7	-0.834790	0.032017	-4.638691	0.256395	-7.222511
8	-0.782029	-0.415654	-3.230845	-2.611045	-1.842611
9	-0.553486	-0.684310	0.806807	-2.329932	7.536716
10	-0.152950	-0.631167	4.269423	0.929594	3.625279
11	0.314451	-0.266140	3.858769	2.712877	-6.227402
12	0.774056	0.245786	0.317747	1.186774	-5.283791
13	1.300573	0.910372	-5.674758	-3.114979	7.737588

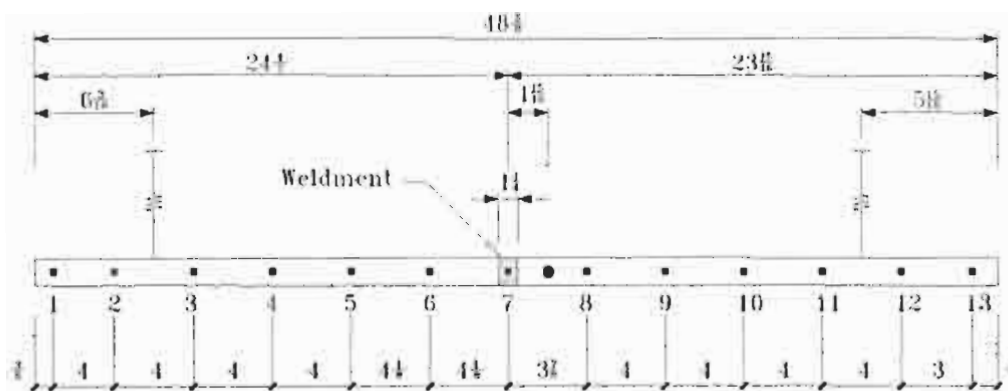
**Figure C.8 Modal Analysis Reporting Sheet for #14 S3
Reinforcing Rod Specimen**

Date: 2/16/2000

Specimen: #14 W1

of Average: 10

Sensitivity: Ch1 (Hammer: 10V) Ch2 (Accelerometer: 0.16V)



- : accel location
- : impact locations

Unit = inch

Location	Mode 1 121.25 Hz	Mode 2 332.50 Hz	Mode 3 645.00 Hz	Mode 4 1058.75 Hz	Mode 5 1558.75 Hz
1	1.585883	-0.373505	-7.662610	1.201084	10.835970
2	1.058499	-0.153848	-1.125759	-0.162674	-4.662353
3	0.431370	0.088993	4.942249	-1.012855	-9.113645
4	-0.180933	0.255652	5.859303	-0.353667	4.717238
5	-0.636174	0.281865	1.618427	0.784393	10.450650
6	-0.892324	0.207816	-3.154223	1.060300	1.706024
7	-1.015594	0.063539	-6.257472	0.386378	-9.250368
8	-1.001195	-0.115088	-5.666794	-0.731469	-6.683199
9	-0.755189	-0.257359	-0.351419	-1.013579	8.240518
10	-0.344931	-0.275335	4.907272	-0.037551	8.462012
11	0.243642	-0.149884	5.929631	0.957471	-6.238715
12	0.863805	0.070812	1.231554	0.567697	-8.800649
13	1.525925	0.342870	-6.821333	-0.973076	8.795525

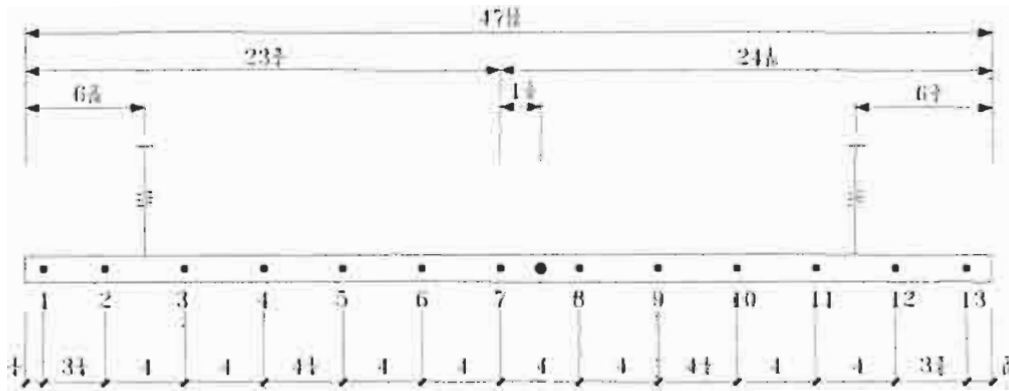
Figure C.9 Modal Analysis Reporting Sheet for #14 W1 Reinforcing Rod Specimen

Date: 3/22/2000

Specimen: #11 Unwelded

of Average: 10

Sensitivity: Ch1 (Hammer: 10V) Ch2 (Accelerometer: 0.31V)



- : accel location
- : impact locations

Unit = inch

Location	Mode 1 100.00 Hz	Mode 2 276.875 Hz	Mode 3 536.875 Hz	Mode 4 886.25 Hz	Mode 5 1305.0 Hz
1	2.642717	-1.651349	-12.759580	7.712157	22.528510
2	1.838160	-0.742463	-2.891993	0.018941	-4.744377
3	0.781463	0.281149	6.644575	-5.584423	-16.148550
4	-0.189853	0.975884	8.877866	-2.889264	4.521648
5	-1.022637	1.150487	2.754236	4.115277	17.972760
6	-1.529532	0.760437	-5.766568	5.724473	-1.309145
7	-1.721360	0.039591	-9.844878	0.269155	-18.400100
8	-1.565722	-0.702880	-6.307574	-5.567464	-3.248002
9	-1.073802	-1.123691	2.105931	-4.479693	17.353050
10	-0.262034	-1.004812	8.744285	2.353817	6.700514
11	0.732218	-0.342951	7.163521	5.684114	-15.419250
12	1.783533	0.664295	-2.021485	0.663831	-6.815749
13	2.706531	1.625058	-12.452360	-7.348738	20.948240

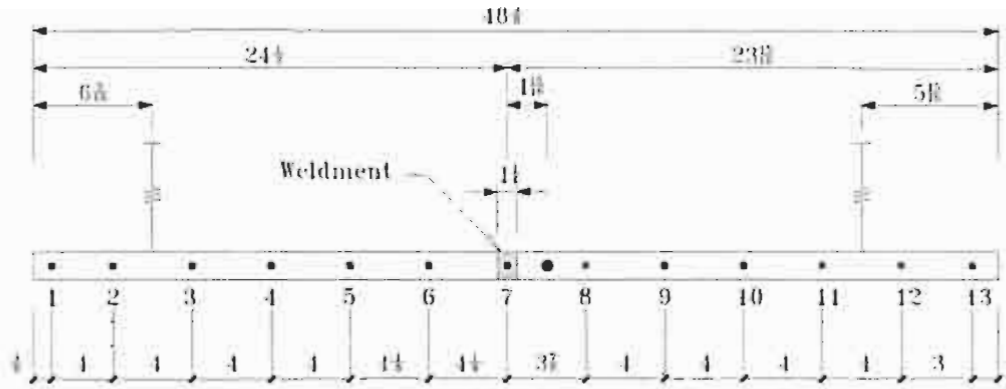
Figure C.11 Modal Analysis Reporting Sheet for #11 Unwelded Reinforcing Rod Specimen

Date: 2/17/2000

Specimen: #11 BP1

of Average: 10

Sensitivity: Ch1 (Hammer: 10V) Ch2 (Accelerometer: 0.31V)



- : accel location
- : impact locations

Unit = inch

Location	Mode 1 100.00 Hz	Mode 2 274.375 Hz	Mode 3 532.50 Hz	Mode 4 879.375 Hz	Mode 5 1295.625 Hz
1	1.847030	-1.252280	-9.772936	5.076704	15.084110
2	1.110341	-0.351164	0.304726	-1.718170	-9.365152
3	0.371269	0.420175	6.894417	-4.239812	-10.240690
4	-0.275397	0.874137	6.898463	-0.901445	8.359417
5	-0.782535	0.897063	1.156594	3.721286	13.442500
6	-1.094588	0.532911	-5.589913	3.938174	-3.650182
7	-1.142325	0.038325	-7.849927	0.255103	-13.104540
8	-1.105056	-0.515821	-5.688565	-3.939499	-4.159839
9	-0.799444	-0.891468	1.057684	-3.799800	13.044800
10	-0.294463	-0.869239	6.839723	0.838403	8.384089
11	0.352750	-0.420367	6.922371	4.202659	-9.766574
12	1.071391	0.329360	0.484914	1.822923	-9.368311
13	1.813612	1.229388	-9.583649	-4.884706	14.210060

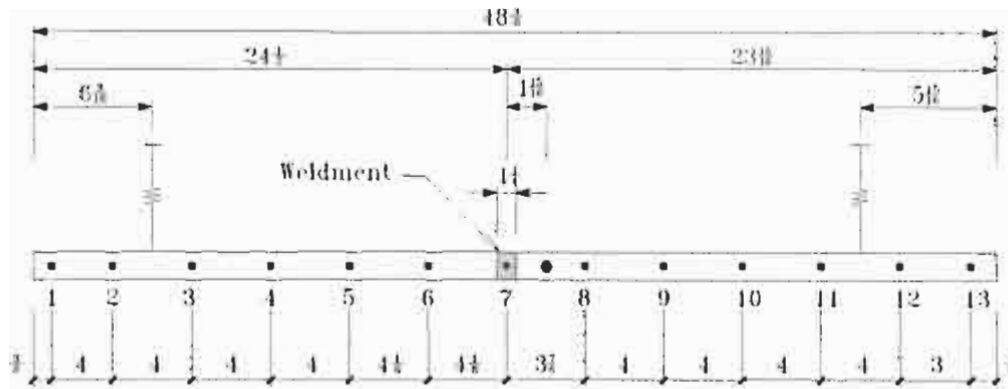
Figure C.12 Modal Analysis Reporting Sheet for #11 BP1 Reinforcing Rod Specimen

Date: 2/18/2000

Specimen: #11 BP2

of Average: 10

Sensitivity: Ch1 (Hammer: 10V) Ch2 (Accelerometer: 0.31V)



- : accel location
- : impact locations

Unit = inch

Location	Mode 1 100.00 Hz	Mode 2 276.25 Hz	Mode 3 533.75 Hz	Mode 4 883.125 Hz	Mode 5 1299.375 Hz
1	1.844336	-1.829320	-7.354769	5.928245	9.903382
2	1.081636	-0.453512	0.778047	-2.684484	-8.200095
3	0.333873	0.712002	5.918875	-5.376110	-7.266950
4	-0.249635	1.313917	5.848812	-1.501779	5.767517
5	-0.788355	1.367194	1.216931	4.648910	10.855750
6	-1.126613	0.849325	-4.494952	5.253962	-2.386171
7	-1.254111	-0.079713	-6.895038	-0.465733	-11.134360
8	-1.122133	-0.860502	-4.405220	-5.241536	-2.244088
9	-0.783699	-1.409509	1.336324	-4.547162	10.984170
10	-0.239303	-1.321655	5.897407	1.576295	5.676335
11	0.307915	-0.747321	6.030140	5.250168	-6.931093
12	1.048425	0.394878	1.057725	2.898295	-8.912643
13	1.845912	1.809306	-7.325980	-5.669753	9.552143

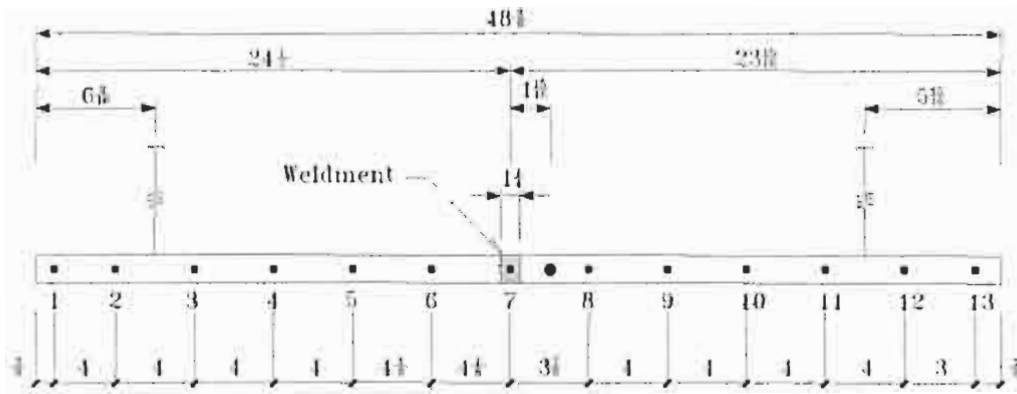
**Figure C.13 Modal Analysis Reporting Sheet for #11 BP2
Reinforcing Rod Specimen**

Date: 2/18/2000

Specimen: #11 BP3

of Average: 10

Sensitivity: Ch1 (Hammer: 10V) Ch2 (Accelerometer: 0.31V)



- : accel location
- : impact locations

Unit = inch

Location	Mode 1 100.00 Hz	Mode 2 276.875 Hz	Mode 3 536.875 Hz	Mode 4 886.25 Hz	Mode 5 1305.0 Hz
1	2.000127	-2.199298	-9.918913	8.113558	12.153690
2	1.210436	-0.706299	-0.492468	-1.709793	-5.098009
3	0.436532	0.603036	6.098875	-5.993570	-7.509105
4	-0.232934	1.408054	6.670134	-1.854766	4.547439
5	-0.777016	1.519382	1.638951	4.892342	9.368880
6	-1.143360	0.926919	-4.950870	5.838734	-1.895793
7	-1.249498	-0.092407	-7.496823	-0.658969	-9.331895
8	-1.100333	-1.011638	-4.200068	-6.047224	-0.083021
9	-0.717203	-1.515284	2.349172	-4.198930	9.829450
10	-0.164492	-1.332784	6.889282	2.515924	3.348181
11	0.518676	-0.478430	5.625820	5.965468	-8.533648
12	1.283863	0.851994	-1.388676	0.860885	-4.190472
13	1.889241	1.959512	-8.330822	-6.495774	9.195808

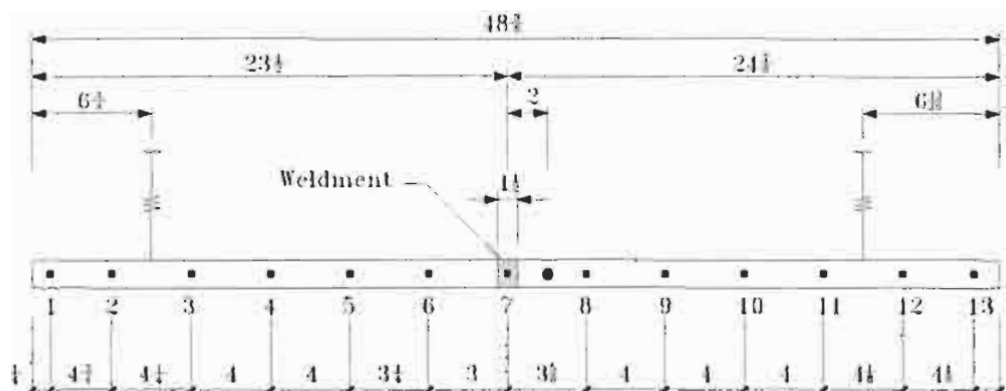
**Figure C.14 Modal Analysis Reporting Sheet for #11 BP3
Reinforcing Rod Specimen**

Date: 2/18/2000

Specimen: #11 PH2

of Average: 10

Sensitivity: Ch1 (Hammer: 10V) Ch2 (Accelerometer: 0.31V)



- : accel location
- : impact locations

Unit = inch

Location	Mode 1 100.625Hz	Mode 2 276.25 Hz	Mode 3 535.625 Hz	Mode 4 883.75 Hz	Mode 5 1302.5 Hz
1	2.117469	-1.432958	-11.306340	5.949988	19.325130
2	1.145229	-0.310468	0.912428	-1.966030	-10.430910
3	0.313116	0.518319	7.507519	-3.918019	-8.583077
4	-0.380621	0.941521	6.532759	-0.201544	10.877470
5	-0.909667	0.908540	0.125914	3.948116	12.211180
6	-1.174007	0.574915	-5.395624	3.865958	-2.870447
7	-1.278506	0.103809	-7.990543	0.750573	-13.700960
8	-1.216963	-0.467840	-6.420005	-3.340027	-7.115093
9	-0.912320	-0.908295	-0.025813	-4.038058	12.017410
10	-0.388289	-0.949050	6.383710	0.137617	11.085000
11	0.292541	-0.533616	7.391312	3.895490	-8.453494
12	1.095364	0.267207	1.289434	2.176243	-11.544940
13	1.942241	1.245265	-8.986640	-4.379912	13.930070

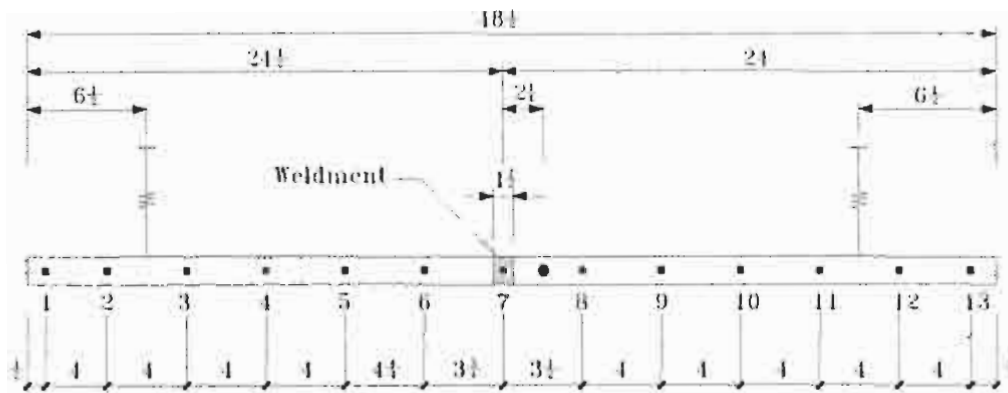
**Figure C.15 Modal Analysis Reporting Sheet for #11 PH2
Reinforcing Rod Specimen**

Date: 3/13/2000

Specimen: #11 S1

of Average: 10

Sensitivity: Ch1 (Hammer: 10V) Ch2 (Accelerometer: 0.31V)



- : accel location
- : impact locations

Unit = inch

Location	Mode 1 100.00 Hz	Mode 2 276.875 Hz	Mode 3 536.25 Hz	Mode 4 885.625 Hz	Mode 5 1304.375 Hz
1	2.159447	-2.344633	-9.587693	8.239686	8.162815
2	1.309640	-0.709273	-0.145854	-2.116835	-4.628910
3	0.474190	0.696692	6.218038	-6.239890	-5.690906
4	-0.279980	1.556741	6.568517	-1.780673	3.670593
5	-0.890904	1.652897	1.368161	5.288912	6.926419
6	-1.287661	0.951174	-5.327599	5.810294	-2.179312
7	-1.397426	-0.086208	-7.607645	-0.525888	-6.918082
8	-1.274419	-1.013342	-4.968988	-6.061039	-1.484940
9	-0.890860	-1.655944	1.436543	-5.321224	6.876401
10	-0.287512	-1.560846	6.513906	1.800774	3.667270
11	0.498072	-0.684424	6.158734	6.468073	-5.623406
12	1.359305	0.732574	-0.270111	2.096109	-4.366010
13	2.226750	2.346337	-9.531126	-8.393258	8.014813

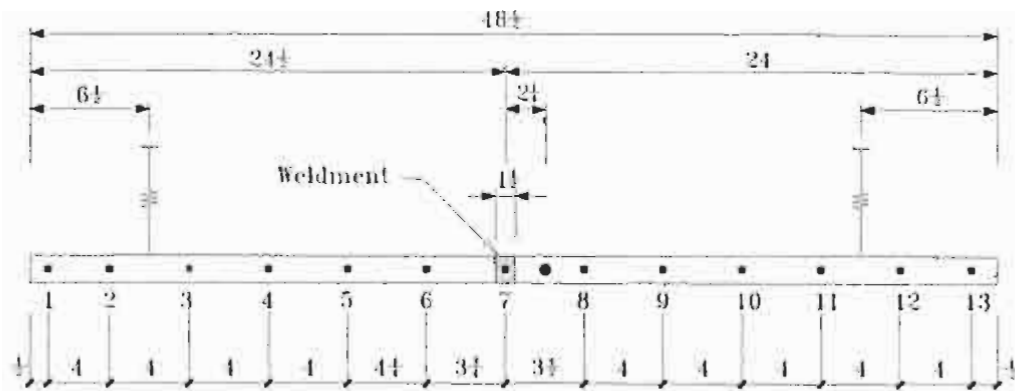
**Figure C.16 Modal Analysis Reporting Sheet for #11 S1
Reinforcing Rod Specimen**

Date: 2/17/2000

Specimen: #11 S2

of Average: 10

Sensitivity: Ch1 (Hammer: 10V) Ch2 (Accelerometer: 0.31V)



- : accel location
- : impact locations

Unit = inch

Location	Mode 1 100.625 Hz	Mode 2 276.875 Hz	Mode 3 537.5 Hz	Mode 4 886.875 Hz	Mode 5 1308.125 Hz
1	1.998368	-1.632762	-7.293608	7.660407	11.665450
2	1.234944	-0.515765	-0.183819	-1.969616	-6.031837
3	0.552547	0.365601	4.320130	-5.954231	-9.839685
4	-0.269283	1.116927	5.184759	-1.556541	6.043432
5	-0.774328	1.203668	1.694386	4.374117	11.107480
6	-1.159222	0.788121	-3.402465	6.026582	-0.699448
7	-1.293099	0.020700	-5.804482	0.069110	-10.260890
8	-1.200346	-0.637775	-4.196924	-5.248274	-3.982984
9	-0.864548	-1.144816	0.563449	-5.386133	9.882747
10	-0.323688	-1.163620	4.807445	0.939641	7.350083
11	0.393967	-0.536106	4.932819	5.889182	-8.307162
12	1.201668	0.485458	0.031875	2.166056	-6.617638
13	2.032878	1.675788	-7.584061	-7.622951	11.809280

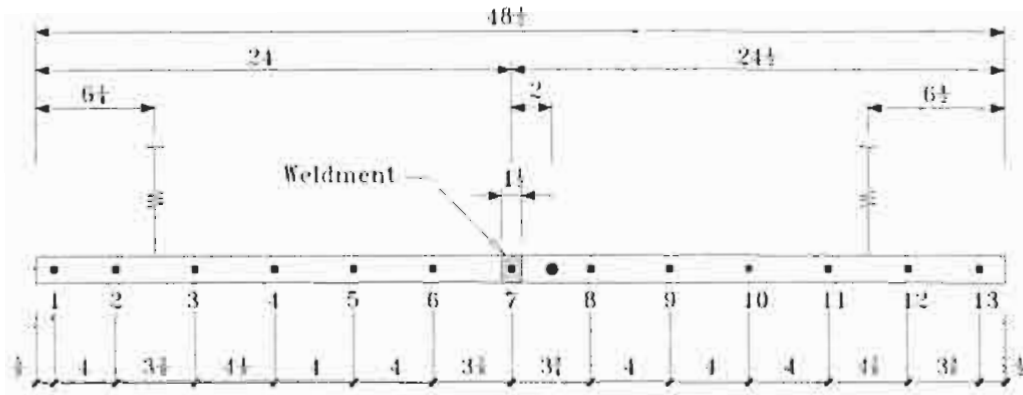
**Figure C.17 Modal Analysis Reporting Sheet for #11 S2
Reinforcing Rod Specimen**

Date: 2/17/2000

Specimen: #11 S3

of Average: 10

Sensitivity: Ch1 (Hammer: 10V) Ch2 (Accelerometer: 0.31V)



- : accel location
- : impact locations

Unit = inch

Location	Mode 1 100.625 Hz	Mode 2 276.25 Hz	Mode 3 536.875 Hz	Mode 4 883.75 Hz	Mode 5 1306.25 Hz
1	2.060574	-1.636298	-10.870840	7.647366	15.663130
2	1.263922	-0.516254	-0.246231	-1.904592	-8.435830
3	0.561470	0.364010	6.397657	-5.809519	-12.082780
4	-0.194638	1.051755	7.810483	-2.430934	5.103025
5	-0.792399	1.179438	2.420612	4.354460	14.145820
6	-1.172996	0.769327	-4.967552	5.869433	-0.709681
7	-1.308116	0.054183	-8.423970	0.535274	-12.905380
8	-1.217759	-0.671395	-6.070173	-5.311109	-4.309259
9	-0.874172	-1.158694	1.049530	-5.205013	12.750130
10	-0.316254	-1.135715	7.199295	1.150866	8.409094
11	0.402947	-0.541248	7.264121	5.766693	-9.865037
12	1.371649	0.688744	-1.777092	0.664403	-5.414910
13	2.070677	1.662800	-10.871840	-7.412736	15.768150

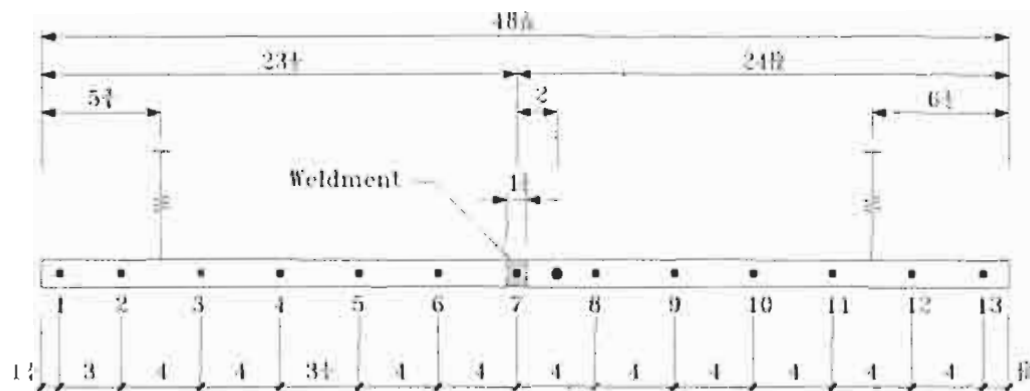
**Figure C.18 Modal Analysis Reporting Sheet for #11 S3
Reinforcing Rod Specimen**

Date: 2/16/2000

Specimen: #11 W1

of Average: 10

Sensitivity: Ch1 (Hammer: 10V) Ch2 (Accelerometer: 0.31V)



- : accel location
- : impact locations

Unit = inch

Location	Mode 1 100.625 Hz	Mode 2 277.50 Hz	Mode 3 536.25 Hz	Mode 4 888.125 Hz	Mode 5 1311.875 Hz
1	1.452180	-0.984744	-5.182952	2.896992	5.133323
2	0.974509	-0.394721	-0.496395	-0.752002	-3.284352
3	0.377329	0.287840	3.960194	-2.991775	-5.470145
4	-0.176771	0.718051	4.444759	-1.022363	3.085349
5	-0.540288	0.843506	1.941122	1.800350	6.956404
6	-0.862340	0.576849	-2.311868	3.138363	0.719752
7	-1.016329	0.105994	-4.996110	0.710197	-6.672929
8	-0.929726	-0.415639	-3.602933	-2.555064	-2.456126
9	-0.675361	-0.752675	0.419355	-2.644084	5.764983
10	-0.261459	-0.749128	4.179811	0.439995	4.375953
11	0.274893	-0.380279	4.327481	2.851153	-4.445312
12	0.878939	0.263163	0.369985	1.336692	-4.729217
13	1.499331	1.007006	-5.565024	-3.196150	6.241135

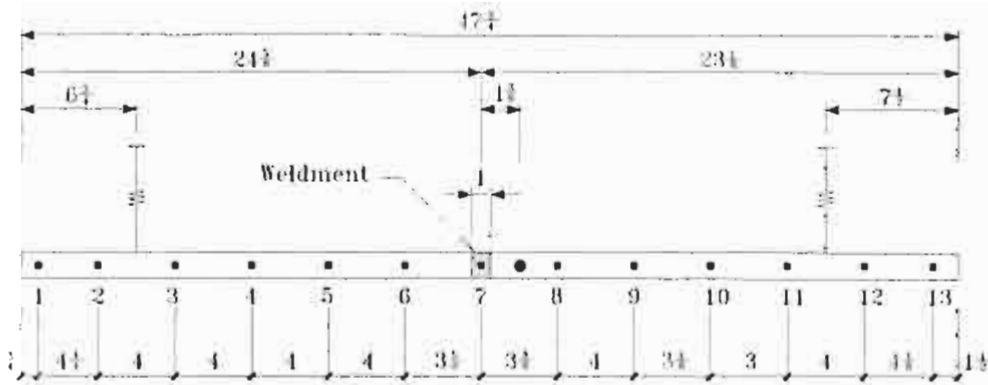
Figure C.19 Modal Analysis Reporting Sheet for #11 W1 Reinforcing Rod Specimen

Date: 2/16/2000

Specimen: #11 W2

of Average: 10

Sensitivity: Ch1 (Hammer: 10V) Ch2 (Accelerometer: 0.31V)



- : accel location
- : impact locations

Unit = inch

Location	Mode 1 103.75 Hz	Mode 2 285.625 Hz	Mode 3 555.00 Hz	Mode 4 912.50 Hz	Mode 5 1349.375 Hz
1	2.474447	-2.173014	-10.736570	7.090058	15.048320
2	1.372937	-0.473978	1.214830	-3.034673	-10.852730
3	0.396063	0.828185	7.911837	-5.911370	-8.947223
4	-0.473240	1.549446	6.929392	-0.326707	10.825250
5	-1.140294	1.490543	0.028013	5.867631	12.097180
6	-1.538924	0.752139	-7.121065	4.886016	-7.739628
7	-1.619068	-0.210797	-8.868468	-1.402014	-14.930300
8	-1.446674	-1.049480	-5.160064	-6.253816	-0.803941
9	-0.962019	-1.578481	2.485761	-4.402927	15.389720
10	-0.396262	-1.494991	7.284328	1.113495	9.463482
11	0.255139	-0.975825	8.162465	5.574709	-6.509051
12	1.245072	0.248959	2.524281	4.095655	-13.395640
13	2.308499	1.801307	-8.124737	-5.180470	10.153870

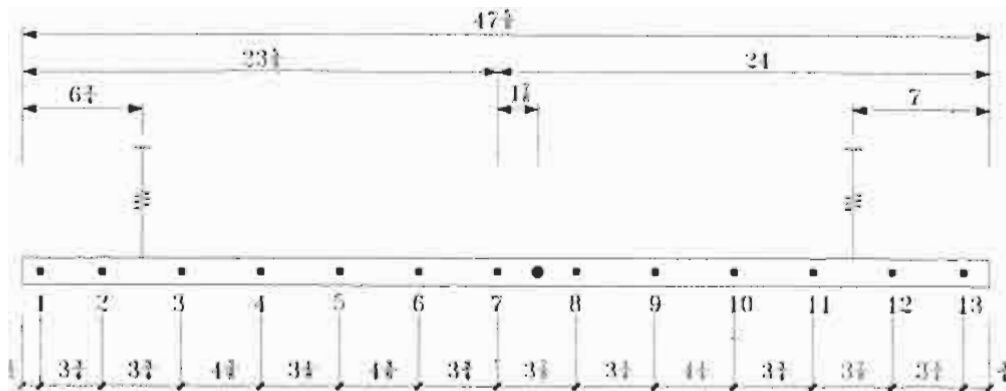
Figure C.20 Modal Analysis Reporting Sheet for #11 W2 Reinforcing Rod Specimen

Date: 3/22/2000

Specimen: #8 Unwelded

of Average: 10

Sensitivity: Ch1 (Hammer: 5V) Ch2 (Accelerometer: 0.625V)



- : accel location
- : impact locations

Unit = inch

Location	Mode 1 74.375 Hz	Mode 2 205.625 Hz	Mode 3 401.875 Hz	Mode 4 662.50 Hz	Mode 5 985.0 Hz
1	2.200758	-2.592322	-14.979340	12.204100	25.030600
2	1.485841	-0.856881	-0.772472	-2.535390	-11.782790
3	0.588085	0.655461	9.210306	-9.422123	-17.415260
4	-0.364774	1.737717	10.096830	-2.296965	11.748380
5	-0.895855	1.867355	3.885321	6.297743	21.589570
6	-1.361436	1.175346	-7.491052	9.218636	-2.997354
7	-1.492352	0.082640	-12.133350	0.658111	-21.642170
8	-1.397013	-1.101767	-8.085062	-8.806037	-5.075965
9	-0.990127	-1.794656	1.609853	-8.128494	19.369480
10	-0.313231	-1.696951	10.469420	2.822892	10.383150
11	0.507950	-0.785564	9.980119	9.377535	-15.404500
12	1.420232	0.747634	0.114064	3.412365	-13.387290
13	2.304044	2.490388	-14.357560	-10.900640	21.611290

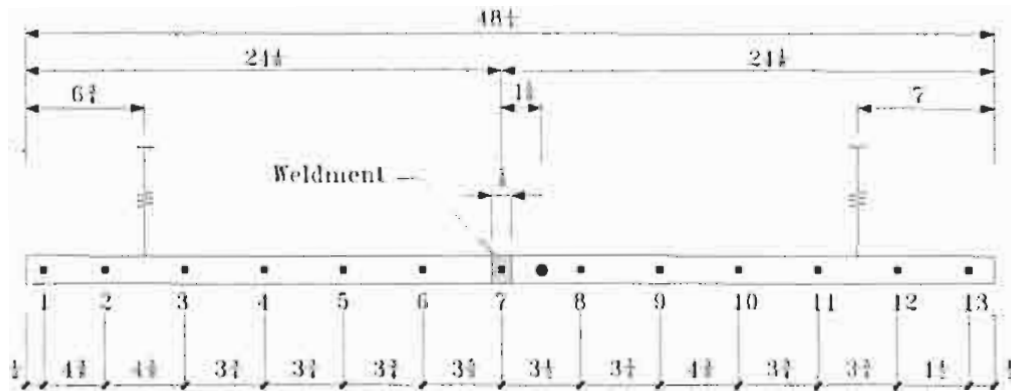
Figure C.21 Modal Analysis Reporting Sheet for #8 Unwelded Reinforcing Rod Specimen

Date: 2/22/2000

Specimen: #8 BP1

of Average: 10

Sensitivity: Ch1 (Hammer: 5V) Ch2 (Accelerometer: 0.625V)



- : accel location
- : impact locations

Unit = inch

Location	Mode 1 73.125 Hz	Mode 2 200.625 Hz	Mode 3 389.375 Hz	Mode 4 645.00 Hz	Mode 5 953.125 Hz
1	1.953285	-1.569237	-8.232833	3.387958	6.831103
2	1.087793	-0.377715	0.577163	-1.193921	-4.349802
3	0.287517	0.612506	6.019255	-2.540130	-3.534349
4	-0.327930	1.082031	5.439490	-0.312011	4.110445
5	-0.810264	1.108139	0.810068	2.412707	5.589521
6	-1.133622	0.680260	-4.496146	2.564949	-1.457467
7	-1.234212	0.035217	-6.589090	0.071095	-5.878393
8	-1.132348	-0.625590	-4.641814	-2.453409	-1.863523
9	-0.827989	-1.070737	0.535534	-2.501604	5.410300
10	-0.260771	-1.049195	5.767020	0.710690	3.375040
11	0.376081	-0.509565	5.668586	2.638552	-4.099304
12	1.091143	0.336338	0.833267	1.359140	-4.376795
13	1.994517	1.546851	-8.238025	-3.522344	6.909818

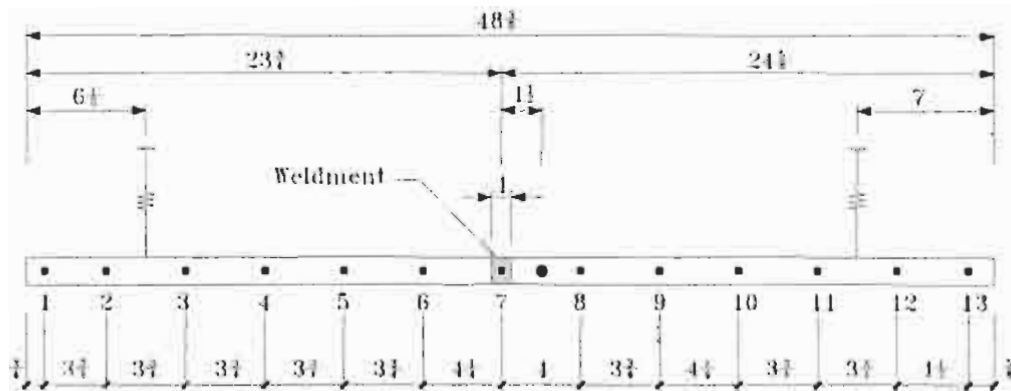
**Figure C.22 Modal Analysis Reporting Sheet for #8 BP1
Reinforcing Rod Specimen**

Date: 2/23/2000

Specimen: #8 BP2

of Average: 10

Sensitivity: Ch1 (Hammer: 5V) Ch2 (Accelerometer: 0.625V)



- : accel location
- : impact locations

Unit = inch

Location	Mode 1 73.125 Hz	Mode 2 200.00 Hz	Mode 3 388.75 Hz	Mode 4 643.125 Hz	Mode 5 952.5 Hz
1	2.259648	-1.432200	-14.990630	6.403974	22.639320
2	1.361204	-0.454320	-0.366165	-1.729661	-12.682270
3	0.476726	0.400371	9.899885	-5.294729	-16.951880
4	-0.183888	0.932827	11.317990	-2.146036	7.683502
5	-0.797637	1.047986	4.117254	3.575035	21.311970
6	-1.244296	0.735645	-5.958352	5.382382	2.601056
7	-1.435001	0.057472	-11.913820	0.617274	-19.514740
8	-1.331274	-0.611597	-8.356189	-4.745988	-5.505231
9	-0.957866	-1.011498	1.166769	-4.695574	18.622050
10	-0.286230	-0.980866	10.474030	1.173634	12.011450
11	0.359278	-0.509021	10.644880	5.123719	-13.911040
12	1.235271	0.305351	1.677838	2.681349	-15.792510
13	2.257210	1.432061	-14.934630	-6.512627	23.295830

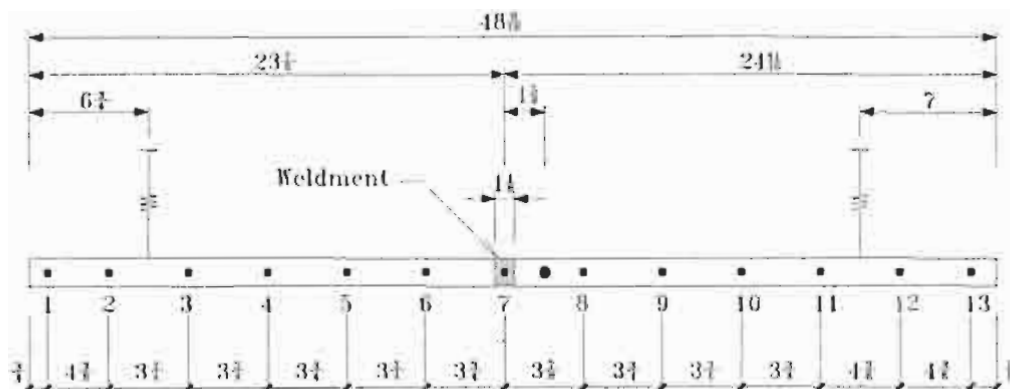
**Figure C.23 Modal Analysis Reporting Sheet for #8 BP2
Reinforcing Rod Specimen**

Date: 2/21/2000

Specimen: #8 PH1

of Average: 10

Sensitivity: Ch1 (Hammer: 5V) Ch2 (Accelerometer: 0.625V)



- : accel location
- : impact locations

Unit = inch

Location	Mode 1 73.750 Hz	Mode 2 206.875 Hz	Mode 3 398.75 Hz	Mode 4 665.00 Hz	Mode 5 976.25 Hz
1	2.079040	-1.678522	-13.157760	5.490192	17.965500
2	1.092242	-0.369889	1.457346	-2.187034	-12.622980
3	0.360334	0.572996	9.382946	-4.325876	-11.697720
4	-0.241286	1.130835	9.494562	-1.078681	9.194222
5	-0.760988	1.207523	2.786676	3.430782	16.927270
6	-1.114621	0.800278	-5.952467	4.320727	0.142814
7	-1.291418	0.072653	-10.275770	0.456602	-15.898250
8	-1.189636	-0.689581	-7.161739	-3.890998	-4.603583
9	-0.862795	-1.174243	1.021390	-4.035428	15.052050
10	-0.355089	-1.204591	8.568519	0.156468	12.700770
11	0.221820	-0.741141	10.193670	4.128885	-8.733235
12	1.061680	0.330805	1.809823	2.372554	-13.172580
13	2.006204	1.651236	-12.928270	-5.295966	17.349620

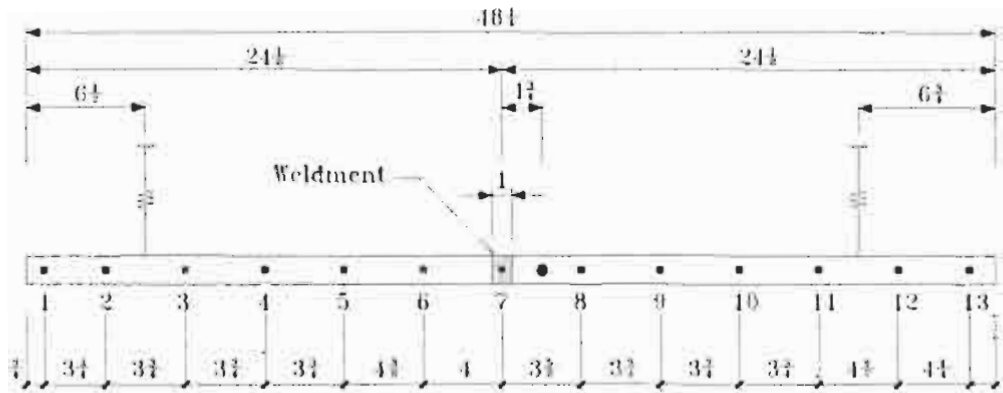
Figure C.25 Modal Analysis Reporting Sheet for #8 PH1 Reinforcing Rod Specimen

Date: 2/22/2000

Specimen: #8 S1

of Average: 10

Sensitivity: Ch1 (Hammer: 5V) Ch2 (Accelerometer: 0.625V)



- : accel location
- : impact locations

Unit = inch

Location	Mode 1 72.500 Hz	Mode 2 200.625 Hz	Mode 3 390.00 Hz	Mode 4 646.875 Hz	Mode 5 955.625 Hz
1	2.430399	-2.304628	-13.513030	9.245727	14.560520
2	1.444904	-0.731492	-0.241381	-2.650688	-8.132593
3	0.549352	0.650830	9.128220	-7.904045	-11.034080
4	-0.206163	1.542003	10.420460	-3.177377	4.899595
5	-0.844656	1.752557	3.845443	5.396210	13.407150
6	-1.381913	1.124497	-6.958481	7.832200	-1.315741
7	-1.515187	-0.029354	-11.179700	-0.134480	-13.315360
8	-1.410587	-0.989055	-7.826989	-7.435764	-3.302613
9	-0.996307	-1.645018	1.293685	-7.159326	11.771300
10	-0.385462	-1.644562	9.410630	0.901027	8.994121
11	0.328370	-0.931539	10.429740	7.631002	-7.676086
12	1.379212	0.630004	0.525530	3.337556	-8.648780
13	2.504292	2.365345	-14.751440	-10.369480	15.613060

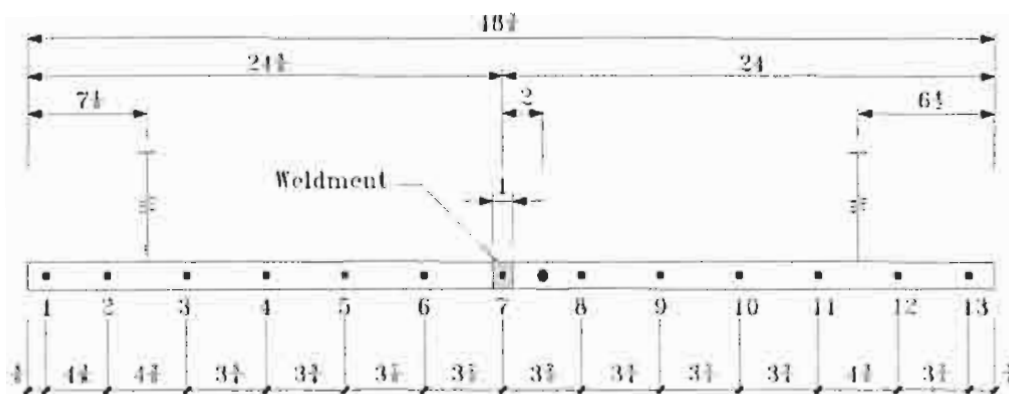
**Figure C.26 Modal Analysis Reporting Sheet for #8 S1
Reinforcing Rod Specimen**

Date: 2/21/2000

Specimen: #8 S2

of Average: 10

Sensitivity: Ch1 (Hammer: 5V) Ch2 (Accelerometer: 0.625V)



- : accel location
- : impact locations

Unit = inch

Location	Mode 1 72.500 Hz	Mode 2 199.375 Hz	Mode 3 388.125 Hz	Mode 4 642.50 Hz	Mode 5 951.25 Hz
1	2.322576	-2.870922	-14.599070	10.918000	16.674710
2	1.286785	-0.723220	0.599624	-3.375706	-8.847980
3	0.342268	1.042950	9.881834	-7.764741	-7.932633
4	-0.349489	1.920580	9.298460	-1.356638	8.201952
5	-0.932146	2.003196	1.818942	7.094379	12.703920
6	-1.317904	1.225406	-7.602349	7.839117	-2.961604
7	-1.451271	-0.072612	-11.429640	-0.380830	-13.178450
8	-1.296723	-1.290648	-6.894214	-8.214065	1.229631
9	-0.904612	-1.979372	2.336042	-6.797413	12.996680
10	-0.308827	-1.878436	9.757956	1.987865	7.304014
11	0.400540	-0.968511	9.891071	8.124833	-8.794019
12	1.366617	0.863315	-0.171632	3.207666	-10.634710
13	2.281647	2.747458	-14.030040	-11.045920	17.914860

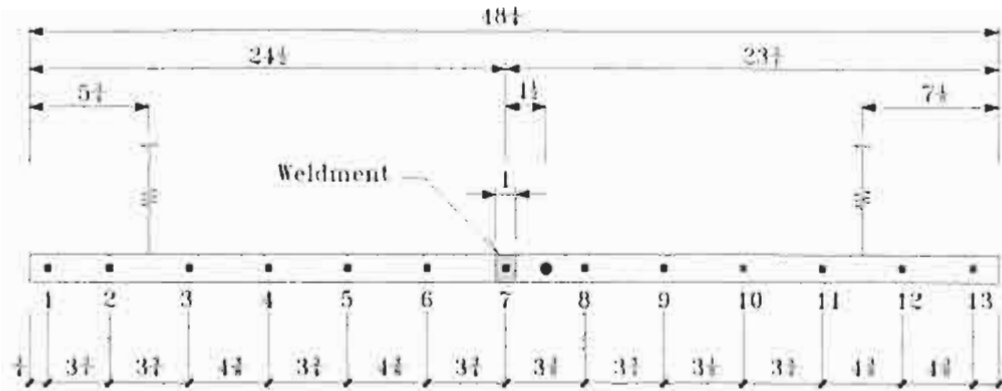
Figure C.27 Modal Analysis Reporting Sheet for #8 S2 Reinforcing Rod Specimen

Date: 2/23/2000

Specimen: #8 S3

of Average: 10

Sensitivity: Ch1 (Hammer: 5V) Ch2 (Accelerometer: 0.625V)



- : accel location
- : impact locations

Unit = inch

Location	Mode 1 73.125 Hz	Mode 2 200.625 Hz	Mode 3 390.625 Hz	Mode 4 645.625 Hz	Mode 5 956.25 Hz
1	2.224443	-2.465880	-11.813170	9.086929	14.780080
2	1.344390	-0.795287	-0.262075	-2.538291	-8.759719
3	0.500413	0.687622	7.833978	-7.786632	-11.440480
4	-0.288418	1.727089	8.410636	-1.887982	8.141359
5	-0.902535	1.825417	2.010779	6.485389	13.562270
6	-1.357675	1.027968	-7.054943	7.174107	-4.733480
7	-1.461119	-0.088987	-10.139830	-0.655191	-14.327730
8	-1.352494	-1.096865	-6.597342	-7.516603	-3.099986
9	-0.956369	-1.801218	1.306843	-7.053002	13.161280
10	-0.459271	-1.843050	7.480780	-0.495077	11.907510
11	0.207145	-1.173562	9.530993	7.105731	-5.975595
12	1.137658	0.383838	2.352286	4.910233	-12.021600
13	2.157576	2.325371	-10.980160	-8.190917	12.885250

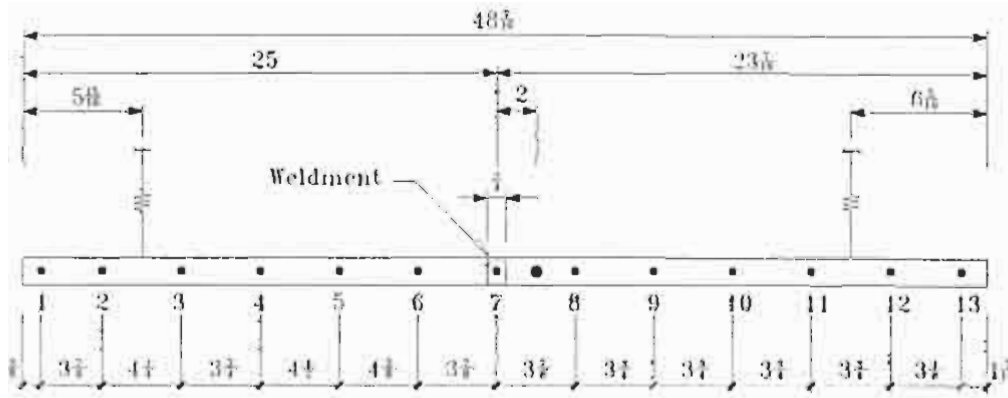
Figure C.28 Modal Analysis Reporting Sheet for #8 S3 Reinforcing Rod Specimen

Date: 2/21/2000

Specimen: #8 W1

of Average: 10

Sensitivity: Ch1 (Hammer: 5V) Ch2 (Accelerometer: 0.625V)



- : accel location
- : impact locations

Unit = inch

Location	Mode 1 71.875 Hz	Mode 2 198.75 Hz	Mode 3 384.375 Hz	Mode 4 639.375 Hz	Mode 5 941.875 Hz
1	2.195383	-3.989592	-13.385830	17.285820	14.636330
2	1.343751	-1.351244	-1.045695	-3.077394	-6.089260
3	0.429946	1.120843	8.232249	-12.637950	-8.970531
4	-0.215533	2.456381	8.931444	-4.340517	5.107193
5	-0.855623	2.637801	1.335188	11.123620	10.785410
6	-1.255579	1.388082	-7.502980	10.590440	-4.795083
7	-1.333693	-0.306183	-9.987376	-2.534464	-11.381800
8	-1.116446	-1.944830	-4.882572	-13.038430	1.556905
9	-0.717591	-2.735176	3.434783	-8.658497	12.373030
10	-0.182409	-2.421941	9.230929	4.906649	4.650730
11	0.451662	-1.041824	8.144313	12.471300	-9.776941
12	1.253517	1.134116	-0.083375	4.415436	-7.536208
13	1.945217	3.206718	-9.858888	-10.774370	8.564082

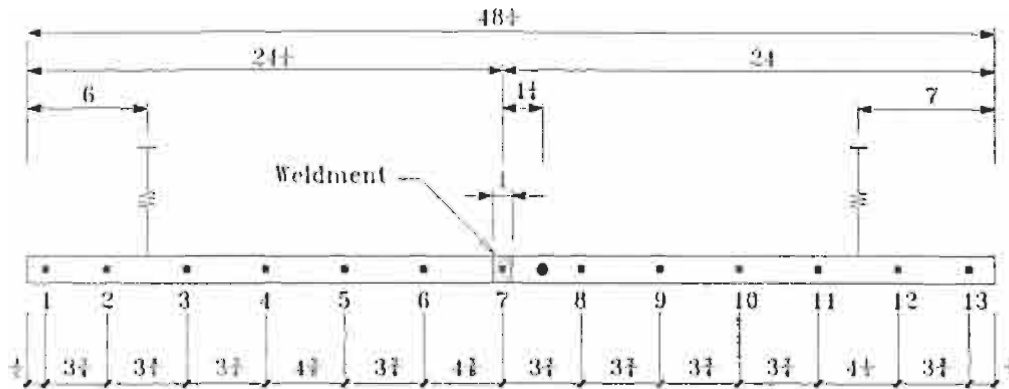
Figure C.29 Modal Analysis Reporting Sheet for #8 W1 Reinforcing Rod Specimen

Date: 2/23/2000

Specimen: #8 W2

of Average: 10

Sensitivity: Ch1 (Hammer: 5V) Ch2 (Accelerometer: 0.625V)



- : accel location
- : impact locations

Unit = inch

Location	Mode 1 72.500 Hz	Mode 2 200.625 Hz	Mode 3 388.125 Hz	Mode 4 646.25 Hz	Mode 5 950.625 Hz
1	2.465713	-1.753986	-14.909290	8.609170	19.989730
2	1.517336	-0.601302	-1.028727	-1.696747	-9.753351
3	0.590503	0.423944	9.094388	-6.774673	-15.082530
4	-0.177332	1.106546	11.048360	-3.038168	5.069979
5	-0.897614	1.264806	3.009487	5.188184	17.975360
6	-1.335144	0.861063	-6.620320	6.791659	0.089825
7	-1.519346	-0.033456	-11.854690	0.301315	-17.520000
8	-1.355235	-0.795173	-7.337601	-6.369437	-2.185292
9	-0.923396	-1.240436	2.234176	-5.423406	17.664560
10	-0.333614	-1.191725	10.162900	1.215538	10.709330
11	0.379792	-0.630547	10.474290	6.303625	-11.694060
12	1.434759	0.539795	-0.305107	2.180642	-10.909640
13	2.338758	1.693935	-14.206130	-7.665238	18.733950

Figure C.30 Modal Analysis Reporting Sheet for #8 W2 Reinforcing Rod Specimen

C.2. MODAL ASSURANCE CRITERION

The modal assurance criterion (MAC) is a measure of the strength of the correlation between two mode shapes. A MAC value close to one indicates a strong correlation, or similarity between modes while a MAC value close to zero indicates a weak correlation. The MAC can be computed using the following expression.

$$\text{MAC}(i, j) = \frac{|\{\phi\}_i \{\phi\}_j^T|^2}{(\{\phi\}_i \{\phi\}_i^T)(\{\phi\}_j \{\phi\}_j^T)} \quad (\text{C.1})$$

Tables C.1 through C.10 present MAC's for #14 specimens which compare experimental and baseline modes. In the tables, i^{th} column represents MAC values between i^{th} experimental mode shape and five FE mode shapes and j^{th} row represents MAC values between j^{th} FE mode shape and five experimental mode shapes. MAC values for #11 and #8 specimens are presented in Tables C.11 through C.20 and Tables C.21 through C.30, respectively.

**Table C.1 Modal Assurance Criteria (FE Model vs. Measured)
for #14 Unwelded Reinforcing Rod Specimen**

Mode	1/M	2/M	3/M	4/M	5/M
1/FE	0.9998	0.0000	0.0018	0.0000	0.0014
2/FE	0.0000	0.9999	0.0001	0.0018	0.0000
3/FE	0.0020	0.0000	0.9999	0.0000	0.0028
4/FE	0.0000	0.0023	0.0000	0.9998	0.0001
5/FE	0.0018	0.0000	0.0028	0.0001	0.9998

**Table C.2 Modal Assurance Criteria (FE Model vs. Measured)
for #14 BP1 Reinforcing Rod Specimen**

Mode	1/M	2/M	3/M	4/M	5/M
1/FE	0.9994	0.0013	0.0352	0.0007	0.0064
2/FE	0.0001	0.9989	0.0023	0.0174	0.0015
3/FE	0.0244	0.0002	0.9973	0.0046	0.0206
4/FE	0.0001	0.0150	0.0010	0.9976	0.0052
5/FE	0.0091	0.0005	0.0188	0.0010	0.9971

**Table C.3 Modal Assurance Criteria (FE Model vs. Measured)
for #14 BP2 Reinforcing Rod Specimen**

Mode	1/M	2/M	3/M	4/M	5/M
1/FE	0.9998	0.0000	0.0101	0.0000	0.0186
2/FE	0.0000	0.9999	0.0000	0.0130	0.0000
3/FE	0.0154	0.0000	0.9993	0.0000	0.0079
4/FE	0.0000	0.0144	0.0001	0.9997	0.0000
5/FE	0.0144	0.0000	0.0135	0.0002	0.9986

**Table C.4 Modal Assurance Criteria (FE Model vs. Measured)
for #14 BP3 Reinforcing Rod Specimen**

Mode	1/M	2/M	3/M	4/M	5/M
1/FE	0.9999	0.0009	0.0217	0.0007	0.0285
2/FE	0.0006	0.9999	0.0003	0.0228	0.0010
3/FE	0.0248	0.0004	0.9994	0.0004	0.0133
4/FE	0.0006	0.0217	0.0001	0.9996	0.0000
5/FE	0.0212	0.0003	0.0176	0.0000	0.9982

**Table C.5 Modal Assurance Criteria (FE Model vs. Measured)
for #14 PH3 Reinforcing Rod Specimen**

Mode	1/M	2/M	3/M	4/M	5/M
1/FE	0.9999	0.0002	0.0103	0.0017	0.0197
2/FE	0.0003	0.9999	0.0004	0.0143	0.0002
3/FE	0.0154	0.0004	0.9988	0.0000	0.0084
4/FE	0.0005	0.0150	0.0001	0.9989	0.0001
5/FE	0.0145	0.0002	0.0116	0.0000	0.9986

**Table C.6 Modal Assurance Criteria (FE Model vs. Measured)
for #14 S1 Reinforcing Rod Specimen**

Mode	1/M	2/M	3/M	4/M	5/M
1/FE	0.9997	0.0013	0.0226	0.0001	0.0173
2/FE	0.0007	0.9997	0.0012	0.0244	0.0012
3/FE	0.0280	0.0006	0.9987	0.0008	0.0249
4/FE	0.0003	0.0246	0.0011	0.9993	0.0001
5/FE	0.0240	0.0002	0.0214	0.0006	0.9921

**Table C.7 Modal Assurance Criteria (FE Model vs. Measured)
for #14 S2 Reinforcing Rod Specimen**

Mode	1/M	2/M	3/M	4/M	5/M
1/FE	0.9997	0.0003	0.0079	0.0002	0.0094
2/FE	0.0003	0.9998	0.0002	0.0098	0.0002
3/FE	0.0107	0.0001	0.9995	0.0005	0.0051
4/FE	0.0001	0.0101	0.0000	0.9993	0.0006
5/FE	0.0087	0.0001	0.0094	0.0001	0.9986

**Table C.8 Modal Assurance Criteria (FE Model vs. Measured)
for #14 S3 Reinforcing Rod Specimen**

Mode	1/M	2/M	3/M	4/M	5/M
1/FE	0.9995	0.0009	0.0120	0.0005	0.0212
2/FE	0.0006	0.9999	0.0007	0.0162	0.0005
3/FE	0.0169	0.0005	0.9991	0.0015	0.0090
4/FE	0.0008	0.0170	0.0004	0.9994	0.0004
5/FE	0.0185	0.0004	0.0130	0.0007	0.9981

**Table C.9 Modal Assurance Criteria (FE Model vs. Measured)
for #14 W1 Reinforcing Rod Specimen**

Mode	1/M	2/M	3/M	4/M	5/M
1/FE	0.9999	0.0019	0.0134	0.0014	0.0184
2/FE	0.0011	0.9999	0.0013	0.0141	0.0005
3/FE	0.0152	0.0009	0.9997	0.0011	0.0090
4/FE	0.0012	0.0148	0.0004	0.9999	0.0005
5/FE	0.0141	0.0007	0.0127	0.0006	0.9990

**Table C.10 Modal Assurance Criteria (FE Model vs. Measured)
for #14 W2 Reinforcing Rod Specimen**

Mode	1/M	2/M	3/M	4/M	5/M
1/FE	1.0000	0.0032	0.0098	0.0034	0.0111
2/FE	0.0024	0.9998	0.0027	0.0113	0.0017
3/FE	0.0121	0.0020	0.9996	0.0019	0.0080
4/FE	0.0023	0.0099	0.0014	0.9997	0.0013
5/FE	0.0100	0.0017	0.0086	0.0007	0.9996

**Table C.11 Modal Assurance Criteria (FE Model vs. Measured)
for #11 Unwelded Reinforcing Rod Specimen**

Mode	1/M	2/M	3/M	4/M	5/M
1/FE	0.9996	0.0007	0.0008	0.0006	0.0009
2/FE	0.0003	0.9999	0.0004	0.0012	0.0006
3/FE	0.0013	0.0005	1.0000	0.0005	0.0017
4/FE	0.0006	0.0010	0.0005	0.9999	0.0006
5/FE	0.0010	0.0006	0.0010	0.0005	0.9998

**Table C.12 Modal Assurance Criteria (FE Model vs. Measured)
for #11 BP1 Reinforcing Rod Specimen**

Mode	1/M	2/M	3/M	4/M	5/M
1/FE	0.9996	0.0004	0.0067	0.0003	0.0135
2/FE	0.0002	0.9999	0.0002	0.0098	0.0001
3/FE	0.0062	0.0002	0.9997	0.0001	0.0057
4/FE	0.0002	0.0089	0.0001	0.9999	0.0004
5/FE	0.0135	0.0001	0.0060	0.0002	0.9991

**Table C.13 Modal Assurance Criteria (FE Model vs. Measured)
for #11 BP2 Reinforcing Rod Specimen**

Mode	1/M	2/M	3/M	4/M	5/M
1/FE	0.9999	0.0008	0.0228	0.0006	0.0290
2/FE	0.0010	0.9999	0.0006	0.0218	0.0005
3/FE	0.0229	0.0007	0.9999	0.0007	0.0165
4/FE	0.0007	0.0216	0.0006	0.9999	0.0003
5/FE	0.0255	0.0008	0.0153	0.0004	0.9996

**Table C.14 Modal Assurance Criteria (FE Model vs. Measured)
for #11 BP3 Reinforcing Rod Specimen**

Mode	1/M	2/M	3/M	4/M	5/M
1/FE	0.9999	0.0042	0.0040	0.0022	0.0083
2/FE	0.0028	0.9998	0.0034	0.0059	0.0033
3/FE	0.0040	0.0020	0.9997	0.0037	0.0032
4/FE	0.0021	0.0051	0.0019	0.9995	0.0024
5/FE	0.0059	0.0018	0.0036	0.0011	0.9990

**Table C.15 Modal Assurance Criteria (FE Model vs. Measured)
for #11 PH2 Reinforcing Rod Specimen**

Mode	1/M	2/M	3/M	4/M	5/M
1/FE	0.9998	0.0057	0.0031	0.0063	0.0066
2/FE	0.0056	0.9998	0.0065	0.0044	0.0038
3/FE	0.0046	0.0047	0.9994	0.0043	0.0024
4/FE	0.0048	0.0057	0.0045	0.9990	0.0041
5/FE	0.0080	0.0042	0.0036	0.0037	0.9983

**Table C.16 Modal Assurance Criteria (FE Model vs. Measured)
for #11 S1 Reinforcing Rod Specimen**

Mode	1/M	2/M	3/M	4/M	5/M
1/FE	0.9998	0.0000	0.0012	0.0000	0.0064
2/FE	0.0000	1.0000	0.0000	0.0016	0.0000
3/FE	0.0013	0.0000	1.0000	0.0000	0.0013
4/FE	0.0000	0.0023	0.0000	0.9999	0.0000
5/FE	0.0036	0.0000	0.0011	0.0000	0.9990

**Table C.17 Modal Assurance Criteria (FE Model vs. Measured)
for #11 S2 Reinforcing Rod Specimen**

Mode	1/M	2/M	3/M	4/M	5/M
1/FE	0.9999	0.0006	0.0027	0.0005	0.0094
2/FE	0.0005	0.9998	0.0007	0.0046	0.0004
3/FE	0.0041	0.0002	0.9996	0.0007	0.0038
4/FE	0.0004	0.0049	0.0003	0.9999	0.0004
5/FE	0.0062	0.0004	0.0034	0.0004	0.9979

**Table C.18 Modal Assurance Criteria (FE Model vs. Measured)
for #11 S3 Reinforcing Rod Specimen**

Mode	1/M	2/M	3/M	4/M	5/M
1/FE	0.9999	0.0006	0.0033	0.0010	0.0105
2/FE	0.0003	0.9998	0.0011	0.0048	0.0005
3/FE	0.0065	0.0002	0.9992	0.0012	0.0032
4/FE	0.0003	0.0074	0.0002	0.9989	0.0014
5/FE	0.0080	0.0003	0.0062	0.0002	0.9984

**Table C.19 Modal Assurance Criteria (FE Model vs. Measured)
for #11 W1 Reinforcing Rod Specimen**

Mode	1/M	2/M	3/M	4/M	5/M
1/FE	0.9999	0.0001	0.0199	0.0002	0.0216
2/FE	0.0000	0.9994	0.0000	0.0205	0.0000
3/FE	0.0243	0.0000	0.9998	0.0001	0.0205
4/FE	0.0000	0.0241	0.0000	0.9995	0.0001
5/FE	0.0243	0.0002	0.0168	0.0001	0.9992

**Table C.20 Modal Assurance Criteria (FE Model vs. Measured)
for #11 W2 Reinforcing Rod Specimen**

Mode	1/M	2/M	3/M	4/M	5/M
1/FE	1.0000	0.0036	0.0185	0.0023	0.0174
2/FE	0.0030	0.9999	0.0029	0.0172	0.0019
3/FE	0.0193	0.0030	0.9998	0.0012	0.0158
4/FE	0.0022	0.0174	0.0026	0.9998	0.0003
5/FE	0.0183	0.0017	0.0137	0.0010	0.9996

**Table C.21 Modal Assurance Criteria (FE Model vs. Measured)
for #8 Unwelded Reinforcing Rod Specimen**

Mode	1/M	2/M	3/M	4/M	5/M
1/FE	0.9992	0.0001	0.0030	0.0001	0.0031
2/FE	0.0000	0.9999	0.0000	0.0029	0.0001
3/FE	0.0039	0.0000	0.9999	0.0003	0.0042
4/FE	0.0000	0.0025	0.0000	0.9998	0.0003
5/FE	0.0041	0.0001	0.0026	0.0000	0.9997

**Table C.22 Modal Assurance Criteria (FE Model vs. Measured)
for #8 BP1 Reinforcing Rod Specimen**

Mode	1/M	2/M	3/M	4/M	5/M
1/FE	0.9998	0.0011	0.0034	0.0002	0.0077
2/FE	0.0002	0.9996	0.0005	0.0045	0.0003
3/FE	0.0034	0.0002	0.9997	0.0004	0.0039
4/FE	0.0003	0.0051	0.0002	0.9997	0.0007
5/FE	0.0048	0.0004	0.0036	0.0000	0.9992

**Table C.23 Modal Assurance Criteria (FE Model vs. Measured)
for #8 BP2 Reinforcing Rod Specimen**

Mode	1/M	2/M	3/M	4/M	5/M
1/FE	0.9995	0.0002	0.0028	0.0000	0.0081
2/FE	0.0001	0.9998	0.0000	0.0039	0.0000
3/FE	0.0032	0.0000	0.9993	0.0000	0.0026
4/FE	0.0000	0.0046	0.0000	0.9996	0.0000
5/FE	0.0038	0.0001	0.0039	0.0000	0.9991

**Table C.24 Modal Assurance Criteria (FE Model vs. Measured)
for #8 BP3 Reinforcing Rod Specimen**

Mode	1/M	2/M	3/M	4/M	5/M
1/FE	0.9996	0.0001	0.0031	0.0002	0.0053
2/FE	0.0019	0.9997	0.0002	0.0060	0.0001
3/FE	0.0027	0.0004	0.9993	0.0001	0.0041
4/FE	0.0006	0.0046	0.0003	0.9992	0.0002
5/FE	0.0052	0.0005	0.0037	0.0001	0.9992

**Table C.25 Modal Assurance Criteria (FE Model vs. Measured)
for #8 PH1 Reinforcing Rod Specimen**

Mode	1/M	2/M	3/M	4/M	5/M
1/FE	0.9993	0.0100	0.0005	0.0036	0.0001
2/FE	0.0069	0.9998	0.0000	0.0042	0.0000
3/FE	0.0006	0.0000	0.9995	0.0000	0.0032
4/FE	0.0051	0.0070	0.0000	0.9990	0.0000
5/FE	0.0003	0.0000	0.0022	0.0001	0.9996

**Table C.26 Modal Assurance Criteria (FE Model vs. Measured)
for #8 S1 Reinforcing Rod Specimen**

Mode	1/M	2/M	3/M	4/M	5/M
1/FE	0.9995	0.0002	0.0021	0.0003	0.0044
2/FE	0.0006	0.9998	0.0005	0.0037	0.0003
3/FE	0.0015	0.0002	0.9997	0.0006	0.0020
4/FE	0.0003	0.0046	0.0005	0.9999	0.0000
5/FE	0.0042	0.0004	0.0023	0.0003	0.9996

**Table C.27 Modal Assurance Criteria (FE Model vs. Measured)
for #8 S2 Reinforcing Rod Specimen**

Mode	1/M	2/M	3/M	4/M	5/M
1/FE	0.9999	0.0024	0.0038	0.0016	0.0125
2/FE	0.0021	0.9999	0.0015	0.0042	0.0031
3/FE	0.0039	0.0018	0.9997	0.0009	0.0005
4/FE	0.0021	0.0056	0.0010	0.9987	0.0001
5/FE	0.0049	0.0014	0.0046	0.0003	0.9875

**Table C.28 Modal Assurance Criteria (FE Model vs. Measured)
for #8 S3 Reinforcing Rod Specimen**

Mode	1/M	2/M	3/M	4/M	5/M
1/FE	0.9999	0.0008	0.0092	0.0005	0.0130
2/FE	0.0003	0.9998	0.0003	0.0116	0.0004
3/FE	0.0100	0.0001	0.9996	0.0006	0.0090
4/FE	0.0006	0.0103	0.0000	0.9994	0.0002
5/FE	0.0090	0.0003	0.0094	0.0000	0.9997

**Table C.29 Modal Assurance Criteria (FE Model vs. Measured)
for #8 W1 Reinforcing Rod Specimen**

Mode	1/M	2/M	3/M	4/M	5/M
1/FE	0.9995	0.0095	0.0080	0.0060	0.0142
2/FE	0.0100	0.9999	0.0064	0.0094	0.0059
3/FE	0.0069	0.0055	0.9999	0.0069	0.0065
4/FE	0.0053	0.0093	0.0053	0.9998	0.0030
5/FE	0.0102	0.0063	0.0053	0.0026	0.9998

**Table C.30 Modal Assurance Criteria (FE Model vs. Measured)
for #8 W2 Reinforcing Rod Specimen**

Mode	1/M	2/M	3/M	4/M	5/M
1/FE	0.9996	0.0003	0.0022	0.0002	0.0099
2/FE	0.0009	0.9999	0.0001	0.0039	0.0002
3/FE	0.0016	0.0004	0.9999	0.0006	0.0024
4/FE	0.0003	0.0047	0.0005	0.9996	0.0000
5/FE	0.0044	0.0003	0.0019	0.0012	0.9993

C.3. SYSTEM IDENTIFICATION RESULTS

The baseline modal parameter (i.e., resonant frequencies and mode shapes) identification results for thirty reinforcing rod specimens are presented here. The convergence of the system identification scheme is demonstrated in Tables C.31 through C.60. Tables C.31 through C.40 present the convergence results for #14 specimens. Tables C.41 through C.50 and Tables C.51 and C.60 present the results for #11 and #8 specimens, respectively. The identified baseline stiffness properties are summarized in Table C.61.

Table C.31 System Identification for #14 Unwelded Reinforcing Rod Specimen

Mode	Frequency of Initial FE Model	Updated Frequencies (Hz)			Frequency of Target Structure	Error (%)	
		Iter. 1	Iter. 2	Iter. 3		Initial	Final
1	131.92	124.04	124.04		122.38	6.06	0.27
2	361.59	340.01	340.00		339.38	6.54	0.19
3	703.16	661.18	661.18		660.63	6.44	0.08
4	1150.2	1081.6	1081.6		1081.3	6.37	0.03
5	1696.6	1595.3	1595.3		1595.6	6.33	0.02

Table C.32 System Identification for #14 BP1 Reinforcing Rod Specimen

Mode	Frequency of Initial FE Model	Updated Frequencies (Hz)			Frequency of Target Structure	Error (%)	
		Iter. 1	Iter. 2	Iter. 3		Initial	Final
1	131.92	124.05			124.38	6.1	0.3
2	361.59	340.03			340.00	6.4	0.0
3	703.16	661.22			659.38	6.6	0.3
4	1150.2	1081.6			1082.5	6.3	0.1
5	1696.6	1595.4			1594.4	6.4	0.1

Table C.33 System Identification for #14 BP2 Reinforcing Rod Specimen

Mode	Frequency of Initial FE Model	Updated Frequencies (Hz)			Frequency of Target Structure	Error (%)	
		Iter. 1	Iter. 2	Iter. 3		Initial	Final
1	126.61	118.99			118.75	6.6	0.2
2	347.11	326.23			327.50	6.0	0.4
3	675.20	634.58			633.13	6.6	0.2
4	1104.9	1038.5			1041.3	6.1	0.3
5	1630.6	1532.5			1528.8	6.7	0.2

Table C.34 System Identification for #14 BP3 Reinforcing Rod Specimen

Mode	Frequency of Initial FE Model	Updated Frequencies (Hz)			Frequency of Target Structure	Error (%)	
		Iter. 1	Iter. 2	Iter. 3		Initial	Final
1	129.89	122.13			121.88	6.6	0.2
2	356.06	334.78			335.63	6.1	0.3
3	692.48	651.09			649.38	6.6	0.3
4	1132.9	1065.2			1068.8	6.0	0.3
5	1671.4	1571.5			1569.4	6.5	0.1

Table C.35 System Identification for #14 PH3 Reinforcing Rod Specimen

Mode	Frequency of Initial FE Model	Updated Frequencies (Hz)			Frequency of Target Structure	Error (%)	
		Iter. 1	Iter. 2	Iter. 3		Initial	Final
1	129.22	121.81			121.88	6.0	0.1
2	354.24	333.92			334.38	5.9	0.1
3	688.97	649.44			647.50	6.4	0.3
4	1127.2	1062.6			1065.0	5.8	0.2
5	1663.1	1567.7			1565.6	6.2	0.1

Table C.36 System Identification for #14 S1 Reinforcing Rod Specimen

Mode	Frequency of Initial FE Model	Updated Frequencies (Hz)			Frequency of Target Structure	Error (%)	
		Iter. 1	Iter. 2	Iter. 3		Initial	Final
1	128.89	120.56			120.63	6.8	0.1
2	353.34	330.50			330.63	6.9	0.0
3	687.23	642.81			641.88	7.1	0.1
4	1124.4	1051.7			1052.5	6.8	0.1
5	1659.0	1551.7			1551.3	6.9	0.0

Table C.37 System Identification for #14 S2 Reinforcing Rod Specimen

Mode	Frequency of Initial FE Model	Updated Frequencies (Hz)			Frequency of Target Structure	Error (%)	
		Iter. 1	Iter. 2	Iter. 3		Initial	Final
1	128.56	121.91			121.88	5.5	0.0
2	352.44	334.20			334.38	5.4	0.1
3	685.49	650.01			649.38	5.6	0.1
4	1121.6	1063.6			1064.4	5.4	0.1
5	1654.9	1569.2			1568.8	5.5	0.0

Table C.38 System Identification for #14 S3 Reinforcing Rod Specimen

Mode	Frequency of Initial FE Model	Updated Frequencies (Hz)			Frequency of Target Structure	Error (%)	
		Iter. 1	Iter. 2	Iter. 3		Initial	Final
1	128.56	122.31			122.50	4.9	0.16
2	352.44	335.32			335.63	5.0	0.09
3	685.49	652.19			651.25	5.3	0.14
4	1121.6	1067.1			1066.9	5.1	0.02
5	1654.9	1574.5			1573.1	5.2	0.09

Table C.39 System Identification for #14 W1 Reinforcing Rod Specimen

Mode	Frequency of Initial FE Model	Updated Frequencies (Hz)			Frequency of Target Structure	Error (%)	
		Iter. 1	Iter. 2	Iter. 3		Initial	Final
1	129.22	121.20			121.25	6.6	0.04
2	354.24	332.26			332.50	6.5	0.07
3	688.97	646.22			645.00	6.8	0.19
4	1127.2	1057.3			1058.8	6.5	0.14
5	1663.1	1559.9			1558.8	6.7	0.07

Table C.40 System Identification for #14 W2 Reinforcing Rod Specimen

Mode	Frequency of Initial FE Model	Updated Frequencies (Hz)			Frequency of Target Structure	Error (%)	
		Iter. 1	Iter. 2	Iter. 3		Initial	Final
1	130.22	123.06			122.50	6.3	0.5
2	356.97	337.33			338.75	5.4	0.4
3	694.24	656.04			654.38	6.1	0.3
4	1135.8	1073.3			1078.1	5.4	0.4
5	1675.5	1583.3			1580.6	6.0	0.2

Table C.41 System Identification for #11 Unwelded Reinforcing Rod Specimen

Mode	Frequency of Initial FE Model	Updated Frequencies (Hz)			Frequency of Target Structure	Error (%)	
		Iter. 1	Iter. 2	Iter. 3		Initial	Final
1	110.83	103.16	103.16		103.13	7.47	0.03
2	304.31	283.24	283.24		283.13	7.48	0.04
3	593.18	552.10	552.11		551.88	7.48	0.04
4	973.26	905.86	905.88		906.25	7.39	0.04
5	1440.7	1340.9	1341.0		1341.9	7.36	0.07

Table C.42 System Identification for #11 BP1 Reinforcing Rod Specimen

Mode	Frequency of Initial FE Model	Updated Frequencies (Hz)			Frequency of Target Structure	Error (%)	
		Iter. 1	Iter. 2	Iter. 3		Initial	Final
1	105.58	99.65	99.68		100.00	5.58	0.32
2	293.53	274.67	274.68		274.38	6.98	0.11
3	562.93	532.81	533.00		532.50	5.71	0.09
4	939.16	878.85	878.88		879.38	6.80	0.06
5	1369.1	1295.0	1295.5		1295.6	5.67	0.01

Table C.43 System Identification for #11 BP2 Reinforcing Rod Specimen

Mode	Frequency of Initial FE Model	Updated Frequencies (Hz)			Frequency of Target Structure	Error (%)	
		Iter. 1	Iter. 2	Iter. 3		Initial	Final
1	106.67	99.93	99.96		100.00	6.67	0.04
2	296.55	276.16	276.16		276.25	7.35	0.03
3	568.66	533.74	533.98		533.75	6.54	0.04
4	948.66	883.48	883.49		883.13	7.42	0.04
5	1382.9	1297.3	1297.9		1299.4	6.43	0.11

Table C.44 System Identification for #11 BP3 Reinforcing Rod Specimen

Mode	Frequency of Initial FE Model	Updated Frequencies (Hz)			Frequency of Target Structure	Error (%)	
		Iter. 1	Iter. 2	Iter. 3		Initial	Final
1	106.67	100.42	100.45		100.63	6.00	0.18
2	296.54	276.99	276.99		276.88	7.10	0.04
3	568.67	536.73	536.92		536.88	5.92	0.01
4	948.63	886.13	886.13		886.25	7.04	0.01
5	1382.9	1304.4	1304.9		1305.0	5.97	0.01

Table C.45 System Identification for #11 PH2 Reinforcing Rod Specimen

Mode	Frequency of Initial FE Model	Updated Frequencies (Hz)			Frequency of Target Structure	Error (%)	
		Iter. 1	Iter. 2	Iter. 3		Initial	Final
1	106.94	100.25	100.27		100.63	6.27	0.36
2	297.31	276.34	276.33		276.25	7.62	0.03
3	570.11	535.89	536.08		535.63	6.44	0.08
4	951.04	884.02	884.01		883.75	7.61	0.03
5	1386.4	1302.3	1302.7		1302.5	6.44	0.02

Table C.46 System Identification for #11 S1 Reinforcing Rod Specimen

Mode	Frequency of Initial FE Model	Updated Frequencies (Hz)			Frequency of Target Structure	Error (%)	
		Iter. 1	Iter. 2	Iter. 3		Initial	Final
1	106.40	100.20	100.24		100.00	6.40	0.24
2	295.73	276.81	276.82		276.88	6.81	0.02
3	567.45	535.35	535.59		536.25	5.82	0.12
4	945.64	885.37	885.42		885.63	6.78	0.02
5	1380.7	1301.6	1302.1		1304.4	5.85	0.18

Table C.47 System Identification for #11 S2 Reinforcing Rod Specimen

Mode	Frequency of Initial FE Model	Updated Frequencies (Hz)			Frequency of Target Structure	Error (%)	
		Iter. 1	Iter. 2	Iter. 3		Initial	Final
1	107.21	100.51	100.54		100.63	6.54	0.09
2	298.08	277.06	277.07		276.88	7.66	0.07
3	571.51	537.30	537.53		537.50	6.33	0.01
4	953.59	886.33	886.36		886.88	7.52	0.06
5	1389.6	1305.6	1306.1		1308.1	6.23	0.15

Table C.48 System Identification for #11 S3 Reinforcing Rod Specimen

Mode	Frequency of Initial FE Model	Updated Frequencies (Hz)			Frequency of Target Structure	Error (%)	
		Iter. 1	Iter. 2	Iter. 3		Initial	Final
1	106.39	100.39	100.41		100.63	5.72	0.22
2	295.79	276.28	276.28		276.25	7.07	0.01
3	567.21	537.02	537.13		536.88	5.65	0.05
4	946.28	883.90	883.93		883.75	7.08	0.02
5	1379.4	1305.0	1305.3		1306.3	5.60	0.08

Table C.49 System Identification for #11 W1 Reinforcing Rod Specimen

Mode	Frequency of Initial FE Model	Updated Frequencies (Hz)			Frequency of Target Structure	Error (%)	
		Iter. 1	Iter. 2	Iter. 3		Initial	Final
1	106.67	100.57	100.60		100.63	6.00	0.03
2	296.49	277.64	277.62		277.50	6.84	0.04
3	568.86	537.41	537.61		536.25	6.08	0.25
4	948.09	888.04	888.01		888.13	6.75	0.01
5	1384.0	1306.4	1306.9		1311.9	5.50	0.38

Table C.50 System Identification for #11 W2 Reinforcing Rod Specimen

Mode	Frequency of Initial FE Model	Updated Frequencies (Hz)			Frequency of Target Structure	Error (%)	
		Iter. 1	Iter. 2	Iter. 3		Initial	Final
1	109.74	103.72	103.74		103.75	5.77	0.01
2	305.03	285.47	285.48		285.63	6.79	0.05
3	585.07	554.64	554.76		555.00	5.42	0.04
4	974.98	912.86	912.90		912.50	6.85	0.04
5	1423.0	1347.3	1347.6		1349.4	5.45	0.13

Table C.51 System Identification for #8 Unwelded Reinforcing Rod Specimen

Mode	Frequency of Initial FE Model	Updated Frequencies (Hz)			Frequency of Target Structure	Error (%)	
		Iter. 1	Iter. 2	Iter. 3		Initial	Final
1	79.313	74.702	74.701		74.375	6.64	0.44
2	218.19	205.50	205.50		205.63	6.11	0.06
3	426.48	401.69	401.68		401.88	6.12	0.05
4	702.27	661.45	661.44		662.50	6.00	0.16
5	1044.10	983.39	983.38		985.00	6.00	0.16

Table C.52 System Identification for #8 BP1 Reinforcing Rod Specimen

Mode	Frequency of Initial FE Model	Updated Frequencies (Hz)			Frequency of Target Structure	Error (%)	
		Iter. 1	Iter. 2	Iter. 3		Initial	Final
1	75.427	72.685	72.684		73.125	3.15	0.60
2	212.59	200.58	200.59		200.63	5.96	0.02
3	402.62	390.46	390.45		389.38	3.40	0.27
4	684.37	645.73	645.75		645.00	6.10	0.12
5	987.89	956.19	956.17		953.13	3.65	0.32

Table C.53 System Identification for #8 BP2 Reinforcing Rod Specimen

Mode	Frequency of Initial FE Model	Updated Frequencies (Hz)			Frequency of Target Structure	Error (%)	
		Iter. 1	Iter. 2	Iter. 3		Initial	Final
1	75.047	72.616	72.610		73.125	2.63	0.70
2	211.46	200.01	200.00		200.00	5.73	0.00
3	400.70	390.37	390.33		388.75	3.07	0.41
4	680.53	643.89	643.85		643.13	5.82	0.11
5	983.61	955.98	955.89		952.50	3.27	0.36

Table C.54 System Identification for #8 BP3 Reinforcing Rod Specimen

Mode	Frequency of Initial FE Model	Updated Frequencies (Hz)			Frequency of Target Structure	Error (%)	
		Iter. 1	Iter. 2	Iter. 3		Initial	Final
1	75.245	75.801	75.872	75.974	78.125	3.69	2.75
2	211.97	211.03	210.06	210.07	210.00	0.94	0.03
3	401.86	406.10	407.17	407.89	405.00	0.78	0.71
4	681.85	679.08	676.10	676.15	674.38	1.11	0.26
5	986.94	995.57	997.58	999.21	991.25	0.43	0.80

Table C.55 System Identification for #8 PH1 Reinforcing Rod Specimen

Mode	Frequency of Initial FE Model	Updated Frequencies (Hz)			Frequency of Target Structure	Error (%)	
		Iter. 1	Iter. 2	Iter. 3		Initial	Final
1	74.475	74.251	74.225		73.750	0.98	0.64
2	209.84	206.65	206.64		206.88	1.43	0.12
3	397.65	397.81	397.63		398.75	0.27	0.28
4	675.38	665.20	665.17		665.00	1.56	0.03
5	976.13	974.99	974.59		976.25	0.01	0.17

Table C.56 System Identification for #8 S1 Reinforcing Rod Specimen

Mode	Frequency of Initial FE Model	Updated Frequencies (Hz)			Frequency of Target Structure	Error (%)	
		Iter. 1	Iter. 2	Iter. 3		Initial	Final
1	75.427	72.620	72.621		72.500	4.04	0.17
2	212.59	200.76	200.76		200.63	5.96	0.06
3	402.62	389.87	389.87		390.00	3.24	0.03
4	684.37	646.29	646.31		646.88	5.80	0.09
5	987.89	954.84	954.83		955.63	3.38	0.08

Table C.57 System Identification for #8 S2 Reinforcing Rod Specimen

Mode	Frequency of Initial FE Model	Updated Frequencies (Hz)			Frequency of Target Structure	Error (%)	
		Iter. 1	Iter. 2	Iter. 3		Initial	Final
1	75.044	72.360	72.359		72.500	3.51	0.19
2	211.49	199.51	199.51		199.38	6.07	0.07
3	400.60	388.84	388.84		388.13	3.21	0.18
4	680.81	642.28	642.30		642.50	5.96	0.03
5	983.06	952.26	952.24		951.25	3.34	0.10

Table C.58 System Identification for #8 S3 Reinforcing Rod Specimen

Mode	Frequency of Initial FE Model	Updated Frequencies (Hz)			Frequency of Target Structure	Error (%)	
		Iter. 1	Iter. 2	Iter. 3		Initial	Final
1	75.431	72.846	72.846		73.125	3.15	0.38
2	212.56	200.65	200.65		200.63	5.95	0.01
3	402.70	391.59	391.58		390.63	3.09	0.24
4	684.12	645.92	645.94		645.63	5.96	0.05
5	988.40	958.91	958.90		956.25	3.36	0.28

Table C.59 System Identification for #8 W1 Reinforcing Rod Specimen

Mode	Frequency of Initial FE Model	Updated Frequencies (Hz)			Frequency of Target Structure	Error (%)	
		Iter. 1	Iter. 2	Iter. 3		Initial	Final
1	74.865	71.688	71.697		71.875	4.16	0.25
2	210.85	198.74	198.74		198.75	6.09	0.01
3	399.94	384.59	384.65		384.38	4.05	0.07
4	678.07	639.57	639.57		639.38	6.05	0.03
5	982.60	942.55	942.68		941.88	4.32	0.08

Table C.60 System Identification for #8 W2 Reinforcing Rod Specimen

Mode	Frequency of Initial FE Model	Updated Frequencies (Hz)			Frequency of Target Structure	Error (%)	
		Iter. 1	Iter. 2	Iter. 3		Initial	Final
1	75.428	72.388	72.394		72.500	4.04	0.15
2	212.58	200.70	200.71		200.63	5.96	0.04
3	402.63	388.24	388.28		388.13	3.74	0.04
4	684.34	646.11	646.13		646.25	5.89	0.02
5	987.95	951.01	951.11		950.63	3.93	0.05

Table C.61 Summary of Identified Baseline Stiffness Parameters (E)

Type of Rod Specimen		Identified Young's Modulus (lb/in ²)
Size	Specimen	
#14	Unwelded	26.5×10 ⁶
	BP1	26.5×10 ⁶
	BP2	26.5×10 ⁶
	BP3	26.5×10 ⁶
	PH3	26.7×10 ⁶
	S1	26.2×10 ⁶
	S2	27.0×10 ⁶
	S3	27.2×10 ⁶
	W1	26.4×10 ⁶
	W2	26.8×10 ⁶
#11	Unwelded	26.0×10 ⁶
	BP1	26.3×10 ⁶
	BP2	26.0×10 ⁶
	BP3	26.2×10 ⁶
	PH2	25.9×10 ⁶
	S1	26.3×10 ⁶
	S2	25.9×10 ⁶
	S3	26.2×10 ⁶
	W1	26.3×10 ⁶
	W2	26.3×10 ⁶
#8	Unwelded	26.6×10 ⁶
	BP1	26.7×10 ⁶
	BP2	26.8×10 ⁶
	BP3	29.4×10 ⁶
	PH1	29.1×10 ⁶
	S1	26.8×10 ⁶
	S2	26.7×10 ⁶
	S3	26.7×10 ⁶
	W1	26.6×10 ⁶
	W2	26.7×10 ⁶

APPENDIX D
TXDOT TENSILE TEST REPORTS FOR REINFORCING ROD SPECIMENS

This appendix contains reproductions of the TxDOT tensile test report sheets for the thirty 48-inch reinforcing rod specimens discussed in Chapters 3, 4, and 5. Each data sheet is identified by the specimen code defined in Chapter 3, Table 3.1.

LAB NO.
 SPECIMEN ID 14C
 SIZE 14
 TECH rh

Test Tensile Test
 Procedure REBAR (TEX 427-A)

Test Date 04-07-2000 Tested By HAMILTON
 Test Time 08:14:53 AM Test Counter N/A
 Elapsed Time 00:04:37 Area 2.2500 In²

Tensile Strgth	106130 PSI	Peak Load	238780 Lbs
Breaking Strgth	71812 PSI	Breaking Load	161580 Lbs
Modulus	1253800 PSI	Correl Coeff	0.9983
2 % Off Strs	80728 PSI	2 % Off Load	181640 Lbs
HOTL Yield Sts	73397 PSI	HOTL Yield Lod	165140 Lbs
Upper Yield Sts	73397 PSI	Lower Yield Sts	73199 PSI
Upper Yield Lod	165140 Lbs	Lower Yield Lod	164700 Lbs

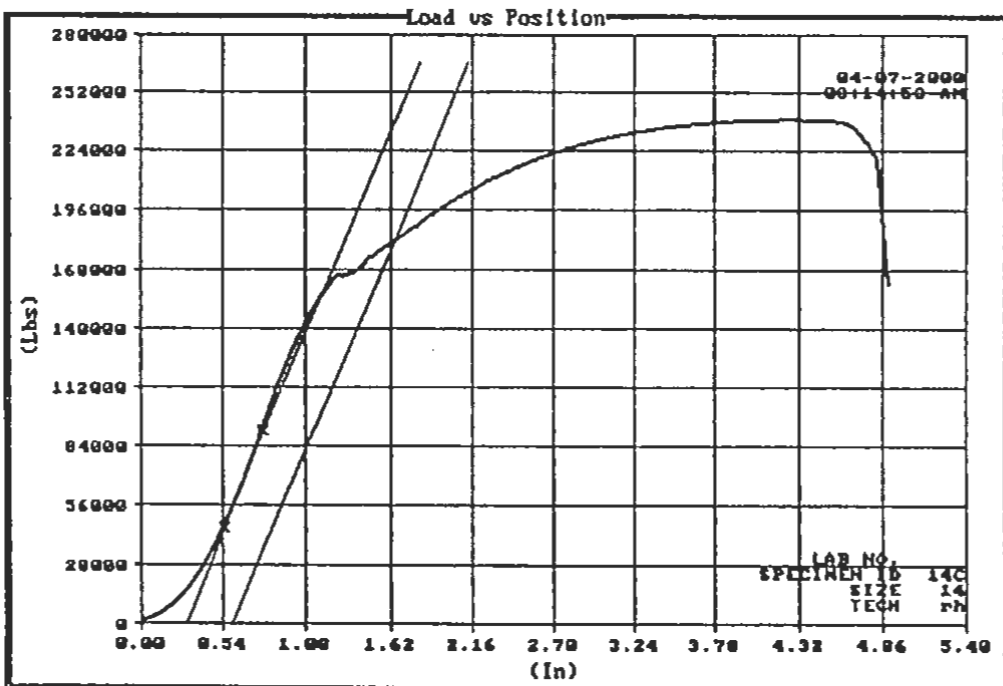


Figure D.1 TxDOT Tensile Test Report for #14 Unwelded Reinforcing Rod Specimen

LAB NO.
 SPECIMEN ID BP2
 SIZE 14
 TECH rh

Test Tensile Test
 Procedure REBAR (TEX 427-A)

Test Date 04-07-2000 Tested By HAMILTON
 Test Time 08:25:58 AM Test Counter N/A
 Elapsed Time 00:03:09 Area 2.2500 In²

Tensile Strgth	81587 PSI	Peak Load	183570 Lbs
Breaking Strgth	81225 PSI	Breaking Load	182760 Lbs
HOTL Yield Sts	73434 PSI	HOTL Yield Lod	165230 Lbs
Upper Yield Sts	73434 PSI	Lower Yield Sts	73362 PSI
Upper Yield Lod	165230 Lbs	Lower Yield Lod	165060 Lbs

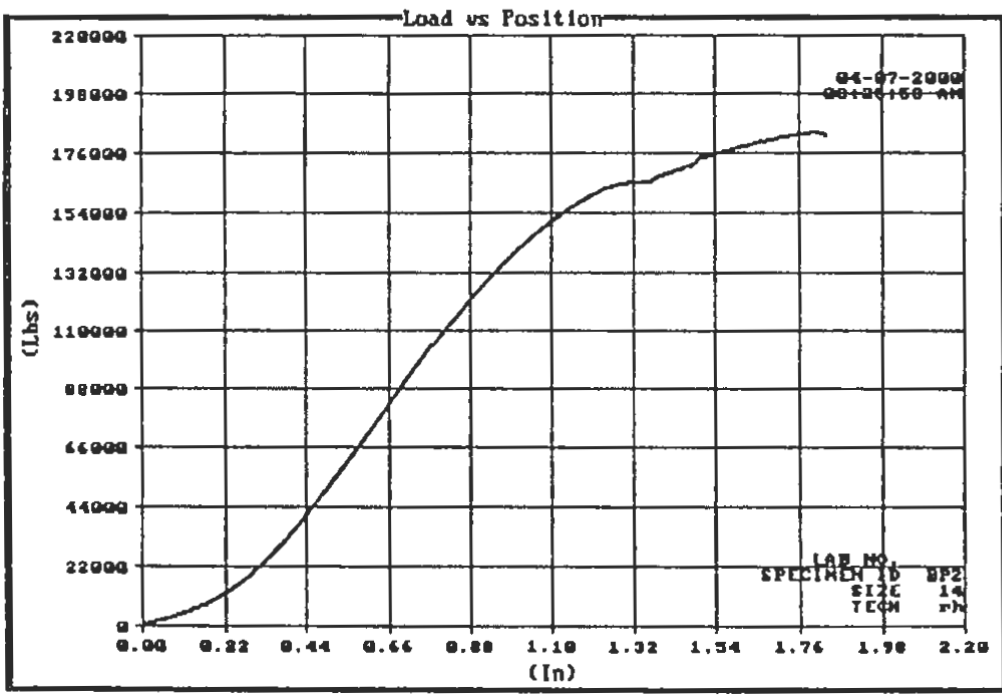


Figure D.3 TxDOT Tensile Test Report for #14 BP2 Reinforcing Rod Specimen

LAB NO.
 SPECIMEN ID BP3
 SIZE 14
 TECH rh

Test Tensile Test
 Procedure REBAR (TEX 427-A)

Test Date 04-07-2000 Tested By HAMILTON
 Test Time 09:15:44 AM Test Counter N/A
 Elapsed Time 00:03:22 Area 2.2500 In²

Tensile Strgth	83196 PSI	Peak Load	187190 Lbs
Breaking Strgth	81273 PSI	Breaking Load	182860 Lbs
HOTL Yield Sts	69118 PSI	HOTL Yield Lod	155510 Lbs
Upper Yield Sts	69118 PSI	Lower Yield Sts	68629 PSI
Upper Yield Lod	155510 Lbs	Lower Yield Lod	154420 Lbs

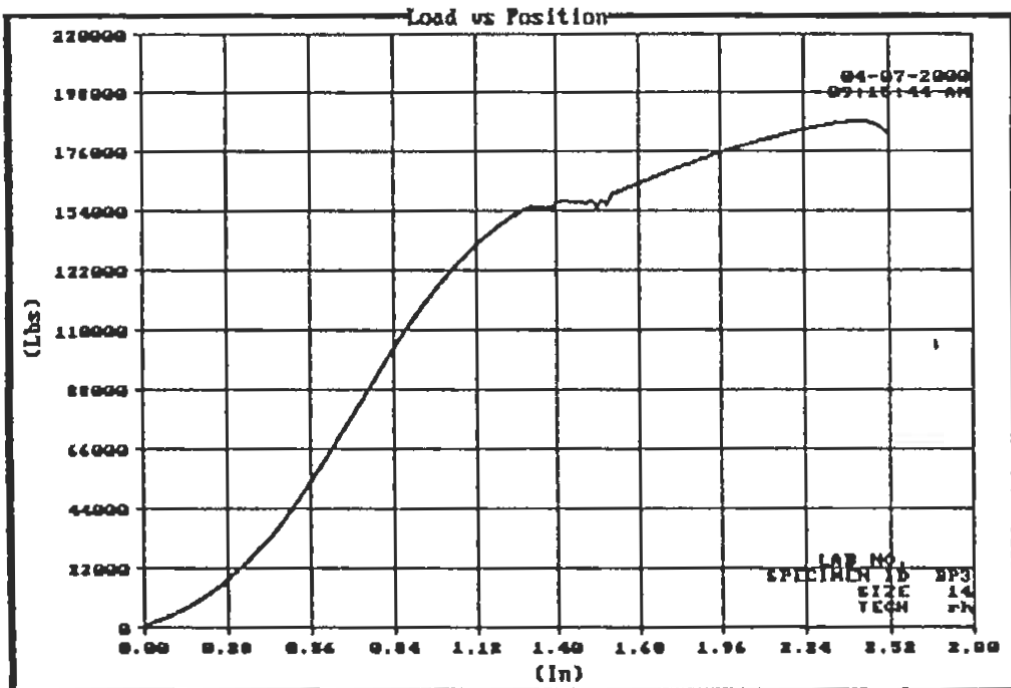


Figure D.4 TxDOT Tensile Test Report for #14 BP3
 Reinforcing Rod Specimen

LAB NO.
SPECIMEN ID
SIZE
TECH

~~PH2~~ PH3
14
rh

Test Tensile Test
Procedure REBAR (TEX 427-A)

Test Date 04-07-2000
Test Time 08:59:21 AM
Elapsed Time 00:03:59

Tested By HAMILTON
Test Counter N/A
Area 2.2500 In²

Tensile Strgth 90481 PSI
Breaking Strgth 89343 PSI
HOTL Yield Sts 69491 PSI
Upper Yield Sts 69491 PSI
Upper Yield Lod 156350 Lbs

Peak Load 203580 Lbs
Breaking Load 201020 Lbs
HOTL Yield Lod 156350 Lbs
Lower Yield Sts 69220 PSI
Lower Yield Lod 155740 Lbs

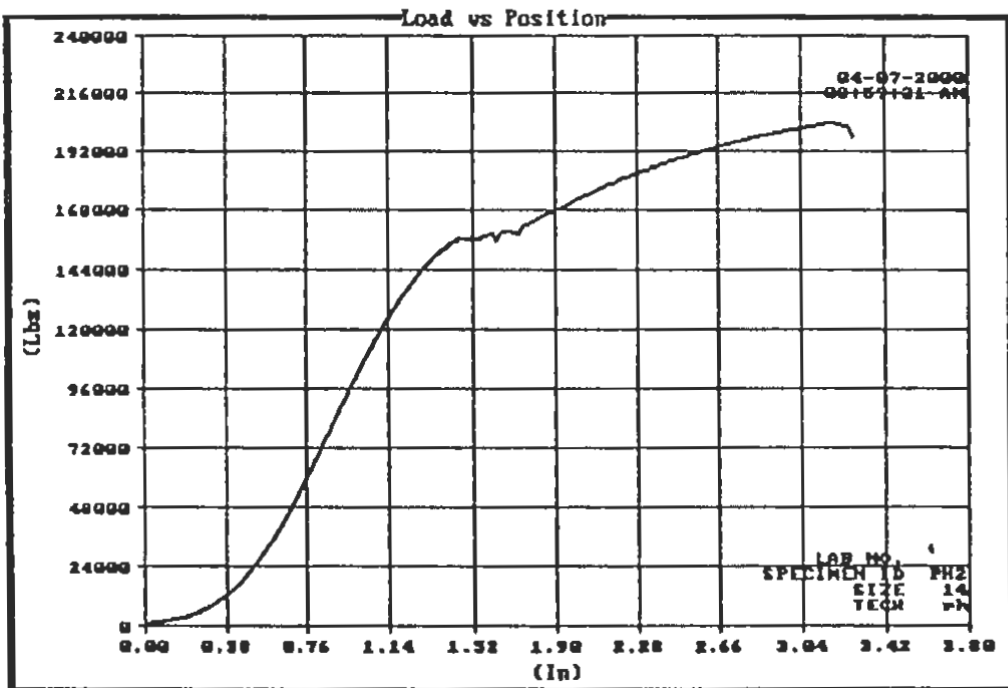


Figure D.5 TxDOT Tensile Test Report for #14 PH3
Reinforcing Rod Specimen

LAB NO.
 SPECIMEN ID S1
 SIZE 14
 TECH rh

Test Tensile Test
 Procedure REBAR (TEX 427-A)

Test Date 04-07-2000 Tested By HAMILTON
 Test Time 09:26:45 AM Test Counter 00000083
 Elapsed Time 00:03:12 Area 2.2500 In»

Tensile Strgth	90353 PSI	Peak Load	203290 Lbs
Breaking Strgth	90052 PSI	Breaking Load	202620 Lbs
HOTL Yield Sts	73720 PSI	HOTL Yield Lod	165870 Lbs
Upper Yield Sts	73720 PSI	Lower Yield Sts	73681 PSI
Upper Yield Lod	165870 Lbs	Lower Yield Lod	165780 Lbs

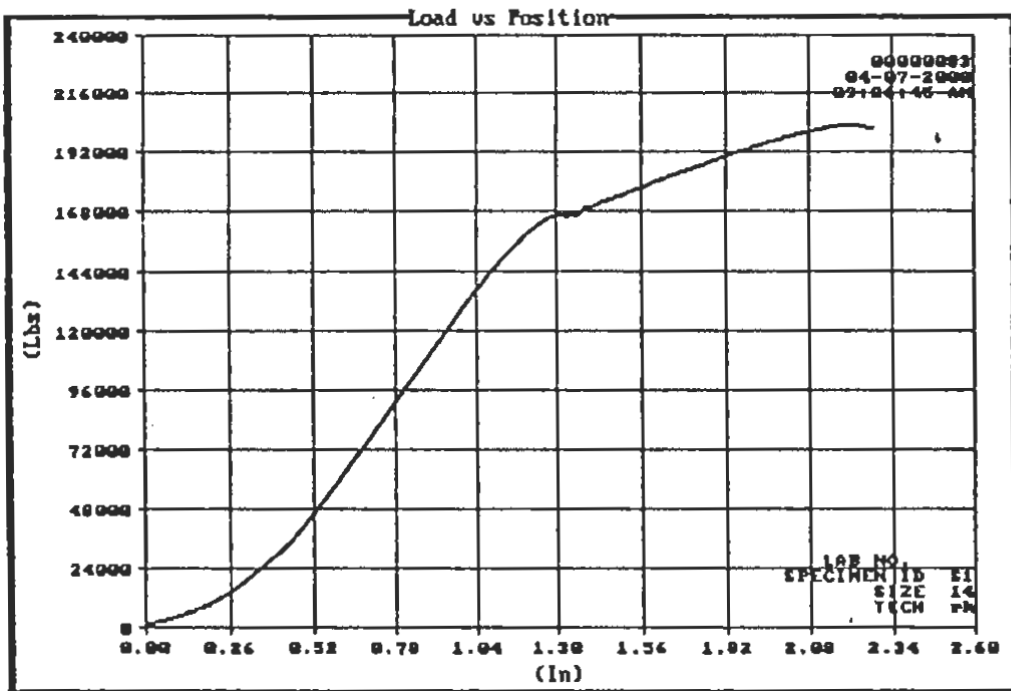


Figure D.6 TxDOT Tensile Test Report for #14 S1 Reinforcing Rod Specimen

LAB NO.
 SPECIMEN ID S2
 SIZE 14
 TECH rh

Test Tensile Test
 Procedure REBAR (TEX 427-A)

Test Date 04-07-2000 Tested By HAMILTON
 Test Time 09:37:42 AM Test Counter 00000084
 Elapsed Time 00:03:31 Area 2.2500 In²

Tensile Strgth	87931 PSI	Peak Load	197840 Lbs
Breaking Strgth	87631 PSI	Breaking Load	197170 Lbs
HOTL Yield Sts	69463 PSI	HOTL Yield Lod	156290 Lbs
Upper Yield Sts	69463 PSI	Lower Yield Sts	69082 PSI
Upper Yield Lod	156290 Lbs	Lower Yield Lod	155430 Lbs

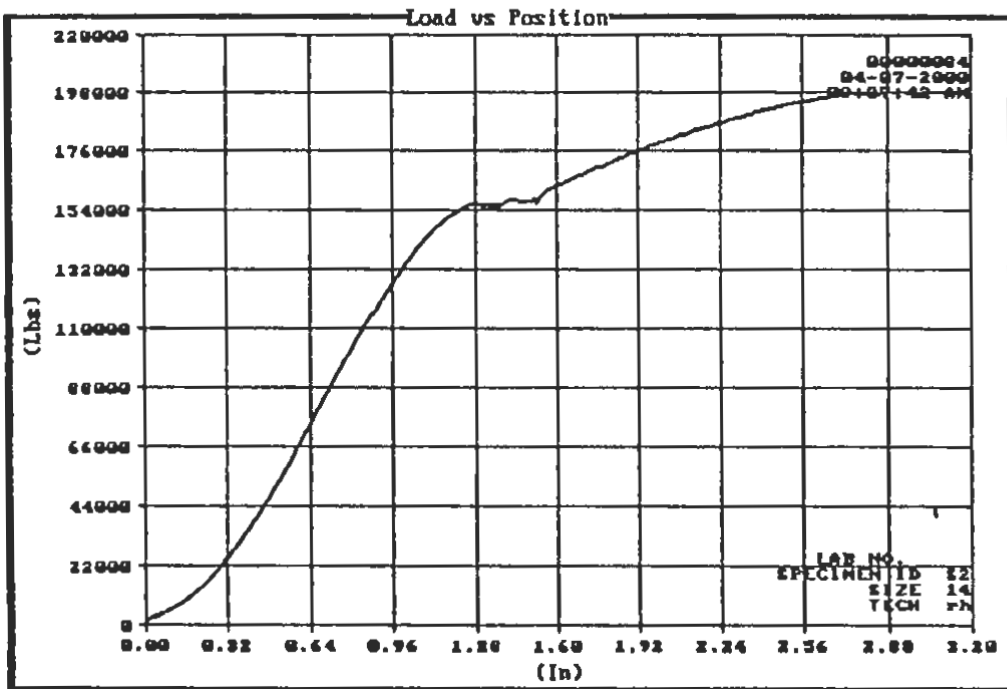


Figure D.7 TxDOT Tensile Test Report for #14 S2 Reinforcing Rod Specimen

LAB NO.
 SPECIMEN ID S3
 SIZE 14
 TECH rh

Test Tensile Test
 Procedure REBAR (TEX 427-A)

Test Date 04-07-2000 Tested By HAMILTON
 Test Time 09:58:59 AM Test Counter N/A
 Elapsed Time 00:02:18 Area 2.2500 In²

Tensile Strgth	88442 PSI	Peak Load	198990 Lbs
Breaking Strgth	86208 PSI	Breaking Load	193970 Lbs
HOTL Yield Sts	69587 PSI	HOTL Yield Lod	156570 Lbs
Upper Yield Sts	69587 PSI	Lower Yield Sts	69501 PSI
Upper Yield Lod	156570 Lbs	Lower Yield Lod	156380 Lbs

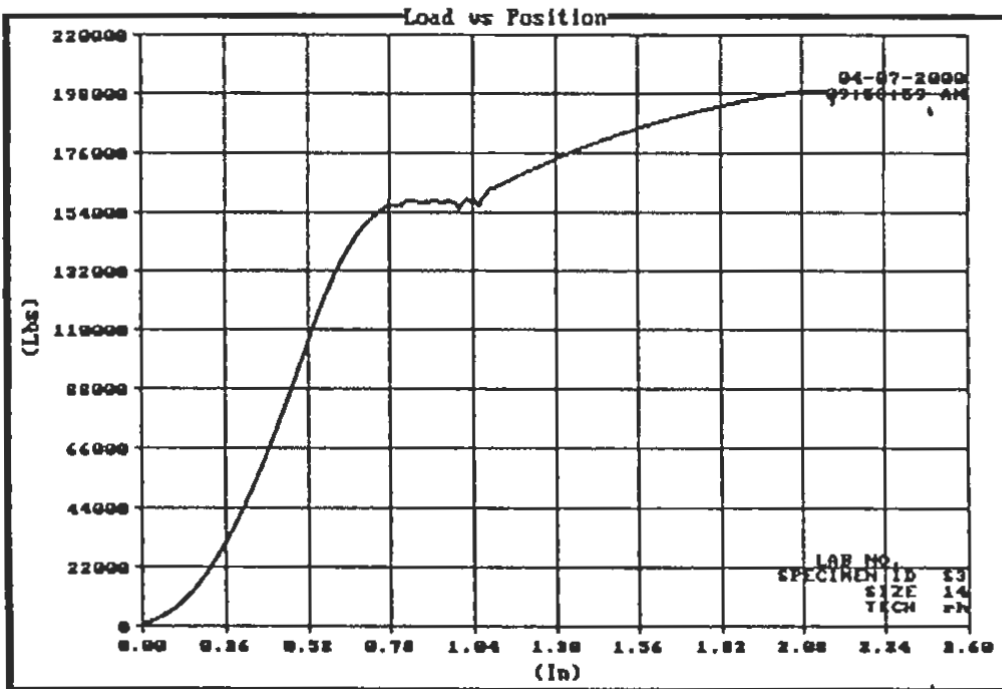


Figure D.8 TxDOT Tensile Test Report for #14 S3 Reinforcing Rod Specimen

LAB NO.
 SPECIMEN ID W1
 SIZE 14
 TECH rh

Test Tensile Test
 Procedure REBAR (TEX 427-A)

Test Date	04-07-2000	Tested By	HAMILTON
Test Time	09:49:28 AM	Test Counter	N/A
Elapsed Time	00:03:22	Area	2.2500 In ²

Tensile Strgth	79444 PSI	Peak Load	178750 Lbs
Breaking Strgth	77476 PSI	Breaking Load	174320 Lbs
HOTL Yield Sts	56079 PSI	HOTL Yield Lod	126180 Lbs
Upper Yield Sts	56079 PSI	Lower Yield Sts	55430 PSI
Upper Yield Lod	126180 Lbs	Lower Yield Lod	124720 Lbs

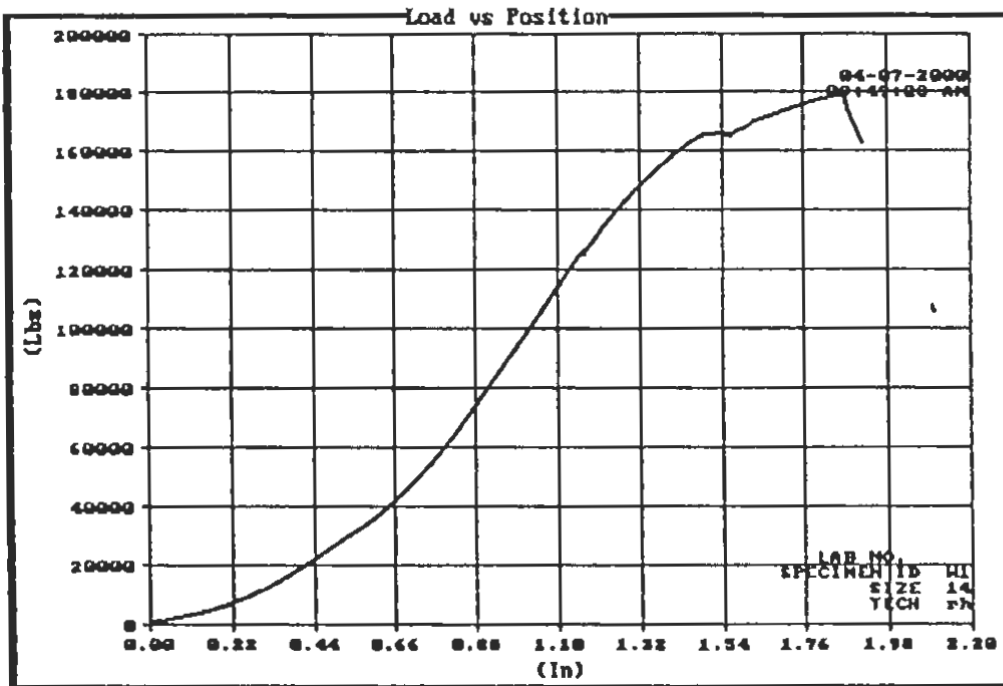


Figure D.9 TxDOT Tensile Test Report for #14 W1 Reinforcing Rod Specimen

LAB NO.
 SPECIMEN ID W2
 SIZE 14
 TECH rh

Test Tensile Test
 Procedure REBAR (TEX 427-A)

Test Date 04-07-2000 Tested By HAMILTON
 Test Time 08:48:39 AM Test Counter N/A
 Elapsed Time 00:03:19 Area 2.2500 In²

Tensile Strgth	78240 PSI	Peak Load	176040 Lbs
Breaking Strgth	73806 PSI	Breaking Load	166060 Lbs
HOTL Yield Sts	69160 PSI	HOTL Yield Lod	155610 Lbs
Upper Yield Sts	69160 PSI	Lower Yield Sts	69010 PSI
Upper Yield Lod	155610 Lbs	Lower Yield Lod	155270 Lbs

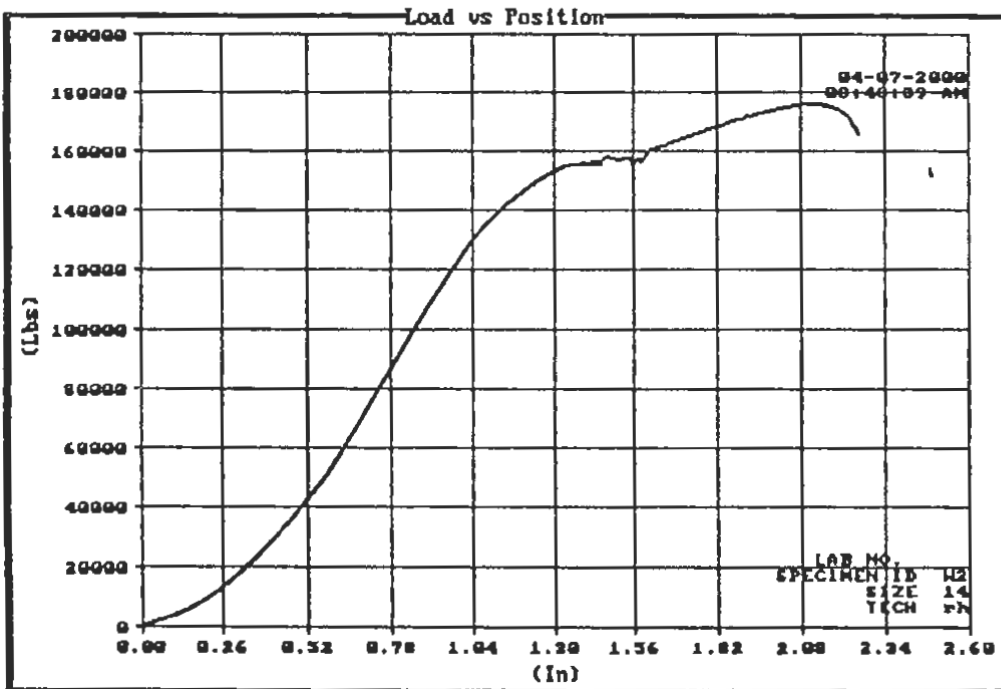


Figure D.10 TxDOT Tensile Test Report for #14 W2 Reinforcing Rod Specimen

LAB NO.
 SPECIMEN ID 11c
 SIZE 11
 TECH rh

Test Tensile Test
 Procedure REBAR W/EXTENSOMETER

Test Date	04-06-2000	Tested By	HAMILTON
Test Time	02:11:09 PM	Test Counter	N/A
Elapsed Time	00:04:46	Area	1.5600 In ²

Tensile Strgth	109890 PSI	Peak Load	171420 Lbs
Breaking Strgth	578 PSI	Breaking Load	.902 Lbs
Modulus	27367000 PSI	Correl Coeff	1.0000
.2 % Off Strs	72638 PSI	.2 % Off Load	113310 Lbs
% Off Strs		HOTL Yield Sts	71375 PSI
HOTL Yield Lod	111340 Lbs	Upper Yield Sts	71375 PSI
Lower Yield Sts	573 PSI	Upper Yield Lod	111340 Lbs
Lower Yield Lod	894 Lbs		

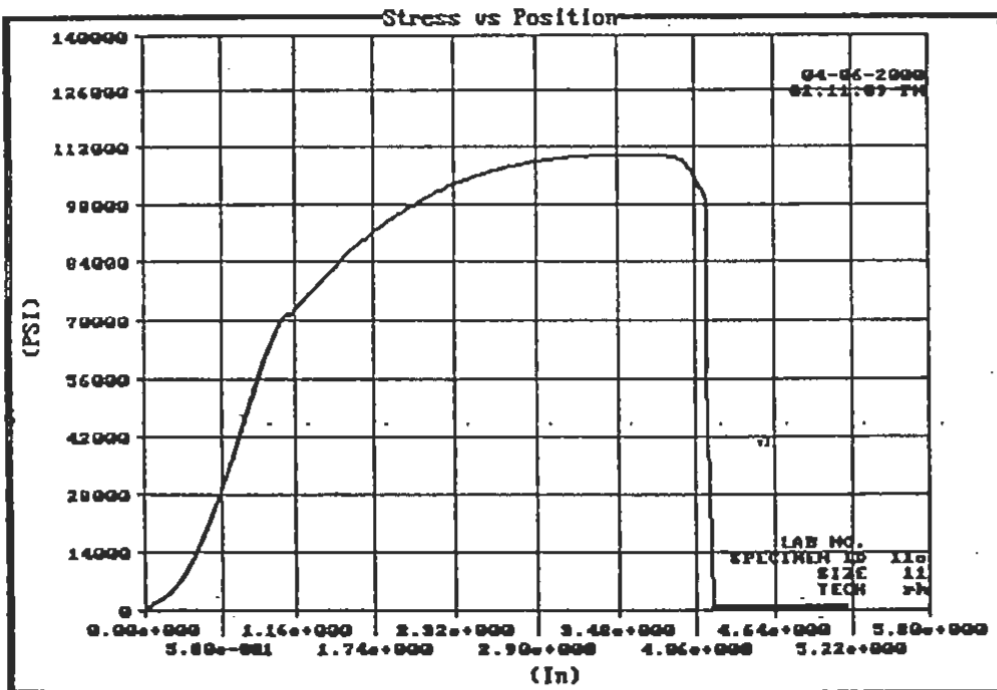


Figure D.11 TxDOT Tensile Test Report for #11 Unwelded Reinforcing Rod Specimen

LAB NO.
 SPECIMEN ID BP1
 SIZE 11
 TECH rh

Test Tensile Test
 Procedure REBAR W/EXTENSOMETER

Test Date	04-06-2000	Tested By	HAMILTON
Test Time	02:50:34 PM	Test Counter	N/A
Elapsed Time	00:02:49	Area	1.5600 In»

Tensile Strgth	85732 PSI	Peak Load	133740 Lbs
Breaking Strgth	81 PSI	Breaking Load	126 Lbs
Modulus	26886000 PSI	Correl Coeff	1.0000
.2 % Off Strs	60258 PSI	.2 % Off Load	94002 Lbs
% Off Strs		HOTL Yield Sts	60640 PSI
HOTL Yield Lod	94599 Lbs	Upper Yield Sts	60640 PSI
Lower Yield Sts	-2267 PSI	Upper Yield Lod	94599 Lbs
Lower Yield Lod	-3536 Lbs		

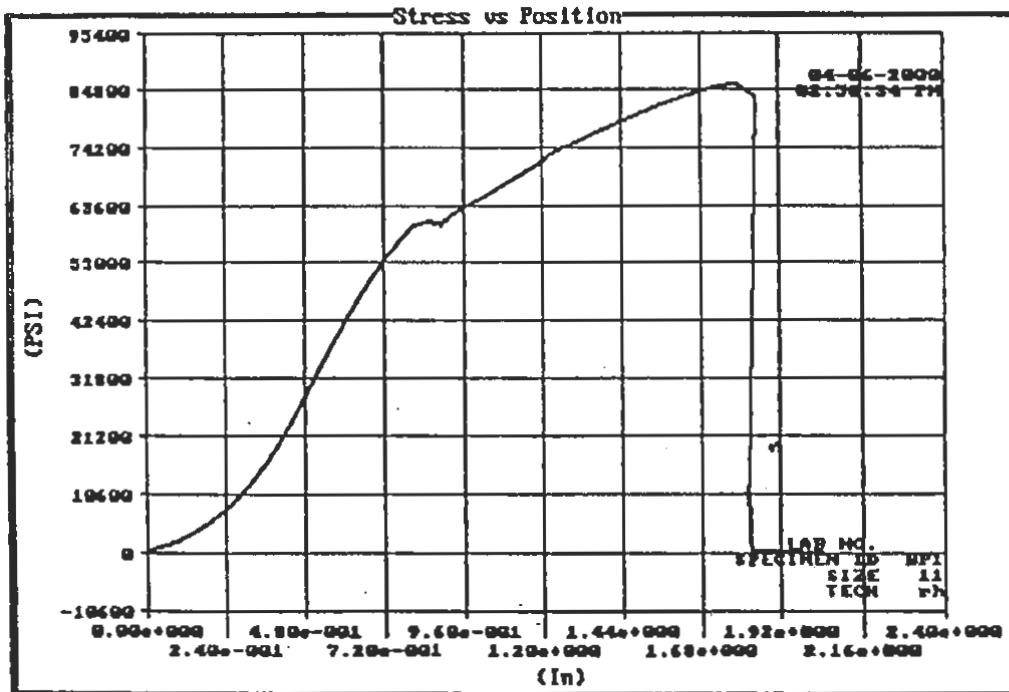


Figure D.12 TxDOT Tensile Test Report for #11 BP1 Reinforcing Rod Specimen

LAB NO.
 SPECIMEN ID BP2
 SIZE 11
 TECH rh

Test Tensile Test
 Procedure REBAR W/EXTENSOMETER

Test Date 04-06-2000
 Test Time 02:42:12 PM
 Elapsed Time 00:02:44

Tested By HAMILTON
 Test Counter N/A
 Area 1.5600 In²

Tensile Strgth 78532 PSI
 Breaking Strgth 109 PSI
 Modulus 26327000 PSI
 .2 % Off Strs 61517 PSI
 % Off Strs
 HOTL Yield Lod
 Lower Yield Sts
 Lower Yield Lod

Peak Load 122510 Lbs
 Breaking Load 170 Lbs
 Correl Coeff 1.0000
 .2 % Off Load 95966 Lbs
 HOTL Yield Sts
 Upper Yield Sts
 Upper Yield Lod

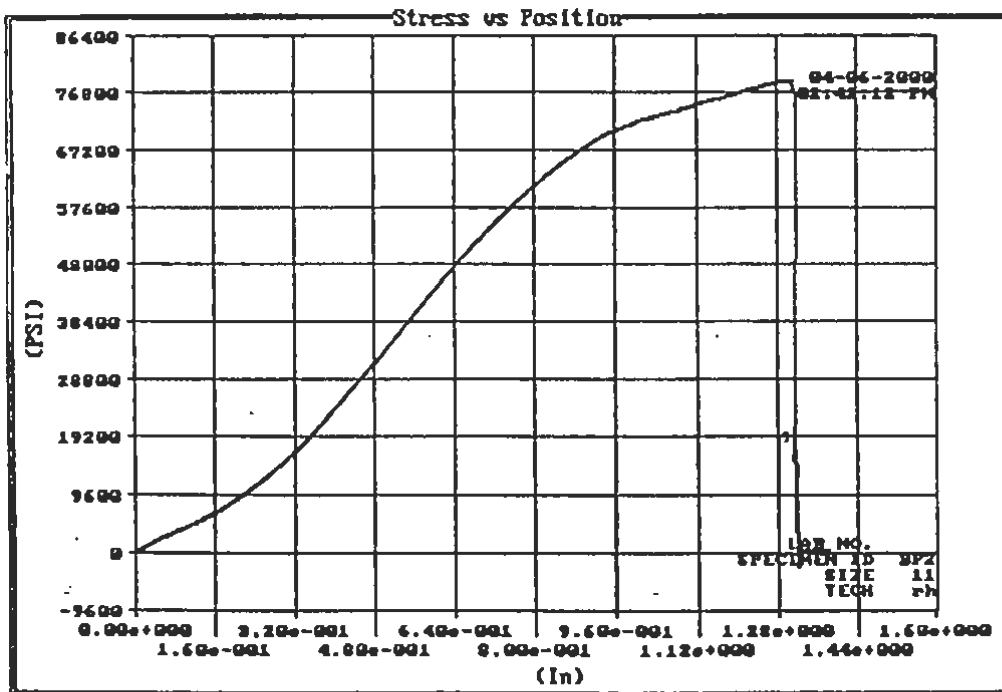


Figure D.13 TxDOT Tensile Test Report for #11 BP2 Reinforcing Rod Specimen

LAB NO.
 SPECIMEN ID BP3
 SIZE 11
 TECH rh

Test Tensile Test
 Procedure REBAR W/EXTENSOMETER

Test Date 04-06-2000 Tested By HAMILTON
 Test Time 02:59:46 PM Test Counter N/A
 Elapsed Time 00:03:02 Area 1.5600 In²

Tensile Strgth	85159 PSI	Peak Load	132850 Lbs
Breaking Strgth	-327 PSI	Breaking Load	-510 Lbs
Modulus	23206000 PSI	Correl Coeff	0.9956
.2 % Off Strs	51538 PSI	.2 % Off Load	80399 Lbs
% Off Strs		HOTL Yield Sts	59603 PSI
HOTL Yield Lod	92980 Lbs	Upper Yield Sts	59603 PSI
Lower Yield Sts	-321 PSI	Upper Yield Lod	92980 Lbs
Lower Yield Lod	-500 Lbs		

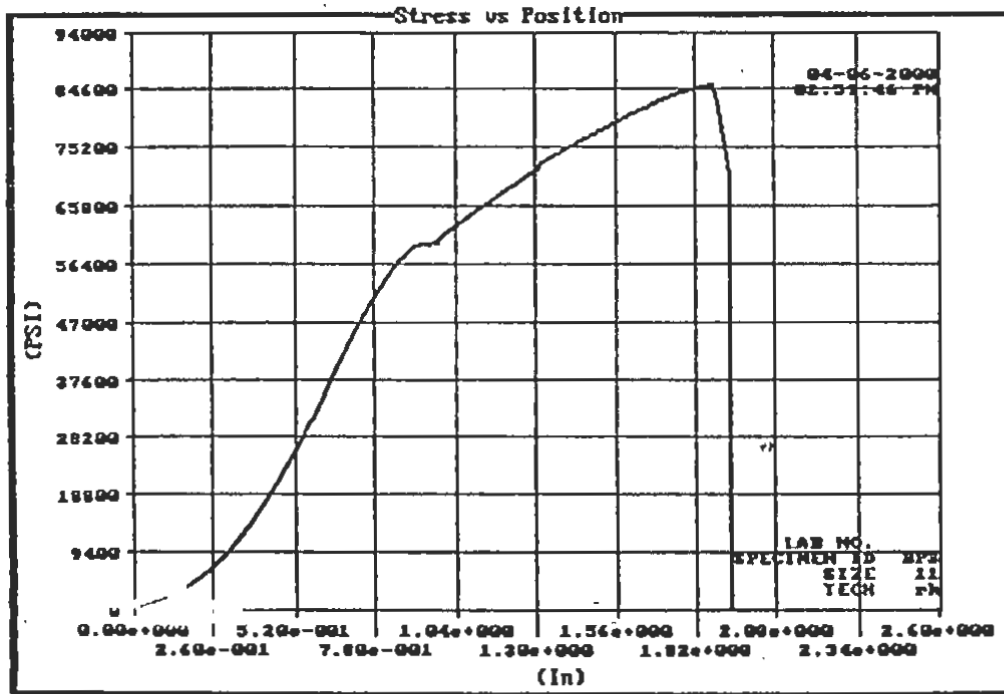


Figure D.14 TxDOT Tensile Test Report for #11 BP3

Reinforcing Rod Specimen

LAB NO.
 SPECIMEN ID PH2
 SIZE 11
 TECH rh

Test Tensile Test
 Procedure REBAR W/EXTENSOMETER

Test Date 04-06-2000 Tested By HAMILTON
 Test Time 03:25:01 PM Test Counter N/A
 Elapsed Time 00:02:54 Area 1.5600 In²

Tensile Strgth	96705 PSI	Peak Load	150860 Lbs
Breaking Strgth	79 PSI	Breaking Load	123 Lbs
Modulus	37796000 PSI	Correl Coeff	0.9997
.2 % Off Strs	70190 PSI	.2 % Off Load	109500 Lbs
% Off Strs		HOTL Yield Sts	70937 PSI
HOTL Yield Lod	110660 Lbs	Upper Yield Sts	70937 PSI
Lower Yield Sts	79 PSI	Upper Yield Lod	110660 Lbs
Lower Yield Lod	124 Lbs		

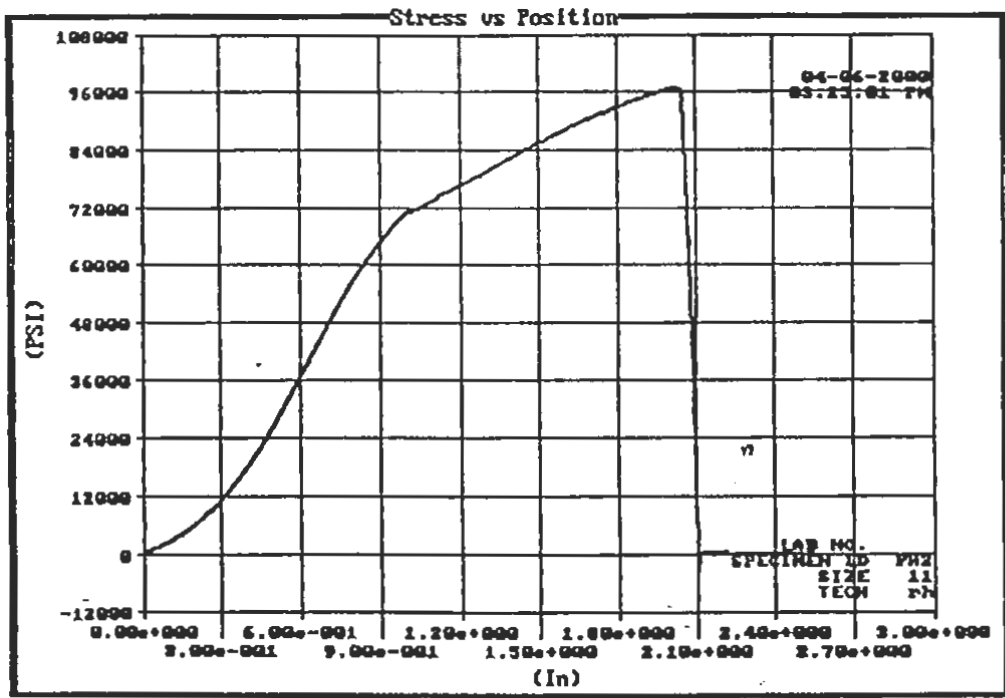


Figure D.15 TxDOT Tensile Test Report for #11 PH2 Reinforcing Rod Specimen

LAB NO.
 SPECIMEN ID S1
 SIZE 11
 TECH rh

Test Tensile Test
 Procedure REBAR W/EXTENSOMETER

Test Date	04-06-2000	Tested By	HAMILTON
Test Time	03:08:18 PM	Test Counter	N/A
Elapsed Time	00:02:26	Area	1.5600 In ²

Tensile Strgth	84410 PSI	Peak Load	131680 Lbs
Breaking Strgth	59 PSI	Breaking Load	92 Lbs
Modulus	25775000 PSI	Correl Coeff	1.0000
.2 % Off Strs	59855 PSI	.2 % Off Load	93374 Lbs
% Off Strs		HOTL Yield Sts	59781 PSI
HOTL Yield Lod	93258 Lbs	Upper Yield Sts	59781 PSI
Lower Yield Sts	57 PSI	Upper Yield Lod	93258 Lbs
Lower Yield Lod	88 Lbs		

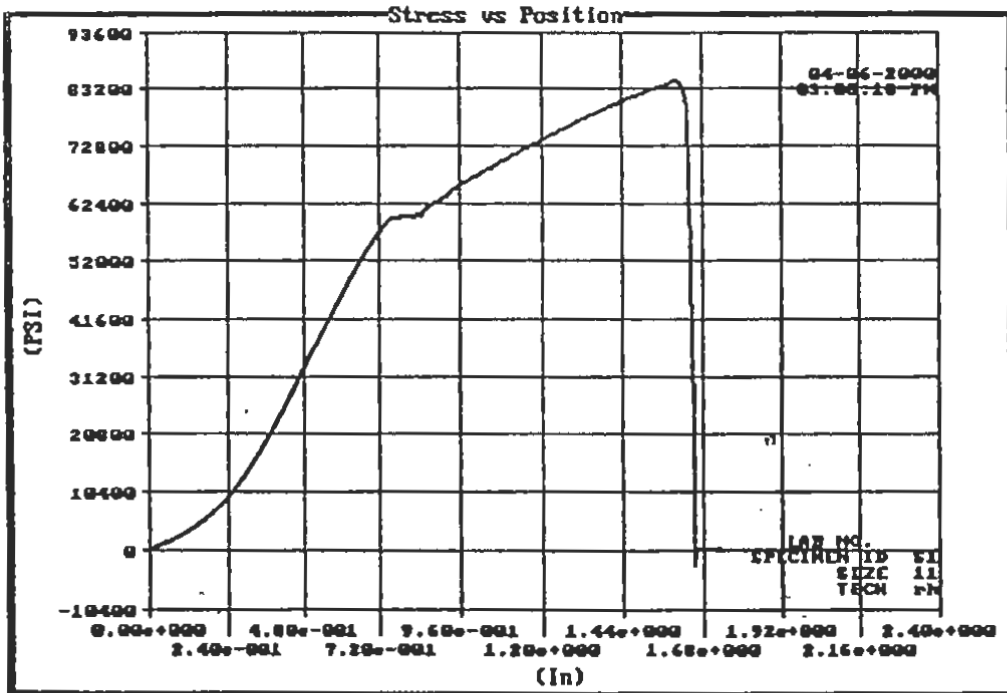


Figure D.16 TxDOT Tensile Test Report for #11 S1 Reinforcing Rod Specimen

LAB NO.
 SPECIMEN ID S2
 SIZE 11
 TECH rh

Test Tensile Test
 Procedure REBAR W/EXTENSOMETER

Test Date 04-06-2000
 Test Time 03:17:01 PM
 Elapsed Time 00:02:28

Tested By HAMILTON
 Test Counter 00000081
 Area 1.5600 In²

Tensile Strgth 85781 PSI
 Breaking Strgth 85699 PSI
 Modulus 27520000 PSI
 .2 % Off Strs 70583 PSI
 % Off Strs
 HOTL Yield Lod 110970 Lbs
 Lower Yield Sts 71063 PSI
 Lower Yield Lod 110860 Lbs

Peak Load 133820 Lbs
 Breaking Load 133690 Lbs
 Correl Coeff 1.0000
 .2 % Off Load 110110 Lbs
 HOTL Yield Sts 71133 PSI
 Upper Yield Sts 71133 PSI
 Upper Yield Lod 110970 Lbs

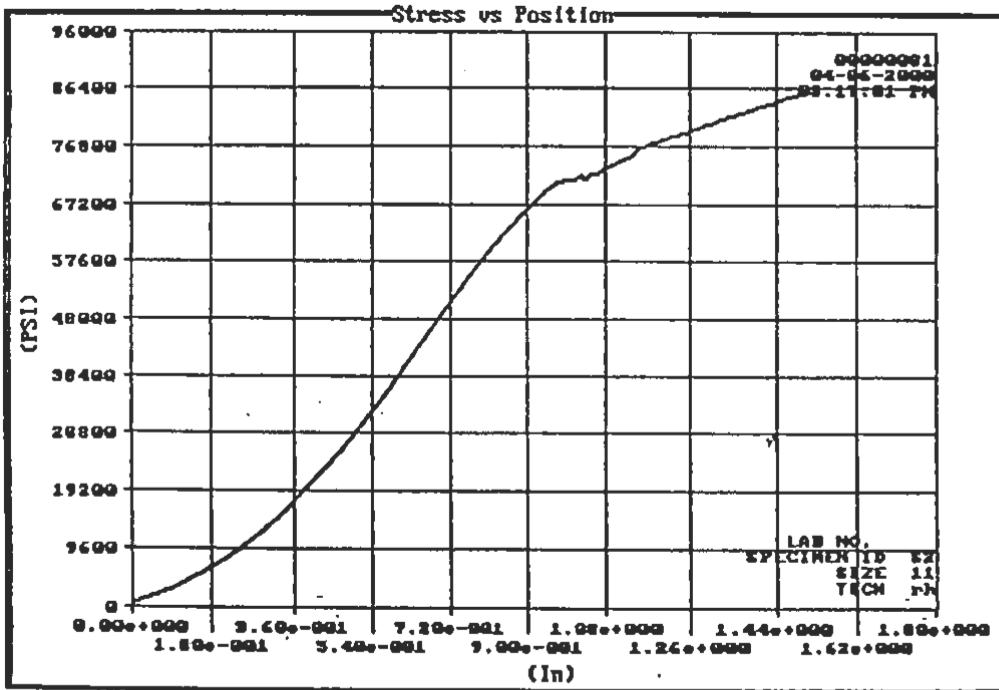


Figure D.17 TxDOT Tensile Test Report for #11 S2
 Reinforcing Rod Specimen

LAB NO.
 SPECIMEN ID S3
 SIZE 11
 TECH rh

Test Tensile Test
 Procedure REBAR W/EXTENSOMETER

Test Date 04-06-2000
 Test Time 02:32:59 PM
 Elapsed Time 00:02:52

Tested By HAMILTON
 Test Counter N/A
 Area 1.5600 In²

Tensile Strgth 84855 PSI
 Breaking Strgth 79 PSI
 Modulus 27672000 PSI
 .2 % Off Strs 71252 PSI
 % Off Strs
 HOTL Yield Lod 111150 Lbs
 Lower Yield Sts 78 PSI
 Lower Yield Lod 122 Lbs

Peak Load 132370 Lbs
 Breaking Load 123 Lbs
 Correl Coeff 0.9999
 .2 % Off Load 111150 Lbs
 HOTL Yield Sts 71253 PSI
 Upper Yield Sts 71253 PSI
 Upper Yield Lod 111150 Lbs

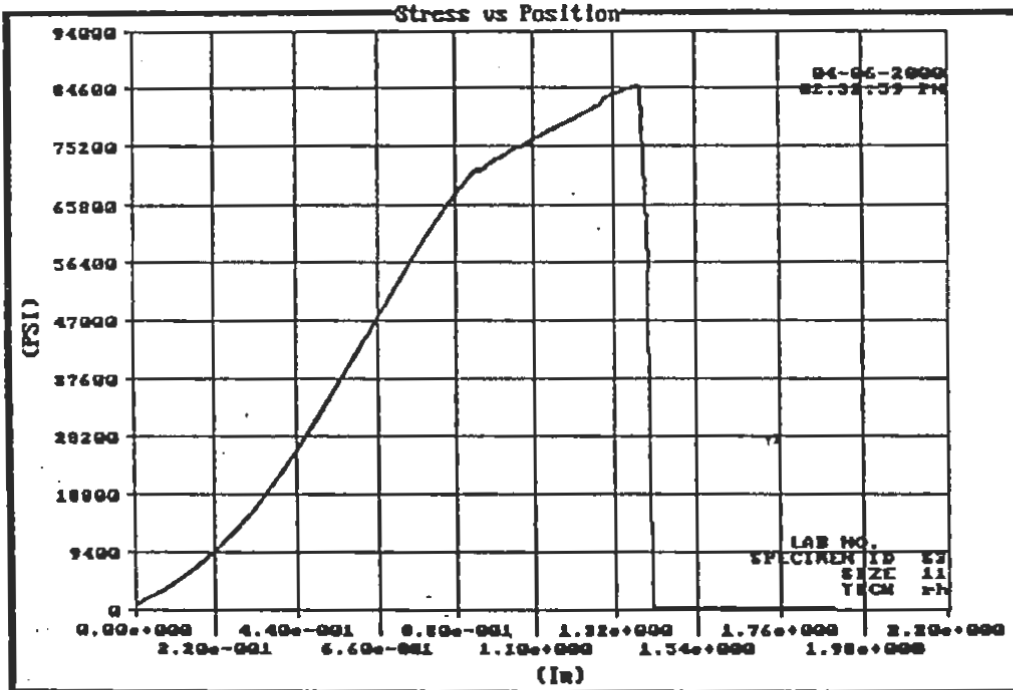


Figure D.18 TxDOT Tensile Test Report for #11 S3 Reinforcing Rod Specimen

LAB NO.
 SPECIMEN ID W1
 SIZE 11
 TECH rh

Test Tensile Test
 Procedure REBAR W/EXTENSOMETER

Test Date 04-06-2000
 Test Time 02:24:15 PM
 Elapsed Time 00:02:49

Tested By HAMILTON
 Test Counter N/A
 Area 1.5600 In²

Tensile Strgth 67923 PSI
 Breaking Strgth 572 PSI
 Modulus 26006000 PSI
 .2 % Off Strs 57433 PSI
 % Off Strs
 HOTL Yield Lod 93797 Lbs
 Lower Yield Sts 571 PSI
 Lower Yield Lod 891 Lbs

Peak Load 105960 Lbs
 Breaking Load 892 Lbs
 Correl Coeff 1.0000
 .2 % Off Load 89595 Lbs
 HOTL Yield Sts 60127 PSI
 Upper Yield Sts 60127 PSI
 Upper Yield Lod 93797 Lbs

u

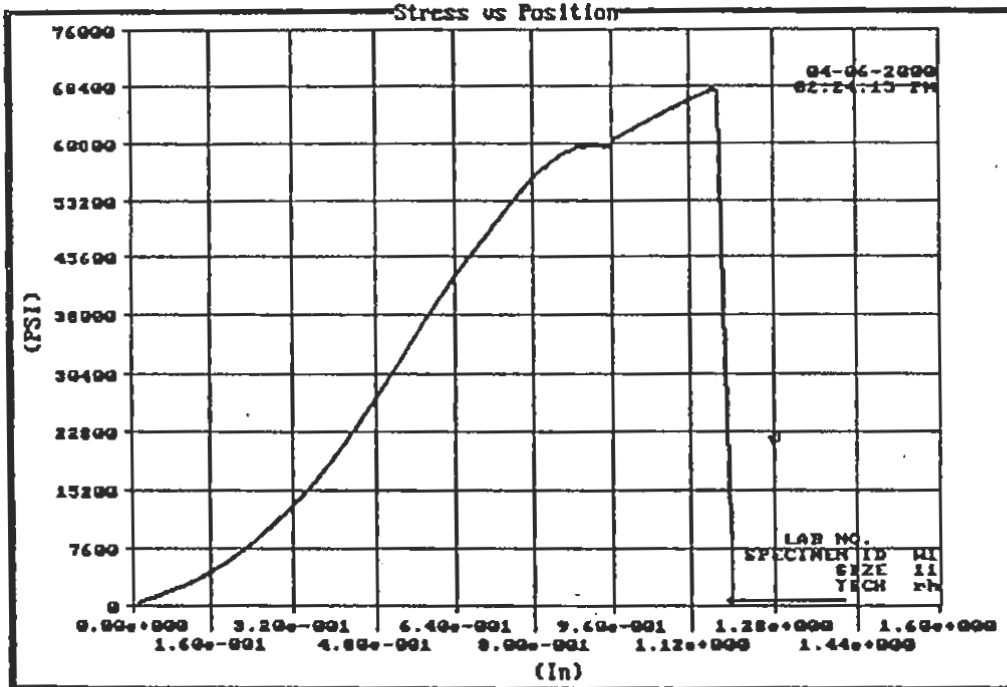


Figure D.19 TxDOT Tensile Test Report for #11 W1 Reinforcing Rod Specimen

LAB NO.
 SPECIMEN ID W2
 SIZE 11
 TECH rh

Test Tensile Test
 Procedure REBAR W/EXTENSOMETER

Test Date 04-06-2000 Tested By HAMILTON
 Test Time 03:33:06 PM Test Counter N/A
 Elapsed Time 00:02:29 Area 1.5600 In²

Tensile Strgth	81422 PSI	Peak Load	127020 Lbs
Breaking Strgth	63442 PSI	Breaking Load	98969 Lbs
Modulus	27144000 PSI	Correl Coeff	1.0000
.2 % Off Strs	59752 PSI	.2 % Off Load	93212 Lbs
% Off Strs		HOTL Yield Sts	59782 PSI
HOTL Yield Lod	93260 Lbs	Upper Yield Sts	59782 PSI
Lower Yield Sts	59596 PSI	Upper Yield Lod	93260 Lbs
Lower Yield Lod	92969 Lbs		

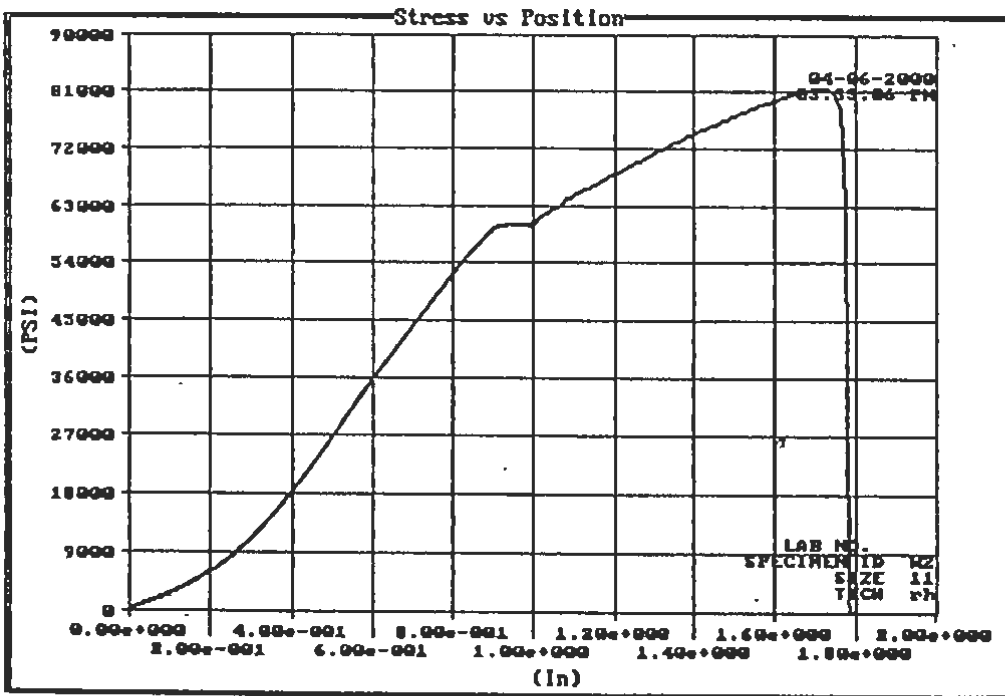


Figure D.20 TxDOT Tensile Test Report for #11 W2 Reinforcing Rod Specimen

LAB NO.
 SPECIMEN ID 8C
 SIZE 8
 TECH rh

Test Tensile Test
 Procedure REBAR W/EXTENSOMETER

Test Date 04-07-2000 Tested By HAMILTON
 Test Time 11:03:15 AM Test Counter N/A
 Elapsed Time 00:02:28 Area 0.7900 In²

Tensile Strgth	106330 PSI	Peak Load	84003 Lbs
Breaking Strgth	96873 PSI	Breaking Load	76530 Lbs
Modulus	27525000 PSI	Correl Coeff	1.0000
.2 % Off Strs	65909 PSI	.2 % Off Load	52068 Lbs
% Off Strs		HOTL Yield Sts	65848 PSI
HOTL Yield Lod	52020 Lbs	Upper Yield Sts	65848 PSI
Lower Yield Sts	65756 PSI	Upper Yield Lod	52020 Lbs
Lower Yield Lod	51947 Lbs		

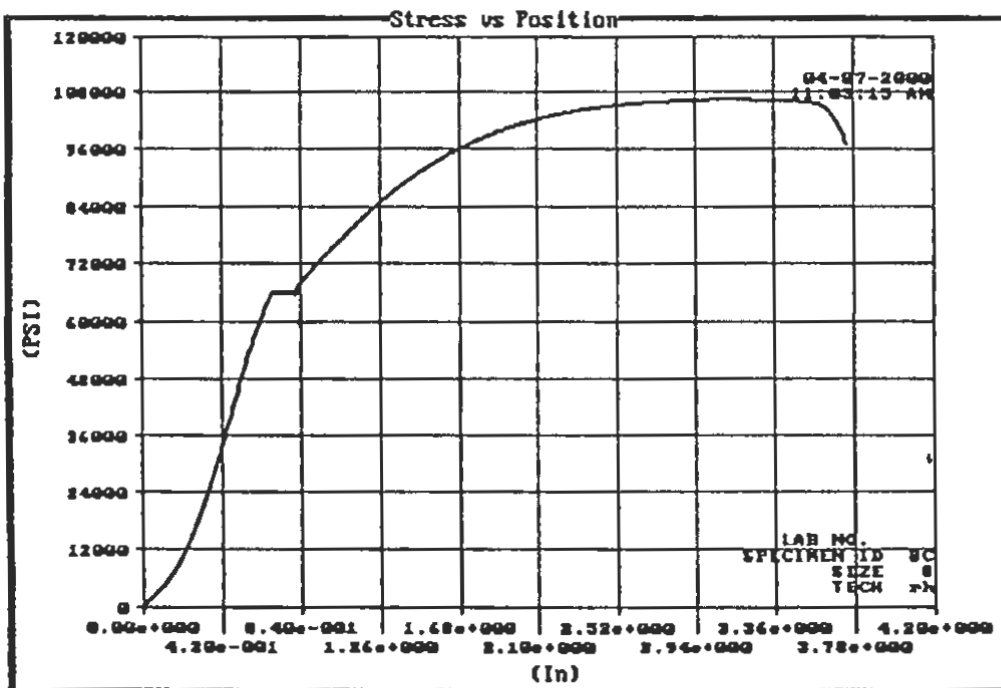


Figure D.21 TxDOT Tensile Test Report for #8 Unwelded Reinforcing Rod Specimen

LAB NO.
 SPECIMEN ID BP1
 SIZE 8
 TECH rh

Test Tensile Test
 Procedure REBAR W/EXTENSOMETER

Test Date 04-07-2000 Tested By HAMILTON
 Test Time 11:15:17 AM Test Counter N/A
 Elapsed Time 00:01:44 Area 0.7900 In²

Tensile Strgth	87808 PSI	Peak Load	69368 Lbs
Breaking Strgth	87513 PSI	Breaking Load	69135 Lbs
Modulus	28316000 PSI	Correl Coeff	1.0000
.2 % Off Strs	63933 PSI	.2 % Off Load	50507 Lbs
% Off Strs		HOTL Yield Sts	63970 PSI
HOTL Yield Lod	50536 Lbs	Upper Yield Sts	63970 PSI
Lower Yield Sts	63866 PSI	Upper Yield Lod	50536 Lbs
Lower Yield Lod	50455 Lbs		

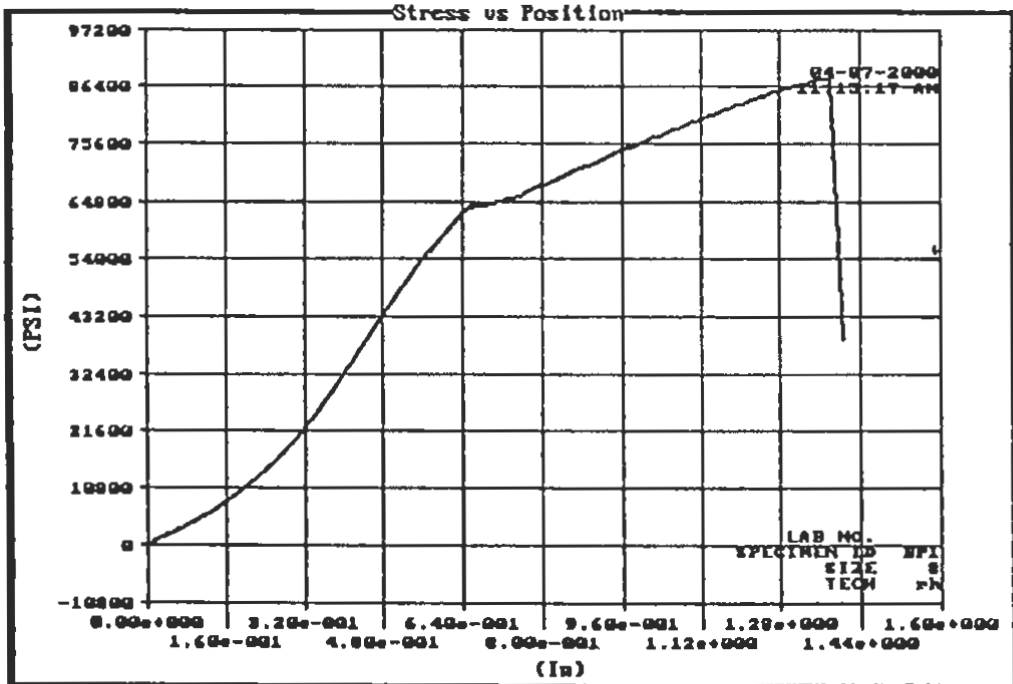


Figure D.22 TxDOT Tensile Test Report for #8 BP1 Reinforcing Rod Specimen

LAB NO.
 SPECIMEN ID BP2
 SIZE 8
 TECH rh

Test Tensile Test
 Procedure REBAR W/EXTENSOMETER

Test Date 04-07-2000 Tested By HAMILTON
 Test Time 11:25:08 AM Test Counter N/A
 Elapsed Time 00:02:58 Area 0.7900 In²

Tensile Strgth	90595 PSI	Peak Load	71570 Lbs
Breaking Strgth	88138 PSI	Breaking Load	69629 Lbs
Modulus	28613000 PSI	Correl Coeff	1.0000
.2 % Off Strs	64276 PSI	.2 % Off Load	50778 Lbs
% Off Strs		HOTL Yield Sts	64233 PSI
HOTL Yield Lod	50744 Lbs	Upper Yield Sts	64233 PSI
Lower Yield Sts	64111 PSI	Upper Yield Lod	50744 Lbs
Lower Yield Lod	50648 Lbs		

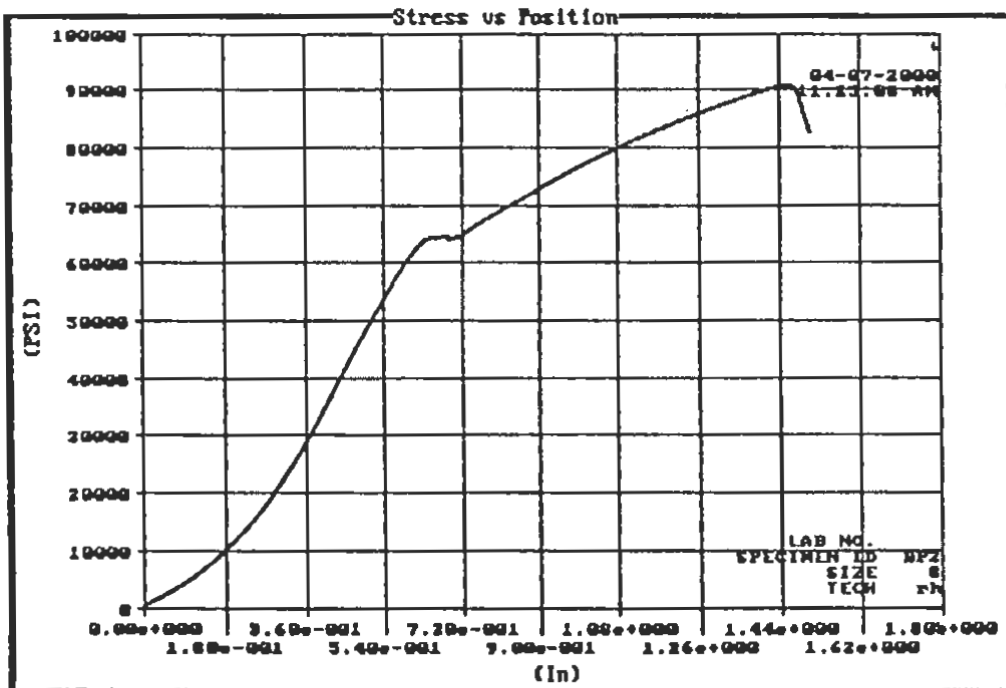


Figure D.23 TxDOT Tensile Test Report for #8 BP2
 Reinforcing Rod Specimen

LAB NO.
 SPECIMEN ID BP3
 SIZE 8
 TECH rh

Test Tensile Test
 Procedure REBAR W/EXTENSOMETER

Test Date 04-07-2000 Tested By HAMILTON
 Test Time 11:45:33 AM Test Counter N/A
 Elapsed Time 00:02:15 Area 0.7900 In²

Tensile Strgth	82809 PSI	Peak Load	65419 Lbs
Breaking Strgth	80201 PSI	Breaking Load	63359 Lbs
Modulus	26378000 PSI	Correl Coeff	1.0000
.2 % Off Strs		.2 % Off Load	
% Off Strs		HOTL Yield Sts	64086 PSI
HOTL Yield Lod	50628 Lbs	Upper Yield Sts	64086 PSI
Lower Yield Sts	63845 PSI	Upper Yield Lod	50628 Lbs
Lower Yield Lod	50438 Lbs		

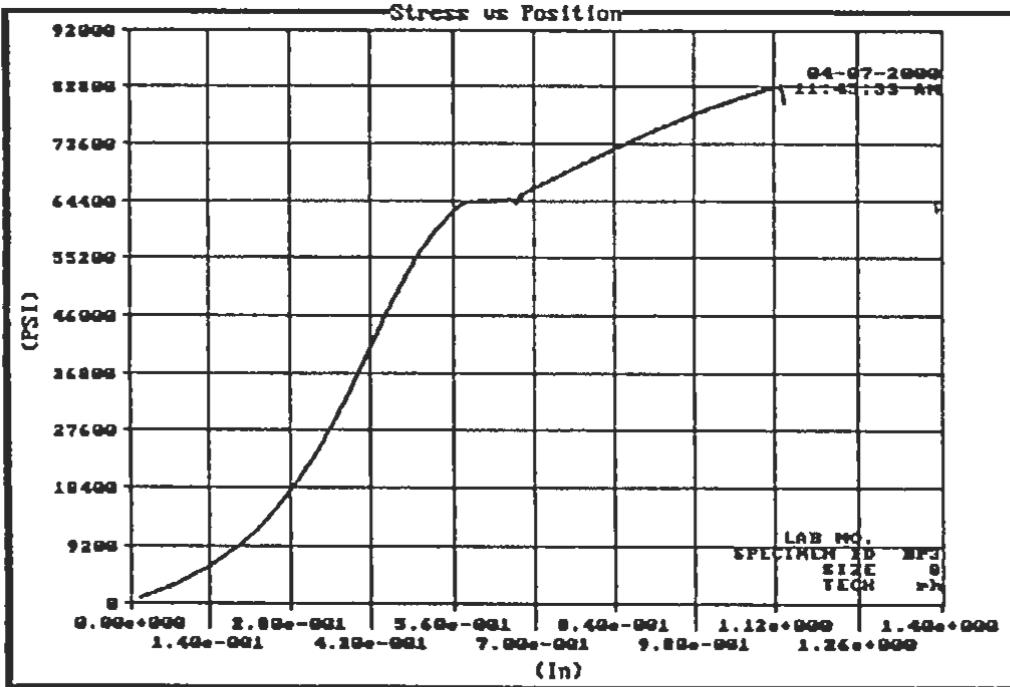


Figure D.24 TxDOT Tensile Test Report for #8 BP3 Reinforcing Rod Specimen

LAB NO.
 SPECIMEN ID s1
 SIZE 8
 TECH rh

Test Tensile Test
 Procedure REBAR W/EXTENSOMETER

Test Date 04-07-2000 Tested By HAMILTON
 Test Time 12:06:34 PM Test Counter N/A
 Elapsed Time 00:02:31 Area 0.7900 In²

Tensile Strgth	86241 PSI	Peak Load	68130 Lbs
Breaking Strgth	78979 PSI	Breaking Load	62394 Lbs
Modulus	26785000 PSI	Correl Coeff	1.0000
.2 % Off Strs	64113 PSI	.2 % Off Load	50650 Lbs
% Off Strs		HOTL Yield Sts	64155 PSI
HOTL Yield Lod	50682 Lbs	Upper Yield Sts	64155 PSI
Lower Yield Sts	63803 PSI	Upper Yield Lod	50682 Lbs
Lower Yield Lod	50404 Lbs		

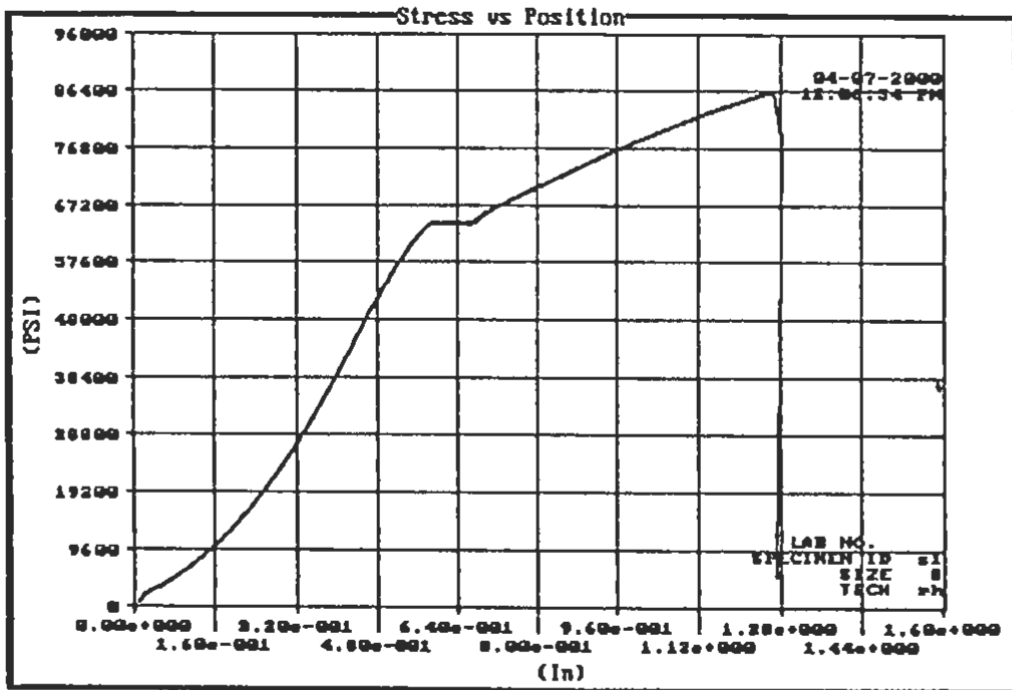


Figure D.26 TxDOT Tensile Test Report for #8 S1 Reinforcing Rod Specimen

LAB NO.
 SPECIMEN ID S2
 SIZE 8
 TECH rh

Test Tensile Test
 Procedure REBAR W/EXTENSOMETER

Test Date 04-07-2000
 Test Time 11:35:56 AM
 Elapsed Time 00:02:52

Tested By HAMILTON
 Test Counter N/A
 Area 0.7900 In²

Tensile Strgth 89094 PSI
 Breaking Strgth 85713 PSI
 Modulus 28181000 PSI
 .2 % Off Strs 64732 PSI
 % Off Strs
 HOTL Yield Lod 51006 Lbs
 Lower Yield Sts 64524 PSI
 Lower Yield Lod 50974 Lbs

Peak Load 70384 Lbs
 Breaking Load 67713 Lbs
 Correl Coeff 1.0000
 .2 % Off Load 51139 Lbs
 HOTL Yield Sts 64565 PSI
 Upper Yield Sts 64565 PSI
 Upper Yield Lod 51006 Lbs

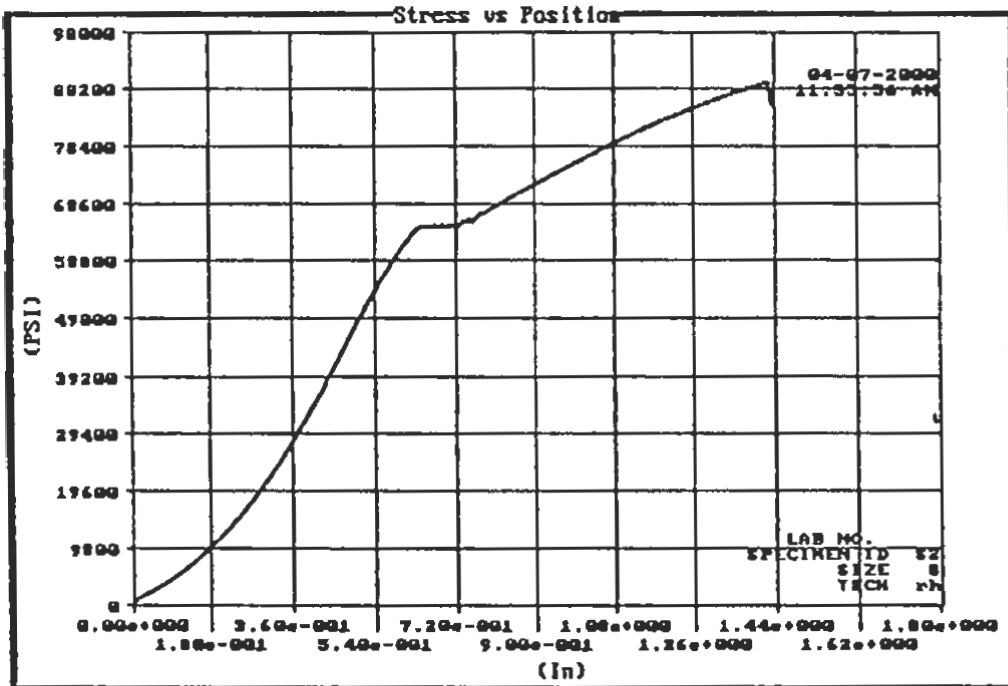


Figure D.27 TxDOT Tensile Test Report for #8 S2 Reinforcing Rod Specimen

LAB NO.
 SPECIMEN ID s3
 SIZE 8
 TECH rh

Test Tensile Test
 Procedure REBAR W/EXTENSOMETER

Test Date	04-07-2000	Tested By	HAMILTON
Test Time	12:14:15 PM	Test Counter	N/A
Elapsed Time	00:03:18	Area	0.7900 In ²

Tensile Strgth	94687 PSI	Peak Load	74803 Lbs
Breaking Strgth	94663 PSI	Breaking Load	74784 Lbs
Modulus	27453000 PSI	Correl Coeff	1.0000
.2 % Off Strs	64291 PSI	.2 % Off Load	50790 Lbs
% Off Strs		HOTL Yield Sts	64343 PSI
HOTL Yield Lod	50831 Lbs	Upper Yield Sts	64343 PSI
Lower Yield Sts	64213 PSI	Upper Yield Lod	50831 Lbs
Lower Yield Lod	50728 Lbs		

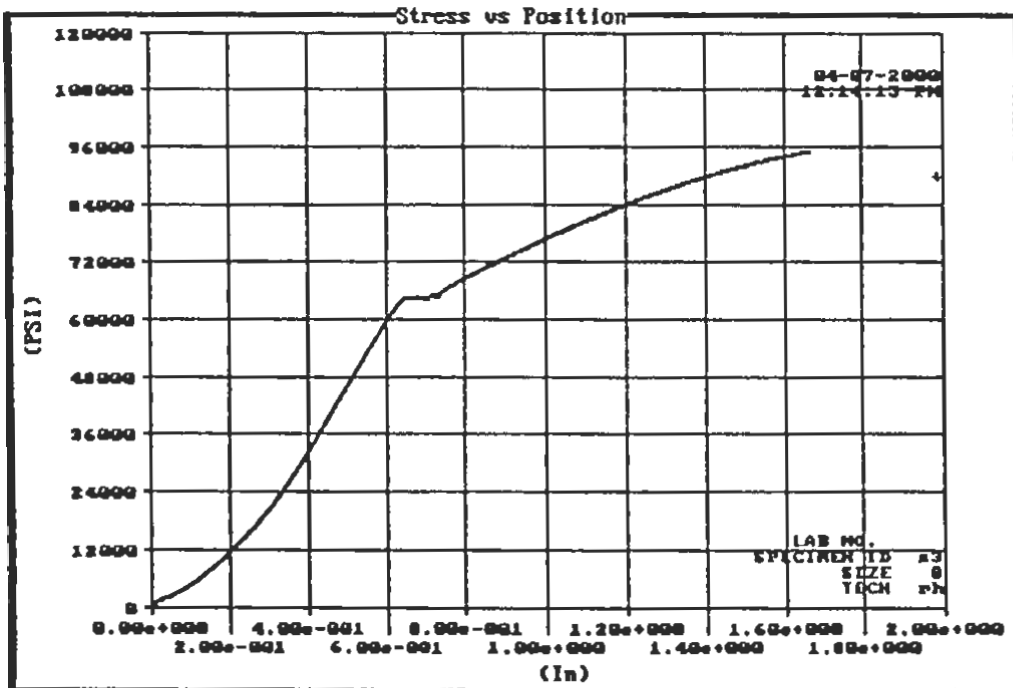


Figure D.28 TxDOT Tensile Test Report for #8 S3 Reinforcing Rod Specimen

LAB NO.
 SPECIMEN ID W1
 SIZE 8
 TECH rh

Test Tensile Test
 Procedure REBAR W/EXTENSOMETER

Test Date 04-07-2000
 Test Time 12:23:44 PM
 Elapsed Time 00:02:33

Tested By HAMILTON
 Test Counter N/A
 Area 0.7900 In²

Tensile Strgth 82967 PSI
 Breaking Strgth 78834 PSI
 Modulus 26489000 PSI
 .2 % Off Strs 62751 PSI
 % Off Strs
 HOTL Yield Lod 51192 Lbs
 Lower Yield Sts 64697 PSI
 Lower Yield Lod 51111 Lbs

Peak Load 65544 Lbs
 Breaking Load 62279 Lbs
 Correl Coeff 0.9998
 .2 % Off Load 49573 Lbs
 HOTL Yield Sts 64800 PSI
 Upper Yield Sts 64800 PSI
 Upper Yield Lod 51192 Lbs

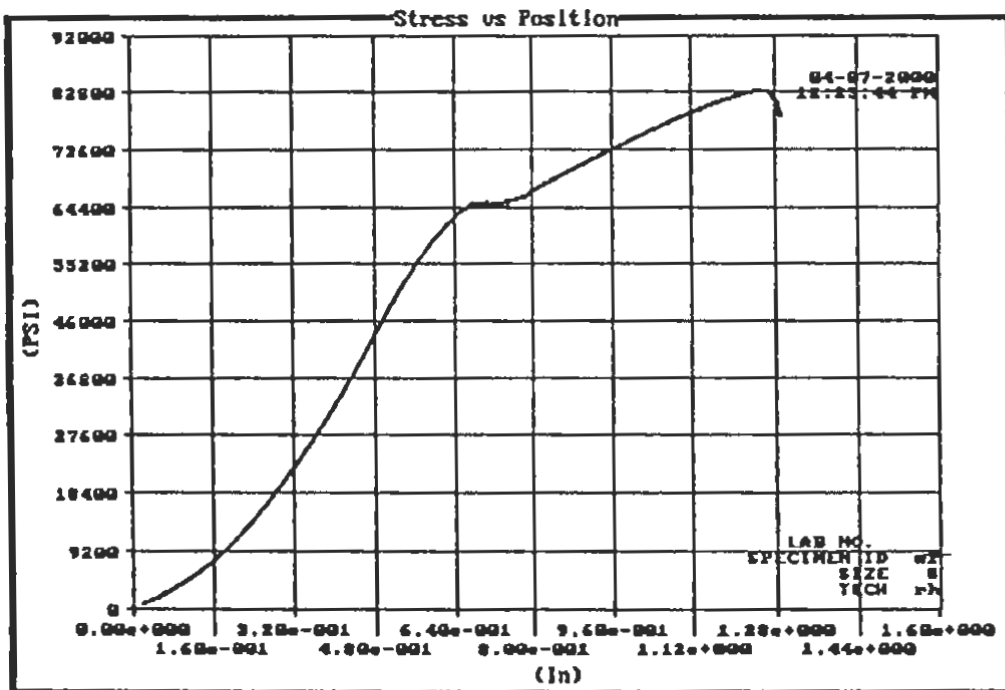


Figure D.29 TxDOT Tensile Test Report for #8 W1 Reinforcing Rod Specimen

LAB NO.
 SPECIMEN ID w2
 SIZE 8
 TECH rh

Test Tensile Test
 Procedure REBAR W/EXTENSOMETER

Test Date 04-07-2000 Tested By HAMILTON
 Test Time 12:31:19 PM Test Counter N/A
 Elapsed Time 00:02:12 Area 0.7900 In²

Tensile Strgth	79191 PSI	Peak Load	62561 Lbs
Breaking Strgth	47270 PSI	Breaking Load	37343 Lbs
Modulus	27057000 PSI	Correl Coeff	0.9999
.2 % Off Strs	62673 PSI	.2 % Off Load	49511 Lbs
% Off Strs		HOTL Yield Sts	64694 PSI
HOTL Yield Lod	51108 Lbs	Upper Yield Sts	64694 PSI
Lower Yield Sts	64521 PSI	Upper Yield Lod	51108 Lbs
Lower Yield Lod	50972 Lbs		

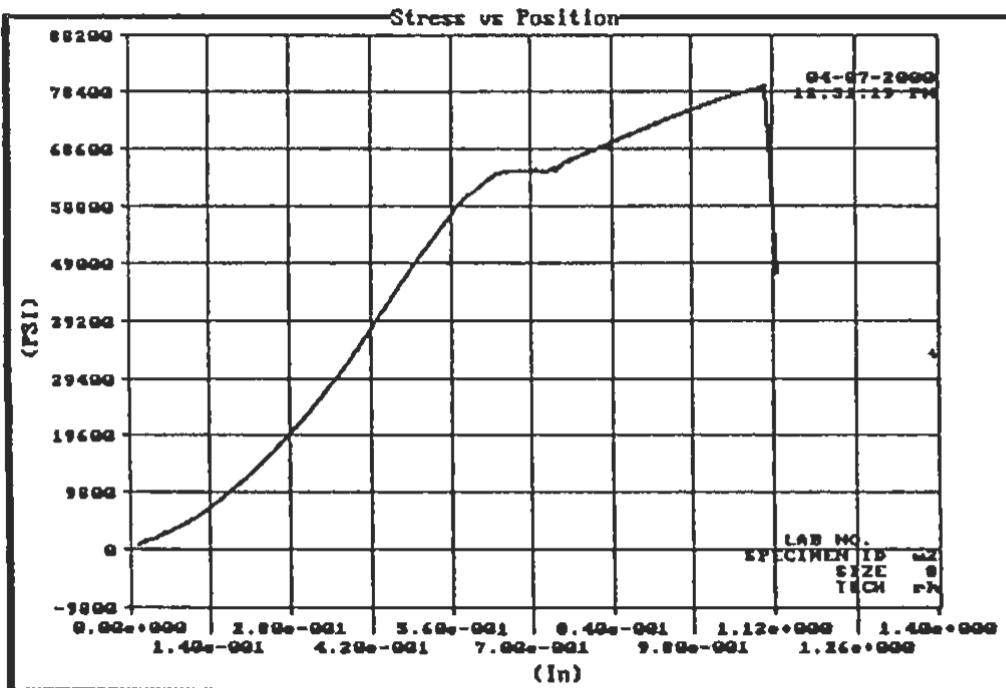


Figure D.30 TxDOT Tensile Test Report for #8 W2 Reinforcing Rod Specimen

APPENDIX E

INDEPENDENT NONDESTRUCTIVE EVALUATION OF WELDED REINFORCING ROD SPECIMENS

E.1 INTRODUCTION

The welded reinforcing rod specimens evaluated in Chapters 3, 4, and 5 were also subjected to a second independent nondestructive evaluation (NDE) process. The objective of this evaluation was to provide an independent review of specimen weld quality using traditional NDE techniques. For comparative purposes two inspection methods were used, dye penetrant inspection and radiographic inspection. A trained but non-certified inspector performed the inspections. The results of this independent review are organized into the following sections; a description of the dye penetrant inspection procedures, the visual and dye penetrant inspection results, the results of the radiographic record interpretations, and a discussion of these NDE results. Table 3.1 summarizes the specimen codes used to identify the specimens discussed in this appendix.

E.2 DYE PENETRANT INSPECTION PROCEDURES

Samples were visually inspected for surface irregularities and discontinuities. Weld samples were then individually inspected using the dye penetrant method. A solvent based cleaner was applied to lint-free cloths, then wiped across the surfaces. Special attention was paid to open crevices and irregular surfaces. After the surface was cleaned, a spray dye penetrant was applied, and then allowed to sit on the surface for a 5 minute dwell time. The sample under inspection was then cleaned using the same technique as stated previously, and then the spray developer was applied to the surface. After five minutes, the sample was visually inspected for evidence of red indications. Figure E.1 depicts a typical specimen weld after cleaning of the weld surface was completed. In Figure E.2 the same view of the specimen weld is shown after application of the dye penetrant and developer.

E.3 RESULTS OF VISUAL / DYE PENETRANT INSPECTION

The irregular surfaces of the bars posed difficulties for the surface inspection with the limited inspection facilities available. The surface irregularity also inhibited the level of cleanliness that could be obtained in the dye penetrant inspections. This difficulty limited the size of the indications that could be identified to those of more gross size. Overflow from larger indications tends to obscure those of smaller size. The following is a detailed summary of the individual specimen inspections.

BP1 (#8): Porosity is visible on the fusion line to the base metal. The top of the joint is fairly flush. Scattered porosity, some large in diameter appear on the sides which also have areas of large reinforcement and overlap. One side of the joint at the base material has some lack of fusion.

BP2 (#8): Porosity is found scattered across the weld, especially at the tie in to the base metal at one side of the joint. The porosity appears at every fusion line between passes from very tiny to fairly large size holes, but do not seem to be very deep.

BP3 (#8): The face of the weld is underfilled. The beads are too long for the joint leading to a form of excessive reinforcement and occasions of overlap. Pinhole porosity can be seen everywhere, including the fusion lines between the layers of beads.

PH1 (#8): Overlaps are present on the sides of the weld in several locations. The face of the weld is flush with the face of the base material. There is large diameter porosity at the fusion line to the base material and pinhole porosity scattered across the surface of the weld.

S1 (#8): The surface of the bar appears to have been overheated; the dirty surface oxidized during welding. Porosity is in the area of the backing bar weld at the fusion line.

S2 (#8): There is an open area in the side of the joint with a large cluster of porosity at this site. The weld has been ground flush at the face.

S3 (#8): The face of the weld has large diameter but shallow porosity while pinhole porosity is scattered across the sides of the weld.

W1 (#8): On the surface can be seen isolated large diameter yet shallow porosity. Pinhole porosity is found on the surface at the fusion lines between layers of beads. The side surface is very irregular with extreme overlap in areas. Undercutting is slight on the face of the weld.

W2 (#8): A large crevice can be seen under an overlap on the side with associated pinhole porosity. A 'chimney' is evident on the face of the weld where the electrode was held in one spot to build up weld metal. A wormhole is in the surface of this buildup as well as other large diameter porosity. The sides of the weld are very irregular with many extreme overlaps. Pinhole porosity also is seen at the overlaps.

BP1 (#11): The surface of the weld has been ground lightly. Pinhole and larger diameter porosity are present under the top layer of beads. Pinhole porosity is scattered on the surface of the weld, particularly at the fusion lines between layers of beads. Shallow lack of fusion appears between some beads. The surface is very irregular with one very large overlap.

BP2 (#11): Pinhole porosity is scattered across the weld cross-section with several instances of large diameter porosity appearing at overlaps and the fusion line to the base metal. The side surface is very irregular. Many overlaps are severe, indicating the welds were made with high heat input.

BP3 (#11): There is pinhole porosity at the fusion lines between bead layers. A surface opening is present behind a large spatter or weld wire adhered to the surface. Large diameter porosity occurs in several places.

PH2 (#11): The surface is very irregular. Pinhole porosity is present at the many overlaps on the sides of the weld. The weld crater on the face has pinhole porosity. Large diameter porosity is open at the fusion line at the base material.

S1 (#11): Shallow pinhole porosity is scattered across the weld cross-section and porosity is visible under the fusion line underneath layers of beads. There is some lack of fusion at the fusion line to the base metal.

S2 (#11): There is pinhole porosity in the face of the weld, lack of fusion between the beads as seen from the side of the weld, as well as overlap and under fill, contributing to surface irregularity. Cluster porosity appears under the overlaps.

S3 (#11): Shallow scattered pinhole porosity is visible across the weld, with larger diameter porosity concentrated near the top of the weld. Lack of fusion can be seen at the fusion line to the base metal.

W1 (#11): Pinhole porosity is scattered across the face of the weld. The surface is very irregular with many overlaps. There is a large opening near the face.

W2 (#11): This weld has no backing bar at inspection. There is apparent lack of fusion at the sidewalls of the joint and under the overlaps. There is root porosity and a large diameter pore in the side.

BP1 (#14): Scattered pinhole porosity and one large diameter pore are visible on the sides. Lack of fusion is apparent at base metal. The surface is irregular.

BP2 (#14): Side surfaces are irregular with ends of beads clearly seen. Pinhole porosity is scattered at all the fusion lines between bead layers.

BP3 (#14): The sidewalls of the joint still can be seen. There is large diameter shallow porosity, and scattered pinhole porosity, with a crack or lack of fusion near bottom third of the joint.

PH3 (#14): Shallow pinhole porosity is scattered across the weld, particularly at the fusion lines between bead layers. Some overlap is on the side.

S1 (#14): This weld has a more even surface than most. There is a small indication of lack of fusion at the tie in to the base metal on the face. Several instances of shallow porosity occur at the fusion line between the weld layers.

S2 (#14): The face of the weld is fairly uniform. Shallow pinhole porosity is distributed across the surfaces with large isolated porosity. There is undercutting at the fusion line to the base metal nearly all the way around the weld.

S3 (#14): There are large amounts of very shallow scattered pinhole porosity, with larger porosity at the fusion line at the base metal.

W1 (#14): There are large diameter scattered porosity and apparent lack of fusion under the overlaps on the side. On one side, there is a large area in which the beads do not fill the cross-section completely.

W2 (#14): Scattered pinhole porosity is present at the weld bead interface between layers. The sides of the weld exhibit marked overlaps in combination with underfill in other areas. A large area of undercutting appears on the face of the weld.

E.4 INTERPRETATION OF RADIOGRAPHIC RECORDS

The radiographic records of each specimen weld recorded by Caltrans after fabrication of the test specimens were shipped to Texas A&M for interpretation. Several images of specimen welds were provided from two perpendicular viewing directions. The results of the interpretation of these records are provided below for each specimen.

BP1 (#8): Some porosity is visible at fusion line to base metal. Shading of X-ray indicates underfill or large variations in weld cross-section dimension.

BP2 (#8): Lack of fusion or very connected linear porosity on one sidewall of the joint at the fusion line to the base metal. Again shading indicated extremely irregular surface, underfill and scattered porosity.

BP3 (#8): Underfill can be seen on the face of the weld. There is lack of fusion at sidewalls of joint. Some porosity can be seen in the radiographs, but not as much as the other BP samples in this size.

PH1 (#8): Large diameter porosity is scattered throughout the weld; some is linear porosity at the fusion lines between the bead layers.

S1 (#8): Massive quantity and large diameter porosity in tack weld. Linear porosity at fusion line of tack weld to base material and weld.

S2 (#8): Large diameter porosity in body of weld located primarily at fusion line. Scattered porosity in weld.

S3 (#8): Large diameter and pinhole scattered porosity are found throughout weld. This bar is not quite as bad as S2.

W1 (#8): Shading indicates extreme underfill in some locations. Lack of fusion exists under top fill pass, also with a large hole. From the radiograph, no porosity is apparent in the weld cross-section.

W2 (#8): Probable cracks are at both toes of weld and may extend to the HAZ. Sides of the weld are very irregular.

BP1 (#11): The weld appears to be of good quality, with very small internal porosity but heavy surface irregularity.

BP2 (#11): A small crack or lack of fusion, probably the latter, extends from toe of weld along fusion line. Isolated instances of large diameter porosity appear near the top surface. No other discontinuities are observed.

BP3 (#11): A small area of lack of fusion is located on one side, which may be surface underfill. The weld has fairly good internal quality, but has an irregular surface area.

PH2 (#11): Scattered porosity is distributed evenly across the weld cross-section. The last weld at the face has heavy larger diameter porosity. Lack of fusion appears at the fusion line to the base metal.

S1 (#11): The condition of this weld is better than the S2 and S3 samples of the same size. One large diameter pore is located near the centerline, as is some lack of fusion between beads.

S2 (#11): Porosity and lack of fusion are evident on the bond line. Linear porosity is present across the weld. Some large diameter porosity and lack of fusion appears in the root area. The S2 sample is in better condition than the S3 sample discussed below.

S3 (#11): Large diameter porosity is present throughout the weld, especially in the top third of the weld. Lack of bond line fusion occurs in several locations such as at the root and in the center of the weld. Porosity is also concentrated at bond lines between passes. On the face of the weld there is porosity and lack of fusion.

W1 (#11): A crack is located in the heat affected zone (HAZ). Large diameter porosity is found on the center near the face of the weld. Lack of bond line fusion or probably underfill is at the root of the weld. The original edges of the joint are distinct. Large diameter porosity is at the bond line on same side as the crack but near the face.

W2 (#11): Wormhole porosity is located at the face. Some lack of fusion appears between the weld beads. Large diameter porosity is at the bond line near the face. The surface appears to be extremely irregular with underfill. One side appears almost to have a crack extending down into the weld metal.

BP1 (#14): Lack of bond line fusion, on one side of the weld joint. One large diameter pore is evident. Overall, the weld has fairly good quality.

BP2 (#14): No discontinuities are visible except the lack of fusion at backing bar welds. The weld is very irregular in density.

BP3 (#14): Some lack of bond line fusion is visible near the bottom third of the weld. The surface of the weld is very irregular.

PH3 (#14): Cluster porosity is seen near the center of the weld cross-section. Small lack of fusion appears near the face.

S1 (#14): Major amounts of large diameter cluster porosity appear in the last welds in the joint face. There is some lack of fusion near root that may be in backing weld.

S2 (#14): Large diameter porosity is scattered throughout entire weld cross-section.

S3 (#14): Large diameter porosity is scattered throughout, though not nearly as many as S2 above. The backing bar tack weld has large quantities of porosity.

W1 (#14): There is a lack of fusion to the base material near face. Lack of fusion (underbead) also appears between passes near the top third of the weld.

W2 (#14): There is a lack of fusion to the base material at the face of the weld. In an overlap, there is large diameter porosity. The bottom two-thirds of the weld cross-section exhibits underfill.

E.5 DISCUSSION OF RESULTS

Indications of discontinuities were located on all of the welds, including surface irregularities, porosity and suspected cracks. Shallow surface porosity was by far the most common indication. The welds for the reinforcing bar were apparently welded with a high to excessive heat input. The welds were characterized by underfill and overlaps visible on the side of the welds at the ends of the weld beads. The backing bars and their associated tack welds were still in place on most of the specimens. All of these tack welds had excessive reinforcement and large diameter cluster porosity, as well as some lack of fusion to the base material. All the welds had the same types of discontinuity, though some samples were worse than the others. Based on the results from the limited NDE inspection, a relative rating of the samples based on the average weld quality was prepared. There is error involved, so an absolute valuation cannot be provided. A comparative evaluation is possible. Table D-1 presents this relative comparison sorted by quality level. Table D-2 presents the same results sorted by specimen identification code and rod size.

E.6 SUMMARY AND CONCLUSIONS

Independent NDE evaluations were performed on the twenty seven welded reinforcing rod specimens tested in Chapters 3, 4, and 5. Two inspection methods, dye penetrant and radiographic record interpretation, were used to establish the relative weldment quality of each specimen.

The welds exhibited indications of irregular surfaces, shallow surface porosity as well as interior porosity, some large in diameter. Undercutting, overlaps and lack of fusion were evident in some welds. Though all the welds did have some type of indication, it was not

apparent for most of the welds that these discontinuities would lead to tensile failure at appreciable low strengths.

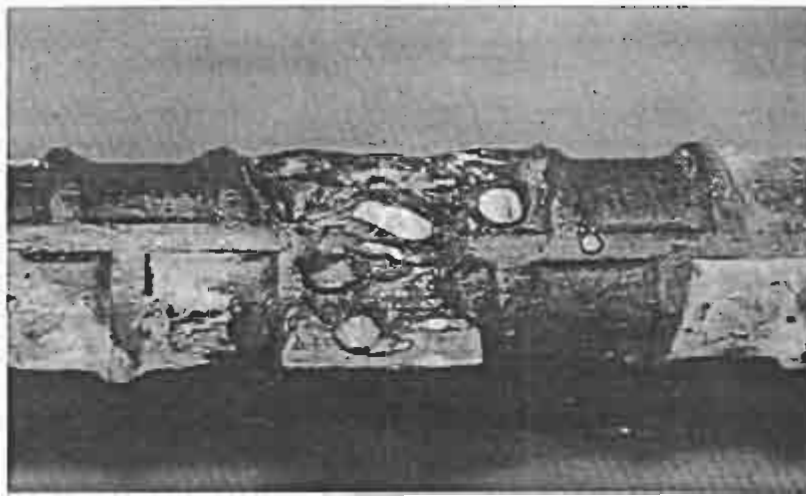
A weld should fail in the heat affected zone (HAZ) located in the base metal immediately adjacent to the weld metal. Failure occurs in the HAZ due to the grain growth created by the high temperatures produced during welding. The HAZ should be minimized in order to reduce the amount of grain growth; this HAZ would typically be smaller in the larger diameter rebar, as the larger cross-section body produces greater amounts of body quenching. This is true for equal heat inputs for the welds. Welds that might fail at lower strengths in this test might have a large quantity of porosity, extreme lack of fusion or cracks. Any of these might sufficiently reduce the weld cross-section as to produce low strength failure.

Table E.1 Welded Specimens Sorted by Relative Weld Quality

<i>Specimen Code</i>	<i>Best</i> ← → <i>Worst</i>			
	<i>1</i>	<i>2</i>	<i>3</i>	<i>4</i>
BP1(#8):	X			
BP2(#8):	X			
BP3(#8):	X			
BP1(#11):	X			
BP3(#11):	X			
S1(#11):	X			
BP1(#14):	X			
BP2(#14):	X			
PH3(#14):	X			
PH1(#8):		X		
S3(#8):		X		
W1(#8):		X		
PH2(#11):		X		
S2(#11):		X		
S1(#14):		X		
S3(#14):		X		
S1(#8):			X	
S2(#8):			X	
BP2(#11):			X	
W2(#11):			X	
BP3(#14):			X	
S2(#14):			X	
W2(#14):			X	
W2(#8):				X
S3(#11):				X
W1(#11):				X
W1(#14):				X

Table E.2 Relative Weld Quality of Specimens Sorted by Specimen Size and Code

<i>Specimen Code</i>	<i>Best</i> ←————→ <i>Worst</i>			
	<i>1</i>	<i>2</i>	<i>3</i>	<i>4</i>
BP1(#8):	X			
BP2(#8):	X			
BP3(#8):	X			
PH1(#8):		X		
S1(#8):			X	
S2(#8):			X	
S3(#8):		X		
W1(#8):		X		
W2(#8):				X
BP1(#11)	X			
BP2(#11)			X	
BP3(#11)	X			
PH2(#11)		X		
S1(#11):	X			
S2(#11):		X		
S3(#11):				X
W1(#11):				X
W2(#11):			X	
BP1(#14)	X			
BP2(#14)	X			
BP3(#14)			X	
PH3(#14)	X			
S1(#14):		X		
S2(#14):			X	
S3(#14):		X		
W1(#14):				X
W2(#14):			X	



**Figure E.1 A Typical Sample Bar with Irregular Surfaces
(Welds apparently were slightly ground)**



**Figure E.2 The Same Bar after the Developer Was Applied
(Note that surface irregularities precluded proper cleaning of the weld area)**